Rational Design and Synthesis of Phosphine Ligands and Their Application in Transition Metal-Catalyzed Reactions

CUMULATIVE DISSERTATION

Sebastian Ahrens

University of Rostock

2025

https://doi.org/10.18453/rosdok_id00005821

Rational Design and Synthesis of Phosphine Ligands and Their Application in Transition Metal-Catalyzed Reactions

CUMULATIVE DISSERTATION

to acquire the academic degree
doctor rerum naturalium (Dr. rer. nat.)
of the Faculty of Mathematics and Natural Sciences
at the University of Rostock

Submitted by
Sebastian Ahrens
born on 16 January 1996 in Güstrow

Rostock, 16 October 2025

The presented work was accomplished at the Leibniz Institute for Catalysis in the research group of Prof. Matthias Beller during the period from October 2021 to July 2025.

Reviewer 1: Prof. Dr. Dr. h.c. mult. Matthias Beller
Leibniz Institute for Catalysis
Applied Homogeneous Catalysis
Albert-Einstein-Straße 29a
18059 Rostock, Germany

Reviewer 2: Prof. Dr. Marko Hapke
Johannes Kepler University Linz
Institute of Catalysis
Altenberger Straße 69
A-4040 Linz, Austria

Reviewer 3: Prof. Dr. Malte Behrens
Kiel University
Institute of Inorganic Chemistry
Max-Eyth-Straße 2
24118 Kiel, Germany

Date of submission: 16 October 2025
Date of defense: 5 May 2026

Statement of Authorship

I hereby affirm that I have written the present thesis by myself without outside assistance. No other resources were utilized than those stated. All references as well as verbatim extracts were quoted, and all sources of information were specifically acknowledged.

Ich versichere hiermit an Eides statt, dass ich die vorliegende Arbeit selbstständig angefertigt und ohne fremde Hilfe verfasst habe. Dazu habe ich keine außer der von mir angegebenen Hilfsmittel und Quellen verwendet. Die den benutzten Werken inhaltlich und wörtlich entnommenen Stellen habe ich als solche kenntlich gemacht.

Rostock, 16 October 2025



Sebastian Ahrens

Note on the use of AI tools: Portions of this thesis were linguistically refined with the assistance of ChatGPT (GPT-5, OpenAI, 2025). The tool was employed exclusively to enhance clarity, grammar, and style; all conceptual, analytical, and interpretive content remains entirely the author's own.

Acknowledgments

First, I would like to sincerely thank my supervisor, **Prof. Dr. Matthias Beller**, for giving me the opportunity to join his research group and to complete my PhD under excellent conditions. I am very grateful for his kindness, support, and consistently positive mindset. His inspiring way of thinking and guidance have offered new ideas and fresh perspectives on my research. Working with him deepened my appreciation for the beauty and excitement of chemistry. I am especially grateful for the freedom to pursue my own ideas, which allowed me to grow both scientifically and personally during my PhD.

I would like to sincerely thank **Dr. Kathrin Junge** for welcoming me into the "Sustainable Redox Reactions" subgroup and for her continuous support throughout my PhD. Your calm and structured approach helped me overcome challenges and made the working environment both motivating and enjoyable. I truly appreciated working in such a friendly and supportive atmosphere. The many cake breaks and group activities you organized created lasting memories.

I am grateful to my industrial collaborators at Symrise AG, **Dr. Johannes Panten** and **Dr. Bernhard Rußbüldt**, for their valuable insights into the industrial R&D sector, for the scientific discussions, and for funding part of my PhD research.

I would like to thank the entire LIKAT analytical and technical departments for their support throughout the years. In particular, I am grateful to **Susann Buchholz**, **Susanne Schareina**, **Andreas Koch**, **PD Dr. Wolfgang Baumann**, and **Dr. Marcus Klahn** for their support in analyzing numerous samples by NMR and HR-MS, and for assisting me with various special measurements. I am also grateful to **Dr. Anke Spannenberg** for her patience and precision in performing the numerous X-ray measurements. Moreover, I sincerely appreciate the support and assistance of all employees of the institute and the University of Rostock.

I am especially grateful to **Dr. Fairoosa Poovan** for her support and valuable scientific discussions, as well as for the many memorable moments we shared throughout our PhD research. Over the years, a great friendship has developed, for which I am thankful.

I would also like to thank **Dr. Dennis Verspeek** for the great time we shared during our PhDs. Working with you in the lab was truly one of the most enjoyable and memorable parts of my entire PhD.

Furthermore, I would like to thank **Dr. Yao Ge** for her guidance at the start of my PhD. Our scientific discussions were a constant source of motivation, and I am truly grateful for her support during the early stages of my research.

I am also grateful to all current and former members of the subgroup “Sustainable Redox Reactions” for a supportive and collaborative working atmosphere. In particular, I would like to thank my current and former labmates, **Dr. Rafał Kusy**, **Dr. Soumyashree Jena**, **Dr. Shuxin Mao**, **Dr. Ruiyang Qu**, **Jianglin Duan**, and **Faral Akhtar**, for many helpful discussions, inspiring conversations, and the unforgettable moments we shared. I would also like to thank **Katja Andres** for her great assistance in the laboratory and for always being willing to help.

Furthermore, I am grateful to **Dr. Niklas Both, Dr. Johannes Fessler** and **Dr. Florian Bourriquen** for many excellent discussions about chemistry. I also want to thank **Dr. Leonardo Scarpa**, **Dr. Carolin Stein**, **German Lopez Robledo**, **Dr. Haifeng Qi**, **Jacqueline Maslack**, **Dr. David Leonard**, **Dr. Raquel Jimenez Rama**, and **Dr. Jorge Quesada Sanchez** for the great moments we shared in the lab and office, which truly made my PhD special. I deeply appreciate all of your valuable input, support, and encouragement, which I will always remember with great appreciation.

Above all, I would like to thank my parents, **Gabriela** and **Frank**, for their continuous support throughout my entire education. I am deeply grateful for their encouragement and for all their love. I cannot thank you enough for always being there for me.

Finally, I would like to thank my partner **Laura** for bringing so much happiness into my life, especially during the more challenging times of my PhD. I am incredibly grateful for her constant support, whether it was discussing chemistry, proofreading, or just being there to listen and share thoughts about my work. Her support has made my scientific journey possible, and I am truly thankful for the time we have shared and look forward to the next chapters of our lives together.

Abstract

The development of sustainable catalytic methodologies is essential to minimizing the resource and energy demands of modern chemical synthesis. By avoiding stoichiometric activating agents and decreasing overall energy consumption, catalytic processes can substantially reduce CO_2 emissions and environmental impact. In homogeneous catalysis, performance is governed not only by the intrinsic properties of the metal center but also by the steric and electronic characteristics of the ligand environment. Through rational design and systematic optimization, ligand frameworks can be tailored to achieve high activity and selectivity while maintaining low catalyst loadings.

This work reports the synthesis of novel benzofurylphosphine ligands, and the development of cobalt-based catalytic systems derived from them, which enable the isomerization of allylamines to enamines with activities comparable to those of rhodium catalysts currently employed in industry. The cobalt catalyst developed herein efficiently converted a wide range of allylamines, and its reaction pathway was elucidated through comprehensive mechanistic studies. Moreover, the newly synthesized benzofurylphosphine ligands were applied in the palladium-catalyzed telomerization of 1,3-butadiene, where the resulting catalytic systems exhibited both excellent activity and high yields.

In addition, this study presents the development of ruthenium catalyst systems that enable the site-selective isotopic labeling of 2-propylbenzimidazole derivatives. A machine learning approach was applied to the generated dataset to predict activity-selectivity relationships of the ruthenium catalysts. The developed systems achieved good to excellent results in deuterium labeling. Furthermore, the general applicability of the method was demonstrated through the successful labeling of pharmaceutical compounds. Finally, the reaction mechanism of the ruthenium catalysts was elucidated using spectroscopic methods and control experiments.

Kurzzusammenfassung

Die Entwicklung nachhaltiger chemischer Transformationen stellt einen zentralen Ansatz für einen ressourcenschonenden Umgang mit Rohstoffen dar. Durch den Verzicht auf stöchiometrische Aktivierungsreagenzien und hohe externe Energiezufuhr leisten Katalysatorsysteme einen wesentlichen Beitrag zur Verringerung des CO_2-Ausstoßes in der chemischen Industrie. Ein entscheidender Aspekt ist dabei die gezielte Modifikation der Katalysatoren: Neben dem aktiven Zentrum – dem Metall – spielt in der homogenen Katalyse insbesondere die Struktur der verwendeten Liganden eine entscheidende Rolle für die Aktivität und Selektivität. Gezielte Synthesen und Optimierungen von Ligandenstrukturen und den resultierenden Katalysatorsystemen ermöglichen hohe Ausbeuten bei gleichzeitig reduziertem Katalysatoreinsatz.

In dieser Arbeit wird die Synthese neuartiger Benzofurylphosphin-Liganden sowie die Entwicklung darauf basierender Cobalt-Katalysatoren beschrieben, welche die Isomerisierung von Allylaminen zu Enaminen mit einer Aktivität ermöglichen, die der von industriell genutzten Rhodium-Katalysatoren entspricht. Darüber hinaus konnte das entwickelte Cobalt-Katalysatorsystem erfolgreich auf eine Reihe von Allylaminen angewendet und umfassend mechanistisch untersucht werden. Die neuartigen Benzofurylphosphin-Liganden fanden zudem Anwendung in der Palladium-katalysierten Telomerisierung von 1,3-Butadien, wobei die neuartigen Katalysatorsysteme sowohl eine ausgezeichnete Aktivität als auch hohe Ausbeuten erreichten.

Darüber hinaus wurden im Rahmen dieser Arbeit Ruthenium-Katalysatorsysteme entwickelt, die eine gezielte Isotopenmarkierung von 2-Propylbenzimidazol-Derivaten ermöglichen. Im Forschungsprojekt kam zudem ein Ansatz des maschinellen Lernens zum Einsatz, der auf Grundlage der generierten Daten präzise Prognosen zu Aktivitäts- und Selektivitätsbeziehungen der Ruthenium-Katalysatoren lieferte. Die resultierenden Katalysatorsysteme erzielten gute bis sehr gute Ergebnisse bei der Deuterium-Markierung. Die allgemeine Relevanz der Methode wurde zudem durch die erfolgreiche Isotopenmarkierung von Arzneistoffen belegt. Darüber hinaus wurde der Reaktionsmechanismus der neuartigen Ruthenium-Katalysatoren mithilfe spektroskopischer Methoden und Kontrollexperimenten eingehend untersucht.

Table of Contents

1 Introduction 1

1.1 Olefin Isomerization – From Biological Relevance to Applications 1

1.1.1 Transition Metal-Catalyzed Isomerization of Olefins 3

1.1.2 Homogeneous Noble Metal Catalysts for Olefin Isomerization 5

1.1.3 Homogeneous Cobalt Catalysts in Selective Olefin Isomerization: Recent Advances and Perspectives 8

1.1.4 Noble vs. Non-Noble Metal Catalysts: Advances and Challenges 11

1.2 Bridging Traditional Reaction Optimization and Artificial Intelligence in Chemistry and Catalysis 13

1.3 Hydrogen Isotope Exchange via Transition Metal Catalysis 16

1.3.1 Regioselective Deuteration of Aromatic C(sp^2)–H Bonds 17

1.3.2 Site-Selective Deuterium Incorporation into Unactivated C(sp^3)–H Bonds 19

2 Objectives of this Work 21

3 Summary of Published Articles 23

3.1 Cobalt(0)-Catalyzed Isomerization of Allylamines Promoted by Monodentate Benzofuran Phosphines 23

3.2 Development of Highly Efficient and Selective Palladium Catalysts for Telomerization of 1,3-Butadiene with Alcohols 31

3.3 Machine Learning–Guided Site-Selective Ru-Catalyzed C(sp^3)–H Activation of Benzimidazole Derivatives 35

4 Conclusion and Outlook 41

5 List of Abbreviations 43

6 References 45

7 Published Articles 55

7.1 Cobalt(0)-Catalyzed Isomerization of Allylamines Promoted by Monodentate Benzofuran Phosphines 55

7.2 Development of highly efficient and selective palladium catalysts for telomerization of 1,3-butadiene with alcohols 68

7.3 Synthesis of non-equivalent diamides and amido-esters via Pd-catalysed carbonylation 73

7.4 1,2-Bis(di(benzofuran-2-yl)phosphino)ethane 86

7.5 General and Anti-Markovnikov Selective Ni-Catalyzed Alkylation of Arenes and Heteroarenes with Non-Activated Olefins 94

7.6 Manganese *N*,*N*,*N*-pincer complex-catalyzed epoxidation of unactivated aliphatic olefins 100

8 Appendix 109

8.1 Curriculum Vitae 109

8.2 Publication List 110

8.3 Conference Presentations 110

1 Introduction

1.1 Olefin Isomerization – From Biological Relevance to Applications

Olefins are ubiquitous structural motifs in chemistry and biology (**Scheme 1.1A1**); their distinctive electronic and stereochemical properties govern transformations spanning from fundamental biosynthetic processes in living cells to advanced methodologies in synthetic chemistry.[1] While nature has evolved a plethora of complex isomerases to mediate biosynthesis, regulate metabolism, and generate structural diversity, the stereospecific synthesis of C(sp^2)–C(sp^2) bonds with small molecule catalysts remains a persistent challenge.[2] Among the most remarkable biochemical processes is the one found in the mammalian visual system, where photon absorption initiates vision through the *cis*–*trans* isomerization of the chromophore retinal (**Scheme 1.1A2**).[3] The photoreceptor protein opsin binds retinal in its chromophore pocket, where it is covalently bound to a lysine residue through a Schiff base.[4] The photoinduced isomerization of 11-*cis*-retinal to all-*trans*-retinal induces a conformational change in rhodopsin, thereby activating the receptor and launching the highly conserved phototransduction cascade that translates the molecular event into an electrical signal.[5] The biological significance of rhodopsins is pervasive across all domains of life, operating as photoreceptors or light-driven ion pumps.[6]

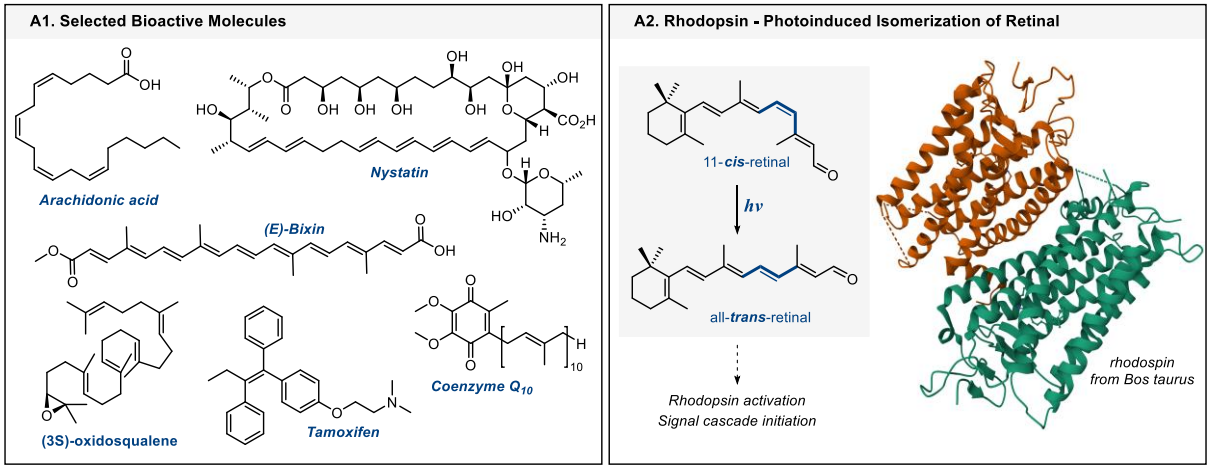

Scheme 1.1: (**A1**) Biologically relevant molecules bearing double bonds.[Adapted from 2] (**A2**) Crystal structure of rhodopsin from *Bos taurus*[7]; photoinduced isomerization of 11-*cis*-retinal to all-*trans*-retinal.

Across nature, C-C double-bond migrations are pivotal to cellular metabolism, wherein isomerases catalyze essential intramolecular transformations (**Scheme 1.2**). For instance, during the β-oxidation

of unsaturated fatty acids, enoyl-CoA isomerase (EC 5.3.3.8) catalyzes the isomerization of unsaturated acyl-CoA, shifting a (*E*/*Z*)-Δ^3double bond to a (*E*)-Δ^2 double bond (**Scheme 1.2A1**).[8] The formed (2*E*)-enoyl-CoA intermediate enters the *β*-oxidation cycle, allowing complete degradation of the unsaturated fatty acids and energy generation in eukaryotic cells. The importance of isomerases is further exemplified in the biosynthesis of cholesterol, where two key transformations are catalyzed by isopentenyl diphosphate isomerase (EC 5.3.3.2)[9] and sterol-$\Delta^{8}/^{7}$-isomerase (EC 5.3.3.5)[10], shown in **Scheme 1.2A1**. Cholesterol is a vital lipid that fulfills multiple functions in the human body. It contributes to membrane architecture, serves as a precursor for steroid hormones and vitamin D, and acts as a substrate in bile acid formation.[11] Moreover, the functional diversity of isomerases is demonstrated by the 9-*cis*/all-*trans*-*β*-carotene and prolycopene isomerases, which mediate *cis*–*trans* isomerization in polyenes – essential steps in the biosynthesis of carotenoids and related natural pigments. (**Scheme 1.2A2**).

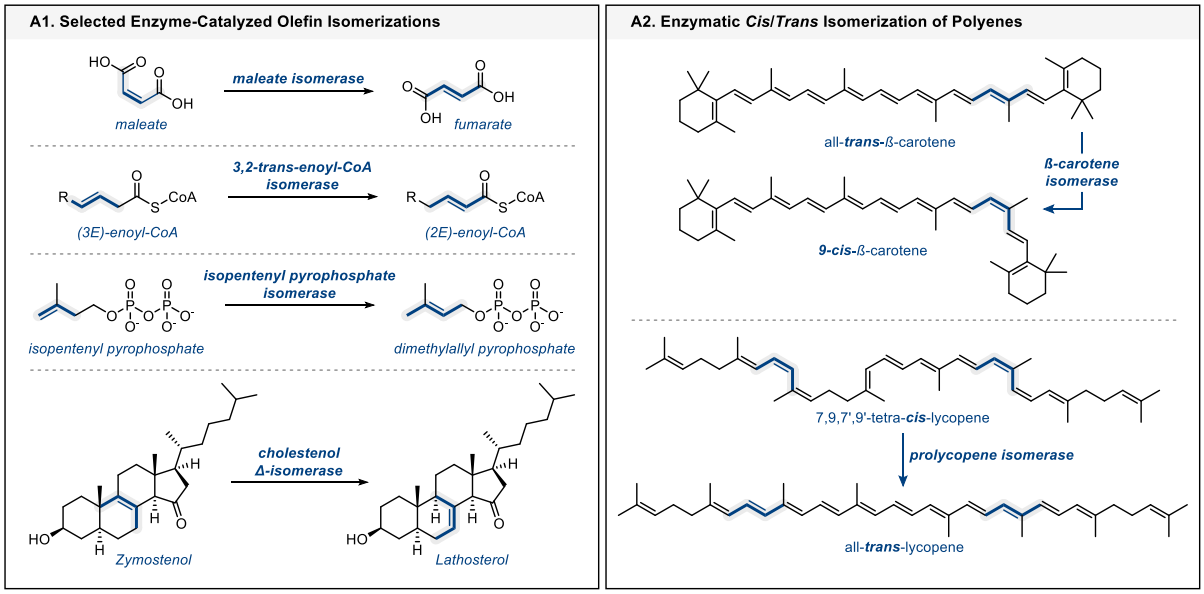

Scheme 1.2: (**A1**) Selected examples of biologically relevant enzyme-catalyzed olefin isomerization. (**A2**) Enzyme-catalyzed *cis*/*trans*-isomerization of polyenes. [Adapted from 2]

Isomerases achieve stereoselective double-bond migration by orienting the substrate within the active site, where hydrogen bonding, electrostatic effects, and hydrophobic interactions of amino acid residues stabilize the transition state ($\Delta G^{\ddagger}$) and direct the formation of a single stereoisomer. For instance, maleylacetoacetate isomerase (MAAI, EC 5.2.1.2) binds its substrate in the active site through Lys125, Arg175, and Glu31, while employing glutathione (GSH) as a cofactor (**Scheme 1.3**).[12] The catalytically active glutathione thiolate (GS^-), stabilized by interactions with Ser14, Gln111, and residues of the α1-helix, mediates the isomerization via a reversible Michael addition to 4-maleylacetoacetate (4-MAA, **Scheme 1.3**).[12] Rotation around the newly formed C–C bond in the thioether intermediate, followed by *β*-elimination, regenerates GSH and produces 4-fumarylacetoacetate (4-FAA).[13]

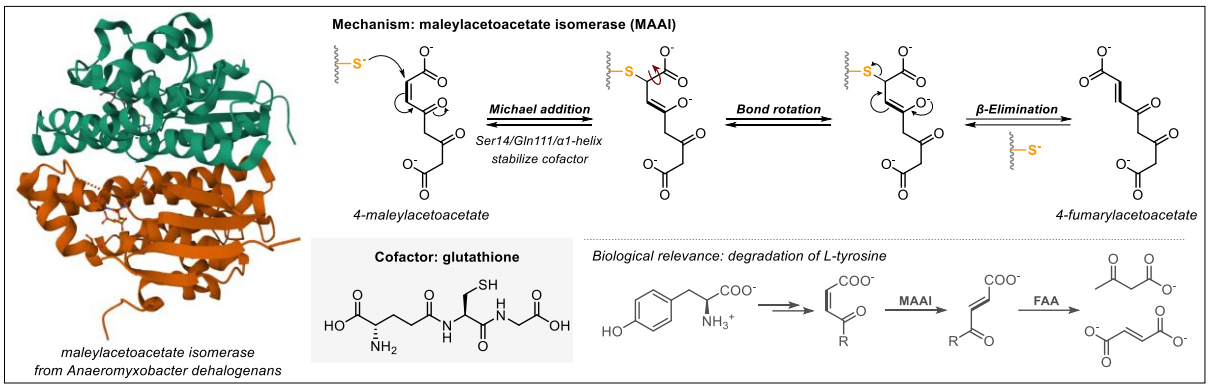

Scheme 1.3: Mechanism and crystal structure of maleylacetoacetate isomerase from *Anaeromyxobacter dehalogenans*[14] (2CP-1) with bound dicarboxyethyl glutathione and citrate in the active site.

All the aforementioned examples of olefin isomerization in biological systems highlight the remarkable capacity of natural catalysts to control double bonds with high precision and efficiency in complex molecular frameworks (**Scheme 1.1-1.3**). These transformations serve as meaningful functional blueprints, emphasizing that, despite major advances, organic chemistry still faces significant challenges in achieving comparable levels of activity and stereoselectivity in processes that evolution has optimized over millions of years.[2] Bridging the gap between biological precision and synthetic chemistry continues to drive chemists toward new catalytic strategies.

1.1.1 Transition Metal-Catalyzed Isomerization of Olefins

Since the mid-20th century, transition-metal-mediated olefin isomerization, often termed "chain walking", has been recognized by chemists.[15] Initially dismissed as an undesired side reaction pathway, C-C double bond isomerization has become a strategic synthetic tool, that offers a versatile platform for transforming accessible, low-cost olefins into regio- and/or stereoselective, higher-value products that are in demand in the pharmaceutical, food, flavor, and fragrance industries.[16-18] Moreover, in terms of sustainable and environmentally friendly chemistry, transition-metal-catalyzed olefin isomerization represents a near-ideal transformation that fulfills several of the *Twelve Principles of Green Chemistry*, including energy efficiency, waste prevention, catalysis, and less hazardous synthesis, as articulated by Paul T. Anastas and John C. Warner in 1998.[19]

In general, double bond migration can be differentiated into either positional- or geometrical-isomerization (**Scheme 1.4**).[1] The latter arises from restricted rotation around C(sp^2)-C(sp^2) double bonds or within ring systems. As a result, distinct isomers with (*E*)- or (*Z*)- configurations are formed. In contrast, positional olefin isomerization is characterized by the migration of a double bond over one or several bonds without altering the molecular skeleton (**Scheme 1.4**).[20]

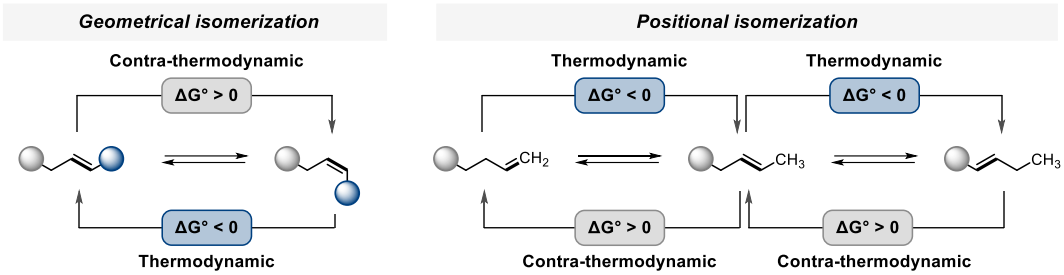

Scheme 1.4: Thermodynamic versus contra-thermodynamic pathways of olefin isomerization.[Adapted from 20]

Typically, the selective synthesis of a defined (regio)isomer via olefin isomerization requires tailored catalysts and optimized reaction conditions, as the small energy gaps between isomers often lead to undesired mixtures.[21] As shown in **Scheme 1.5**, olefin isomerization can be either thermodynamically or kinetically controlled. Under thermodynamic control, the reaction overcomes an activation barrier ($\Delta G_1^{\ddagger}$) to form the most stable isomer.[22] Typically, the isomerization of simple terminal olefins to internal olefins is thermodynamically favored and thus can be achieved utilizing different catalysts, e.g. acids[23], bases[24], or metal hydrides[25] (**Scheme 1.5A**). Moreover, the isomerization of terminal olefins is associated with relatively low activation energy ($\Delta G_1^{\ddagger}$, **Scheme 1.5A**), as internal double bonds are more stabilized by increased substitution through hyperconjugation and by lower steric repulsion.

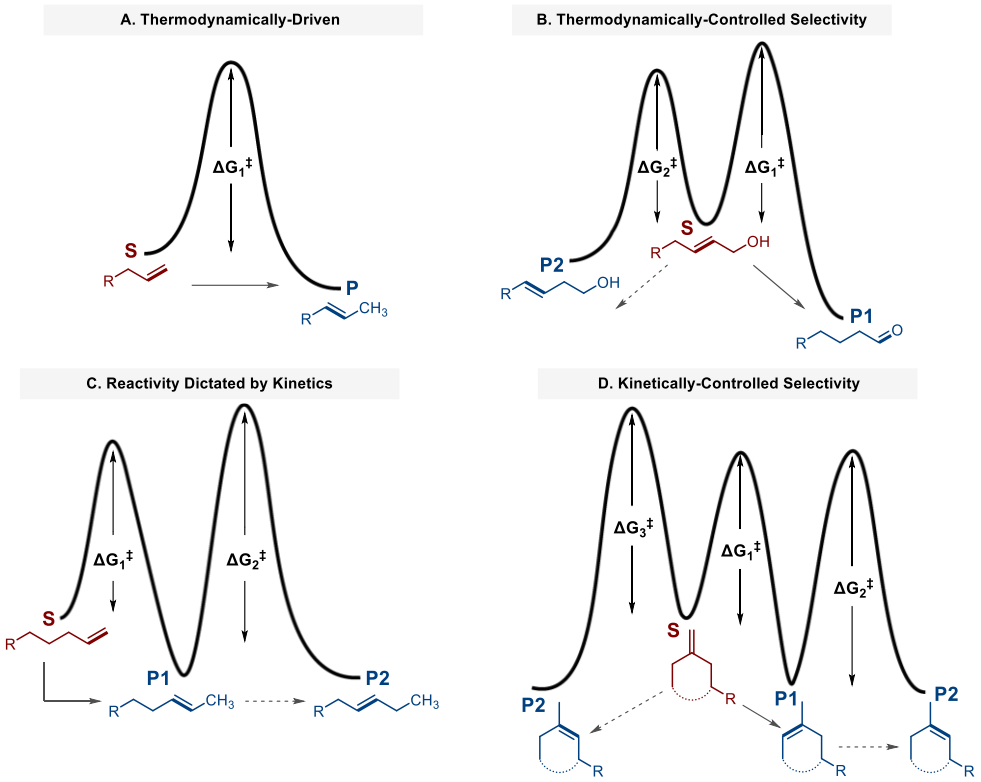

Scheme 1.5: Thermodynamic vs. kinetic control in olefin isomerization: comparison of energy profiles.[Adapted from 22]

In reactions with multiple theoretical isomers as products, the thermodynamically stable species tends to be the dominant product although its formation requires a higher activation energy than the kinetically favored species ($\Delta G_2^{\ddagger} > \Delta G_1^{\ddagger}$, **Scheme 1.5B**). For instance, alkenyl alcohols can isomerize to the corresponding carbonyl compounds via catalyst-mediated chain-walking under thermodynamic control, affording the most stable conjugated product.[26] If the target product does not represent the most stable isomer, isomerization becomes significantly more challenging (**Scheme 1.5C**), since the activation energy barriers ($\Delta G_1^{\ddagger}$ and $\Delta G_2^{\ddagger}$) of the isomers differ only slightly.[27, 28] For example, achieving regioselective mono-isomerization of linear terminal olefins requires tailored catalysts to suppress chain walking. In recent years, a variety of systems, including Ir-,[29] Ru-,[30] Pd-[31] and Co-based catalysts,[32] have been developed to promote mono-isomerization. However, controlling regioselective isomerization in larger molecular scaffolds (**Scheme 1.5D**), whereby multiple products arise from competing reaction pathways with different activation barriers ($\Delta G^{\ddagger}$), remains an active research area of olefin valorization.

1.1.2 Homogeneous Noble Metal Catalysts for Olefin Isomerization

In the 1980s, Otsuka and Noyori made an important contribution to the field of transition metal-catalyzed olefin isomerization.[33] Since then, extensive efforts have been devoted to the enantioselective isomerization of allylamines to enamines using the subsequently developed chiral cationic Rh(I)–BINAP complexes [2,2′-bis(diphenylphosphino)-1,1′-binaphthalene]. Due to its exceptional selectivity and close to quantitative yield (>98% *ee*, TON of 200.000), the Rh-catalyzed isomerization of *N,N*-diethylgeranylamine (DEGA) to citronellal-enamine became a key step in the Takasago process for the synthesis of (-)-menthol, which is still amongst the largest technical applications of homogeneous asymmetric catalysis (**Scheme 1.6A1**).[34] Extensive mechanistic investigations, supported by computational studies, elucidated the catalytic cycle of the isomerization, which proceeds via a Rh(η^3-enamine) intermediate and an inner-sphere 1,3-hydrogen shift.[35] The absolute configuration of the product is determined by the chirality of the Rh-BINAP ligand (*R/S*) and the (*E/Z*) stereochemistry of the allylamine (**Scheme 1.6A1**).[15]

Afterwards, numerous studies have focused on the isomerization of olefins bearing other stabilizing substituents (e.g., -OH, -OR, or -COR), leading to the thermodynamically favored conjugated product.[15] In particular, the isomerization of primary alkenyl alcohols to the corresponding aldehydes has been widely investigated (**Scheme 1.6A2**).[18] Relative to the high catalyst efficiency observed in Rh-catalyzed allylamine isomerization, Tani *et al.* reported that their previously developed Rh-BINAP complexes exhibited significantly reduced activity and low enantioselectivity in the isomerization of primary alkenyl alcohols.[36] However, Fu and co-workers demonstrated in 2000 that Rh(I) phosphaferrocene complexes enable the isomerization of primary allylic alcohols, yielding the corresponding chiral aldehydes with good yields and high enantioselectivity (**Scheme 1.6A2**).[37, 38]

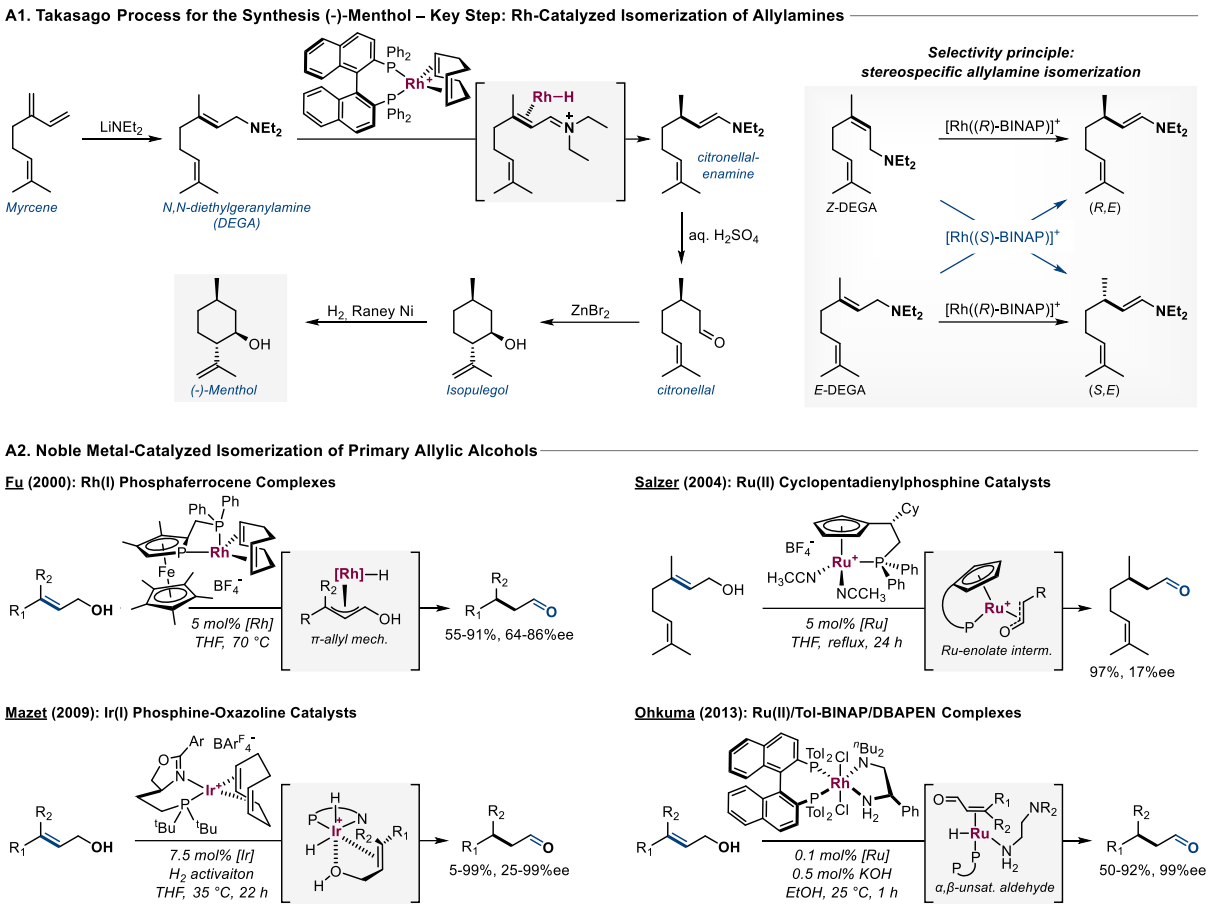

Scheme 1.6: (**A1**) Takasago process for the synthesis of menthol; stereochemical control in the Rh-catalyzed isomerization of allylamines.[Adapted from 15] (**A2**) Noble metal catalysts for the isomerization of primary allylic alcohols.

Building on Fu's pioneering work, Salzer and co-workers reported Ru(II) complexes bearing modified chiral Cp-phosphine ligands that catalyze the isomerization of primary alkenyl alcohols.[39] Although good catalytic activity was observed, the systems delivered poor enantioselectivity (**Scheme 1.6A2**). Subsequent studies by Mazet and co-workers on Crabtree's catalyst resulted in the development of Ir(I) complexes bearing chiral phosphine-oxazoline ligands.[40] These Ir-based catalytic systems demonstrated high activity and enantioselectivity in the isomerization of primary (*E*)-allylic alcohols (**Scheme 1.6A2**). Follow-up works by Mazet and Andersson fine-tuned the catalytic system and adapted the Ir oxazoline catalysts for more sophisticated substrates.[41]

Among the catalysts reported for the isomerization of primary allylic alcohols, the Ru(II) complexes developed by Ohkuma and co-workers with a dual ligand system consisting of tol-BINAP and dbapen (2-dibutylamino-1-phenylethylamine) operate with one of the lowest catalyst loadings reported to date.[42] The Ru catalyst effectively converted (*E*)- and (*Z*)-allylic alcohols into the corresponding chiral aldehydes with high yields (**Scheme 1.6A2**).

Despite their efficiency in the isomerization of primary allylic alcohols, the majority of reported noble metal catalysts exhibited only limited activity when applied to secondary alkenyl alcohols. A pioneering work in the field of olefin isomerization was introduced by Grotjahn and co-workers, who reported a highly active cationic Cp Ru(I)-based complex that catalyzes the long-distance isomerization of alkenyl alcohols into the corresponding ketones (**Scheme 1.7**).[43] Notably, the developed Ru complex exhibited high catalyst efficiency while isomerizing a broad range of olefins. Continuing in the area of long-range isomerization, Mazet and co-workers developed a Pd-dtbpe complex [1,2-bis(di-*tert*-butylphosphino)ethane] that enables the remote isomerization of *α,β*-unsaturated carbonyl compounds (**Scheme 1.7**).[44] In addition, the Pd catalyst displayed versatility by enabling the isomerization of both primary and secondary alcohols to the corresponding carbonyl compounds.

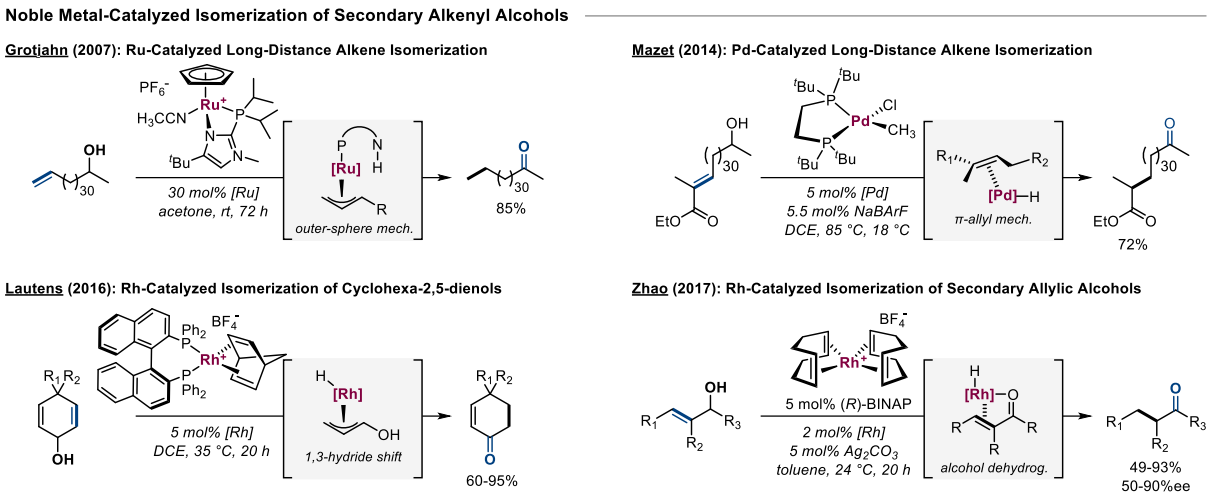

Scheme 1.7: Selected noble metal catalysts for the isomerization of secondary alkenyl alcohols to carbonyls compounds.

Moreover, Lautens and co-workers reported the Rh-catalyzed isomerization of cyclohexa-2,5-dienols to disubstituted cyclohexanones, underscoring the utility of transition-metal-catalyzed isomerization for cyclic scaffold modification (**Scheme 1.7**).[45] Following this work, Zhao and co-workers reported the first enantioselective isomerization of secondary allylic alcohols, providing direct access to *α*-chiral ketones (**Scheme 1.7**).[46] This transformation was accomplished with an *in situ* generated Rh catalyst, using $[Rh(COD)_2]BF_4$ and (*R*)-BINAP, affording moderate to high yields together with good enantioselectivities of the ketones.

As discussed above, noble metal catalysts effectively mediate the isomerization of a wide range of challenging substrates, including unreactive and cyclic olefins. Their reactivity remains a pivotal factor in the development of future catalytic concepts. In contrast to the isomerization strategies discussed here that rely on directing groups, the isomerization of simple terminal or internal aliphatic olefins has been accomplished with several noble-metal catalysts.

1.1.3 Homogeneous Cobalt Catalysts in Selective Olefin Isomerization: Recent Advances and Perspectives

For decades, noble metal complexes have dominated the field of homogeneous catalysis, owing to their robustness and high reactivity. However, concerns regarding their scarcity, cost, and toxicity have shifted increasing attention toward earth-abundant base metals, which offer higher abundance, lower cost, and reduced toxicity.[17] In particular, Co-based systems are increasingly investigated for olefin isomerization owing to their higher reactivity compared with other base metals.[17]

Since 1960, $HCo(CO)_4$ has been recognized as a catalyst for olefin isomerization, with pioneering contributions from the groups of Orchin and Rosenberg.[47] Building on this early work, Periasamy and co-workers reported in 1987 an *in situ* Co catalyst system composed of $CoCl_2$, PPh_3, and $NaBH_4$ that transformed terminal alkenes such as dec-1-ene, allylbenzene and safrole into internal (*E*)-alkenes (**Scheme 1.8**).[48] Despite its utility, the developed system required equimolar amounts of the Co catalyst, limiting its practical applicability. In 2009, Oshima and co-workers unveiled an *in situ* Co-NHC catalyst, generated from $CoCl_2$, IMes·HCl and $Me_2PhSiCH_2MgCl$, for the isomerization of simple aliphatic olefins into internal (*E*)-olefins.[49] Interestingly, mechanistic studies suggested a Co-cyclopropane intermediate, as depicted in **Scheme 1.8**. However, the applicability of this catalytic system was considerably limited by requiring 50 mol% of the Grignard reagent.

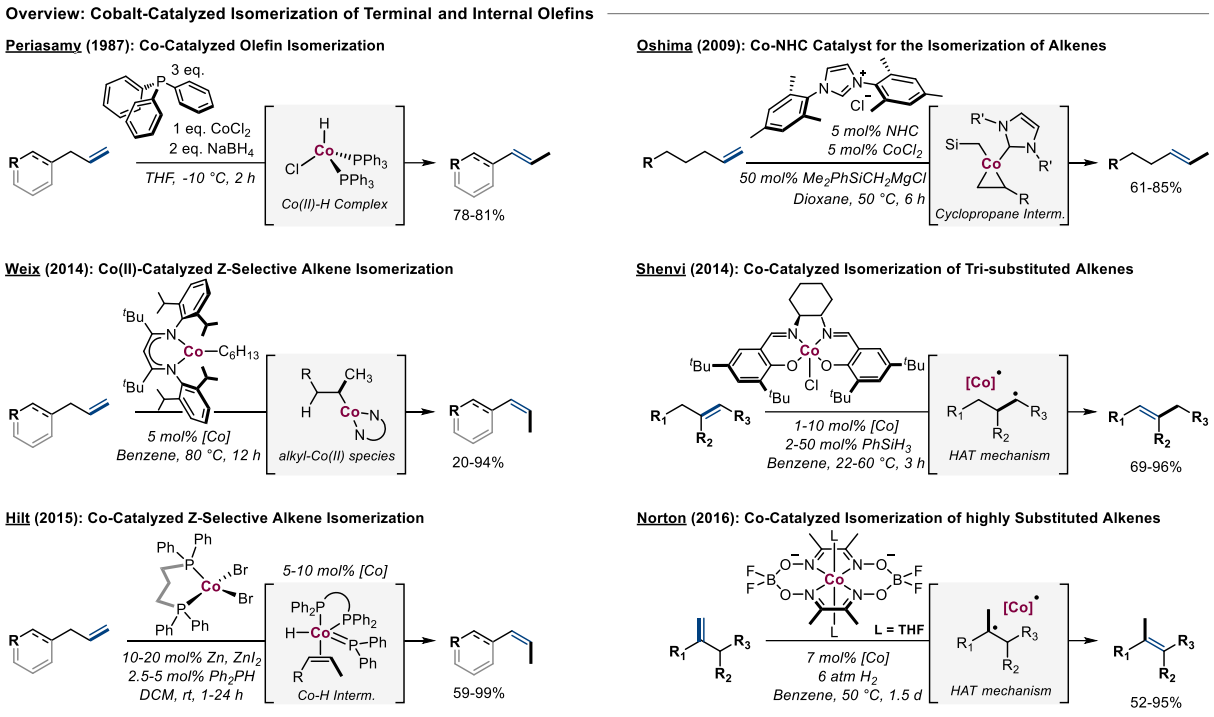

Scheme 1.8: Overview of reported Co catalysts applied in olefin isomerization.

A groundbreaking study on Co-catalyzed olefin isomerization was reported in 2014 by Holland, Weix, and co-workers, who disclosed a Co-β-diketiminate catalyst for the (Z)-selective isomerization of terminal alkenes to internal (Z)-olefins (**Scheme 1.8**).[50] Although the catalyst was effective for the model substrate hex-1-ene, its scope was limited, as other olefins provided lower yields and poor regioselectivity. Following their initial study, Holland and co-workers reported in 2021 a modified Co-β-diketiminate complex with improved (E/Z) ratios and broader applicability (**Scheme 1.9**).[51]

In 2014, Shenvi and co-workers described a Co-salen catalyst capable of promoting both positional isomerization and cycloisomerization of olefins.[52] The catalytic system enabled the conversion of terminal olefins into di-, tri-, and even tetrasubstituted olefins, displaying broad functional group tolerance and affording good to excellent yields (**Scheme 1.8**). However, its utility in (E/Z)-selective transformations is limited, with only three substrates evaluated, affording modest results.

Building on the work of Holland and Weix on (Z)-selective isomerization, Hilt and co-workers developed an *in situ* Co catalyst composed of [$CoBr_2$(L)] (L = dppp, bdpp, or dpppBuEt), Zn, ZnI_2, and Ph_2PH for the isomerization of terminal olefins (**Scheme 1.8**).[32] Both functionalized and simple olefins were converted into the target (Z)-isomers with high yields and moderate to good (E/Z)- selectivities. However, the Co catalyst gave increased (E)-isomer formation with aryl-substituted substrates and afforded exclusively the (E)-isomer from allyl ethers or allylbenzene, demonstrating its limited applicability.

In 2016, another innovative Co-based catalytic system was presented by Norton and co-workers, employing a cobaloxime complex under 6 atm H_2 for the mono-isomerization of highly substituted olefins (**Scheme 1.8**).[53] The developed Co catalyst converted 1,1-disubstituted olefins with high chemoselectivity and displayed broad tolerance toward functional groups, including ketones, carbonates, and pyridines. Notably, even alkenyl alcohols underwent isomerization, leading to the formation of the corresponding ketones or aldehydes. Despite its broad applicability, the cobaloxime catalyst is limited by its (E/Z) selectivity and relatively high catalyst loading (7 mol% [Co]).

A significant advancement in the regioselective isomerization of exocyclic olefins was reported by Liu, Jiao, and co-workers in 2018. (**Scheme 1.9**).[22] Their developed Co NNP pincer catalyst enabled the isomerization of exocyclic olefins with six- to eight-membered rings, affording the corresponding isomers with good to high stereoselectivity. Mechanistic studies, including DFT calculations and deuterium labeling experiments, indicate a metal hydride pathway for the olefin isomerization.

In 2020, the first Co-catalyzed isomerization of conjugated dienes was reported by Diver and co-workers using a cobaloxime-based catalyst (**Scheme 1.9**).[54] A range of different conjugated dienes underwent isomerization, although the system was applied to only a limited number of substrates and afforded low to moderate (E/Z) selectivity. Mechanistic studies, including radical clock experiments, revealed Co-centered radical intermediates as key species.

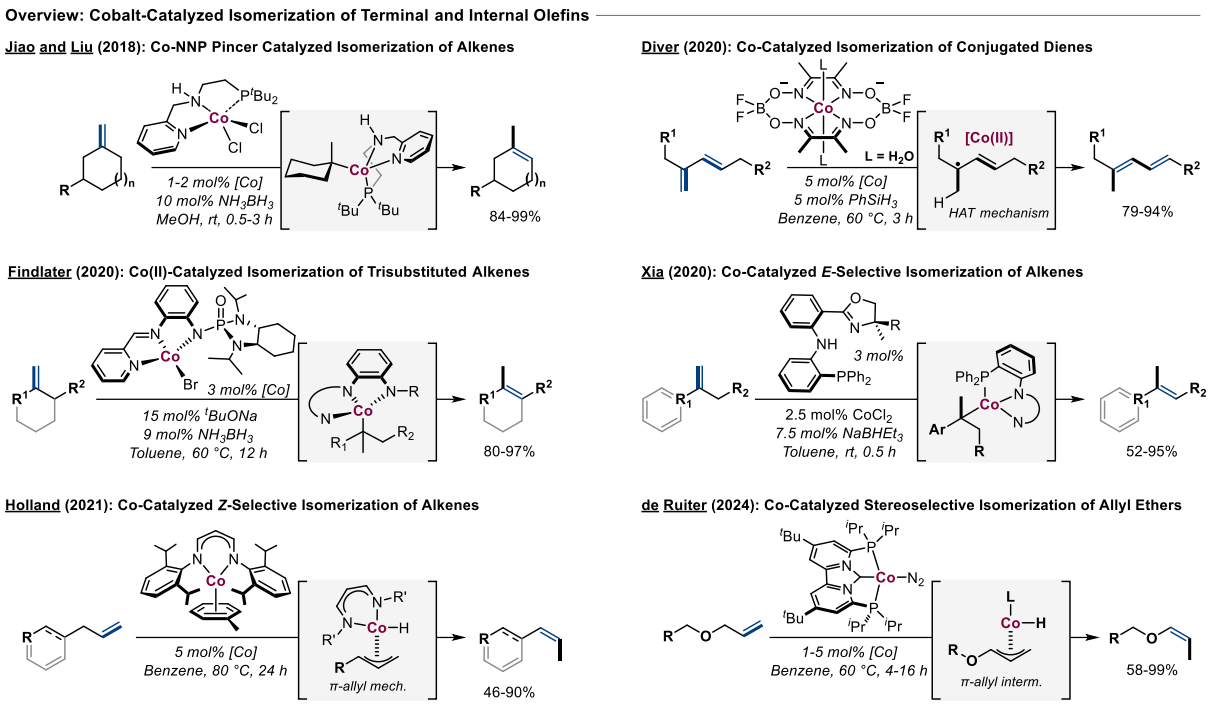

Scheme 1.9: Overview of reported Co catalysts applied in olefin isomerization.

Another notable example was described by Findlater and co-workers, employing an *in situ* generated Co pincer complex for the isomerization of 1,1-disubstituted olefins, thereby enabling the synthesis of trisubstituted internal olefins (**Scheme 1.9**).[55] The catalyst exhibited high stereoselectivity across a broad range of olefins, showed good functional group tolerance, and even promoted the isomerization of dienes to afford fully conjugated products. Building on this work, Xia and co-workers presented another Co pincer catalyst for the isomerization of 1,1-disubstituted olefins.[56] However, in comparison to Findlater's system, the catalyst exhibited a considerably more limited substrate scope.

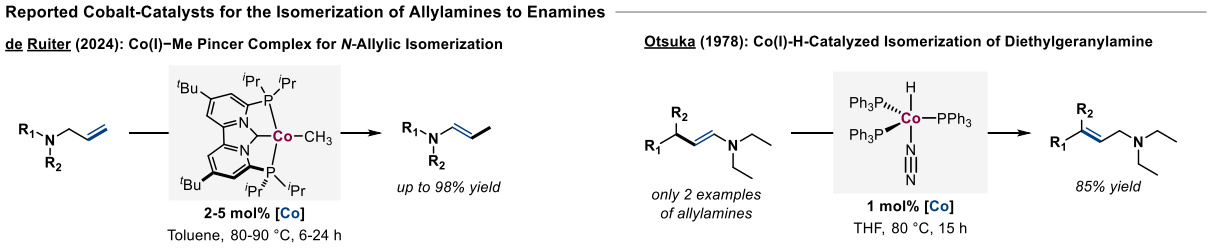

Scheme 1.10: Overview of reported Co-catalysts for the isomerization of allylamines to enamines.

Although significant progress has been made in Co-catalyzed olefin isomerization, substrates with heteroatoms in proximity to the double bond remain difficult for base-metal catalysts, particularly when the heteroatom is located at the homoallylic position, as exemplified by allyl ethers, allyl alcohols,

and allylamines. In this context, the groups of Chen and Ji have recently investigated the Co-catalyzed isomerization of allyl ethers.[57, 58] In 2024, de Ruiter and co-workers developed Co $PC_{NHC}P$ complexes for the (*E*)- and (*Z*)-selective isomerization of allyl ethers (**Scheme 1.9**).[57-59] Although both developed Co catalysts exhibited good functional-group tolerance, their regioselectivity was generally only moderate. In comparison to allyl ethers, the isomerization of allylamines to enamines has so far been realized with only two Co catalysts (**Scheme 1.10**). The earliest example, described by Otsuka and Ikeda in the late 1970s, involved the industry-relevant isomerization of *N,N*-diethylgeranylamine (DEGA).[60] Since then, only one additional Co catalyst has been reported by de Ruiter and co-workers for terminal allylamines, employing the same system previously used for the isomerization of allyl ethers.[61]

1.1.4 Noble vs. Non-Noble Metal Catalysts: Advances and Challenges

Since catalytic activities are always reported under system-specific optimized conditions (e.g., temperature, reaction time, concentration), reliable comparisons across studies remain inherently difficult. Nonetheless, evaluating different catalysts and their reaction parameters in the same model reaction offers an approximate indication of relative performance. To enable a systematic comparison of state-of-the-art noble and non-noble metal catalysts, we assessed their performance in the positional isomerization of estragole to (*E*)-anethole, an industrially relevant transformation studied with a wide range of homogeneous catalysts (**Scheme 1.11**).

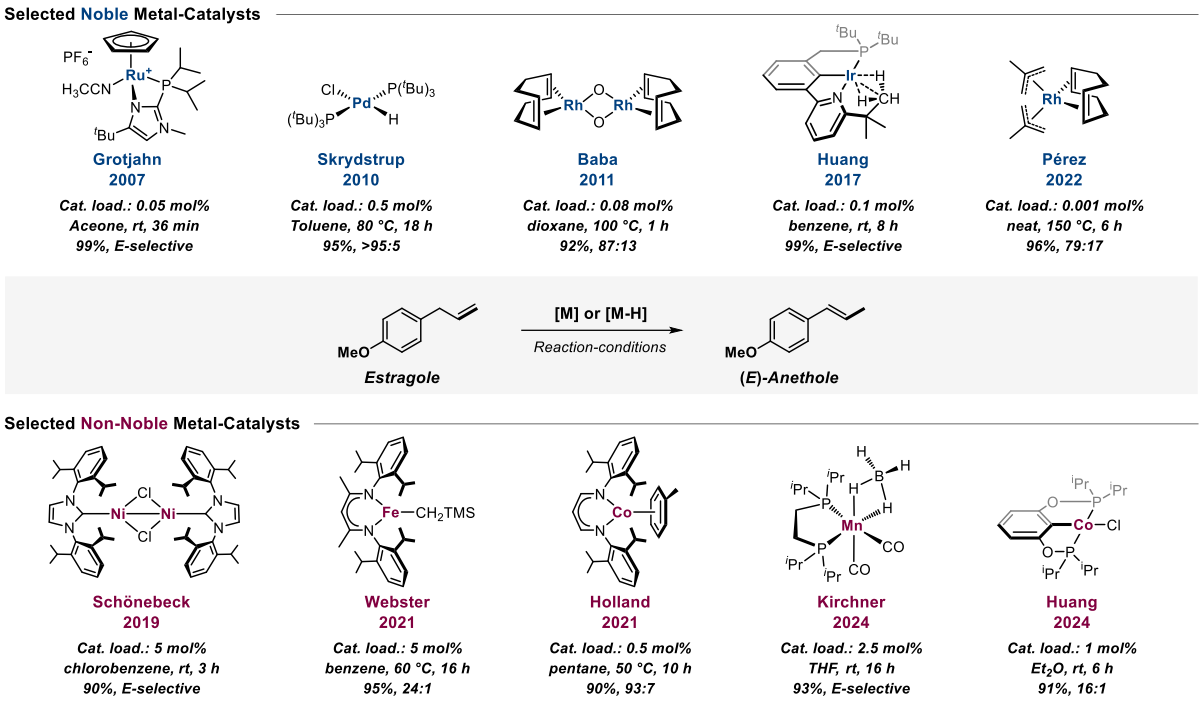

Scheme 1.11: Comparison of selected homogenous catalysts for the isomerization of estragole to (*E*)-anethole.

For instance, Grotjahn's Ru catalyst isomerizes estragole to (*E*)-anethole with only 0.05 mol% catalyst loading at room temperature in less than 1 h.[30] In comparison, Skrydstrup reported a Pd–H complex in 2010 that produces (*E*)-anethole with good selectivity, although it requires higher temperature and a higher catalyst loading (0.5 mol% [Pd]).[31] More recently, Huang described an Ir pincer catalyst with an activity comparable to the Grotjahn system, operating at 0.1 mol% under ambient conditions.[29] Likewise, even simple Ru and Rh precursors, as reported by Baba and Pérez, catalyze the isomerization of estragole to (*E*)-anethole in high yields with low catalyst loadings, albeit under elevated reaction temperatures.[62, 63]

Focusing on non-noble-metal catalysts, Schönebeck reported in 2019 a Ni–NHC dimer that catalyzes the isomerization of estragole at room temperature with 5 mol% loading, affording 90% (*E*)-anethole.[64] Subsequently, Webster introduced an Fe-*β*-diketiminate complex that delivered 95% yield of (*E*)-anethole with a similar catalyst loading, although at elevated reaction temperatures (**Scheme 1.11**).[65] In the same year, Holland and co-workers reported a structurally related Co *β*-diketiminate complex that afforded comparable yield and selectivity with only 0.5 mol% catalyst loading.[51] In 2024, Kirchner presented a Mn borohydride complex that enabled the efficient isomerization of estragole at room temperature with 2.5 mol% catalyst loading.[66] Most recently, Huang and co-workers described a Co pincer complex that operates at 1 mol% loading and afforded 91% yield of (*E*)-anethole.[67]

In contrast to the noble-metal catalysts discussed above, the reported non-noble-metal systems for the isomerization of estragole to (*E*)-anethole typically require catalyst loadings one to two orders of magnitude higher. As shown in **Scheme 1.11**, Co generally displays the highest activity among the non-noble metals, yet Co catalysts remain notably less active than Ru, Rh, or Ir. Improving the activity of non-noble-metal catalysts to approach that of noble metals remains a central goal in the pursuit of more sustainable catalysis.

1.2 Bridging Traditional Reaction Optimization and Artificial Intelligence in Chemistry and Catalysis

The development of new reactions and methodologies stands at the core of chemical innovation, and various strategies have been devised to discover new catalytic systems.[68, 69] Traditionally, researchers have relied on a trial-and-error approach, in which new reactions are identified through empirical testing.[70, 71] The success of this method depends entirely on the knowledge and experience of the researcher. Although it has led to numerous important discoveries, the trial-and-error process remains unpredictable, labor-intensive, and often slow. To overcome these limitations, high-throughput screening (HTS) has emerged as a more systematic approach in recent decades.[72] In catalysis, HTS enables automated and parallel testing, allowing large numbers of reactions to be analyzed in a significantly shorter time and thereby accelerating the discovery process. Another advantage of this strategy lies in its ability to generate structured datasets, which can reveal useful correlations between catalyst structure and performance or even lead to the discovery of entirely new catalysts.[73] But HTS also faces fundamental limitations: the combinatorial variety of chemical possibilities in multi-component systems can quickly exceed the capacity of HTS methods. Furthermore, in catalysis, the often time-consuming synthesis of catalysts restricts the number of candidates that can be tested, thereby limiting the applicability of HTS. Over the past decade, computational approaches for reaction prediction have gained increasing importance in both academia and industry, as they can lower failure rates and substantially accelerate discovery.[74-77] Applied machine learning (ML)–the use of self-learning algorithms to address specific tasks–provides a powerful framework across the sciences, from property prediction in drug discovery to synthesis planning in chemistry (**Scheme 1.12A1**).[74] Its potential has been greatly enhanced by recent advances in computational hardware and cloud infrastructure, which have substantially lowered the barriers to adopting ML in chemistry and related fields.[78]

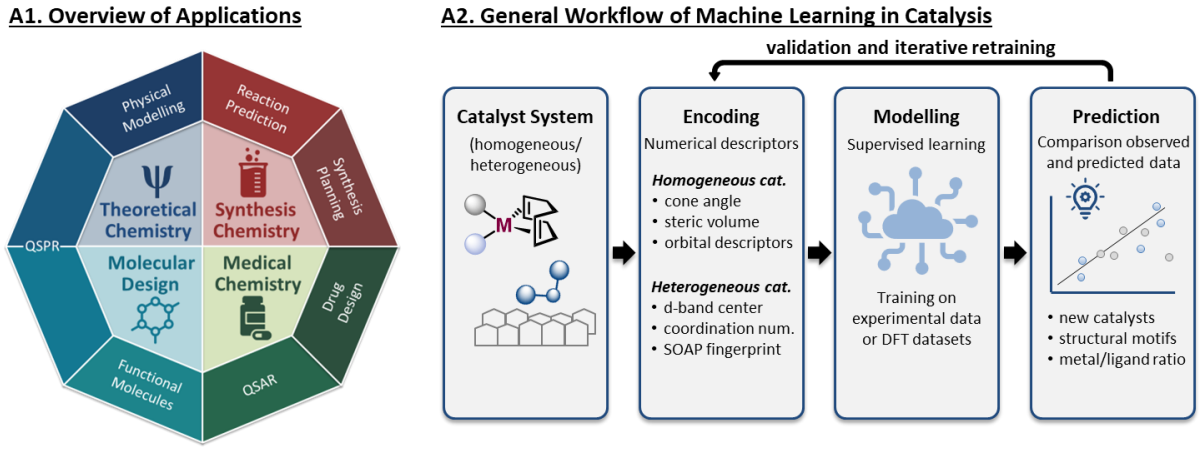

Scheme 1.12: (**A1**) ML in chemistry: overview of application fields.[Adapted from 74] (**A2**) General workflow of ML in catalysis.

The application of ML in catalysis is typically structured as a three-step workflow—encoding, modeling, and prediction—that is embedded in a closed-loop cycle, continuously refining and improving catalyst performance with each iteration (**Scheme 1.12A2**).

The first step involves transforming chemical entities into chemically meaningful, computer-readable molecular representations. This process is non-trivial, as it requires thorough consideration of dataset quality and compatibility with model architectures.[74] Since chemists conventionally depict molecules in graphical formats, e.g., Lewis structures, graph-based or graph-inspired representations have been applied to tasks ranging from quantitative structure-property relationships to yield prediction.[74] These encodings span from simple one-dimensional projections, such as SMILES, to more complex matrix-based formats.[74] Although simple graph encodings are available, most applications rely on sophisticated model architectures to capture nonlinear interactions. A common limitation of these methods is their strong dependence on large datasets; for smaller datasets, strategies such as pretraining or data augmentation are often required to ensure reliable performance (**Scheme 1.13**).[74]

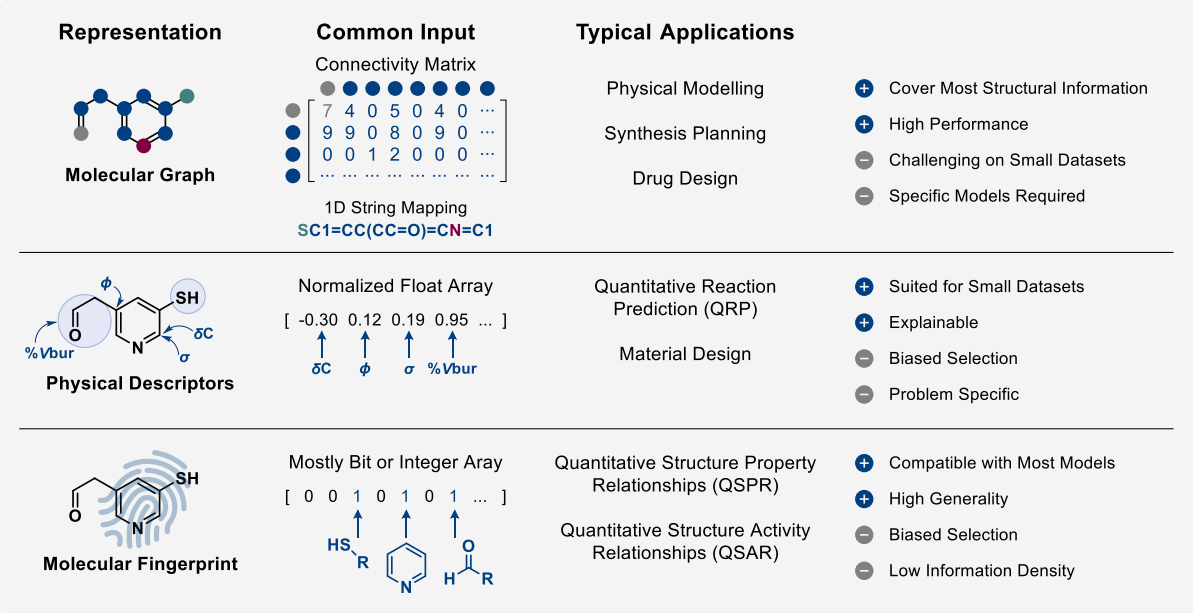

Scheme 1.13: Different strategies to represent molecules for machine learning applications.[Adapted from 74]

More advanced encoding strategies include physical descriptors, often derived from quantum mechanical or molecular dynamics simulations (**Scheme 1.13**).[74] These descriptors are highly interpretable and can provide mechanistic insights at electronic or steric levels, which is particularly valuable in data-scarce systems and can help to prevent overfitting in ML models.[74] Nevertheless, their selection is often opaque or biased towards specific datasets, which limits their transferability across domains in comparison to more flexible, data-driven representations.[74]

Molecular fingerprints represent another widely used strategy for encoding molecular information (**Scheme 1.13**).[74] Structural features are encoded into binary or integer vectors, with each entry indicating the presence or frequency of specific motifs such as atom environments, rings, or functional groups. This direct mapping provides a link between molecular structure and model understanding, as relevant features can often be associated with well-defined connectivity patterns. Nevertheless, the predictive power of these models is typically confined to the chemical space in which they were developed, thereby limiting their applicability across broader domains.[73]

Once the chemical system is encoded, supervised learning algorithms are trained to establish correlations between structural features and experimental data, such as conversion, yield, regioselectivity, or enantioselectivity, thereby linking molecular representations to experimental observations (**Scheme 1.13**).[73] In the prediction stage of ML, the trained model is applied to new data to generate chemically relevant hypotheses that go beyond simply ranking parameters such as temperature, solvents, or concentrations. Well-trained models can propose entirely new classes of structures or highlight structural motifs associated with improved selectivity, activity, or stability (**Scheme 1.13**). Moreover, by combining ML with high-throughput screening, closed-loop discovery cycles can be established in which experiments generate structured data and models analyze the results to propose subsequent steps. This self-driving approach is particularly powerful for addressing the complexity of catalytic reactions, accelerating optimization, and yielding more accurate predictions.[79] For instance, Doyle, Dreher, and co-workers demonstrated in 2018 that ML is capable of accurately predicting yields in Pd-catalyzed C–N cross-coupling reactions and of identifying non-intuitive ligand and base combinations that substantially improved both selectivity and yield.[79]

Looking ahead, ML represents a powerful new tool for all fields of chemistry, including catalysis, offering opportunities to design improved or entirely new catalytic systems, accelerate reaction optimization, and minimize costly and time-consuming trial-and-error experimentation.[80] Additionally, ML promotes the systematic exploration of chemical systems and facilitates the development of sustainable synthesis strategies, thereby opening new avenues for catalysis research.[81]

1.3 Hydrogen Isotope Exchange via Transition Metal Catalysis

Since the 1960s, hydrogen–deuterium exchange has emerged as a valuable tool across many areas of chemistry, ranging from nuclear science and analytical chemistry to organic synthesis and medicinal chemistry.[82-84] Deuterium-labeled compounds differ from their protium analogues in vibrational properties and bond strength: C–D bonds exhibit a lower zero-point energy (1.2–1.5 kcal mol^{-1}) and a higher bond dissociation energy than C–H bonds, resulting in slower cleavage rates.[85] These differences, referred to as the kinetic isotope effect (KIE), leave most physical properties unchanged but significantly alter chemical reactivity and metabolic stability.[86] In medicinal chemistry, deuterium incorporation can prolong half-life, improve pharmacokinetics, and reduce adverse effects.[86] Therefore, the development of deuterated drugs has attracted considerable attention in recent years. In 2017, deutetrabenazine was approved as the first deuterated pharmaceutical, followed by four further approvals and more than 20 candidates currently in clinical trials (**Scheme 1.14A1**).[82]

In addition to their enhanced stability, deuterated molecules used in optoelectronics display distinct characteristics (**Scheme 1.14A2**).[82] For instance, multideuterated aryl and heteroaryl compounds promote stronger π–π interactions and exhibit distinct crystallization properties compared to their hydrogen analogues.[87] These structural variations can considerably affect their photophysical properties, including emission efficiency and quantum yield.[82, 88, 89]

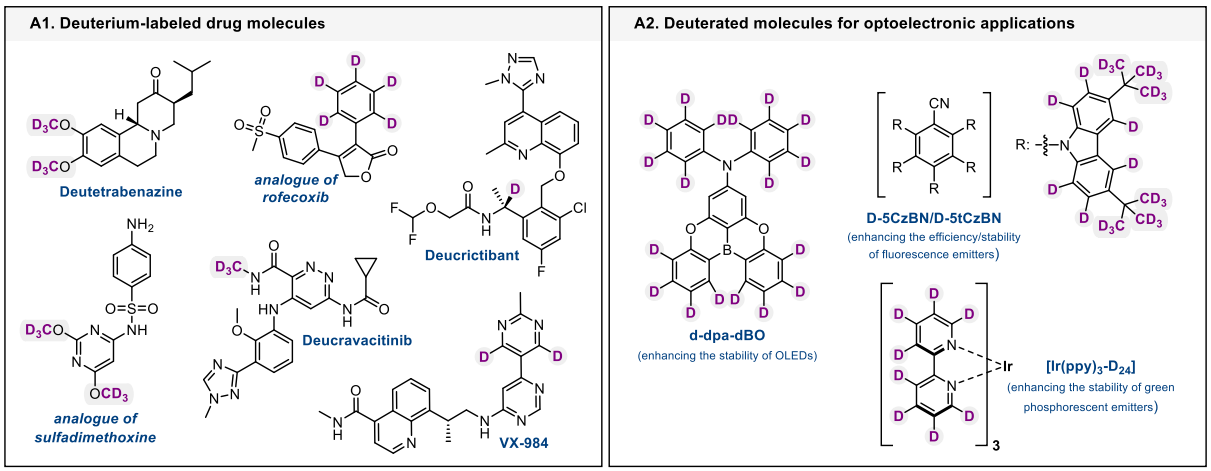

Scheme 1.14: Relevance of deuterated molecules. (**A1**) Selected deuterated drug molecules. [Adapted from 90] (**A2**) Deuterated optoelectronic molecules. [Adapted from 82]

With the growing relevance of deuterated compounds, considerable efforts have been devoted to the development of new methodologies and scalable strategies for their synthesis. Hitherto, these advances have enabled access to a broad spectrum of isotopically modified compounds (**Scheme 1.14**). The following chapter will provide an overview of the achieved results and outline current limitations as well as future perspectives in hydrogen-deuterium exchange.

1.3.1 Regioselective Deuteration of Aromatic C(sp^2)–H Bonds

Within the field of transition-metal-catalyzed hydrogen–deuterium exchange (HIE), Ir complexes have emerged as benchmark systems for the *ortho*-selective deuterium-labeling of arenes bearing directing groups (DG, **Scheme 1.15A1**).[91, 92] Early studies on the Crabtree catalyst demonstrated the potential of Ir-catalyzed HIE, although these reactions generally required elevated catalyst loadings and extended reaction times.[93, 94] Kerr and co-workers later disclosed two distinct classes of Ir-based catalysts: cationic Ir complexes with sterically demanding *N*-heterocyclic carbene ligands in combination with a phosphine donor[95, 96], and neutral chloride Ir complexes[97, 98] (**Scheme 1.15A1**). Both systems delivered improved deuterium incorporation and greater practicality relative to earlier methods, enabling reactions to proceed under mild conditions − typically at room temperature and low pressure of D_2 and with short reaction − while achieving high levels of deuterium incorporation (>90%).[99]

Building on these results, Muri[100], Tamm[101], and Kerr[102] developed Ir complexes with bidentate ligands incorporating a phosphine donor unit. Since then, Ir-based catalysts have found broad application in the *ortho*-selective deuteration of arenes, displaying remarkable tolerance toward ketone[103], ester[104], amide[103], carboxylic acid[105], nitro[106], and heteroaryl substituents[107-112] (**Scheme 1.15A1**).

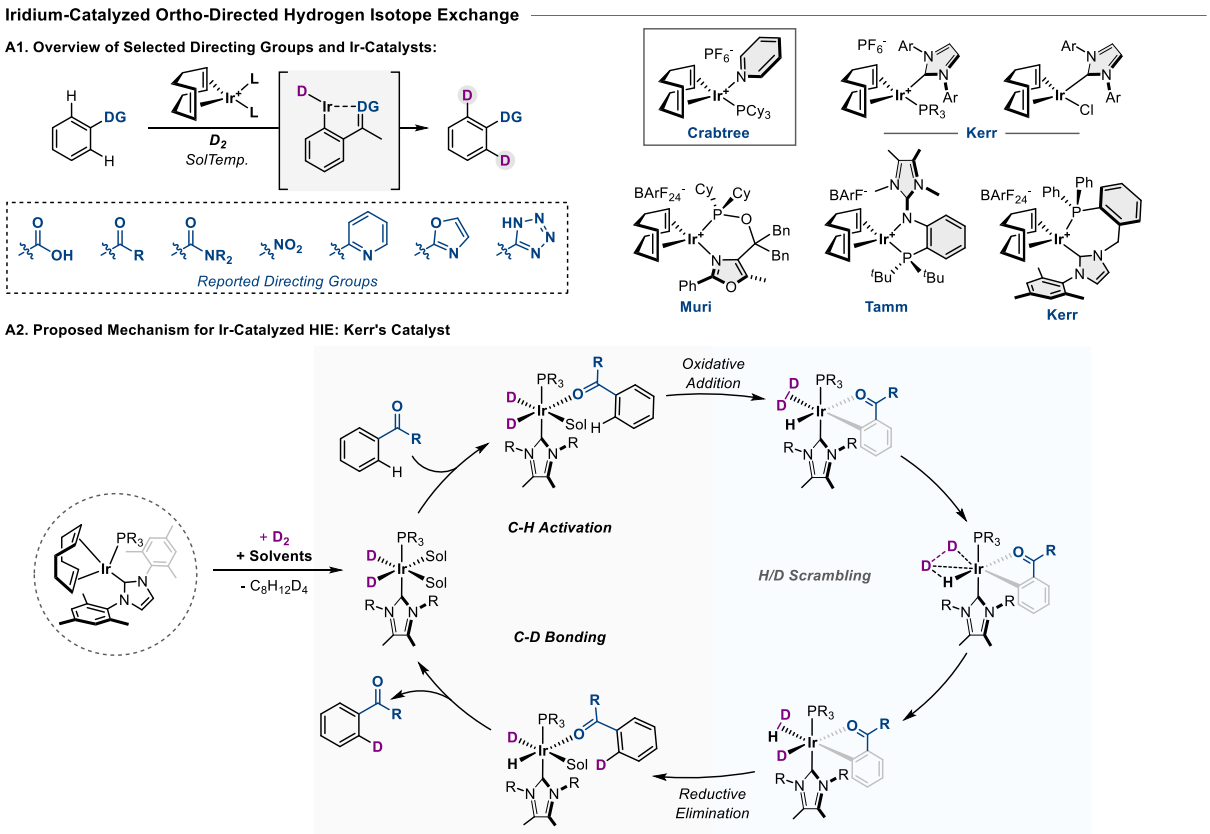

Scheme 1.15: (**A1**) Ir-catalyzed *ortho*-directed **HIE** in arenes; overview of selected directing groups and Ir catalysts. (**A2**) Proposed mechanism of Kerr's catalyst for the **HIE** in arenes. [Adapted from 113]

As shown in **Scheme 1.15A2**[113], the Ir-catalyzed *ortho*-directed HIE of arenes is initiated by coordination of the DG to the catalyst, which places the *ortho*-C–H bond into close proximity to the metal center and thereby facilitates its activation via oxidative addition. In the presence of molecular deuterium, the reaction proceeds via a five-membered cyclometalated iridium dideuteride–hydride intermediate. Owing to the fluxionality of the hydrides, repeated H/D scrambling can occur within the complex. Finally, reductive elimination releases the *ortho*-deuterated arene and regenerates the Ir catalyst.

Given the scarcity and high cost of Ir, considerable efforts have been devoted to the development of alternative metal catalysts for HIE of aromatic molecules. In particular, Rh-, Ru-, and Pd-based systems have been explored, with Pt and Ag investigated to a lesser extent (**Scheme 1.16**). These catalysts not only facilitate HIE of simple arenes but also enable isotope exchange in aromatic heterocycles, which typically represent more challenging substrates. For example, Li and co-workers reported a Rh catalyst for the HIE of benzoquinoline, achieving high and site-selective deuterium incorporation (98%).[114] Nikonov later described a Ru–NHC catalyst that enabled complete deuterium incorporation of quinoline derivatives, with overall deuterium incorporation of approx. 80%.[115] Moreover, Zhang and colleagues reported a Rh catalyst that facilitated selective deuterium incorporation at the C1 and C2 positions of indole derivatives, reaching levels above 90% D incorporation (**Scheme 1.16**).[116]

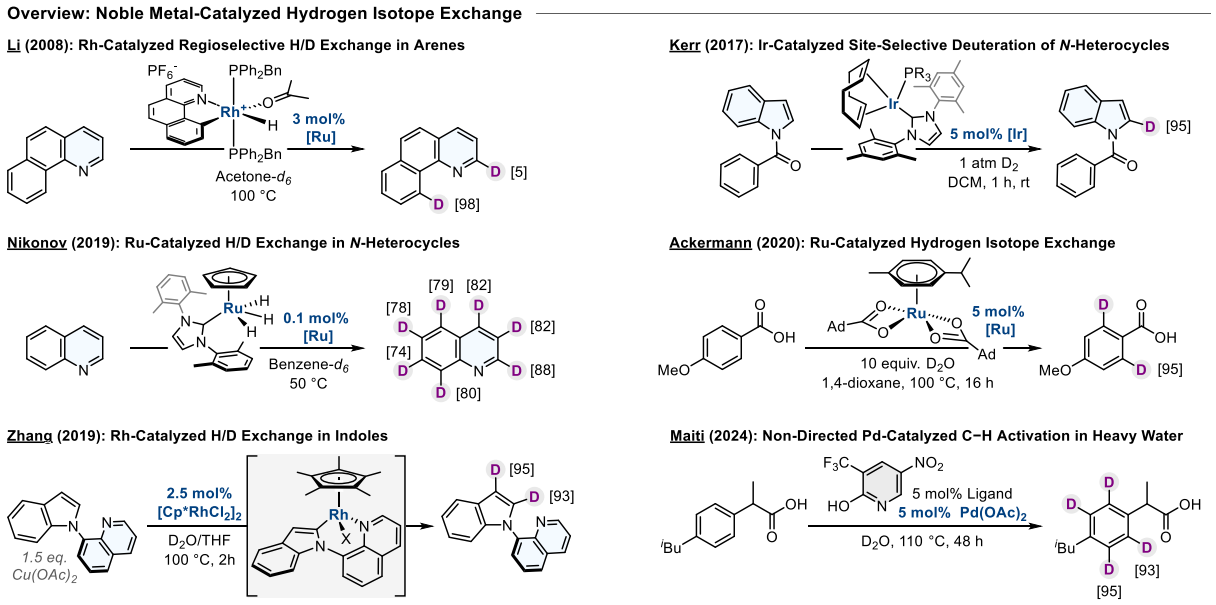

Scheme 1.16: Selected examples of noble-metal catalysts developed for HIE in arenes:

More recently, Ackermann and co-workers reported the *ortho*-selective deuteration of benzoic acid derivatives using a Cp–Ru(II) complex, with D_2O in dioxane serving as the deuterium source (**Scheme 1.16**).[117] The developed catalyst system achieved high deuterium incorporation (>90%). Building on these findings, Maiti and co-workers developed an *in situ* generated Pd catalyst that enabled both

ortho- and *meta*-selective deuterium labeling of substrates bearing carbonyl directing groups, including pharmaceutically relevant molecules, achieving high levels of deuterium incorporation.[118]

Compared to the well-established *ortho*-directed HIE of arenes, particularly with Ir catalysts, *meta*-selective deuterium labeling has remained far less explored (**Scheme 1.17**). In 2019, the groups of Werz and Maiti[119], as well as Yu and Dai[120], independently reported Pd catalysts for *meta*-selective deuterium labeling of arenes. Both approaches rely on the preinstallation of bulky directing groups that enforce geometry-controlled C–H activation of the Pd center, specifically at the *meta*-position. In both studies, phenylacetic acids were employed as substrates with the directing groups introduced via an ester linkage. Although the substrate scope was relatively limited, both catalytic systems exhibited good meta selectivity and high levels of deuterium incorporation (**Scheme 1.17**).

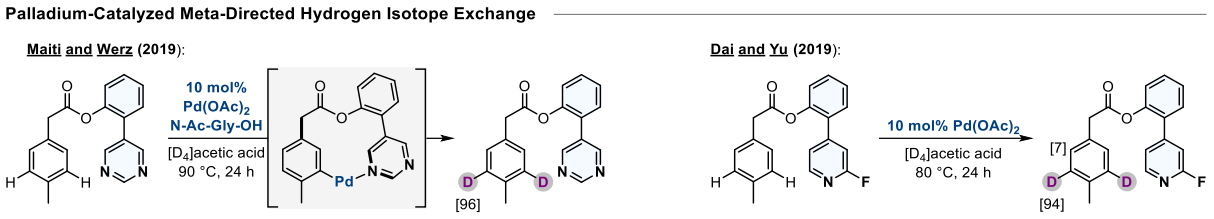

Scheme 1.17: Overview of Pd-based catalysts reported for meta-directed HIE in arenes.

Despite extensive research on C(sp^2)–H exchange in arenes and the development of numerous catalytic systems, the deuterium labeling of C(sp^3)–H bonds remains comparatively underexplored.[86, 121] Their intrinsically lower reactivity, combined with the lack of electronic activation, makes selective functionalization particularly challenging. As a result, only a limited number of catalytic systems for C(sp^3)–H deuterium exchange have been developed, which will be discussed in the following section.

1.3.2 Site-Selective Deuterium Incorporation into Unactivated C(sp^3)–H Bonds

The activation of aliphatic C–H bonds represent a long-standing challenge in catalysis because of their high bond dissociation energies and lack of electronic activation. Recent advances, however, have shown that HIE of C(sp^3)–H bonds can be achieved either through direct π-coordination of an olefin to a transition metal or with the assistance of directing groups. Early studies by Shi[122] and Beller[123] demonstrated that aliphatic alcohols and amines can undergo deuterium incorporation using commercially available Ru precatalysts (**Scheme 1.18**).

In 2008, Jia reported the β-selective deuteration of aromatic alcohols employing [Ru(*p*-cymene)Cl_2]$_2$ in combination with 2-aminoethanol as a ligand, achieving high levels of deuterium incorporation.[124] In subsequent work, Beller and co-workers described the α,β-deuteration of amines using the Shvo catalyst, which afforded nearly quantitative isotope incorporation. Building on these pioneering results, pincer-type ruthenium complexes such as Ru–PNN and Ru–MACHO were developed and

proved highly effective for both amines and alcohols, enabling α- and β-deuteration with enhanced reactivity under milder conditions. For instance, in 2015, Chidambaram and co-workers employed the Ru–MACHO complex to achieve α- and α,β-deuteration of alcohols, further underscoring the potential of these systems for selective aliphatic HIE.[125] Another noteworthy Ru catalyst was developed by the Szymczak group, demonstrating the stereoretentive deuteration of α-chiral amines and thereby providing an elegant method for the synthesis of chiral deuterated amines (**Scheme 1.18**).[126]

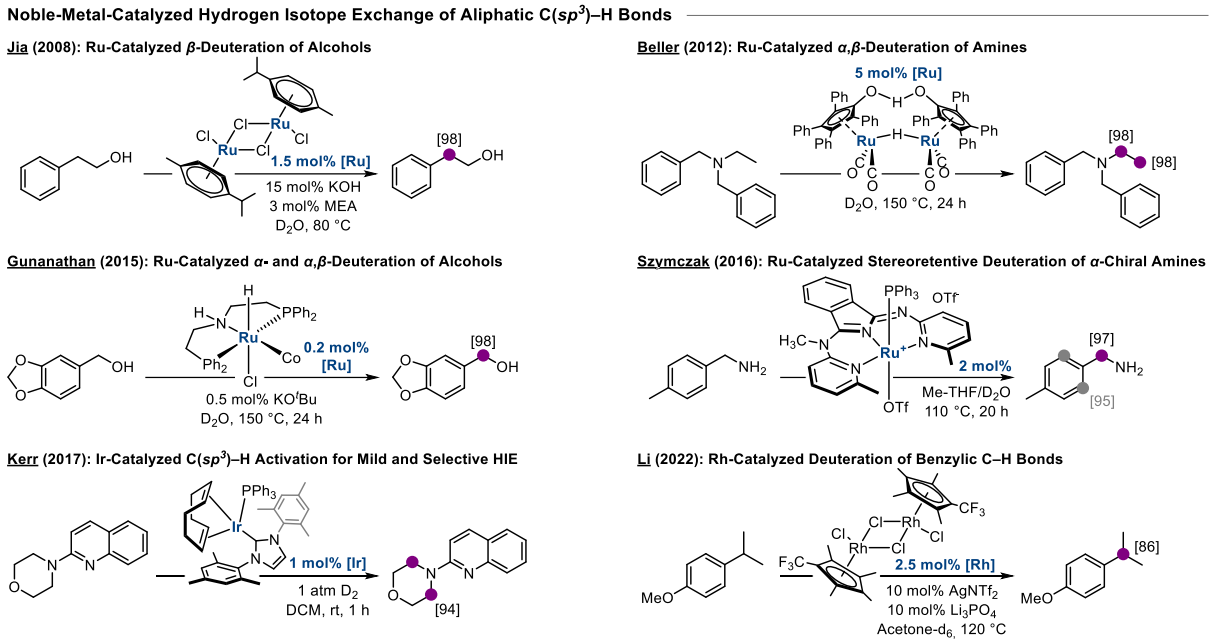

Scheme 1.18: Selected examples of noble metal-catalyzed HIE of aliphatic C(sp^3)–H bonds.

To date, numerous additional catalytic systems have been developed, further expanding the substrate scope of HIE. [106, 122] Although HIE has evolved into a powerful tool for isotopic labeling, many methodologies still require extensive substrate-specific optimization of catalytic systems, thereby limiting their general applicability. Moreover, limitations including incomplete isotope incorporation and restricted functional group tolerance highlight the necessity for novel methodologies to enhance both the efficiency and the scope of HIE processes.

2 Objectives of this Work

In recent years, Co catalysts have emerged as promising tools for olefin isomerization, unlocking new opportunities in base-metal catalysis. The pioneering studies of Shenvi[52] and Norton[53] demonstrated that even highly demanding tri- and tetrasubstituted olefins can be isomerized in moderate to high yields using Co-based systems. Nevertheless, Co catalysts still face significant challenges – most notably poor regioselectivity, limited activity, and insufficient robustness – which currently restrict their broader application in synthetic chemistry and industrial processes.

With this in mind, the first objective of this work is to develop a Co-based catalytic system for the isomerization of allylamines to enamines, with particular emphasis on the industry-relevant substrate *N*,*N*-diethylgeranylamine (DEGA). Since the Takasago process relies on the Rh-catalyzed isomerization of DEGA, the development of an alternative Co catalyst would be of considerable economic interest. Building on Otsuka's work, this challenge will be addressed through the screening of Co hydride complexes and the systematic variation of ligand structures, with the aim of achieving higher catalytic activity, enhanced selectivity, and improved mechanistic understanding.

The second objective of this work is the development of Ru catalysts for site-selective H/D exchange in aliphatic benzimidazole derivatives. Although methodologies for deuterium labeling have been extensively studied in recent years, achieving selective H/D exchange at C(sp^3)–H sites remains a major challenge. This study aims to establish a Ru-based catalyst platform capable of both positional and complete deuteration. To achieve this goal, a machine learning approach will be employed to predict activity–selectivity relationships during catalyst screening, thereby accelerating the identification of promising catalysts. The integration of experimental and computational strategies is expected to provide novel Ru catalysts and key insights into H/D exchange selectivity.

Another objective of this work is the development of new Pd-based catalysts for the telomerization of 1,3-butadiene to 1-methoxy-2,7-octadiene. As current methods often require elevated temperatures or sophisticated catalysts, this study aims to establish milder and more sustainable reaction conditions while maintaining high selectivity and yield.

The following chapter summarizes the results presented in the published articles included in this thesis. The first section addresses the development of novel Co catalysts for the isomerization of allylamines using benzofuryl phosphines. The second section builds on previous work concerning novel phosphine ligands and extends their application to the Pd-catalyzed telomerization of butadiene. Finally, the third section discusses the Ru-catalyzed deuteration of benzimidazole derivatives.

3 Summary of Published Articles

3.1 Cobalt(0)-Catalyzed Isomerization of Allylamines Promoted by Monodentate Benzofuran Phosphines

This study explores the development of a Co catalyst that converts aliphatic and aromatic allylamines into their corresponding enamines. The starting point of our work was Otsuka's report of the first reported isomerization of (*E*)-allylamines to the corresponding (*E*)-enamines catalyzed by a Co(I)-hydride complex. After initial screening of various Co catalysts and ligands, including mono-, bi-, and tri-dentate phosphines, we discovered that tri(furan-2-yl)phosphine (TFP, **L1**) combined with $Co(OAc)_2$ and DIBAL-H in THF achieved 81% yield of **1b** with good selectivity (**Scheme 3.1**).

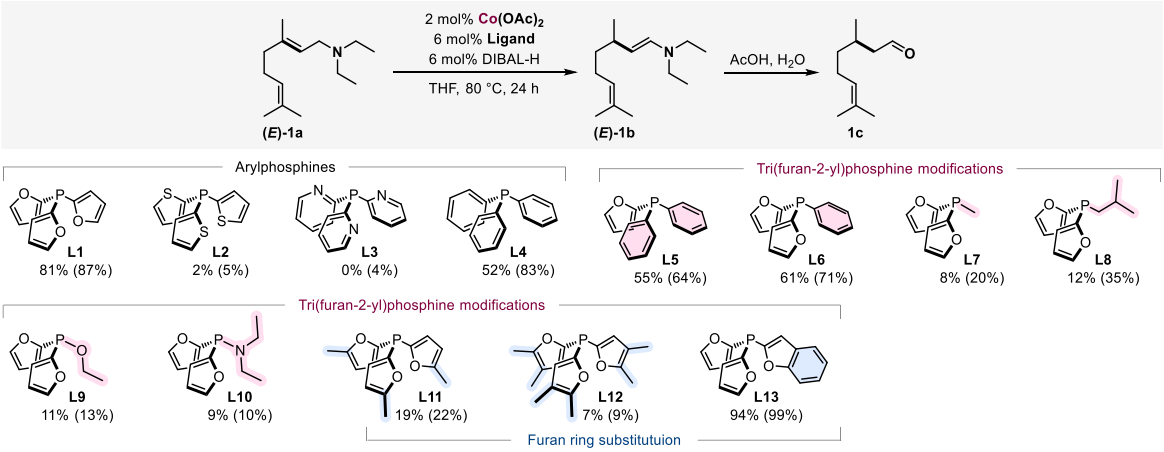

Scheme 3.1: Initially examined ligands for the Co-catalyzed isomerization of allylamine **1a**. Conditions: 2.5 mmol of **1a**, 1.5 mL THF, $Co(OAc)_2$, ligand, DIBAL-H, 80 °C, 24 h. After catalysis, **1b** was hydrolyzed by the addition of 1.5 mL of a 5% AcOH solution, yielding **1c**. Conversion of **1a** and yield of **1c** were determined by GC using *n*-hexadecane as internal standard. The numbers in parentheses represent the conversion.

We next turned our attention towards the synthesis of furan-based phosphines (**L4-L12**) to enhance catalytic performance (**Scheme 3.1**). The substitution of furyl residues with benzene rings led to a significant decrease in the yield of **1b** (**L5**-**L6**). Likewise, exchanging one furyl unit with an alkyl-, diethylamine or -ethoxy unit resulted in a reduced catalyst activity (**L7**-**L10**). Interestingly, the addition of methyl groups to the furan ring also led to a considerably decrease in the yield of **1b**, probably due to steric reasons (**L11**-**L12**). However, introducing a benzofuran residue in place of one furan ring (benzofuran-2-yldi(furan-2-yl)phosphine, **L13**) improved the catalyst performance, achieving complete conversion of **1a** and 94% yield of **1b** (**Scheme 3.1**). Applying optimized reaction conditions, it was

possible to reduce the catalyst loading to 0.1 mol% $Co(acac)_2$ while also using fewer equivalents of the ligand (**L13**) and reductant (1:2 metal to ligand/reductant ratio). To elucidate the origin of the enhanced catalytic performance of **L13**, we systematically studied the performance of several benzofuryl phosphines, including their electronic and steric properties (**L13**-**L27**, **Scheme 3.2**).

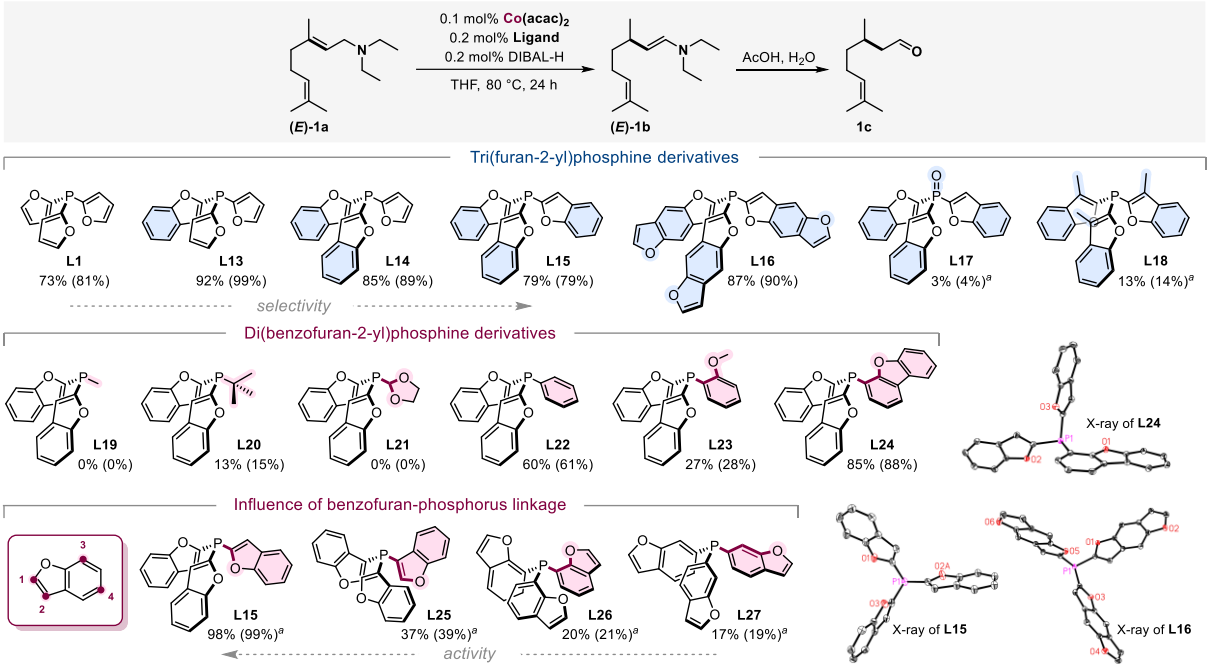

Scheme 3.2: Overview of synthesized and tested benzofuryl phosphines. Conditions: 2.5 mmol of **1a**, 1.5 mL THF, $Co(acac)_2$, ligand, DIBAL-H, 80 °C, 24 h. Conversion of **1a** and yield of **1c** were determined by GC using *n*-hexadecane as internal standard. The numbers in parentheses represent the conversion of **1a**. [a]Catalyst loading: 0.5 mol% $Co(acac)_2$, 1 mol% ligand and 1 mol% DIBAL-H. Molecular structure of **L15**, **L16,** and **L24**. Displacement ellipsoids correspond to 30% probability, hydrogen atoms are omitted for clarity.

In comparison to the mono-substituted benzofuryl phosphine **L13**, further replacement of furyl substituents with benzofuryl ones increased the selectivity of the catalytic system, although the activity was slightly reduced (**L13**-**L15**). Application of tri(benzofuran-2-yl)phosphine (**L15**) afforded the best selectivity for the isomerization of **1a**, with negligible side-product formation. Increasing the reaction temperature from 80 °C to 100 °C enabled the complete conversion of **1a** and almost quantitative yield of **1b** (with 0.1 mol% catalyst loading). Notably, the developed Co system exhibited catalytic activity and selectivity comparable to currently applied Rh catalysts.

When phosphine oxide **L17** was employed, only trace amounts of **1b** were obtained, indicating that oxidation of **L15** leads to deactivation of the corresponding Co catalyst (**Scheme 3.2**). Similarly, the activity of the catalytic system was considerably decreased by the presence of a methyl group at the C3 position of the benzofuran residue (**L18**), probably due to steric hindrance.

We extended our studies by synthesizing a series of di(benzofuran-2-yl) phosphine derivatives (**L19**-**L24**). Introducing an alkyl group (**L19**-**L21**) led to a substantial decrease in catalytic activity. Notably, aryl substituents (**L22**-**L24**) showed significantly better results, with phenyl- (**L22**, 60%) and dibenzofuran- (**L24**, 85%) derivatives leading to high yields of **1b**. These results suggest that the presence of a sp^2 oxygen atom seems to be crucial (**L15**, **L24**) to generate a highly active Co catalyst, since the ligands containing sp^3 oxygen atoms (**L21**, **L23**) gave significantly lower yields of **1b**.

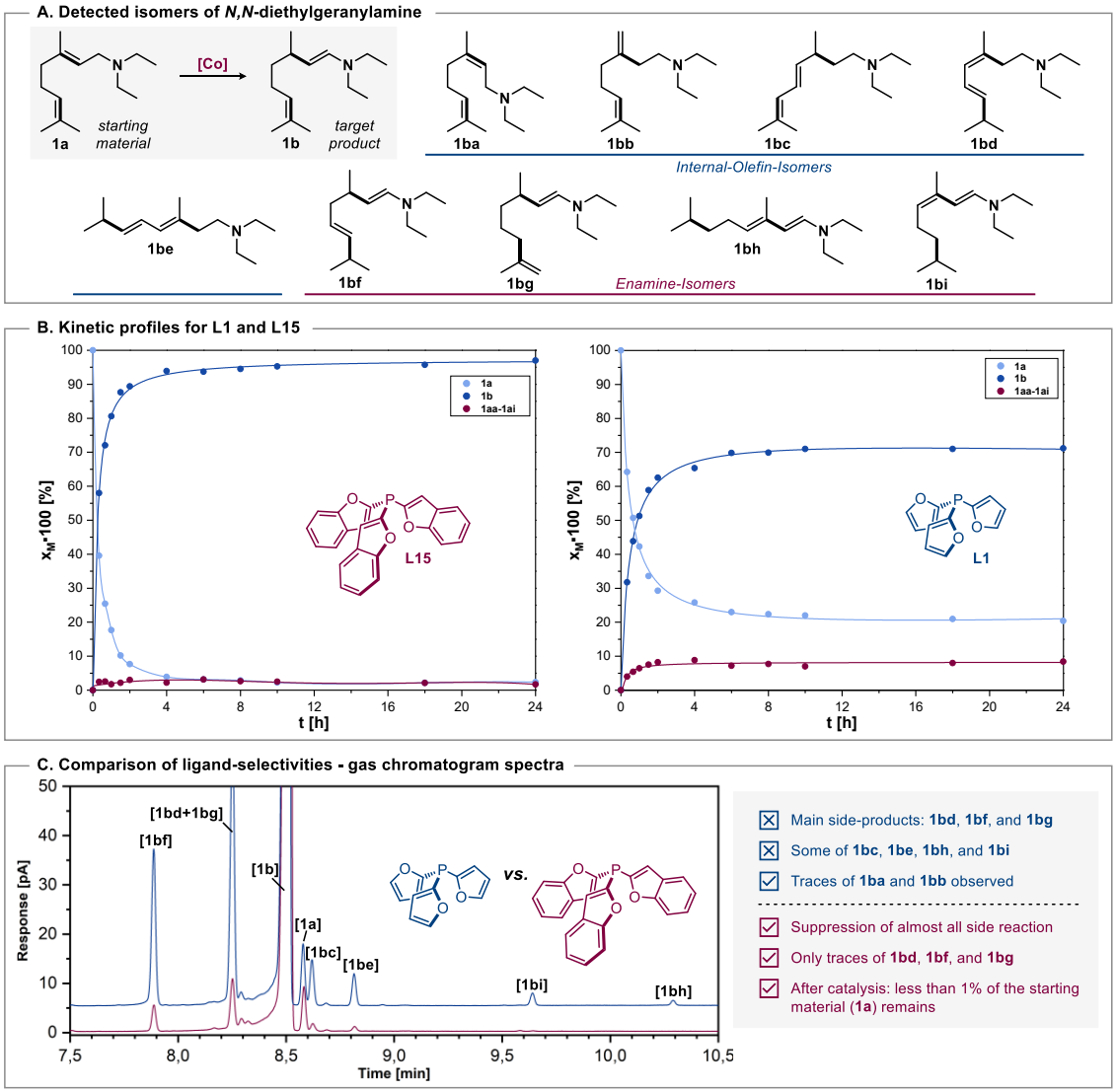

Scheme 3.3: (A) Identified isomers of **1a** after catalysis. (B) Kinetic profiles of **L1** and **L15**. (C) Comparison of ligand selectivities **L1** and **L15** - GC spectra of product mixtures after the Co-catalyzed isomerization. Reaction conditions: 2.5 mmol of **1a**, 1.5 mL THF, 1 mol% $Co(acac)_2$, 2 mol% DIBAL-H/ligand, 100 °C.

After identifying benzofuran phosphines as the most suitable ligands, we investigated the influence of the benzofuran-phosphorus linkage. (**Scheme 3.2**). While **L15** (P-C2) showed high activity, **L25** (P–C3) was notably less active. Phosphines with P–C5 (**L27**) or P–C7 (**L26**) linkages displayed even lower activity. These results highlight the importance of an sp^2 oxygen atom two bonds away from the phosphorus atom for the formation of the catalytically active Co species.[127]

With **L15** established as the most selective benzofuryl phosphine and the reaction conditions optimized, we next investigated the side-products of **1a** to elucidate the reaction mechanism (**Scheme 3.2A**). Of note, **L1** was used as a less selective ligand in larger-scale reactions to allow isomer isolation. Overall, we identified five internal olefin isomers (**1ba**-**1bd**) and four enamine isomers (**1be**-**1bi**). It is particularly noteworthy that tri(benzofuran-2-yl)phosphine (**L15**) prevents (*Z*)-(*E*) isomerization and chain-walking of double bonds of **1a**. For example, the formation of isomers **1be**, **1bh** and **1bi** was fully suppressed when **L15** was used instead of **L1**. In addition, **L15** afforded considerably lower amounts of **1bd**, **1bf**, and **1bg** compared to **L1**.

Additionally, we recorded the formation of undesired side-products (**1ba**-**1bi**) during the Co-catalyzed isomerization over time for **L15** and **L1** (**Scheme 3.2B**). In the case of **L1**, the reaction furnished 65% of **1b** along with 8% side-products after 4 h of reaction. In comparison, **L15** converted over 95% of substrate **1a** to product **1b** within 4 h, with minimal formation of undesired isomers. After 24 h reaction time, **1b** was obtained in 98% yield, accompanied by 2% side products.

To investigate the scope and limitations of the optimized catalytic system, we synthesized and evaluated a broad range of aliphatic and aromatic allylamine derivatives (**1a**-**31a**, **Scheme 3.4**). The newly developed Co catalyst effectively converted the (*E*)- and (*Z*)-isomer of diethyl-geranylamine (**1a**) into the corresponding enamines with yields of 98% and 97%. Similarly, geranylamine derivatives bearing ethyl- (**2a**), ethyl-methyl- (**3a**), di-methyl- (**4a**) and isopropyl- (**5a**) were also successfully isomerized. We further demonstrated that even cyclic aliphatic geranylamine derivatives with pyrrolidine- (**6a**) and morpholine- (**7a**) substituents underwent conversion to the corresponding enamines. However, no catalytic activity was observed in the case of aryl geranylamine derivatives (**8a**–**9a**), demonstrating the importance of the amine moiety for the efficient catalysis. We then systematically synthesized and tested a series of internal and terminal (*E*)-allylamines (**10a**-**21a, Scheme 3.4**).

Notably, our developed system enabled the isomerization of a broad range of internal allylamines, including challenging substrates such as **15a** and **16a**, as well as the industry-relevant farnesal derivative **10a**, which was selectively converted with 79% yield. Remarkably, terminal allylamines (**19a**-**20a**) were also converted to the respective enamines. Despite the broad substrate tolerance, the catalyst was incompatible with allylamine **14a** bearing an ester group. Furthermore, we demonstrated that aromatic allylamines bearing functional groups, such as *tert*-butyl (**23a**), chloro- (**24a**), trifluoromethyl- (**25a**), or methoxy- (**26a**) were isomerized to the corresponding enamines in high yields. More challenging substrates, including C3-substituted allylamine derivatives (**29a**-**30a**) and even the di-

functionalized allylamine **31a**, were also successfully converted. Finally, to highlight the industrial relevance of our developed Co catalyst, we successfully performed the isomerization of **1a** on a multi-100-gram scale, producing 311 g of citronellal (**1c**) with high selectivity (96% yield).

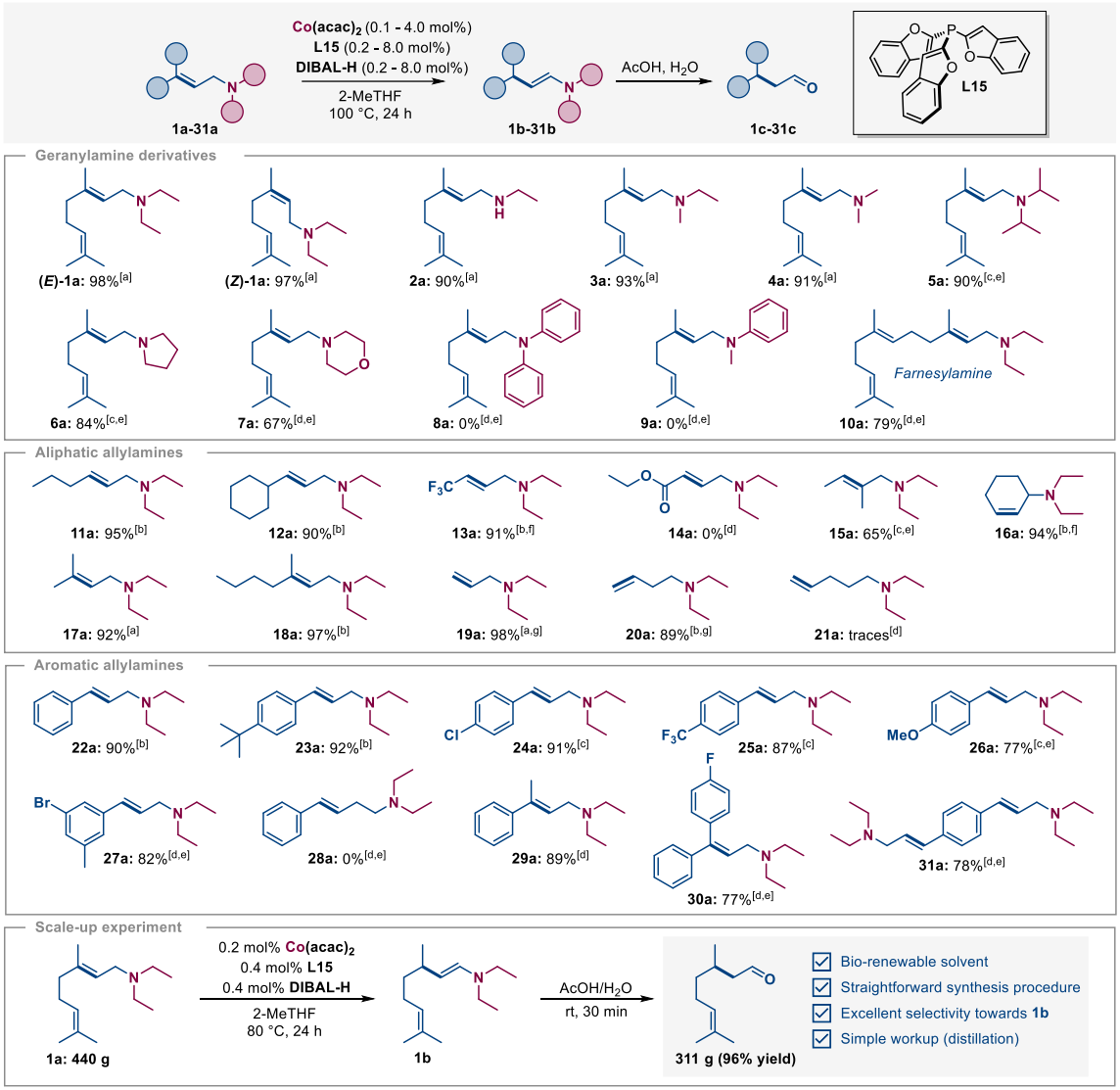

Scheme 3.4: Co-catalyzed isomerization of various aliphatic and aromatic allylamines to their corresponding enamines. Values below the structures represent the isolated yield(s) of aldehydes. Conditions: substrate (0.5 - 2.5 mmol), 2-MeTHF or THF, 100 °C, 24 h. Note: Product **10c** represents the sum of the isomers. [a] Catalyst: 0.1 mol% $Co(acac)_2$, 0.2 mol% **L15** & DIBAL-H. [b] Catalyst: 1 mol% $Co(acac)_2$, 2 mol% **L15** & DIBAL-H. [c] Catalyst: 2 mol% $Co(acac)_2$, 4 mol% **L15** & DIBAL-H. [d] Catalyst: 4 mol% $Co(acac)_2$, 8 mol% **L15** & DIBAL-H. [e] Reaction time: 48 h. [f] Isolated as an enamine. [g] GC-yield.

To gain insights into the origin of the catalyst reactivity, we first carried out a series of crystallization experiments. The treatment of $Co(acac)_2$ and **L15** (ratio 1:2) in anhydrous THF with two equivalents DIBAL-H resulted in the reduction of the Co(II)-precursor to Co(0) and the release of H_2. Dark red, platelet-shaped crystals of **Co-2** suitable for single-crystal X-ray diffraction were obtained after crystallization. The molecular structure of **Co-2** was determined by SC-XRD, disclosing a homoleptic tetrahedral Co d^9 complex [CoL_4] with four coordinating ligands (**Scheme 3.5A**).

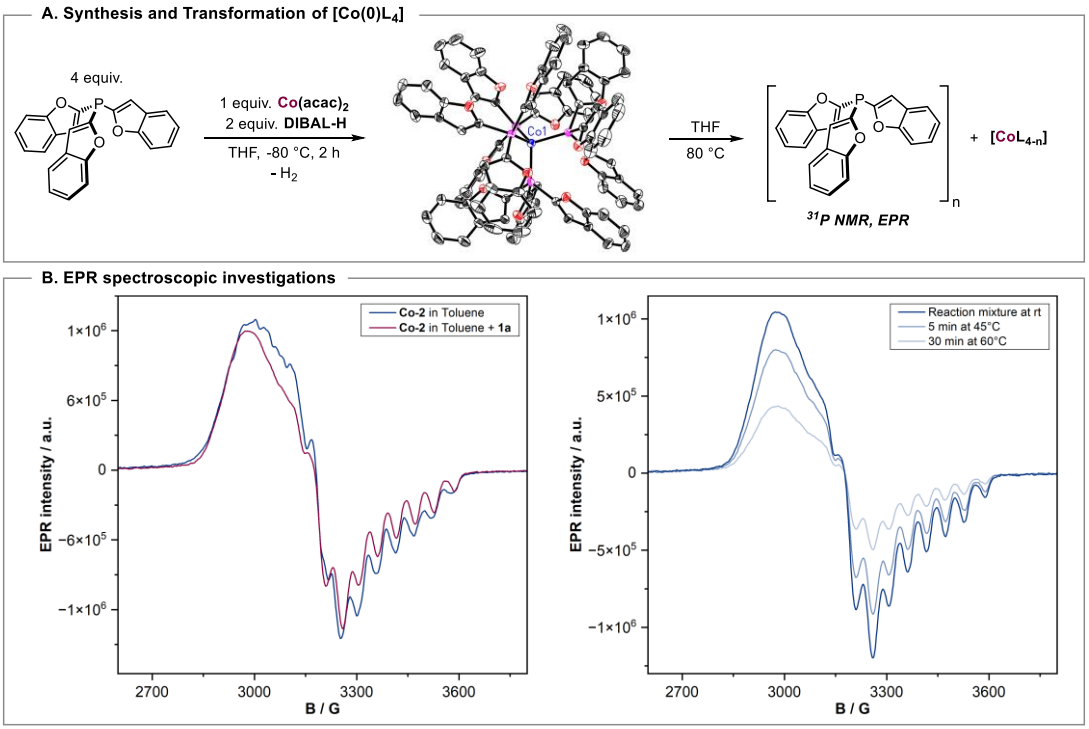

Scheme 3.5: (A) Solid-state structure of Co-2 at 30% probability ellipsoids. Hydrogen atoms are omitted for clarity. (B) Recorded EPR spectra of Co-2 in toluene, measured at 95 K.

Although control experiments revealed slightly differences in the activities of the isolated **Co-2** and the *in situ* catalyst, applying a slightly higher catalyst loading of **Co-2** (0.3 mol%) led to a quantitative yield of **1b**. Despite **Co-2** not being the active species, which may represent an off-cycle resting state that forms *in situ* the active Co catalyst, we conducted a detailed study of **Co-2** to better understand its properties and role in the catalytic system. Since **Co-2** has formal 17 valence-electrons and therefore has a radical character, a set of EPR measurements were performed (**Scheme 3.5B**).

Due to the limit coordination sphere of **Co-2**, we postulated that the Co complex undergoes ligand dissociation to generate a vacant coordination site for substrate binding. To prove this hypothesis, we performed EPR titration experiments of **Co-2** in toluene, with or without substrate **1a**. The addition of **1a** to **Co-2** in toluene led to a slightly shifted and decreased signal in the EPR spectra, suggesting the presence of an *in situ* formed Co(0) substrate complex ($g_{\parallel} = g_{\parallel} = 2.188$ and $g_{\perp} = 1.989$, $A_{\parallel} = 105.5$, $A_{\perp}$

= 150.0 MHz). Similarly, we observed a signal shift for the addition of THF to **Co-2** in toluene (g‖ = 2.187 and g⊥ = 1.989, A‖= 106.2, A⊥ = 151.5 MHz). Moreover, NMR experiments also suggested the presence of free ligand (**L15**) when **Co-2** was dissolved in THF-d_8 compared to toluene-d_8. Based on these combined results, we conclude that **Co-2** represents a precatalyst that undergoes ligand dissociation in the presence of THF or **1a**, leading to the active Co species.

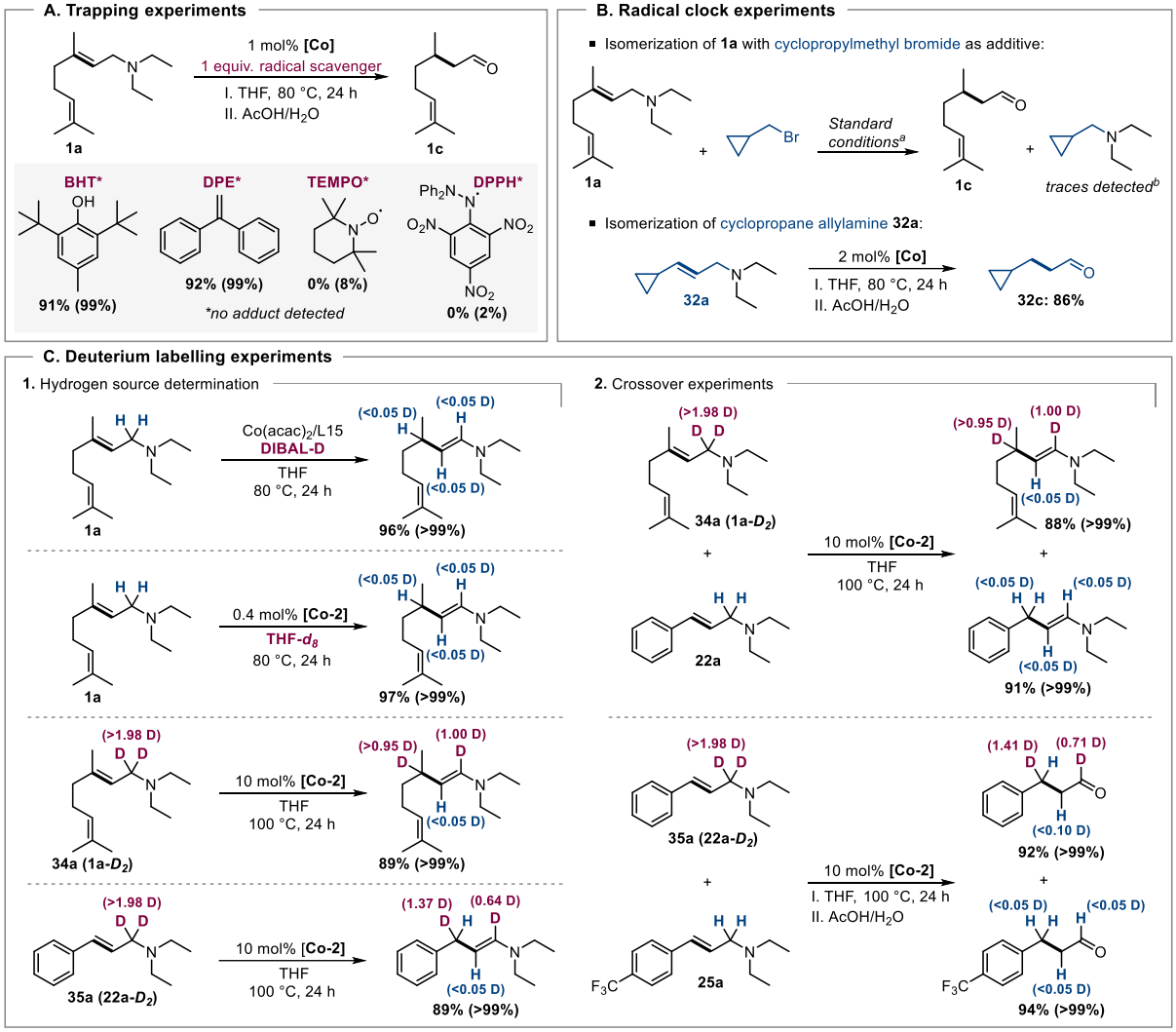

Scheme 3.6: Mechanistic control experiments. (A) Trapping experiments with radical scavengers. (B) Radical clock experiments. [a]Standard conditions: 2.5 mmol of **1a**, 1.5 mL THF, 1 mol% $Co(acac)_2$, 2 mol% **L15** and DIBAL-H, 80 °C, 24 h. (D) Deuterium labelling experiments.

In situ EPR measurements of the catalyst solution revealed no radical intermediates. The addition of radical scavengers (TEMPO, Galvinoxyl, or DPPH) to the model reaction with substrate **1a** completely suppressed isomerization, although no adducts were detected by GC–MS or LC–MS, suggesting catalyst

deactivation via coordination to the metal center (**Scheme 3.6**). In contrast, DHT and BPE did not affect the catalytic activity. Moreover, radical clock experiments with cyclopropane-containing substrates showed no evidence of ring opening for either (bromomethyl)cyclopropane or allylamine **32a** and **33a**. These combined results rule out free radical intermediates in the isomerization.

Moreover, a broad range of isotope-labeling experiments was performed to further elucidate the reaction mechanism. No deuterium incorporation was observed when the model reaction of **1a** was conducted in THF-d_8 or with DIBAL-D, excluding both as potential hydrogen sources. In contrast, isomerization of the γ-deuterated substrates **1a-D$_2$ (34a)** and **22a-D$_2$ (35a)** afforded the corresponding enamines with α-deuterium incorporation, consistent with a 1,3-hydrogen shift. To distinguish between inter- and intramolecular pathways, H/D crossover experiments were conducted. No deuterium transfer was detected in the resulting products, thereby excluding both radical and metal-hydride species in the reaction mechanism. In addition, no hydride species were observed by ^{1}H NMR analysis.

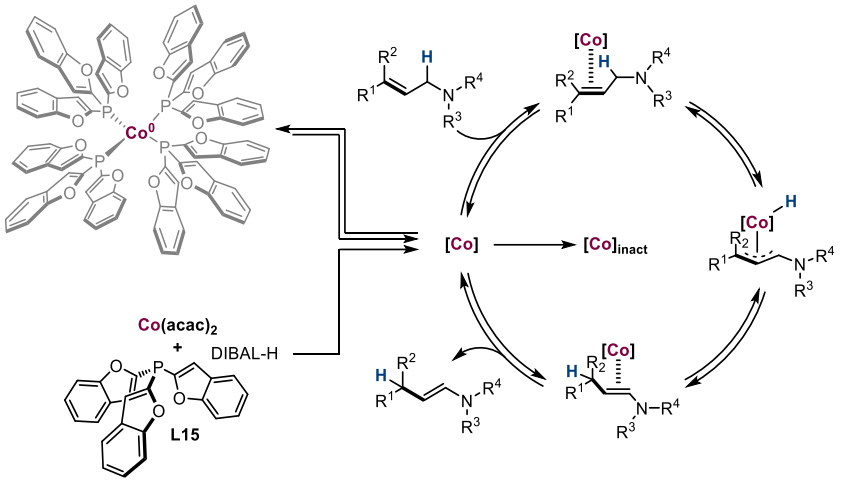

Scheme 3.7: Proposed mechanism for the Co-catalyzed isomerization of allylamines to enamines.

Based on our mechanistic studies, we propose an inner-sphere allyl mechanism (**Scheme 3.7**). The active Co species is generated either from Co(acac)$_2$ or the defined precatalyst **Co-2**. Coordination of the allylamine then affords a metal–substrate intermediate, as supported by EPR measurements. Subsequent C–H activation of the allylic position constitutes the rate-determining step and furnishes a Co-H species. Reinsertion of the hydride into the allylic system produces the product intermediate, which releases the desired enamine. During the process, the catalyst gradually converts into an inactive species (**Scheme 3.7**).

3.2 Development of Highly Efficient and Selective Palladium Catalysts for Telomerization of 1,3-Butadiene with Alcohols

Pd-catalyzed telomerization reactions have attracted considerable attention as atom-economic transformations, with the telomerization of 1,3-butadiene to 1-methoxy-2,7-octadiene (1-MODE) being of particular interest due to its industrial relevance as an intermediate in the production of 1-octene. Although numerous homogeneous Pd catalysts have been reported, most systems still require sophisticated catalysts or ligands to achieve high yields of 1-MODE. Since triphenylphosphine derivatives with electron-donating substituents have been extensively studied, we aimed to investigate our recently developed monodentate phosphines containing furyl- and benzofuryl-substituents (**Scheme 3.8**), which offer distinct electronic and steric properties, in the Pd-catalyzed telomerization of 1,3-butadiene.[128]

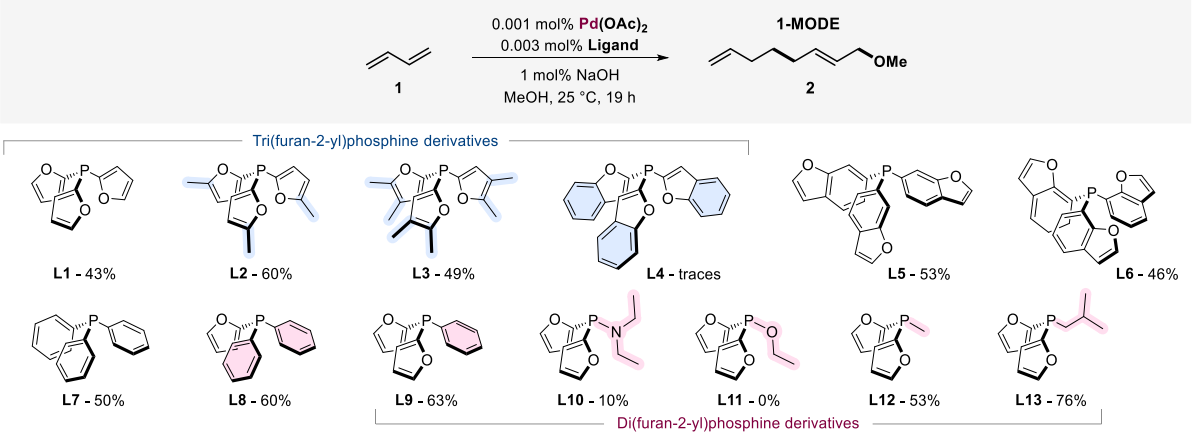

Scheme 3.8: Initially evaluated ligands for the Pd-catalyzed telomerization of 1,3-butadiene. Conditions: 1.5 mL MeOH per 1.0 g butadiene, condensed 1,3-butadiene, Ar atmosphere, 25 °C, stirring 750 rpm, 19 h. Yields were determined by GC analysis using isooctane as internal standard.

We started our ligand screening with the commercially available tri(2-furyl)phosphine (**L1**), which provided a 43% yield of 1-MODE (**Scheme 3.8**). The more electron-rich derivatives **L2** and **L3**, bearing additional methyl groups on the furan ring, increased the catalyst performance slightly. Interestingly, no activity of the Pd catalyst was observed when tri(benzofuran-2-yl)phosphine (**L4**) was used. However, when structurally related benzofuryl phosphines **L5** and **L6** were used, we obtained 53% and 46% yield of 1-MODE. In comparison to simple triphenylphosphine (**L7**), the replacement of one or two phenyl units with a furyl ring increased the yield to 60% (**L8**) and 63% (**L9**), respectively. Considering the satisfactory yield obtained with **L9**, additional di-furyl phosphine derivatives (**L10**-**L13**) were evaluated. Notably, the catalyst performance was significantly increased when an isobutyl residue (**L13**) was incorporated, which yielded 76% of 1-MODE.

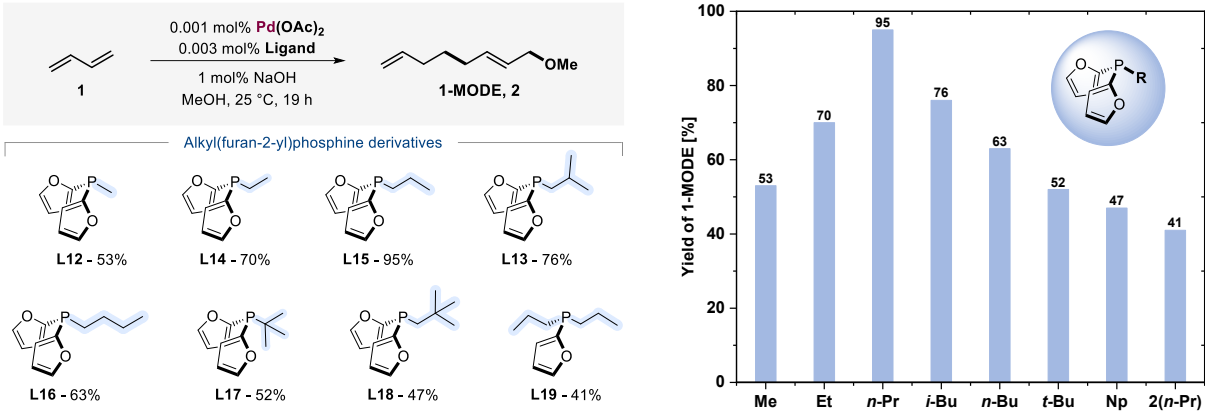

Scheme 3.9: Screening of di(furan-2-yl) phosphines: variation of the alkyl chain length. Conditions: 1.5 mL MeOH per 1.0 g butadiene, condensed 1,3-butadiene, Ar atmosphere, 25 °C, stirring 750 rpm, 19h. Yields were determined by GC analysis using isooctane as internal standard.

In order to further enhance the performance of the catalyst, we proceeded to modify the ligand structure by synthesizing a library of alkyl di-furyl phosphines (**L12**-**L19**, **Scheme 3.9**). The systematic synthesis of di-furyl phosphines, bearing linear alkyl residues (**L14**-**L16**) and branched alkyl residues (**L17**-**L18**), enabled us to identify di(furan-2-yl)(propyl)phosphine (**L15**), which gave an excellent yield of 95% (**Scheme 3.9**). Owing to the excellent performance of **L15**, the impact of temperature and the metal-to-ligand ratio was subsequently investigated.

Table 3.1: Optimization of reaction conditions and control experiments.

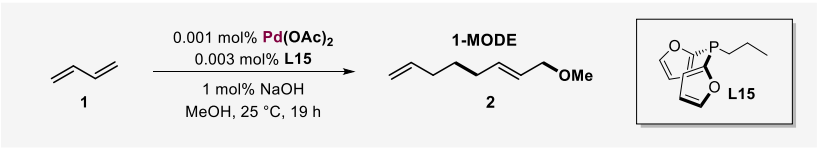

Entry	Changes from standard conditions			Yield [%]
	$Pd(OAc)_2$ [mol%]	**L15** [mol%]	Temp. [°C]	
1	1	3	**0**	10
2	1	3	**25**	95
3	1	3	**50**	93
4	1	3	**70**	52
5	1	**-**	25	-
6	1	**1**	25	50
7	1	**5**	25	42
8	**0.5**	3	25	35

Conditions: 1.5 mL MeOH per 1.0 g butadiene, condensed 1,3-butadiene, Ar atmosphere, 25 °C, stirring 750 rpm, 19 h. Yields were determined by GC analysis using isooctane as internal standard.

Surprisingly, raising the reaction temperature did not improve the catalyst performance (**Table 3.1**, entries 1-4). At 50 °C, the yield remained comparable to the telomerization at room temperature, with a yield of 93%. However, the activity of the catalyst decreased significantly at 70 °C and 90 °C, yielding 40% and 52% of 1-MODE, respectively. Lowering the reaction temperature to 0 °C was also unfavorable, whereby only 10% of 1-MODE were obtained.

Furthermore, investigating the ligand-to-metal ratio revealed its critical impact on the formation of the active Pd species (**Table 3.1**, entries 5-7). The initially applied ratio of 1:3 (ligand:metal) proved to be most favorable for the Pd-catalyzed telomerization. Reducing the ratio to 1:1 resulted in a yield of 50%, while increasing it to 1:5 further lowered the yield to 43%. Notably, no product was formed in the absence of the ligand (**L13**), indicating the crucial role of **L13** during catalysis.

To further investigate the activity of our new developed telomerization catalyst towards different alcohols, we performed the catalysis in different mixtures of alcohols (**Scheme 3.10**). When a 2:1 ratio of MeOH to EtOH was applied, the catalytic system exhibited high selectivity for methanol, affording the products 1-MODE and 1-EtODE in a 10:1 ratio (Condition A). Notably, performing the telomerization using a 1:1 ratio of MeOH to EtOH resulted in a negligible higher yield of 1-EtODE (Condition B). A similarly high selectivity for MeOH was observed when a 1:1 ratio of MeOH to BuOH was used, yielding 1-MODE and 1-BuODE in a 9:1 ratio (Condition C). The preferred formation of 1-MODE as the primary product can be ascribed to the favored protonation of the Pd-(η^3,η^1-octadienediyl)-complex by MeOH (**Scheme 3.11**).

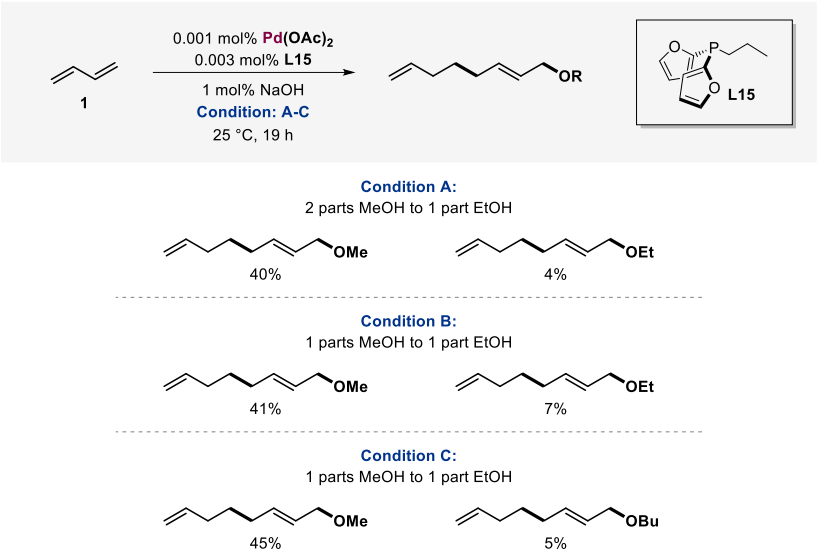

Scheme 3.10: Chemoselective Pd-catalyzed telomerization using alcohol mixtures. Conditions: 1.5 mL MeOH per 1.0 g butadiene, condensed 1,3-butadiene, Ar atmosphere, 25 °C, stirring 750 rpm, 19 h. Yields were determined by GC analysis using isooctane as internal standard.

Control experiments demonstrated that our developed alkyl di(furan-2-yl) phosphines exhibited high air stability despite their electron-rich character, which makes these ligands highly attractive for further applications under semi-anaerobic conditions. For example, in the case of **L15**, only trace amounts of phosphine oxide were detected after overnight stirring under air. The complete oxidation of **L15** required the use of hydrogen peroxide in excess, affording di(furan-2-yl)(propyl)phosphine oxide (**L18**). The resulting molecular structure of **L18** was determined by SC-XRD. Importantly, when **L18** was applied as the ligand, only negligible amounts of 1-MODE were detected, indicating deactivation of the Pd catalyst. Finally, the mechanism shown in **Scheme 3.11** was postulated according to the studies of Jolly *et al.* and literature data.

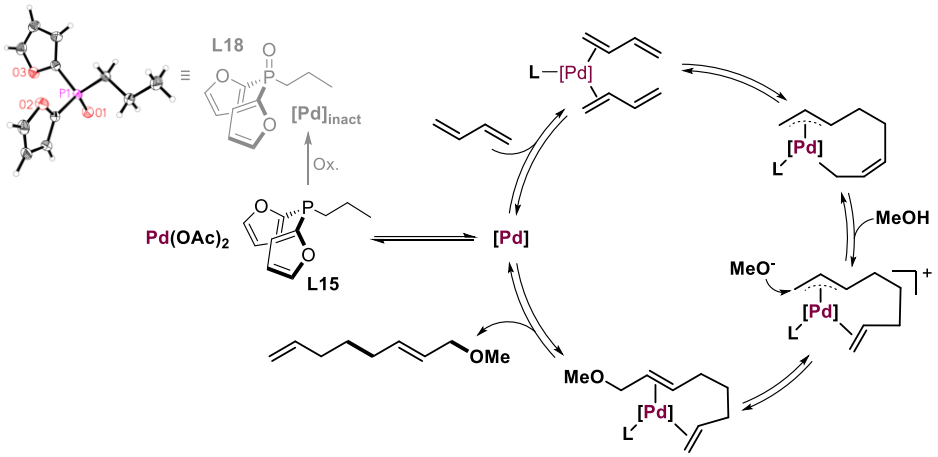

Scheme 3.11: Proposed mechanism for the Pd-catalyzed telomerization of 1,3-butadien. Solid-state structure of **L18** at 30% probability ellipsoids.

3.3 Machine Learning–Guided Site-Selective Ru-Catalyzed C(sp^3)–H Activation of Benzimidazole Derivatives

Recent studies have demonstrated that Ru catalysts can promote HIE at C(sp^3)–H bonds.[123, 125] However, most known systems rely on alcohol or amine functionalities as directing groups, enabling primarily α- and β-deuteration. The present work aims to develop a more general platform, using 2-propylbenzimidazole (**1a**) as the model substrate, to achieve site-selective HIE at the β- and γ-positions as well as complete deuteration along the alkyl chain. Machine learning is employed as a predictive framework to correlate structural features with catalytic activity and selectivity, providing quantitative insights that guide the rational design of improved Ru-based HIE catalysts.

After extensive screening of diverse ligand motifs in the Ru-catalyzed HIE of **1a**, machine learning predictions enabled the identification of the three catalyst systems shown in **Scheme 3.12** as the most active and selective. These Ru catalysts were subsequently used to optimize the reaction conditions and explore the substrate scope.

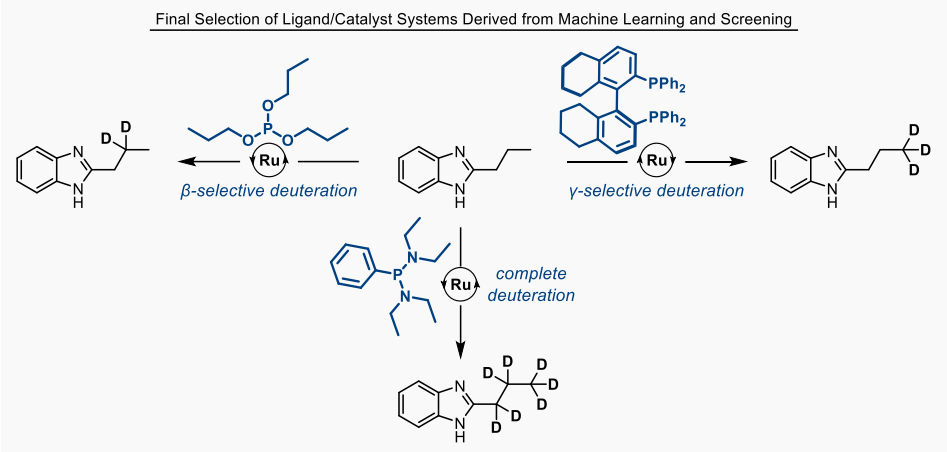

Scheme 3.12: Ru-catalyzed hydrogen deuterium exchange in 2-propylbenzimidazole – catalytic systems identified by machine learning and optimized through multiple screening rounds.

It should be emphasized that neither the machine learning part nor the related ligand screening studies are part of the results presented and discussed in this thesis.

To gain further insight into the catalytic performance, key reaction parameters – including the Ru precursors, Ag additives, deuterium sources, solvent, temperature, and reaction time – were systematically investigated to evaluate their influence on activity and selectivity. Among the Ru precursors tested, the Ru(II) dimers (**Ru-1**, **Ru-2,** and **Ru-3**) provided over 75%D_γ with negligible deuterium incorporation at the β-position (**Scheme 3.13A**). The optimal result was obtained with

[Ru(*p*-cymene)Cl_2]$_2$ (**Ru-3**), which showed excellent *γ*-selectivity, yielding 80%D_γ and 0%D_β. In contrast, the Ru-COD-complexes (**Ru-4** and **Ru-5**) showed reduced D_γ-incorporation (below 75%) and 5%D_β. When the isolated Ru-complex ([Ru(H_8-BINAP)Cl_2], **Ru-6**) was employed, comparable activity to **Ru-3** was observed (74%D_γ), but the selectivity was significantly reduced (16%D_β).

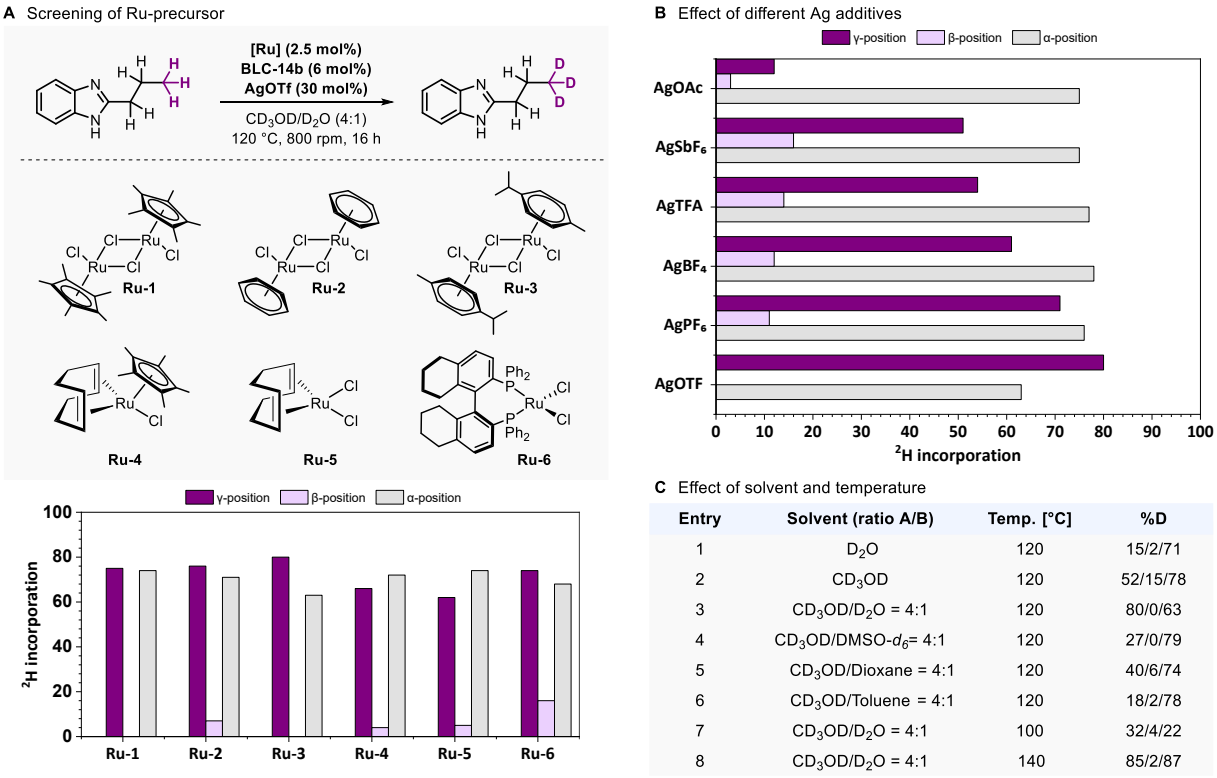

Entry	Solvent (ratio A/B)	Temp. [°C]	%D
1	D_2O	120	15/2/71
2	CD_3OD	120	52/15/78
3	CD_3OD/D_2O = 4:1	120	80/0/63
4	CD_3OD/DMSO-d_6= 4:1	120	27/0/79
5	CD_3OD/Dioxane = 4:1	120	40/6/74
6	CD_3OD/Toluene = 4:1	120	18/2/78
7	CD_3OD/D_2O = 4:1	100	32/4/22
8	CD_3OD/D_2O = 4:1	140	85/2/87

Scheme 3.13: Optimization of reaction conditions for the *γ*-selective HIE of compound **1a**. General reaction conditions: 0.5 mmol of **1a**, 2.5 mol% [Ru], 6 mol% BLC-14b, 30 mol% Ag additive, solvent-mixture: 0.4 mL CD_3OD & 0.1 mL D_2O. Yields were determined by ^{1}H NMR. (**A**) Screening of various Ru precursors. (**B**) Evaluation of different Ag additives. (**C**) Investigation of solvent mixtures and temperature effects.

Next, we investigated the effect of different Ag additives on the Ru-catalyzed HIE of the model substrate **1a** (**Scheme 3.13B**). AgOAc exhibited the lowest activity, with only 12%D_γ and 5%D_β. In contrast, $AgSbF_6$ and AgTFA showed significantly improved activity, achieving HIE efficiencies greater than 55%D at the *γ*-position, however, both additives also led to more than 10%D_β. Similarly, $AgBF_4$ and $AgPF_6$ yielded comparable results, with HIE efficiencies of 76%D_γ and 78%D_γ, respectively, while *β*-incorporation again exceeded 10%. Notably, the best result was achieved with AgOTF, which delivered 80%D_γ with no detectable *β*-incorporation, demonstrating excellent *γ*-selectivity (**Scheme 3.13B**).

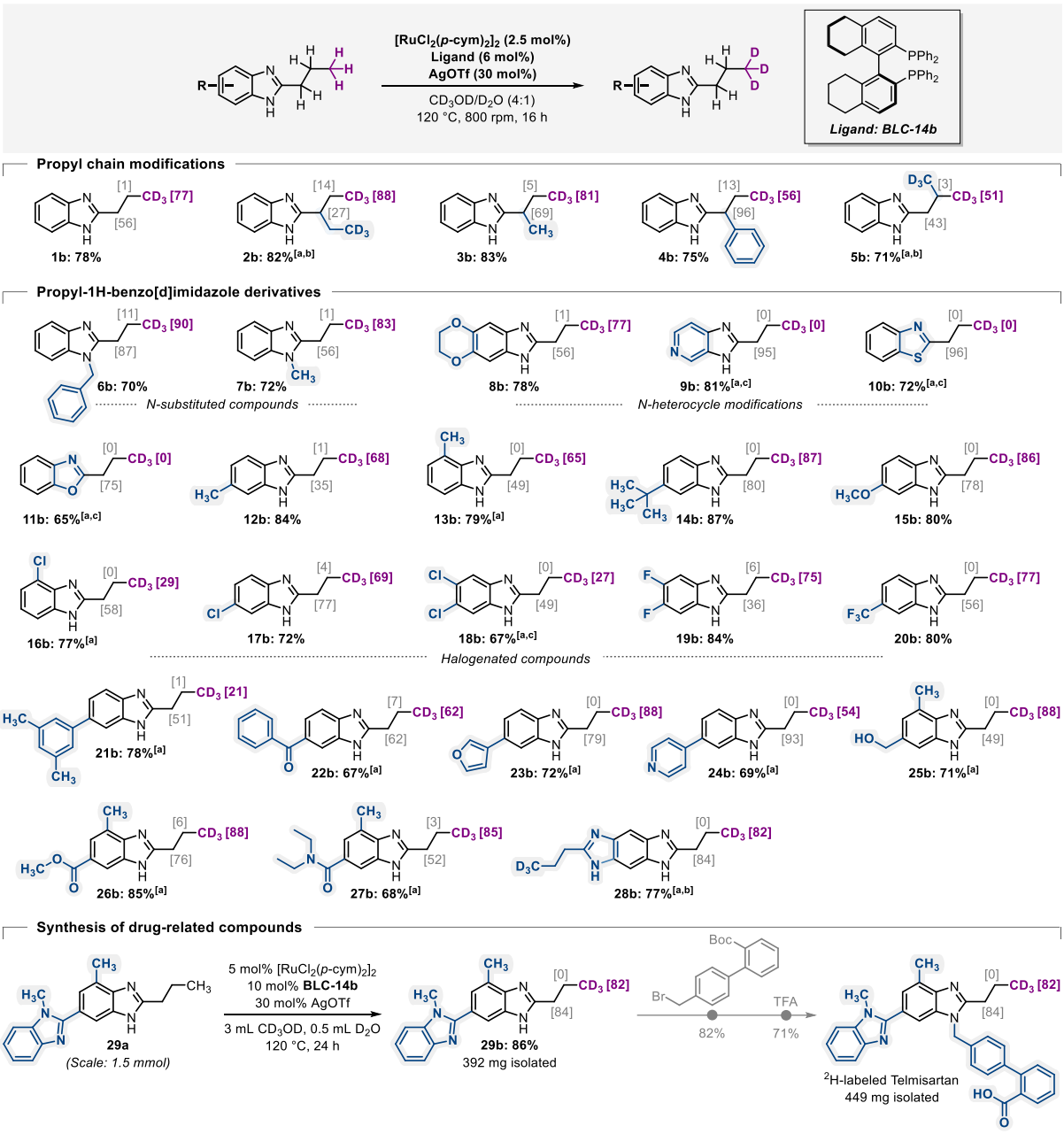

Scheme 3.14.: Ru-catalyzed γ-selective deuterium labeling of benzo[d]imidazole derivatives. Values below the structures represent the isolated yield(s) of the deuterium-labeled compounds (**1a-29a**). Standard reaction conditions: 0.5 mmol substrate, 2.5 mol% [Ru], 0.4 mL CD_3OD, 0.1 ml D_2O, 120 °C, 16 h. [a] Catalyst loading: 5 mol% [Ru]. [b] Reaction time: 48 h. [c] Solvent-mixture: 0.8 mL CD_3OD & 0.2 mL D_2O.

We further investigated the influence of the deuterium source and solvent on the γ-selective HIE (**Scheme 3.13C**). Under the applied reaction conditions, D_2O resulted in low catalytic activity, with only 15%D_γ and 2%D_β. When CD_3OD was used, deuterium incorporation increased to 52%D_γ, but selectivity

decreased, with *β*-incorporation of 15%D. The best result was achieved using a CD_3OD/D_2O (4:1) mixture, which provided high *γ*-selectivity with 80%D_γ and no *β*-incorporation (**Scheme 3.13C**, entry 3). In contrast, solvent mixtures including CD_3OD with DMSO, dioxane, or toluene gave inferior results, with D_γ-incorporation below 50%D (**Scheme 3.13C**, entries 4-6). Furthermore, testing different reaction temperatures showed that neither lower nor higher temperature (**Scheme 3.13C**, entries 7-8) improved the results, with the best catalytic performance observed at 120 °C.

We explored the scope and limitations of the optimized catalysts, starting with an investigation on the effect of different alkyl substituents on the *γ*-selective HIE in 2-propyl-1*H*-benzo[*d*]imidazole derivatives (**Scheme 3.14**, **1a-5a**). Compared to our model substrate **1a**, benzo[*d*]imidazole derivatives bearing methyl- (**2a**) and ethyl- (**3a**) groups in the *α*-position showed increased deuterium incorporation, exceeding 80%D_γ. In contrast, phenyl- (**4a**) and isobutyl- (**5a**) derivatives exhibited slightly reduced HIE, with approx. 50%D_γ incorporation. Interestingly, *N*-substitution of the benzo[*d*]imidazole with benzyl- (**6a**) or methyl- (**7a**) resulted in an increased yield and good degrees of deuteration (>80%D_γ, **Scheme 3.14**).

To investigate the effect of structure-related *N*-heterocycles of benzo[*d*]imidazole on the catalytic performance and the resulting HIE, a series of derivatives (**8a–11a**) was evaluated. Notably, we achieved high deuterium incorporation efficiency and good selectivity for the dioxane derivative **8a** (77%D_γ and 1%D_β). Attempts to extend the HIE catalyst to other *N*-heterocycles, including imidazopyridine (**9a**), benzo[*d*]thiazole (**10a**), and benzo[*d*]oxazole (**11a**), were unsuccessful under the optimized conditions, however, in each case, significant deuterium incorporation was observed at the *α*-position (**Scheme 3.14**). Subsequently, we prepared several benzo[*d*]imidazole derivatives containing a propyl residue (**12a–29a**) and systematically studied the Ru-catalyzed HIE. Both *para*- and *ortho*-substituted alkyl substituent (**12a–14a**) showed good compatibility, exhibiting moderate to high levels of deuterium incorporation. The presence of an electron-donating group in *para*-position, such as methoxy- (**15a**), increased the deuterium incorporation to 86%D_γ. Furthermore, the applied reaction conditions demonstrated broad tolerance toward electron-deficient benzo[*d*]imidazole derivatives bearing C(sp^2)–X bonds (**16a–19a**) and a trifluoromethyl group (**20a**), while maintaining good *γ*-selectivity. It is noteworthy that benzo[*d*]imidazole derivatives containing pyridine- (**24a**) and furan- (**23a**) moieties were also well tolerated, yielding 54%D_γ and 88%D_γ, respectively. Moreover, sterically demanding benzo[*d*]imidazole derivatives bearing hydroxyl- (**25a**), ester- (**26a**), and amide- (**27a**) groups were further evaluated, displaying excellent deuterium incorporation (>85%D_γ). Furthermore, the challenging difunctionalized substrate **28a** was successfully converted under the optimized conditions (82%D_γ), highlighting the robustness of the developed protocol.

To further demonstrate the versatility of the developed system, we applied our Ru catalyst to the benzo[d]imidazole derivative **29a**, a known drug precursor for the synthesis of Telmisartan (AT1 receptor blocker). To our delight, efficient deuterium incorporation was achieved on a 400 mg scale, providing the ^{2}H-labeled product **29b** with 82%D_γ incorporation and no β-deuterium incorporation, and an isolated yield of 86%. Finally, compound **29b** was converted into deuterium-labeled Telmisartan via a two-step synthesis, affording 449 mg of the target drug molecule.

We extended our investigation of the HIE of 2-propyl-1*H*-benzo[*d*]imidazole derivatives by employing the optimized Ru catalyst (tripropyl phosphite, TPP) to achieve selective β-deuteration (**Scheme 3.15**, Method A). For the model substrate **1a**, excellent selectivity was observed, with 70%D_β and only 2%D_γ. While the catalyst exhibited limited selectivity for the *tert*-butyl- (**3c**) and fluoro- (**6c**) derivatives, high levels of β-deuteration were achieved (88%D and 72%D, respectively). In contrast, the methoxy- (**4c**) and chloro- (**5c**) derivatives displayed significantly better selectivity, further demonstrating the catalyst's efficiency (**Scheme 3.15**, Method A).

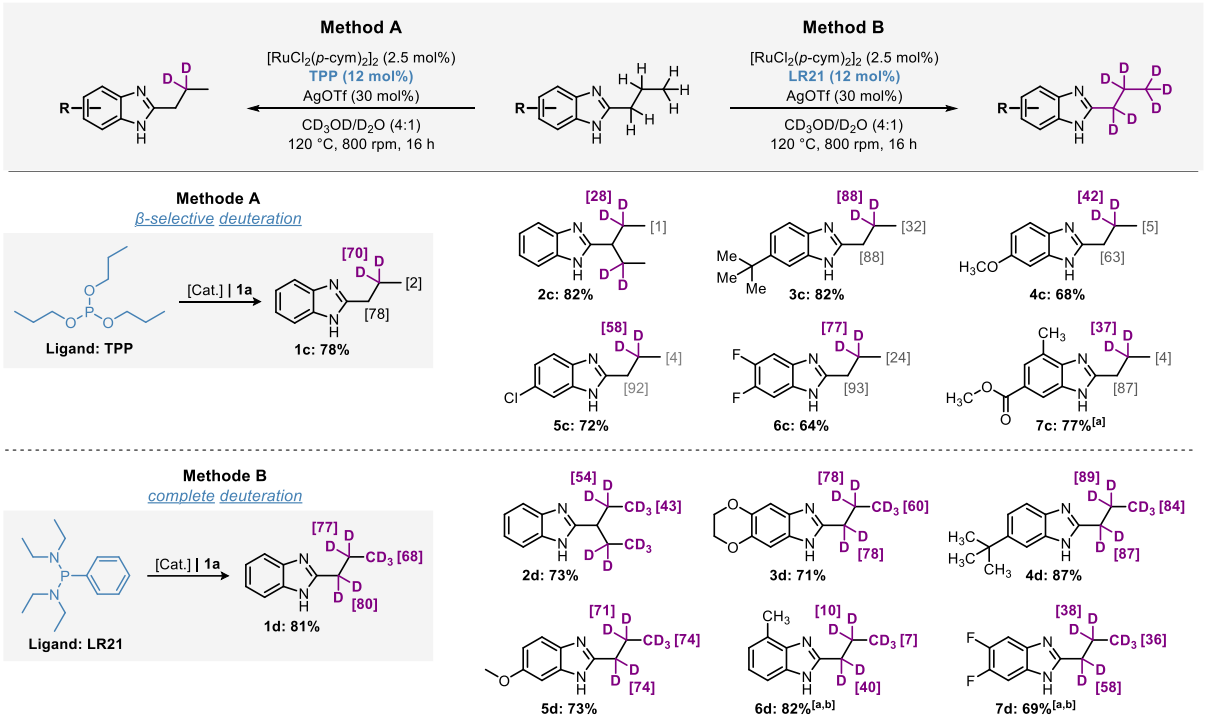

Scheme 3.15: Ru-catalyzed β -selective and complete deuterium labeling of benzo[*d*]imidazole derivatives. Values below the structures represent the isolated yield(s) of the deuterium labeled compounds. Standard reaction conditions: 0.5 mmol substrate, 2.5 mol% [Ru], 0.4 mL CD_3OD, 0.1 ml D_2O, 120 °C, 16 h. [a] Catalyst loading: 5 mol% [Ru]. [b] Reaction time: 48 h.

Finally, we investigated the complete deuteration of 2-propyl-1*H*-benzo[*d*]imidazole derivatives (**Scheme 3.15**, Method B). For substrate **1a**, we achieved a notable average deuterium incorporation of 75%D. A modest decrease in activity was observed for derivative **2d** with 58%D. High deuterium incorporation was achieved for the dioxane derivative **3d** (72%D), as well as the *tert*-butyl (**4d**, 87%D) and methoxy (**5d**, 73%D) substituted analogues. In contrast, substrate **6d**, bearing a methyl group in the *ortho* position, showed limited reactivity with the Ru catalyst.

In total, the developed catalytic system proved broadly applicable to benzimidazole derivatives, affording good to high levels of deuterium incorporation across *β*-, *γ*-, and fully deuterated products. The method's robustness and functional group tolerance underscore its potential for late-stage isotopic labeling of pharmaceutically relevant compounds. Furthermore, the integration of machine learning into catalyst design provided valuable structure–activity insights, highlighting how data-driven approaches can accelerate the development of Ru-based HIE methodologies.

4 Conclusion and Outlook

In this thesis, novel benzofurylphosphine ligands were developed that, in combination with Co precursors, form highly active and selective Co(0) catalysts for allylamine isomerization. These catalysts exhibit catalytic performance similar to that of Rh systems and enable scalable, industrially relevant transformations. In parallel, machine-learning-guided design of Ru catalysts further advanced site-selective deuterium labeling, demonstrating how data-driven ligand optimization can accelerate innovation in catalytic and medicinal chemistry.

Initially, a new class of monodentate benzofurylphosphine ligands has been synthesized. In combination with Co(II) acetylacetonate and DIBAL-H, the newly developed benzofurylphosphines generate Co(0) catalysts that isomerize structurally diverse aliphatic and aromatic allylamines into the corresponding enamines. These Co-based systems exhibit high activity and selectivity, comparable to state-of-the-art rhodium catalysts. Furthermore, the industrial relevance of these new Co *in situ* catalysts was demonstrated through successful scale-up experiments. Extensive mechanistic investigations–including deuterium labeling, radical trapping experiments, and kinetic studies –were conducted and revealed a π-allyl mechanism. The activity of the *in situ* generated Co(0) catalyst was found to correlate with the presence of furan-2-yl substituents on the phosphine ligand, while selectivity increased with a higher number of benzofuran-2-yl groups. These structure-activity correlations, together with the synthesized ligand library, provide a valuable platform for the design of next-generation catalysts. Since the Takasago process relies on asymmetric isomerization of allylamines, developing chiral benzofurylphosphine ligands could offer a promising strategy to replace Rh catalysts with a Co-based system.

Owing to the broad application of aromatic monodentate phosphines in catalysis, benzofurylphosphines represent an alternative structural motif with distinct electronic and steric properties that can enhance catalyst performance. This concept was demonstrated in the Pd-catalyzed telomerization of 1,3-butadiene to 1-methoxy-2,7-octadiene, where the use of (benzo-)furylphosphine ligands resulted in an increased activity compared to previously employed triphenylphosphine ligands.

Furthermore, a series of Ru-based catalysts has been synthesized and applied to the deuterium labeling of 2-propylbenzimidazole derivatives. The development of these catalytic systems was guided by a machine-learning framework, which enabled systematic, data-driven exploration of catalyst structures and reaction conditions. The refinement process revealed that phosphite and phosphinamine ligands were particularly effective, leading to Ru catalysts with improved selectivity. Through systematic optimization and iterative refinement of the catalytic systems, highly active Ru catalysts were obtained,

enabling site-selective β-, γ- and full deuteration of C(sp^3)–H bonds. Moreover, the generality of this methodology was demonstrated through its successful application to a broad range of benzimidazole derivatives, including pharmaceutically relevant compounds. Notably, the developed Ru catalysts afforded good-to-high levels of deuterium incorporation. These results establish a promising blueprint for analogous catalytic systems and illustrate how the integration of machine learning with catalyst design can drive innovative advances in medicinal and isotopic labeling chemistry.

5 List of Abbreviations

ΔG	difference of Gibbs free energy
^{i}Pr	*iso*-propyl
^{n}Bu	*n*-butyl
^{n}Pr	*n*-propyl
^{t}Bu	*tert*-butyl
2-MeTHF	2-methyltetrahydrofuran
acac	acetylacetonate
AcOH	acetic acid
Ad	adamantyl
AI	artificial intelligence
Ar	aryl
$BAr^{F}{}_{4}^{-}$	tetrakis(3,5-bis(trifluoromethyl)phenyl)borate
BINAP	[1,1-binaphthalene]-2,2-diyl)bis(diphenylphosphane)
cym	cymene
Cp	cyclopentadienyl
Cy	cyclohexyl
COD	cycloocta-1,5-diene
DCE	1,2-dichloroethane
DCM	dichloromethane
DFT	density-functional theory
dipp	2,6-diisopropylphenyl
ee	enantiomeric excess
EPR	electron paramagnetic resonance
Et	ethyl
et al.	et alii
equiv.	equivalent

GC	gas chromatography
L	ligand
Me	methyl
MeOH	methanol
MEA	ethanolamine
Mes	mesityl
MS	mass spectrometry
n.d.	not determined
NHC	*N*-heterocyclic carbene
NMR	nuclear magnetic resonance
Np	neopentyl
Ph	phenyl
R	(organic) rest
rt	room temperature
TEMPO	2,2,6,6-tetramethylpiperidinyloxyl
THF	tetrahydrofuran
XRD	X-ray diffraction

6 References

(1) Molloy, J. J.; Morack, T.; Gilmour, R. Positional and Geometrical Isomerisation of Alkenes: The Pinnacle of Atom Economy. *Angew. Chem. Int. Ed.* **2019**, *58* (39), 13654-13664.

(2) Neveselý, T.; Wienhold, M.; Molloy, J. J.; Gilmour, R. Advances in the E → Z Isomerization of Alkenes Using Small Molecule Photocatalysts. *Chem. Rev.* **2022**, *122* (2), 2650-2694.

(3) Kiser, P. D.; Golczak, M.; Palczewski, K. Chemistry of the Retinoid (Visual) Cycle. *Chem. Rev.* **2014**, *114* (1), 194-232.

(4) Terakita, A. The opsins. *Genome Biol.* **2005**, *6* (3), 213.

(5) Lamb, T. D.; Pugh, E. N., Jr. Phototransduction, Dark Adaptation, and Rhodopsin Regeneration The Proctor Lecture. *Invest. Ophthalmol. Vis. Sci.* **2006**, *47* (12), 5138-5152.

(6) Kandori, H. Ion-pumping microbial rhodopsins. *Front. Mol. Biosci.* **2015**, *2, 52.*

(7) Palczewski, K.; Kumasaka, T.; Hori, T.; Behnke, C. A.; Motoshima, H.; Fox, B. A.; Trong, I. L.; Teller, D. C.; Okada, T.; Stenkamp, R. E.; et al. Crystal Structure of Rhodopsin: A G Protein-Coupled Receptor. *Science* **2000**, *289* (5480), 739-745.

(8) Janssen, U.; Fink, T.; Lichter, P.; Stoffel, W. Human Mitochondrial 3,2-trans-Enoyl-CoA Isomerase (DCI): Gene Structure and Localization to Chromosome 16p13.3. *Genomics* **1994**, *23* (1), 223-228.

(9) Wu, Z.; Wouters, J.; Poulter, C. D. Isopentenyl Diphosphate Isomerase. Mechanism-Based Inhibition by Diene Analogues of Isopentenyl Diphosphate and Dimethylallyl Diphosphate. *J. Am. Chem. Soc.* **2005**, *127* (49), 17433-17438.

(10) Wilton, D. C.; Rahimtula, A. D.; Akhtar, M. The reversibility of the Δ^8-cholestenol–Δ^7-cholestenol isomerase reaction in cholesterol biosynthesis. *Biochem. J.* **1969**, *114* (1), 71-73.

(11) Capell-Hattam, I. M.; Brown, A. J. Sterol Evolution: Cholesterol Synthesis in Animals Is Less a Required Trait Than an Acquired Taste. *Curr. Biol.* **2020**, *30* (15), R886-R888.

(12) Polekhina, G.; Board, P. G.; Blackburn, A. C.; Parker, M. W. Crystal Structure of Maleylacetoacetate Isomerase/Glutathione Transferase Zeta Reveals the Molecular Basis for Its Remarkable Catalytic Promiscuity. *Biochemistry* **2001**, *40* (6), 1567-1576.

(13) Seltzer, S.; Hane, J. Maleylacetoacetate cis-trans isomerase: One-step double cis-trans isomerization of monomethyl muconate and the enzyme's probable role in benzene metabolism. *Bioorg. Chem.* **1988**, *16* (4), 394-407.

(14) Kim, J.; Toro, R.; Bhosle, R.; Al Obaidi, N. F.; Morisco, L. L.; Wasserman, S. R.; Sojitra, S.; Washington, E.; Scott Glenn, A.; Chowdhury, S.; et al. Crystal structure of Maleylacetoacetate isomerase from Anaeromyxobacter dehalogenans 2CP-1, target EFI-507175. **2013**.

(15) Massad, I.; Suresh, R.; Segura, L.; Marek, I. Stereoselective synthesis through remote functionalization. *Nat. Synth.* **2022**, *1* (1), 37-48.

(16) Massad, I.; Marek, I. Alkene Isomerization through Allylmetals as a Strategic Tool in Stereoselective Synthesis. *ACS Catal.* **2020**, *10* (10), 5793-5804.

(17) Zhang, S.; Findlater, M. Cobalt-Catalyzed Isomerization of Alkenes. *Synthesis* **2021**, *53* (16), 2787-2797.

(18) Liu, X.; Liu, Q. Catalytic asymmetric olefin isomerization: Facile access to chiral carbon-stereogenic olefinic compounds. *Chem Catal.* **2022**, *2* (11), 2852-2864.

(19) Anastas, P. T.; Warner, J. C. *Green Chemistry: Theory and Practice*; Oxford University Press, 1998.

(20) Obeid, A.-H.; Hannedouche, J. Iron-Catalyzed Positional and Geometrical Isomerization of Alkenes. *Adv. Synth. Catal.* **2023**, *365* (8), 1100-1111.

(21) Liu, C.-F.; Wang, H.; Martin, R. T.; Zhao, H.; Gutierrez, O.; Koh, M. J. Olefin functionalization/isomerization enables stereoselective alkene synthesis. *Nat. Catal.* **2021**, *4* (8), 674-683.

(22) Liu, X.; Zhang, W.; Wang, Y.; Zhang, Z. X.; Jiao, L.; Liu, Q. Cobalt-Catalyzed Regioselective Olefin Isomerization Under Kinetic Control. *J. Am. Chem. Soc.* **2018**, *140* (22), 6873-6882.

(23) Meek, J. S. The determination of a mechanism of isomerization of maleic acid to fumaric acid. *J. Chem. Educ.* **1975**, *52* (8), 541.

(24) Bank, S.; Schriesheim, A.; Rowe, C. A., Jr. An Understanding of the Stereoselectivity of Base-Catalyzed Olefin Isomerization Based on a Thermodynamically More Stable cis-Allylic Anion. *J. Am. Chem. Soc.* **1965**, *87* (14), 3244-3245.

(25) McGrath, D. V.; Grubbs, R. H. The mechanism of aqueous ruthenium(II)-catalyzed olefin isomerization. *Organometallics* **1994**, *13* (1), 224-235.

(26) Mantilli, L.; Mazet, C. Iridium-catalyzed isomerization of primary allylic alcohols under mild reaction conditions. *Tetrahedron Lett.* **2009**, *50* (28), 4141-4144.

(27) Perdriau, S.; Chang, M.-C.; Otten, E.; Heeres, H. J.; de Vries, J. G. Alkene Isomerisation Catalysed by a Ruthenium PNN Pincer Complex. *Chem. Eur. J.* **2014**, *20* (47), 15434-15442.

(28) Becica, J.; Glaze, O. D.; Wozniak, D. I.; Dobereiner, G. E. Selective Isomerization of Terminal Alkenes to (*Z*)-2-Alkenes Catalyzed by an Air-Stable Molybdenum(0) Complex. *Organometallics* **2018**, *37* (3), 482-490.

(29) Wang, Y.; Qin, C.; Jia, X.; Leng, X.; Huang, Z. An Agostic Iridium Pincer Complex as a Highly Efficient and Selective Catalyst for Monoisomerization of 1-Alkenes to trans-2-Alkenes. *Angew. Chem. Int. Ed.* **2017**, *56* (6), 1614-1618.

(30) Larsen, C. R.; Grotjahn, D. B. Stereoselective alkene isomerization over one position. *J. Am. Chem. Soc.* **2012**, *134* (25), 10357-10360.

(31) Gauthier, D.; Lindhardt, A. T.; Olsen, E. P. K.; Overgaard, J.; Skrydstrup, T. In Situ Generated Bulky Palladium Hydride Complexes as Catalysts for the Efficient Isomerization of Olefins. Selective Transformation of Terminal Alkenes to 2-Alkenes. *J. Am. Chem. Soc.* **2010**, *132* (23), 7998-8009.

(32) Schmidt, A.; Nödling, A. R.; Hilt, G. An Alternative Mechanism for the Cobalt-Catalyzed Isomerization of Terminal Alkenes to (*Z*)-2-Alkenes. *Angew. Chem. Int. Ed.* **2015**, *54* (3), 801-804.

(33) Tani, K.; Yamagata, T.; Akutagawa, S.; Kumobayashi, H.; Taketomi, T.; Takaya, H.; Miyashita, A.; Noyori, R.; Otsuka, S. Metal-assisted terpenoid synthesis. 7. Highly enantioselective isomerization of prochiral allylamines catalyzed by chiral diphosphine rhodium(I) complexes. Preparation of optically active enamines. *J. Am. Chem. Soc.* **1984**, *106* (18), 5208-5217.

(34) Dylong, D.; Hausoul, P. J. C.; Palkovits, R.; Eisenacher, M. Synthesis of (−)-menthol: Industrial synthesis routes and recent development. *Flavour Fragr. J.* **2022**, *37* (4), 195-209.

(35) Inoue, S.; Takaya, H.; Tani, K.; Otsuka, S.; Sato, T.; Noyori, R. Mechanism of the asymmetric isomerization of allylamines to enamines catalyzed by 2,2'-bis(diphenylphosphino)-1,1'binaphthyl-rhodium complexes. *J. Am. Chem. Soc.* **1990**, *112* (12), 4897-4905.

(36) Tani, K. Asymmetric isomerization of allylic compounds and the mechanism. *Pure Appl. Chem.* **1985**, *57* (12), 1845-1854.

(37) Tanaka, K.; Qiao, S.; Tobisu, M.; Lo, M. M. C.; Fu, G. C. Enantioselective Isomerization of Allylic Alcohols Catalyzed by a Rhodium/Phosphaferrocene Complex. *J. Am. Chem. Soc.* **2000**, *122* (40), 9870-9871.

(38) Tanaka, K.; Fu, G. C. A Versatile New Catalyst for the Enantioselective Isomerization of Allylic Alcohols to Aldehydes: Scope and Mechanistic Studies. *J. Org. Chem.* **2001**, *66* (24), 8177-8186.

(39) Doppiu, A.; Salzer, A. A New Route to Cationic Half-Sandwich Ruthenium(II) Complexes with Chiral Cyclopentadienylphosphane Ligands. *Eur. J. Inorg. Chem.* **2004**, (11), 2244-2252.

(40) Mantilli, L.; Gerard, D.; Torche, S.; Besnard, C.; Mazet, C. Iridium-catalyzed asymmetric isomerization of primary allylic alcohols. *Angew. Chem. Int. Ed.* **2009**, *48* (28), 5143-5147.

(41) Li, H.; Mazet, C. Catalyst-Directed Diastereoselective Isomerization of Allylic Alcohols for the Stereoselective Construction of C(20) in Steroid Side Chains: Scope and Topological Diversification. *J. Am. Chem. Soc.* **2015**, *137* (33), 10720-10727.

(42) Arai, N.; Sato, K.; Azuma, K.; Ohkuma, T. Enantioselective Isomerization of Primary Allylic Alcohols into Chiral Aldehydes with the tol-binap/dbapen/Ruthenium(II) Catalyst. *Angew. Chem. Int. Ed.* **2013**, *52* (29), 7500-7504.

(43) Grotjahn, D. B.; Larsen, C. R.; Gustafson, J. L.; Nair, R.; Sharma, A. Extensive Isomerization of Alkenes Using a Bifunctional Catalyst: An Alkene Zipper. *J. Am. Chem. Soc.* **2007**, *129* (31), 9592-9593.

(44) Lin, L.; Romano, C.; Mazet, C. Palladium-Catalyzed Long-Range Deconjugative Isomerization of Highly Substituted α,β-Unsaturated Carbonyl Compounds. *J. Am. Chem. Soc.* **2016**, *138* (32), 10344-10350.

(45) Kress, S.; Johnson, T.; Weisshar, F.; Lautens, M. Synthetic and Mechanistic Studies on the Rhodium-Catalyzed Redox Isomerization of Cyclohexa-2,5-dienols. *ACS Catal.* **2016**, *6* (2), 747-750.

(46) Liu, T. L.; Ng, T. W.; Zhao, Y. Rhodium-Catalyzed Enantioselective Isomerization of Secondary Allylic Alcohols. *J. Am. Chem. Soc.* **2017**, *139* (10), 3643-3646.

(47) Hendrix, W. T.; Von Rosenberg, J. L. The mechanism of the rearrangement of the hydrocobalt carbonyl catalyzed isomerization of 3-phenylpropene. *J. Am. Chem. Soc.* **1976**, *98* (16), 4850-4852.

(48) Satyanarayana, N.; Periasamy, M. Isomerization of olefins catalysed by a $CoCl_2/Ph_3P/NaBH_4$ system. *J. Organomet. Chem.* **1987**, *319* (1), 113-117.

(49) Kobayashi, T.; Yorimitsu, H.; Oshima, K. Cobalt-Catalyzed Isomerization of 1-Alkenes to (*E*)-2-Alkenes with Dimethylphenylsilylmethylmagnesium Chloride and Its Application to the Stereoselective Synthesis of (*E*)-Alkenylsilanes. *Chem. Asian J.* **2009**, *4* (7), 1078-1083.

(50) Chen, C.; Dugan, T. R.; Brennessel, W. W.; Weix, D. J.; Holland, P. L. *Z*-Selective Alkene Isomerization by High-Spin Cobalt(II) Complexes. *J. Am. Chem. Soc.* **2014**, *136* (3), 945-955.

(51) Kim, D.; Pillon, G.; DiPrimio, D. J.; Holland, P. L. Highly *Z*-Selective Double Bond Transposition in Simple Alkenes and Allylarenes through a Spin-Accelerated Allyl Mechanism. *J. Am. Chem. Soc.* **2021**, *143* (8), 3070-3074.

(52) Crossley, S. W. M.; Barabé, F.; Shenvi, R. A. Simple, Chemoselective, Catalytic Olefin Isomerization. *J. Am. Chem. Soc.* **2014**, *136* (48), 16788-16791.

(53) Li, G.; Kuo, J. L.; Han, A.; Abuyuan, J. M.; Young, L. C.; Norton, J. R.; Palmer, J. H. Radical Isomerization and Cycloisomerization Initiated by H• Transfer. *J. Am. Chem. Soc.* **2016**, *138* (24), 7698-7704.

(54) Delgado, K. R.; Youmans, D. D.; Diver, S. T. Mild Isomerization of Conjugated Dienes Using Co-Mediated Hydrogen Atom Transfer. *Org. Lett.* **2020**, *22* (2), 750-754.

(55) Zhang, S.; Bedi, D.; Cheng, L.; Unruh, D. K.; Li, G.; Findlater, M. Cobalt(II)-Catalyzed Stereoselective Olefin Isomerization: Facile Access to Acyclic Trisubstituted Alkenes. *J. Am. Chem. Soc.* **2020**, *142* (19), 8910-8917.

(56) Liu, H.; Cai, C.; Ding, Y.; Chen, J.; Liu, B.; Xia, Y. Cobalt-Catalyzed *E*-Selective Isomerization of Alkenes with a Phosphine-Amido-Oxazoline Ligand. *ACS Omega* **2020**, *5* (20), 11655-11670.

(57) Huang, G.; Ke, M.; Tao, Y.; Chen, F. Specific *Z*-Selectivity in the Oxidative Isomerization of Allyl Ethers to Generate Geometrically Defined *Z*-Enol Ethers Using a Cobalt(II)(salen) Complex Catalyst. *J. Org. Chem.* **2020**, *85* (8), 5321-5329.

(58) Li, N.; You, M.; Qiu, X.; Deng, M.; Kang, G.; Liu, H.; Deng, S.-Z.; Ji, B. Cobalt-Catalyzed Chemoselective Isomerization of 2-Substituted Allyl Ethers Induced by Hydrogen Atom Transfer. *Asian J. Org. Chem.* **2022**, *11* (11), e202200488.

(59) Raje, S.; Garhwal, S.; Młodzikowska-Pieńko, K.; Sheikh Mohammad, T.; Raphaeli, R.; Fridman, N.; Shimon, L. J. W.; Gershoni-Poranne, R.; de Ruiter, G. N_2 Dissociation vs Reversible 1,2-Methyl Migration in $PC_{NHC}P$ Cobalt(I) Complexes in the Stereoselective Isomerization (*E*/*Z*) of Allyl Ethers. *JACS Au* **2024**, *4* (11), 4234-4248.

(60) Kumobayashi, H.; Akutagawa, S.; Otsuka, S. Metal-assisted terpenoid syntheses. 6. Enantioselective hydrogen migration in prochiral allylamine systems by chiral cobalt catalysts. *J. Am. Chem. Soc.* **1978**, *100* (12), 3949-3950.

(61) Raje, S.; Sheikh Mohammad, T.; de Ruiter, G. A Neutral $PC_{NHC}P$ Co(I)–Me Pincer Complex as a Catalyst for *N*-Allylic Isomerization with a Broad Substrate Scope. *J. Org. Chem.* **2024**, *89* (7), 4319-4325.

(62) Motokura, K.; Nakayama, K.; Miyaji, A.; Baba, T. "Ligand-Consuming" Formation of Rhodium-Hydride Species from $[Rh(OH)(cod)]_2$ Without any Additional Hydride Sources for Catalytic Olefin Isomerizations and Cyclobutene Synthesis. *ChemCatChem* **2011**, *3* (9), 1419-1421.

(63) Sanz-Navarro, S.; Mon, M.; Domenech-Carbo, A.; Greco, R.; Sanchez-Quesada, J.; Espinos-Ferri, E.; Leyva-Perez, A. Parts-per-million of ruthenium catalyze the selective chain-walking reaction of terminal alkenes. *Nat. Commun.* **2022**, *13* (1), 2831.

(64) Kapat, A.; Sperger, T.; Guven, S.; Schoenebeck, F. *E*-Olefins through intramolecular radical relocation. *Science* **2019**, *363* (6425), 391-396.

(65) Woof, C. R.; Durand, D. J.; Fey, N.; Richards, E.; Webster, R. L. Iron Catalyzed Double Bond Isomerization: Evidence for an Fe(I)/Fe(III) Catalytic Cycle. *Chem. Eur. J.* **2021**, *27* (19), 5972-5977.

(66) Blaha, I.; Weber, S.; Dülger, R.; Veiros, L. F.; Kirchner, K. Alkene Isomerization Catalyzed by a Mn(I) Bisphosphine Borohydride Complex. *ACS Catal.* **2024**, *14* (17), 13174-13180.

(67) Jiayan Du, J. L., Guixia Liu, Zheng Huang. Cobalt-Catalyzed Regio- and Stereoselective Isomerization of Terminal Alkenes to *trans*-2-Alkenes. *Chin. J. Org. Chem.* **2024**, *44* (9), 2889-2897.

(68) Meuwly, M. Machine Learning for Chemical Reactions. *Chem. Rev.* **2021**, *121* (16), 10218-10239.

(69) Tu, Z.; Stuyver, T.; Coley, C. W. Predictive chemistry: machine learning for reaction deployment, reaction development, and reaction discovery. *Chem. Sci.* **2023**, *14* (2), 226-244.

(70) Chen, Y.; Feng, J.; Wang, X.; Zhang, C.; Ke, D.; Zhu, H.; Wang, S.; Suo, H.; Liu, C. Iterative Approach of Experiment–Machine Learning for Efficient Optimization of Environmental Catalysts: An Example of NOx Selective Reduction Catalysts. *Environ. Sci. Technol.* **2023**, *57* (46), 18080-18090.

(71) Strieth-Kalthoff, F.; Sandfort, F.; Kühnemund, M.; Schäfer, F. R.; Kuchen, H.; Glorius, F. Machine Learning for Chemical Reactivity: The Importance of Failed Experiments. *Angew. Chem. Int. Ed.* **2022**, *61* (29), e202204647.

(72) Bajorath, J. Integration of virtual and high-throughput screening. *Nat. Rev. Drug Discov.* **2002**, *1* (11), 882-894.

(73) Benavides-Hernández, J.; Dumeignil, F. From Characterization to Discovery: Artificial Intelligence, Machine Learning and High-Throughput Experiments for Heterogeneous Catalyst Design. *ACS Catal.* **2024**, *14* (15), 11749-11779.

(74) Pflüger, P. M.; Kühnemund, M.; Katzenburg, F.; Kuchen, H.; Glorius, F. An evolutionary algorithm for interpretable molecular representations. *Chem* **2024**, *10* (5), 1391-1405.

(75) Dalmau, D.; Sigman, M. S.; Alegre-Requena, J. V. Machine learning workflows beyond linear models in low-data regimes. *Chem. Sci.* **2025**, *16* (19), 8555-8560.

(76) Strieth-Kalthoff, F.; Sandfort, F.; Segler, M. H. S.; Glorius, F. Machine learning the ropes: principles, applications and directions in synthetic chemistry. *Chem. Soc. Rev.* **2020**, *49* (17), 6154-6168.

(77) Schrader, M. L.; Schäfer, F. R.; Schäfers, F.; Glorius, F. Bridging the information gap in organic chemical reactions. *Nat. Chem.* **2024**, *16* (4), 491-498.

(78) Kitchin, J. R. Machine learning in catalysis. *Nat. Catal.* **2018**, *1* (4), 230-232.

(79) Ahneman, D. T.; Estrada, J. G.; Lin, S.; Dreher, S. D.; Doyle, A. G. Predicting reaction performance in C–N cross-coupling using machine learning. *Science* **2018**, *360* (6385), 186-190.

(80) Pflüger, P. M.; Glorius, F. Molecular Machine Learning: The Future of Synthetic Chemistry? *Angew. Chem. Int. Ed.* **2020**, *59* (43), 18860-18865.

(81) Abraham, B. M.; Jyothirmai, M. V.; Sinha, P.; Viñes, F.; Singh, J. K.; Illas, F. Catalysis in the digital age: Unlocking the power of data with machine learning. *Rev. Comput. Mol. Sci.* **2024**, *14* (5), e1730.

(82) Lim, H. N.; Shin, I.; Hong, W. P. Recent Advances in Transition Metal-Catalyzed Multideuteration of (Hetero)Arenes via Hydrogen Isotope Exchange. *Eur. J. Org. Chem.* **2025**, *28* (23), e202500236.

(83) Michelotti, A.; Roche, M. 40 Years of Hydrogen–Deuterium Exchange Adjacent to Heteroatoms: A Survey. *Synthesis* **2019**, *51* (06), 1319-1328.

(84) Atzrodt, J.; Derdau, V.; Fey, T.; Zimmermann, J. The Renaissance of H/D Exchange. *Angew. Chem. Int. Ed.* **2007**, *46* (41), 7744-7765.

(85) Di Martino, R. M. C.; Maxwell, B. D.; Pirali, T. Deuterium in drug discovery: progress, opportunities and challenges. *Nat. Rev. Drug Discov.* **2023**, *22* (7), 562-584.

(86) Kopf, S.; Bourriquen, F.; Li, W.; Neumann, H.; Junge, K.; Beller, M. Recent Developments for the Deuterium and Tritium Labeling of Organic Molecules. *Chem. Rev.* **2022**, *122* (6), 6634-6718.

(87) Li, L.; Jakowski, J.; Do, C.; Hong, K. Deuteration and Polymers: Rich History with Great Potential. *Macromolecules* **2021**, *54* (8), 3555-3584.

(88) Cai, Z.; Yan, W.; Guo, R.; Liu, H.; Huo, P.; Yu, G.; Bian, Z.; Liu, Z. Warm-White-Light Perdeuterated Dy(III) Complex with a Photoluminescence Quantum Yield of up to 72% in Deuterated Chloroform. *Inorg. Chem.* **2023**, *62* (17), 6560-6564.

(89) Dong, X.; Shen, S.; Qin, Y.; Xie, X.; Pang, Z.; Gao, H.; Liu, G.; Lee, C.-S.; Wang, P.; Wang, Y. Novel Deuterated Benzothiadiazole Derivatives with Enhancing High-Lying Reverse Intersystem Crossing for High-Efficiency Organic Light-Emitting Diodes. *J. Phys. Chem. C* **2024**, *128* (2), 974-983.

(90) Stinglhamer, M.; Kuhlmann, J. H.; Martinelli, E.; Perulli, S.; Sandvoss, M.; Mück-Lichtenfeld, C.; Derdau, V.; García Mancheño, O. Site-selective Photoredox-Catalyzed Late-stage Benzylic Hydrogen Isotope Exchange. *Angew. Chem. Int. Ed.* **2024**, *63* (50), e202411567.

(91) Kerr, W. J.; Knox, G. J.; Paterson, L. C. Recent advances in iridium(I) catalysis towards directed hydrogen isotope exchange. *J. Labelled Compd. Radiopharm.* **2020**, *63* (6), 281-295.

(92) Herbert, J. M. Deuterium exchange promoted by iridium complexes formed *in situ*. *J. Labelled Compd. Radiopharm.* **2010**, *53* (11-12), 658-661.

(93) Hesk, D.; Das, P. R.; Evans, B. Deuteration of acetanilides and other substituted aromatics using [Ir(COD)(Cy_3P)(Py)]PF_6 as catalyst. *J. Labelled Compd. Radiopharm.* **1995**, *36* (5), 497-502.

(94) Ellames, G. J.; Gibson, J. S.; Herbert, J. M.; McNeill, A. H. The scope and limitations of deuteration mediated by Crabtree's catalyst. *Tetrahedron* **2001**, *57* (46), 9487-9497.

(95) Brown, J. A.; Irvine, S.; Kennedy, A. R.; Kerr, W. J.; Andersson, S.; Nilsson, G. N. Highly active iridium(i) complexes for catalytic hydrogen isotope exchange. *Chem. Commun.* **2008**, (9), 1115-1117.

(96) Nilsson, G. N.; Kerr, W. J. The development and use of novel iridium complexes as catalysts for ortho-directed hydrogen isotope exchange reactions. *J. Labelled Compd. Radiopharm.* **2010**, *53* (11-12), 662-667.

(97) Cochrane, A. R.; Irvine, S.; Kerr, W. J.; Reid, M.; Andersson, S.; Nilsson, G. N. Application of neutral iridium(I) N-heterocyclic carbene complexes in ortho-directed hydrogen isotope exchange. *J. Labelled Compd. Radiopharm.* **2013**, *56* (9-10), 451-454.

(98) Kerr, W. J.; Knox, G. J.; Reid, M.; Tuttle, T. Catalyst design in C–H activation: a case study in the use of binding free energies to rationalise intramolecular directing group selectivity in iridium catalysis. *Chem. Sci.* **2021**, *12* (19), 6747-6755.

(99) Cross, P. W. C.; Herbert, J. M.; Kerr, W. J.; McNeill, A. H.; Paterson, L. C. Isotopic Labelling of Functionalised Arenes Catalysed by Iridium(I) Species of the [(cod)Ir(NHC)(py)]PF_6 Complex Class. *Synlett* **2016**, *27* (01), 111-115.

(100) Parmentier, M.; Hartung, T.; Pfaltz, A.; Muri, D. Iridium-Catalyzed H/D Exchange: Ligand Complexes with Improved Efficiency and Scope. *Chem. Eur. J.* **2014**, *20* (36), 11496-11504.

(101) Jess, K.; Derdau, V.; Weck, R.; Atzrodt, J.; Freytag, M.; Jones, P. G.; Tamm, M. Hydrogen Isotope Exchange with Iridium(I) Complexes Supported by Phosphine-Imidazolin-2-imine P,N Ligands. *Adv. Synth. Catal.* **2017**, *359* (4), 629-638.

(102) Kerr, W. J.; Knox, G. J.; Reid, M.; Tuttle, T.; Bergare, J.; Bragg, R. A. Computationally-Guided Development of a Chelated NHC-P Iridium(I) Complex for the Directed Hydrogen Isotope Exchange of Aryl Sulfones. *ACS Catal.* **2020**, *10* (19), 11120-11126.

(103) Valero, M.; Weck, R.; Güssregen, S.; Atzrodt, J.; Derdau, V. Highly Selective Directed Iridium-Catalyzed Hydrogen Isotope Exchange Reactions of Aliphatic Amides. *Angew. Chem. Int. Ed.* **2018**, *57* (27), 8159-8163.

(104) Devlin, J.; Kerr, W. J.; Lindsay, D. M.; McCabe, T. J. D.; Reid, M.; Tuttle, T. Iridium-Catalysed ortho-Directed Deuterium Labelling of Aromatic Esters–An Experimental and Theoretical Study on Directing Group Chemoselectivity. *Molecules* **2015**, *20* (7), 11676-11698.

(105) Krüger, J.; Manmontri, B.; Fels, G. Iridium-Catalyzed H/D Exchange. *Eur. J. Org. Chem.* **2005**, (7), 1402-1408.

(106) Kerr, W. J.; Mudd, R. J.; Owens, P. K.; Reid, M.; Brown, J. A.; Campos, S. Hydrogen isotope exchange with highly active iridium(I) NHC/phosphine complexes: a comparative counterion study. *J. Labelled Compd. Radiopharm.* **2016**, *59* (14), 601-603.

(107) Brown, J. A.; Cochrane, A. R.; Irvine, S.; Kerr, W. J.; Mondal, B.; Parkinson, J. A.; Paterson, L. C.; Reid, M.; Tuttle, T.; Andersson, S.; et al. The Synthesis of Highly Active Iridium(I) Complexes and their Application in Catalytic Hydrogen Isotope Exchange. *Adv. Synth. Catal.* **2014**, *356* (17), 3551-3562.

(108) Lockley, W. J. S. Hydrogen isotope labelling using iridium(I) dionates. *J. Labelled Compd. Radiopharm.* **2010**, *53* (11-12), 668-673.

(109) Cochrane, A. R.; Idziak, C.; Kerr, W. J.; Mondal, B.; Paterson, L. C.; Tuttle, T.; Andersson, S.; Nilsson, G. N. Practically convenient and industrially-aligned methods for iridium-catalysed hydrogen isotope exchange processes. *Org. Biomol. Chem.* **2014**, *12* (22), 3598-3603.

(110) Atzrodt, J.; Derdau, V.; Kerr, W. J.; Reid, M.; Rojahn, P.; Weck, R. Expanded applicability of iridium(I) NHC/phosphine catalysts in hydrogen isotope exchange processes with pharmaceutically-relevant heterocycles. *Tetrahedron* **2015**, *71* (13), 1924-1929.

(111) Kerr, W. J.; Lindsay, D. M.; Reid, M.; Atzrodt, J.; Derdau, V.; Rojahn, P.; Weck, R. Iridium-catalysed ortho-H/D and -H/T exchange under basic conditions: C–H activation of unprotected tetrazoles. *Chem. Commun.* **2016**, *52* (40), 6669-6672.

(112) Burhop, A.; Prohaska, R.; Weck, R.; Atzrodt, J.; Derdau, V. Burgess iridium(I)-catalyst for selective hydrogen isotope exchange. *J. Labelled Compd. Radiopharm.* **2017**, *60* (7), 343-348.

(113) Jiang, Z.-J.; Bai, J.-F.; Gao, Z. Transition-Metal-Catalyzed Deuteration via Hydrogen Isotope Exchange. *SynOpen* **2024**, *08* (04), 328-359.

(114) Chen, S.; Song, G.; Li, X. Chelation-assisted rhodium hydride-catalyzed regioselective H/D exchange in arenes. *Tetrahedron Lett.* **2008**, *49* (48), 6929-6932.

(115) Mai, V. H.; Gadzhiev, O. B.; Ignatov, S. K.; Nikonov, G. I. H/D exchange in N-heterocycles catalysed by an NHC-supported ruthenium complex. *Catal. Sci. Technol.* **2019**, *9* (13), 3398-3407.

(116) Wu, J.; Qian, B.; Lu, L.; Yang, H.; Shang, Y.; Zhang, J. Access to the C2 C–H olefination, alkylation and deuteration of indoles by rhodium(iii) catalysis: an opportunity for diverse syntheses. *Org. Chem. Front.* **2021**, *8* (12), 3032-3040.

(117) Müller, V.; Weck, R.; Derdau, V.; Ackermann, L. Ruthenium(II)-Catalyzed Hydrogen Isotope Exchange of Pharmaceutical Drugs by C–H Deuteration and C–H Tritiation. *ChemCatChem* **2020**, *12* (1), 100-104.

(118) Teja, C.; Kolb, S.; Colonna, P.; Grover, J.; Garcia-Argote, S.; Lahiri, G. K.; Pieters, G.; Werz, D. B.; Maiti, D. Deuteration and Tritiation of Pharmaceuticals by Non-Directed Palladium-Catalyzed C–H Activation in Heavy and Super-Heavy Water. *Angew. Chem. Int. Ed.* **2024**, *63* (48), e202410162.

(119) Bag, S.; Petzold, M.; Sur, A.; Bhowmick, S.; Werz, D. B.; Maiti, D. Palladium-Catalyzed Selective meta-C–H Deuteration of Arenes: Reaction Design and Applications. *Chem. Eur. J.* **2019**, *25* (40), 9433-9437.

(120) Xu, H.; Liu, M.; Li, L.-J.; Cao, Y.-F.; Yu, J.-Q.; Dai, H.-X. Palladium-Catalyzed Remote meta-C–H Bond Deuteration of Arenes Using a Pyridine Template. *Org. Lett.* **2019**, *21* (12), 4887-4891.

(121) Li, N.; Li, J.; Qin, M.; Li, J.; Han, J.; Zhu, C.; Li, W.; Xie, J. Highly selective single and multiple deuteration of unactivated C(sp^3)-H bonds. *Nat. Commun.* **2022**, *13* (1), 4224.

(122) Kang, Q.-K.; Li, Y.; Chen, K.; Zhu, H.; Wu, W.-Q.; Lin, Y.; Shi, H. Rhodium-Catalyzed Stereoselective Deuteration of Benzylic C–H Bonds via Reversible η^6-Coordination. *Angew. Chem. Int. Ed.* **2022**, *61* (11), e202117381.

(123) Neubert, L.; Michalik, D.; Bähn, S.; Imm, S.; Neumann, H.; Atzrodt, J.; Derdau, V.; Holla, W.; Beller, M. Ruthenium-Catalyzed Selective α,β-Deuteration of Bioactive Amines. *J. Am. Chem. Soc.* **2012**, *134* (29), 12239-12244.

(124) Tse, S. K. S.; Xue, P.; Lau, C. W. S.; Sung, H. H. Y.; Williams, I. D.; Jia, G. Ruthenium-Catalyzed Regioselective Deuteration of Alcohols at the β-Carbon Position with Deuterium Oxide. *Chem. Eur. J.* **2011**, *17* (49), 13918-13925.

(125) Chatterjee, B.; Gunanathan, C. Ruthenium Catalyzed Selective α- and α,β-Deuteration of Alcohols Using D_2O. *Org. Lett.* **2015**, *17* (19), 4794-4797.

(126) Hale, L. V. A.; Szymczak, N. K. Stereoretentive Deuteration of α-Chiral Amines with D_2O. *J. Am. Chem. Soc.* **2016**, *138* (41), 13489-13492.

(127) Ahrens, S.; Kusy, R.; Spannenberg, A.; Vuong, T. H.; Rabeah, J.; Russbueldt, B. M. E.; Panten, J.; Jiao, H.; Junge, K.; Beller, M. Cobalt(0)-Catalyzed Isomerization of Allylamines Promoted by Monodentate Benzofuran Phosphines. *J. Am. Chem. Soc.* **2025**, *147* (35), 31859-31870.

(128) Souza, E. L. S. d.; Ahrens, S.; Spannenberg, A.; Neumann, H.; Junge, K.; Correia, C. R. D.; Jackstell, R.; Beller, M. Development of highly efficient and selective palladium catalysts for telomerization of 1,3-butadiene with alcohols. *Chem. Commun.* **2025**, *61* (50), 9083-9086.

7 Published Articles

This chapter contains the original publications of the research presented in this thesis. The author's contribution to each publication is outlined.

7.1 Cobalt(0)-Catalyzed Isomerization of Allylamines Promoted by Monodentate Benzofuran Phosphines

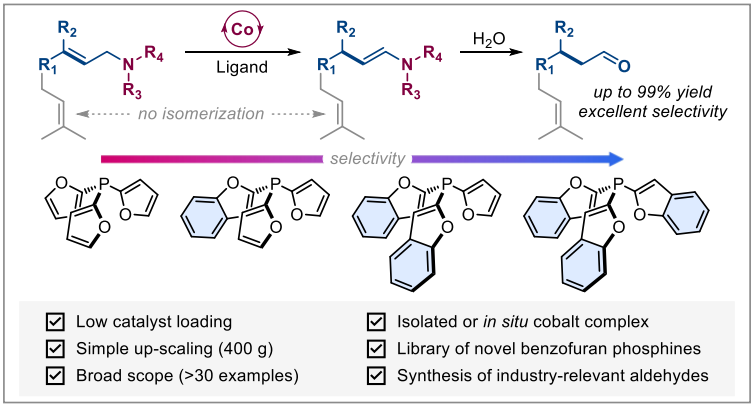

Ahrens, S.; Kusy, R.; Spannenberg, A.; Vuong, T. H.; Rabeah, J.; Rußbüldt, B. M. E.; Panten, J.; Jiao, H.; Junge, K.; Beller, M. *J. Am. Chem. Soc.* **2025**, *147* (35), 31859-31870.

DOI: 10.1021/jacs.5c09017. Electronic supporting information is available online.

Author's Contribution

The author conceptualized and designed the project. The author synthesized and characterized ligands and complexes, optimized reaction conditions, evaluated substrate scope, and conducted catalytic and mechanistic experiments. Furthermore, the author prepared the initial manuscript and supporting information. The author's contribution approximately accounts 80%.

Sebastian Ahrens
(PhD student)

Prof. Matthias Beller
(Supervisor)

JACS
JOURNAL OF THE AMERICAN CHEMICAL SOCIETY
pubs.acs.org/JACS

Open Access
This article is licensed under CC-BY 4.0

Article

Cobalt(0)-Catalyzed Isomerization of Allylamines Promoted by Monodentate Benzofuran Phosphines

Sebastian Ahrens, Rafał Kusy, Anke Spannenberg, Thanh H. Vuong, Jabor Rabeah, Bernhard M. E. Russbueldt, Johannes Panten,* Haijun Jiao,* Kathrin Junge,* and Matthias Beller*

Cite This: J. Am. Chem. Soc. 2025, 147, 31859−31870

Read Online

ACCESS | Metrics & More | Article Recommendations | Supporting Information

ABSTRACT: Isomerization of C−C double bonds is an efficient tool for converting bulk olefins into high-value compounds. Herein we describe a newly developed homogeneous cobalt-based system which enables the isomerization of allylamines to enamines with similar activity and selectivity to noble metal catalysts. The catalyst activity was bound to the presence of furan-2-yl substituents of the phosphine ligand, while the selectivity was increased with the number of benzofuran-2-yl groups. The resulting cobalt(0) catalysts allowed the isomerization of various aliphatic and aromatic allylamines, including the synthesis of industry-relevant products with high catalytic activity. Potential industrial application of our system was substantiated by the scale-up experiment, which provided 311 g of citronellal in 96% yield. We proposed a plausible mechanism based on EPR and NMR analysis combined with deuterium labeling, radical trapping experiments, and kinetic studies.

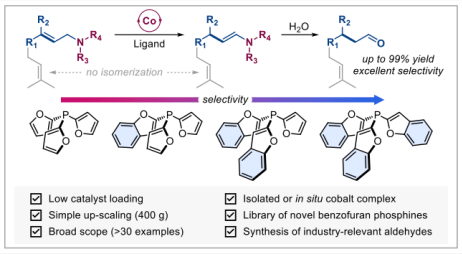

INTRODUCTION

Transition-metal-catalyzed isomerization of olefins is an atom- and energy-efficient transformation which enables conversion of accessible low-cost alkenes into higher-value products, which are in demand in pharmaceutical, food, flavor, and fragrance industries.[1] Although a wide range of systems for olefin isomerization has been reported in the last decades, the vast majority of efficient and industry-relevant catalysts are based on noble metals such as Pd,[2] Ir,[3] Pt,[4] and Ru.[5] However, more recently, the attention has shifted to base metals such as Fe,[6] Co,[7,8] and Ni,[9,10] due to their higher abundance, lower cost, and lower toxicity.[11]

In particular, the application of Co complexes as catalysts in olefin isomerization reactions is of growing interest (Scheme 1A). Liu (Scheme 1A1) and Findlater (Scheme 1A2) employed Co pincer complexes in the isomerization of methylenecyclohexane derivatives, allowing the stereoselective synthesis of trisubstituted alkenes.[12] In 2020, Diver reported a radical-triggered double isomerization of disubstituted-1,3-dienes catalyzed by cobaloxime complexes (Scheme 1A3).[13] In 2020, (*Z*)-selective isomerization of terminal olefins was disclosed by Holland (Scheme 1A4).[14] More recently, Lu presented a Co-catalyzed multipositional isomerization of conjugated dienes via a metal-hydride mechanism. While significant progress has been made in olefin isomerization, the application of Co-based catalysts remains limited to the transformation of relatively simple substrates, such as terminal or unfunctionalized olefins. In particular, the isomerization of internal olefins containing heteroatoms (O, N, or S), (e.g., the transformation of allylamines to enamines) remains a challenge for any base-metal catalyst.[15] Otsuka et al. reported isomerization of (*E*)-allylamines to the corresponding (*E*)-allylenamines catalyzed by Co(I)-hydride, but the presented scope was limited to two examples.[16]

In 2024, the group of de Ruiter developed a neutral $PC_{NHC}P$ Co(I)-pincer complex for the isomerization of terminal (*E*)-allylamines and (*E*)-allylamides (Scheme 1A5).[17] The importance of allylamine isomerization is reflected in the Takasago process, which allows menthol synthesis and constitutes one of the largest industrial applications of homogeneous asymmetric catalysis (Scheme 1B).[18] It encompasses the Rh-catalyzed isomerization of *N*,*N*-diethylgeranylamine (**1a**) to citronellal enamine (**1b**), which we chose as our model reaction. Herein, we report the development of a novel *in situ* generated Co(0) catalyst from tri(benzofuran-2-yl)phosphine as a ligand, which is capable of converting structurally diverse and industry-relevant aliphatic and aromatic allylamines into the corresponding enamines in up to quantitative yields (Scheme 1C).

Received: June 3, 2025
Revised: July 27, 2025
Accepted: July 28, 2025
Published: August 19, 2025



ACS Publications
© 2025 The Authors. Published by American Chemical Society

https://doi.org/10.1021/jacs.5c09017
J. Am. Chem. Soc. 2025, 147, 31859−31870

Downloaded via LEIBNIZ INST FOR CATALYSIS (LIKAT) on October 17, 2025 at 05:17:42 (UTC).
See https://pubs.acs.org/sharingguidelines for options on how to legitimately share published articles.

Scheme 1. Transition-Metal-Catalyzed Isomerization of Olefins

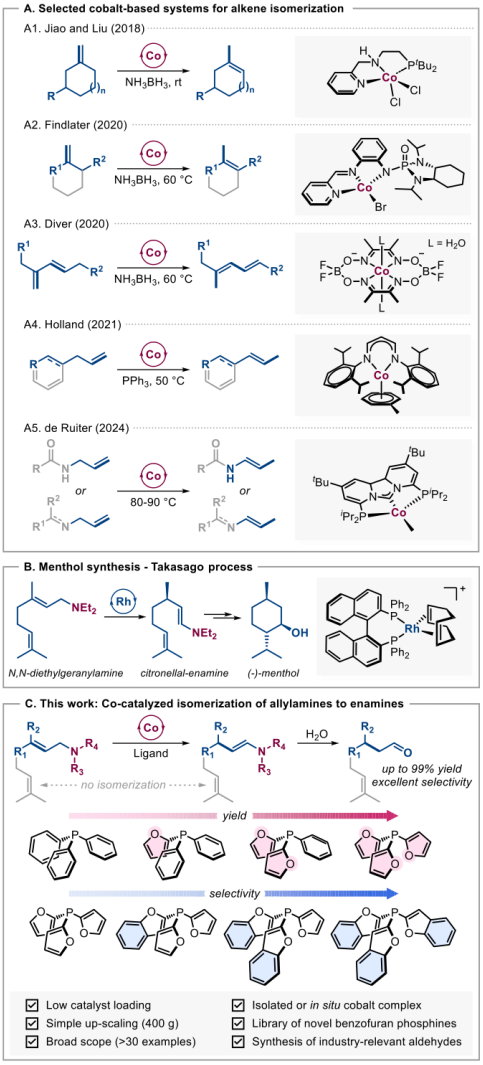

RESULTS AND DISCUSSION

Catalyst Development and Optimization of the Reaction System. We initiated our investigations on the Co-catalyzed isomerization of allylamines by screening Co pincer complexes bearing different (PNP, NNN, and NNP) pincer ligands (see SI section 2 for details, Table S1). Recently, these Co complexes have been described as catalysts for the isomerization of various olefins.[19] Unfortunately, only negligible reactivity was observed for the isomerization of allylamines in the presence of these Co pincer complexes. Hence, we focused on *in situ*-generated Co catalysts using commercially available and newly developed bi- and monodentate ligands. After testing more than 40 different phosphines (see SI section 3), we discovered a surprisingly high activity for tri(furan-2-yl)-phosphine (TFP, **L1**).

The combination of $Co(OAc)_2$, DIBAL-H, and **L1** performed well for the isomerization of *N*,*N*-diethylgeranylamine **1a** and yielded 81% of **1b** with good selectivity (Scheme 2). Other aromatic phosphines bearing heterocycles, such as thiophene **L2** or pyridine **L3**, led to the deactivation of the catalyst, while the use of triphenylphosphine **L4** gave a much lower yield. To evaluate the effect of the furan moiety in more detail, we prepared a library of furan-based phosphines **L4**–**L12**. The yield increased with the replacement of the benzene ring with furyl one **L4**–**L6**, confirming the crucial importance of this moiety.

Scheme 2. Co-Catalyzed Isomerization of Allylamine 1a: Testing Different Phosphines[a]

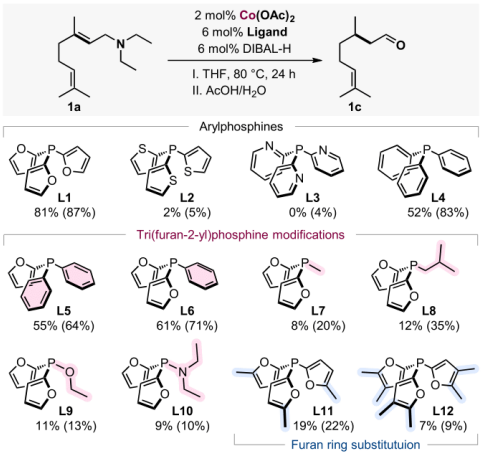

[a]Reaction conditions: 2.5 mmol of **1a**, 1.5 mL of THF, $Co(OAc)_2$, ligand, DIBAL-H, 80 °C, 24 h. After catalysis, **1b** was hydrolyzed by the addition of 1.5 mL of a 5% acetic acid solution, yielding **1c**. [b]Conversion of **1a** and yield of **1c** were determined by GC analysis using *n*-hexadecane as an internal standard. The numbers in parentheses represent the conversion.

In the case of difurylphosphines bearing alkyl substituents (−Me, **L7**; −*i*Bu, **L8**), a significantly lower reactivity of the catalyst was detected compared to the aromatic phosphines. A similar activity was observed while using **L9** and **L10**, bearing a diethylamine or an ethoxy unit, respectively. Finally, the presence of a monosubstituted (**L11**) or disubstituted furan ring (**L12**) with a methyl group suppressed the catalytic activity, probably due to steric reasons.

Interestingly, the performance of the Co catalyst was considerably improved by the exchange of one furan ring with a benzofuran moiety (**L13**), leading to the complete conversion of **1a** to the desired product **1b** in 94% yield (Table S3, entry 13). To understand the superior performance of **L13** compared to **L1**, we altered the electronic and steric properties of TFP (Scheme 3). To our delight, we observed that further replacement of furyl substituents with benzofuryl ones (**L14**,

https://doi.org/10.1021/jacs.5c09017
J. Am. Chem. Soc. 2025, 147, 31859−31870

Scheme 3. Overview of Synthesized and Tested Benzofuran Phosphines[a]

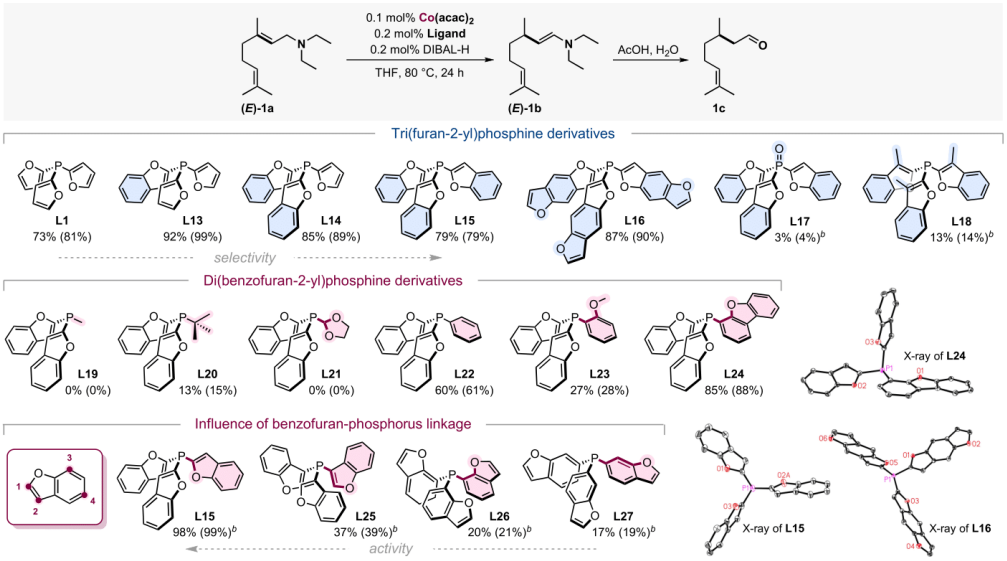

[a]Reaction conditions: 2.5 mmol of **1a**, 1.5 mL of THF, $Co(acac)_2$, selected phosphine, DIBAL-H, 80 °C, 24 h. Conversion of **1a** and yield of **1c** were determined by GC analysis using *n*-hexadecane as an internal standard. The numbers in parentheses represent the conversion of **1a**. In the molecular structures of **L15**, **L16**, and **L24**, displacement ellipsoids correspond to 30% probability, and hydrogen atoms have been omitted for clarity. [b]Catalyst loading: 0.5 mol % $Co(acac)_2$, 1 mol % benzofuran phosphine and DIBAL-H.

L15) led to an increase in selectivity. Moreover, the use of 0.1 mol % $Co(acac)_2$ and tri(benzofuran-2-yl)phosphine **L15** as a ligand at 100 °C enabled the full conversion of **1a** and production of **1b** in almost quantitative yield (SI section 6).

Of note, the application of benzofuran phosphines such as **L15** in homogeneous catalysis has been rarely described.[20,21] The ligand **L15**, previously reported by the Santelli[20] group, was characterized by X-ray diffraction (see SI section 8). The employment of tris(benzo[1,2-*b*:4,5-*b*′]difuran-2-yl)phosphine **L16** gave slightly lower selectivity. Only traces of **1b** were detected for phosphine oxide **L17**,[22] which clearly demonstrates that oxidation of phosphine **L15** leads to the deactivation of the corresponding Co catalyst. Moreover, the presence of the methyl group at the C3 position of the benzofuran ring in phosphine **L18** hampered catalytic activity significantly, probably due to steric hindrance. A similar trend was observed for **L11** and **L12** (Scheme 2).

Subsequently, we investigated the influence of the replacement of one benzofuran-2-yl moiety with different substituents. In the case of alkyl groups like methyl (**L19**) or dioxolane (**L21**), no catalytic activity was observed, which was consistent with the previous observations for **L7** and **L8** (Scheme 2). Better results were observed after the introduction of aryl substituents (**L22**–**L24**). The presence of an sp^2 oxygen atom seems to be crucial (**L15**, **L24**), since the ligands containing sp^3 oxygen atoms (**L21**, **L23**) were inefficient. Interestingly, **L24** exhibited higher activity compared to **L15**, albeit with inferior selectivity.

Once we had proved that benzofuran phosphines were the most suitable ligands, we examined the influence of the benzofuran-phosphorus linkage. Much lower activity was observed for phosphine with a phosphorus atom linked to the benzofuran rings at the C3 position (**L25**). The performance of phosphines with a phosphorus atom bonded to a benzene ring of benzofuran (**L26**, **L27**) was comparable to the performance of triphenylphosphine **L4**. The above examples indicate that the vicinity of an sp^2 oxygen atom two bonds away from the phosphorus atom is essential for catalytic activity.

Having identified **L15** as the most efficient ligand, the influence of crucial reaction parameters such as catalyst loading, precursors, ligand ratio, solvents, and reductants was investigated (Table 1). $Co(acac)_2$ and $Co(acac)_3$ showed enhanced reactivity compared to other Co(II) precursors such as $CoCl_2$, $CoBr_2$, $Co(OTf)_2$, or $Co(BF_4)_2$ (see SI section 6 for details). In some cases, decomposition of the resulting Co complexes was indicated by a brown precipitate after catalysis.

Due to the slightly better catalytic performance and the lower usage of reductant equivalents for $Co(acac)_2$ compared to $Co(acac)_3$, we continued our investigations with $Co(acac)_2$ (Table 1, entry 1). Furthermore, the addition of different reductants such as DIBAL-H, $AlEt_3$, $LiAlH_4$, or $LiAlH[O^tBu]_3$ led to an active Co catalyst (SI section 6). The best reactivity of the *in situ* Co catalyst was achieved with two equivalents of DIBAL-H. Notably, the active Co(0) catalyst was not generated under a molecular hydrogen atmosphere (Table 1, entry 7).

Any further alterations of the optimized catalyst system did not provide the desired product (Table 1, entries 3–6), indicating that all components are crucial to form the active catalytic species. Of note, by increasing the temperature, we were able to reduce the catalyst amount to 0.075 mol % (Table 1, entry 9). To the best of our knowledge, this is one of the lowest

https://doi.org/10.1021/jacs.5c09017
J. Am. Chem. Soc. 2025, 147, 31859−31870

Table 1. Co-Catalyzed Isomerization of Allylamine 1a: Optimization of the Reaction Conditions

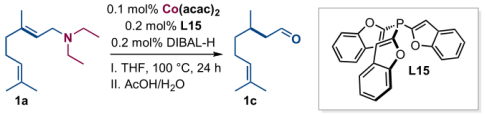

entry	changes from standard conditions	yield [%][a]
1[b]	none	98 (99)
2[c]	$Co(acac)_3$ as Co precursor	97 (99)
3	without $Co(acac)_2$	traces
4	without **L15**	0 (5)
5	without DIBAL-H	traces
6	only using **L15** as catalyst	–
7[d]	H_2 was used as the H source	traces
8	toluene was used as a solvent	21 (23)
9[e]	0.075 mol % [Co], 2-MeTHF, 120 °C	96 (98)

[a]Conversion of **1a** and yield of **1b** were determined by GC analysis using *n*-hexadecane as an internal standard. [b]Reaction conditions: 2.5 mmol of **1a**, 100 °C, 24 h. [c]Catalyst: 0.1 mol % $Co(acac)_3$, 0.2 mol % **L15**, 0.3 mol % DIBAL-H. [d]20 bar H_2 [e]Optimized reaction conditions: 1.5 mL of 2-MeTHF, 0.075 mol % $Co(acac)_2$, 0.15 mol % DIBAL-H, 0.15 mol % **L15**, 120 °C, 24 h.

base-metal catalyst loadings reported for olefin isomerization reactions.[23]

Having optimal reaction conditions for the isomerization of **1a**, we identified and analyzed side-products to better understand the reaction course. **L1** was used as a less selective ligand in larger-scale reactions to allow isomer isolation. The byproducts were analyzed by 2D-NMR spectroscopy, and their signals were assigned by GC analysis (see SI section 7 for details). In total, five internal olefin isomers (**1ba**–**1bd**) and four enamine isomers (**1be**–**1bi**) could be characterized (Scheme 4A).

It is noteworthy that the formation of isomers **1be**, **1bh**, and **1bi** is completely suppressed using **L15** in comparison to **L1**. Moreover, the production of **1bd**, **1bf**, and **1bg** is significantly lower for **L15**, compared to **L1**. In general, tri(benzofuran-2-yl)phosphine **L15** effectively prevents (*Z*)−(*E*) isomerization and chain-walking of double bonds of **1a**, which makes this ligand particularly interesting for industrial applications.

Substrate Scope and Limitations. We explored the scope and limitations of the optimized system, starting with an investigation of the effects of different N-substituents on the isomerization of allylamines. Thus, several geranylamine derivatives bearing alkyl or aryl residues were prepared (**2a**–**10a**, Scheme 5). Compared to the industrial benchmark substrate diethyl-geranylamine (**1a**), we observed full conversion for other linear alkyl geranylamine derivatives, e.g., ethyl (**2a**), ethyl methyl (**3a**), dimethyl (**4a**), and isopropyl (**5a**) geranylamine. However, the regioselectivity decreased slightly for the methyl-substituted derivatives **3a**, **4a**, and **5a**. In the case of cyclic aliphatic amines like pyrrolidine (**6a**) and morpholine (**7a**) derivatives, we observed lower conversions. No conversion of the *N*,*N*-diaryl derivatives **8a** and **9a** was achieved, even though a significantly higher catalyst loading and harsher reaction conditions (120 °C) were applied. Nevertheless, even well-established Ru and Rh catalysts failed to convert the aryl derivative **8a** to the corresponding enamine.[24] Overall, the screening of different N-substituted geranylamine derivatives revealed the importance of a suitable amine moiety.

Subsequently, we prepared several aliphatic (*E*)-allylamines containing diethylamine residues **10a**–**21a** and systematically studied their isomerization (Scheme 5). Notably, we selectively isomerized the highly challenging and industry-relevant farnesal-

Scheme 4. Suppressed or Promoted Side Reactions of 1a: Comparison of L1 and L15[a]

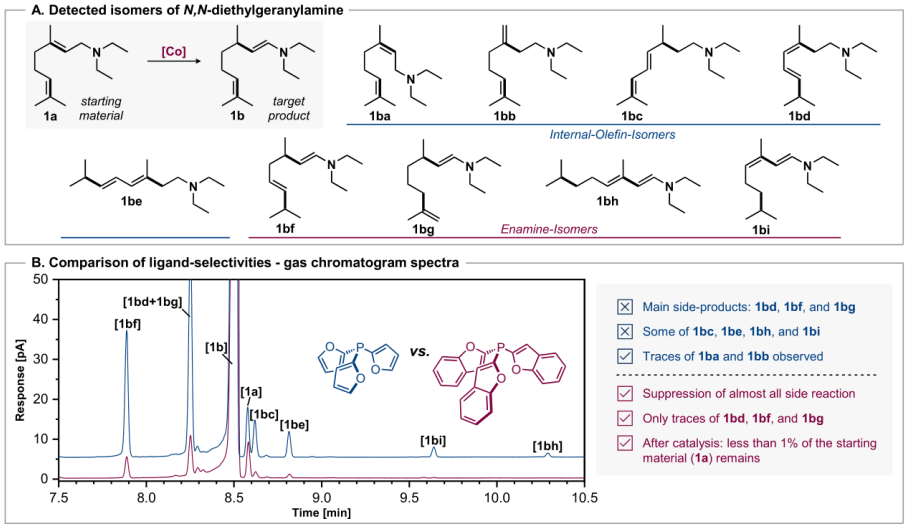

[a](A) Identified isomers of **1a** after catalysis. (B) Comparison of selectivities of ligands **L1** and **L15**: GC spectra of product mixtures after the Co-catalyzed isomerization. Reaction conditions: 2.5 mmol of **1a**, 1.5 mL of THF, 1 mol % $Co(acac)_2$, 2 mol % DIBAL-H/ligand, 100 °C.

https://doi.org/10.1021/jacs.5c09017
J. Am. Chem. Soc. 2025, 147, 31859−31870

Scheme 5. Substrate Scope: Co-Catalyzed Isomerization of Various Allylamine Derivatives[a]

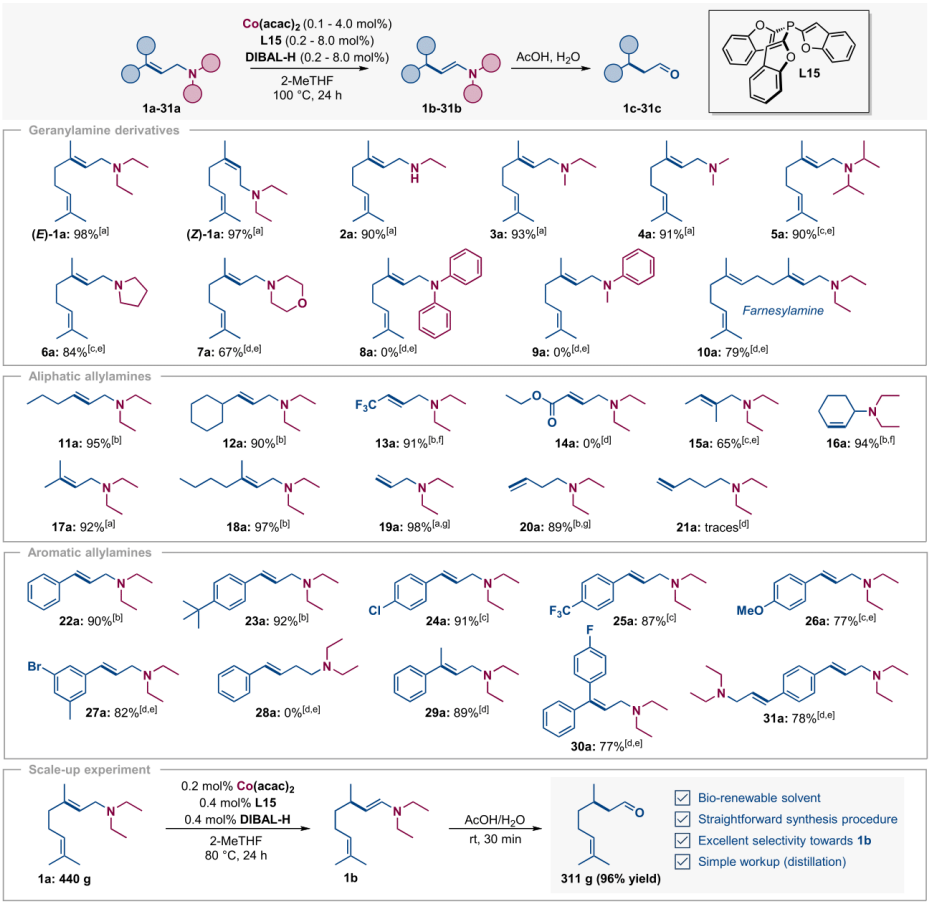

[a]Values below the structures represent the isolated yield(s) of the corresponding aldehydes. Reaction conditions: substrate (0.5−2.5 mmol, see SI section 10 for details), 2-MeTHF or THF, 100 °C, 24 h. Note: Product **10c** represents the sum of the isomers. [a] Catalyst: 0.1 mol % $Co(acac)_2$, 0.2 mol % **L15**, and DIBAL-H. [b] Catalyst: 1 mol % $Co(acac)_2$, 2 mol % **L15**, and DIBAL-H. [c] Catalyst: 2 mol % $Co(acac)_2$, 4 mol % **L15**, and DIBAL-H. [d] Catalyst: 4 mol % $Co(acac)_2$, 8 mol % **L15**, and DIBAL-H. [e] Reaction time: 48 h. [f] Isolated as an enamine. [g] GC yield.

derivative **10a**, obtaining **10c** in 79% yield. Furthermore, internal (*E*)-allylamine derivatives with sterically demanding substituents (**11a**−**13a**) were converted to their corresponding enamines with low catalyst loading and high selectivity. The isomerization of the hex-2-enamine derivative **11a** and the cyclohexane derivative **12a** was realized with only 0.2 mol % catalyst amount. However, our system was incompatible with allylamine bearing ester group **14a**, as were most base metal catalysts described in the literature. We were also able to achieve isomerization of the challenging substrates **15a**, **16a**, or **18a** by increasing the catalyst loading to 1−2 mol %.

Next, we investigated the Co-catalyzed isomerization of terminal allylamine derivatives over several bonds.[24] Generally, olefin migration becomes significantly more challenging with the number of bonds between the double bond and the directing group.[25,26] First, the isomerization of the terminal allylamine **19a** over one C−C bond was performed with 0.1 mol % catalyst loading at 80 °C and gave **19c** in a quantitative yield. To our delight, we achieved the isomerization of **20a** over two C−C bonds with a slightly higher catalyst loading of 1 mol %. However, our system was unable to achieve isomerization of **21a** over three C−C-bonds, as only traces of the desired product were obtained, although full conversion was achieved. The production of **21c** was not observed even at higher temperatures and with increased catalyst loadings.

To further demonstrate the potential applications of our developed system, we synthesized and tested several aromatic allylamine derivatives (**22a**−**31a**, Scheme 5). Amines **22a** and **23a** were successfully converted to their corresponding enamines in nearly quantitative yields. Notably, various

https://doi.org/10.1021/jacs.5c09017
J. Am. Chem. Soc. 2025, 147, 31859−31870

functional groups on the phenyl ring, such as chloro (**24a**), trifluoromethyl (**25a**), or methoxy (**26a**) were tolerated. The isomerization of a more challenging substrate bearing a bromo substituent **27a** was achieved with 4 mol % catalyst loading. In comparison to the aliphatic allylamine **20a**, no isomerization occurred over two C−C bonds for the aromatic allylamine **28a**. Under the same conditions none of the initially tested noble metal catalysts were able to catalyze the isomerization of **28a** (SI section 11.4). Noteworthy, C3-substituted allylamines bearing a methyl (**29a**) or fluorobenzene (**30a**) residue were transformed into the corresponding products in yields over 70%. Furthermore, to demonstrate the synthetic utility of this transformation, our system was successfully applied to the difunctionalized allylamine **31a**. To highlight the industrial significance of our methodology, the isomerization of **1a** was successfully applied on a multigram scale, producing 311 g of citronellal **1c** (Scheme 5). Achieving a yield of 96%, we successfully demonstrated that the developed system also operates efficiently on the molar scale.

Mechanistic Investigations. Determination of the hetero- or homogeneous character of the actual catalyst is often not evident.[27] Thus, we performed the model reaction with the addition of a mercury drop, as a nanoparticle scavenger, which did not affect the catalytic activity. Moreover, transmission electron microscopy (TEM) analysis of the model reaction mixture with or without substrate **1a** did not reveal the formation of metal nanoparticles or clusters (see SI section 9.4 for details). The latter were also not observed by MS (SI section 9.6). The above observations indicated homogeneous catalysis.

To obtain more information, we attempted to isolate the catalytically active Co complex (see SI section 8, **Co-1**). The treatment of $Co(acac)_2$ and **L15** (ratio 1:4) in THF with two equivalents DIBAL-H resulted in the release of H_2 and the formation of a dark brown Co solution at −80 °C (Scheme 6). The reaction mixture was filtered, layered with *n*-pentane, and the crystallization at −30 °C gave dark red platelet crystals. The molecular structure of **Co-2** was determined by SC-XRD, disclosing a homoleptic tetrahedral Co d^9 complex with four coordinating phosphines.

Scheme 6. Synthesis and Transformation of Co-2[a]

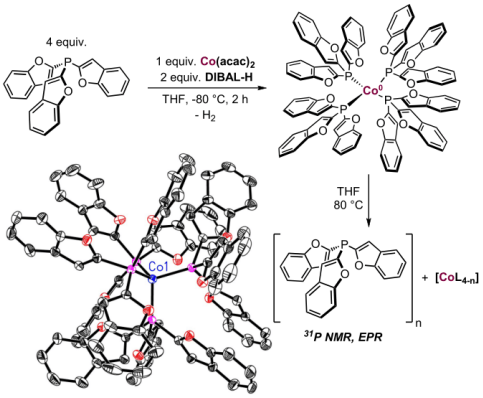

[a]Solid-state structure of **Co-2** at 30% probability ellipsoids. Hydrogen atoms have been omitted for clarity.

Interestingly, we observed the formation of **Co-2** even in the presence of only one equivalent DIBAL-H or **L15.** In subsequent crystallization experiments with substrate **1a** or 1,5-cyclooctadiene (COD), we also observed the formation of **Co-2**, however, the isolation of a Co(0) complex with coordinated **1a** or COD could not be achieved (see SI section 8 for details).

To distinguish between the activities of the isolated complex **Co-2** and the catalyst generated *in situ*, a series of control experiments were carried out (SI section 9). When 0.1 mol % catalyst loading was used, the *in situ* generated Co catalyst with 1:2 metal-to-ligand ratio gave nearly quantitative yield (98%), while the defined **Co-2** catalyst showed significantly lower activity (18% yield). However, increasing the catalyst loading to 0.3 mol % led to a significant enhancement in catalytic performance, affording **1b** in 98% yield. These combined results strongly suggest that the catalytically active Co species differs from the isolated **Co-2** complex, which may represent an off-cycle resting state.

Furthermore, based on the **Co-2** complex with either **L15** or **L1** as ligands, we carried out DFT computations employing *N*,*N*-dimethyl-3-methylbut-2-en-1-amine as a simplified model substrate (see SI section 12 for details). However, the calculated activation barriers for the $[Co(L)_4]$ species were inconclusive and considerably too high to permit the isomerization to proceed under the applied reaction conditions. These observations further support the conclusion that **Co-2** does not represent the catalytically active Co species.

Moreover, EPR measurements of the molecular defined 17 valence-electron Co complex (**Co-2**) were performed to provide more insights into the reaction mechanism. *In situ* EPR analysis of **Co-2** in toluene showed no resonances at room temperature. However, at 95 K, it exhibited an EPR signal of axial symmetry at $g_{\parallel} = 2.190$ and $g_{\perp} = 1.989$, $A_{\parallel} = 103$, $A_{\perp} = 148.5$ MHz (estimated from EPR simulation, SI section 9.5). The coupling of the unpaired electrons ($S = 1/2$) with ^{59}Co nuclear spins ($I = 7/2$, 100%) leads to the well-resolved eight-line hyperfine structure of the parallel component of the EPR signal with $A_{\parallel} = 148.5$ MHz (SI section 9.5). The poorly resolved middle hyperfine lines (second derivative EPR signal) show an additional splitting due to the hyperfine interaction with ^{31}P nucleus ($I = 1/2$). Compared to low-spin Co(II) compounds with $g_{\perp} > g_{\parallel}$, **Co-2** with $g_{\parallel} > g_{\perp}$ can be assigned to Co(0) in a tetragonally distorted octahedral field of the ligands.[28,29]

To further investigate the activity of **Co-2**, titration experiments were conducted in toluene, with or without substrate **1a** or THF. The addition of **1a** to **Co-2** in toluene resulted in slight shifts and decreased signal intensity in the EPR spectra (Scheme 7A), indicating a direct interaction between **1a** and **Co-2** occurs, and consequently another Co(0) complex ($g_{\parallel} = g_{\parallel} = 2.188$ and $g_{\perp} = 1.989$, $A_{\parallel} = 105.5$, $A_{\perp} = 150.0$ MHz) is present.

Similarly, the addition of THF to **Co-2** resulted in a signal shift ($g_{\parallel} = 2.187$ and $g_{\perp} = 1.989$, $A_{\parallel} = 106.2$, $A_{\perp} = 151.5$ MHz), exhibiting similar features to those observed after the addition of **1a** (SI section 9.5). ^{31}P NMR experiments further suggested the presence of free phosphine ligand (**L15**) when **Co-2** was dissolved in THF-d_8 compared to toluene-d_8, showing a peak at −67.93 ppm in the ^{31}P NMR. Based on these combined results, we conclude that the phosphine undergoes dissociation in the presence of THF or **1a**, leading to the formation of the active species.

Next, to rule out a radical pathway, a series of EPR measurements were performed. The reaction mixture, consist-

https://doi.org/10.1021/jacs.5c09017
J. Am. Chem. Soc. 2025, 147, 31859−31870

Scheme 7. Mechanistic Investigations[a]

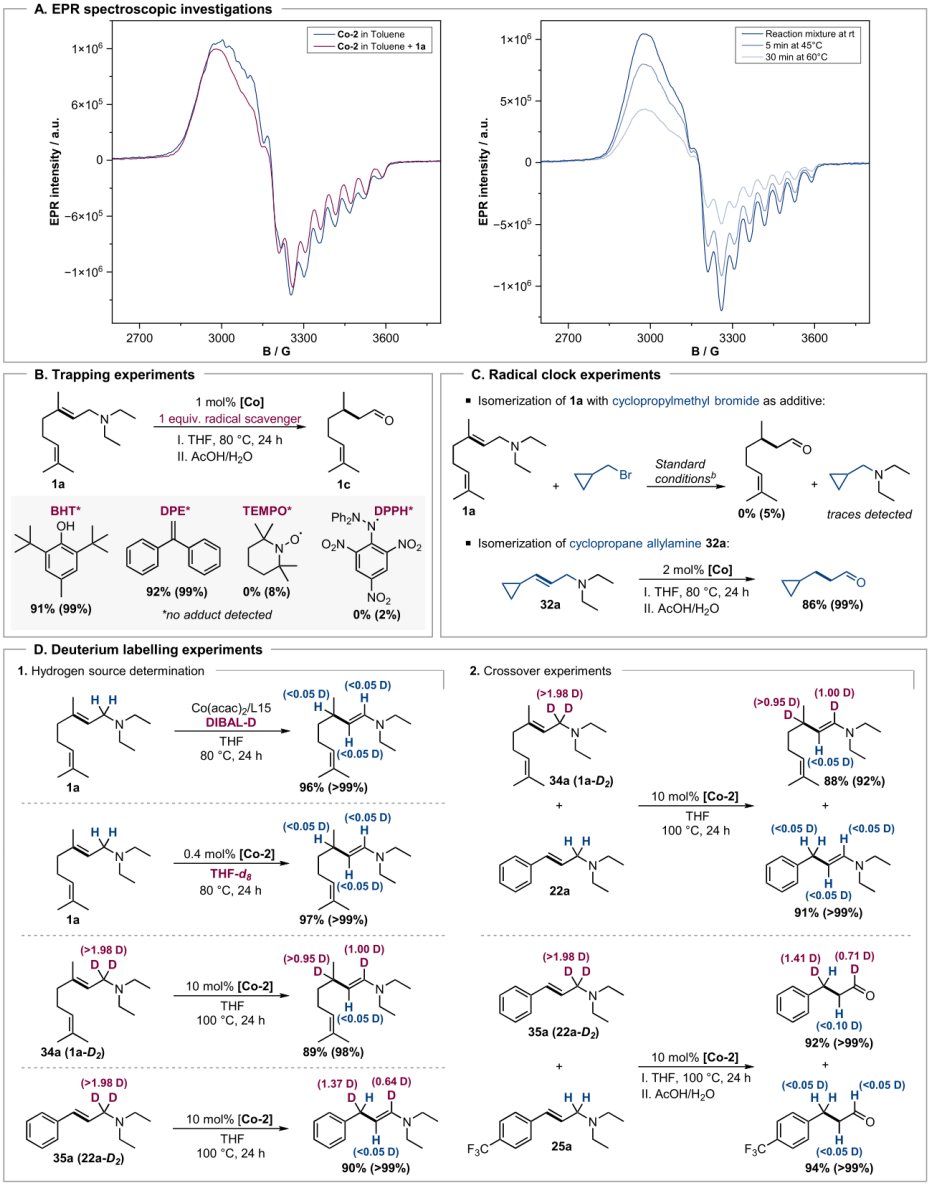

[a](A) Recorded EPR spectra of **Co-2** in toluene, measured at 95 K. (B) Trapping experiments with radical scavengers, reaction-scale: 2.5 mmol of **1a**. (C) Radical clock experiments. [b]Standard conditions: 2.5 mmol of **1a**, 1.5 mL of THF, 1 mol % $Co(acac)_2$, 2 mol % **L15**, and DIBAL-H, 80 °C, 24 h. (D) Deuterium labeling experiments.

ing of **Co-2**, **1a**, and THF, was first heated to 45 °C for 5 min, followed by heating to 60 °C for 30 min (Scheme 7A). No radical intermediate was detected during the *in situ* EPR measurements. To further confirm these results, different radical scavengers were added to the model reaction with substrate **1a**. The application of TEMPO, Galvinoxyl, or DPPH led to

https://doi.org/10.1021/jacs.5c09017
J. Am. Chem. Soc. 2025, 147, 31859−31870

complete suppression of the isomerization (Scheme 7B); however, no adduct was identified by GC-MS and LC-MS. We assume that the addition of these radicals led to the deactivation of the catalyst by coordination to the metal center. On the other hand, the addition of DHT or BPE did not significantly affect the model reaction. Finally, radical clock experiments (Scheme 7C) with cyclopropane-containing substrates were carried out. However, no cyclopropane ring opening could be detected for either (bromomethyl)-cyclopropane or allylamine **32a** and **33a**, which rules out the existence of a free radical intermediate during the isomerization.

Generally, the metal-catalyzed isomerization of C−C double bonds can occur via an inter- or intramolecular pathway.[7,10] The former category encompasses radical (Scheme 8A) and metal hydride mechanisms (Scheme 8B); however, both pathways could already be excluded. In the group of intramolecular processes, one may distinguish between inner- or outer-sphere allyl mechanism (Scheme 8C), oxidative cyclization (Scheme 8D), and a cationic (Scheme 8E) or metalloradical allyl mechanism (Scheme 8F). To identify a plausible mechanistic pathway, we planned and performed a series of further experiments.

First, we performed isotope-labeling experiments (Scheme 7D). No deuterium incorporation was observed when the model reaction of **1a** was performed in THF-d_8 or with DIBAL-D, excluding both compounds as hydrogen sources. On the other hand, the isomerization of the γ-deuterated substrates **1a**-D_2 (**34a**) and **22a**-D_2 (**35a**) led to the respective enamines **34b** and **35b**, with deuterium incorporation in the α-position, indicating the 1,3-hydrogen shift.

Finally, to distinguish between the inter- and intramolecular mechanisms, we performed H/D crossover experiments using γ-deuterated substrates **1a**-D_2 or **22a**-D_2 with **22a** or **25a**, respectively (Scheme 7D). No deuterium incorporation was detected in **22b** or **25b**, excluding a radical (Scheme 7A) or metal hydride mechanism (Scheme 7B). Moreover, no metal hydride was observed by ^{1}H NMR.

Among the intramolecular processes mentioned above, the inner-sphere π-allyl mechanism (Scheme 8C) seems to be the most plausible pathway. First, no EPR activity should exclude the metalloradical allyl pathway (Scheme 8F).[10] Moreover, the cationic mechanism (Scheme 8E) would involve the formation of 2° instead of 3° carbocation, and no rearrangement of 3,3-dimethylbut-1-ene, indicating carbocation formation, was observed (see SI section 9.9).[30] Finally, oxidative cyclization (Scheme 8D) is scarcely described and substantiated in the literature.[31]

Next, we examined the model reaction mixture in time using tri(benzofuran-2-yl) **L15** or tri(furan-2-yl) phosphine **L1** as a ligand (Scheme 9A). In the case of **L15**, over 95% of **1a** was converted into **1b** in 4 h, and the production of unwanted isomers was negligible. In contrast, the maximal conversion of **1a** was about 80% for **L1**, and a substantial amount of byproducts was produced.

Subsequently, we employed variable-time normalization analysis (VTNA) to derive more information about the mechanism.[32] Our initial attempts to determine substrate or catalyst order using VTNA for three different substrate or catalyst concentration profiles were unsuccessful (see SI section 9.10). Hence, we checked the possibility of the catalyst deactivation or product inhibition, which proved to occur due to the lack of curve overlay after the time shift (Scheme 9B).

Scheme 8. Main Pathways: Transition-Metal Catalyzed Isomerization of Allylamines

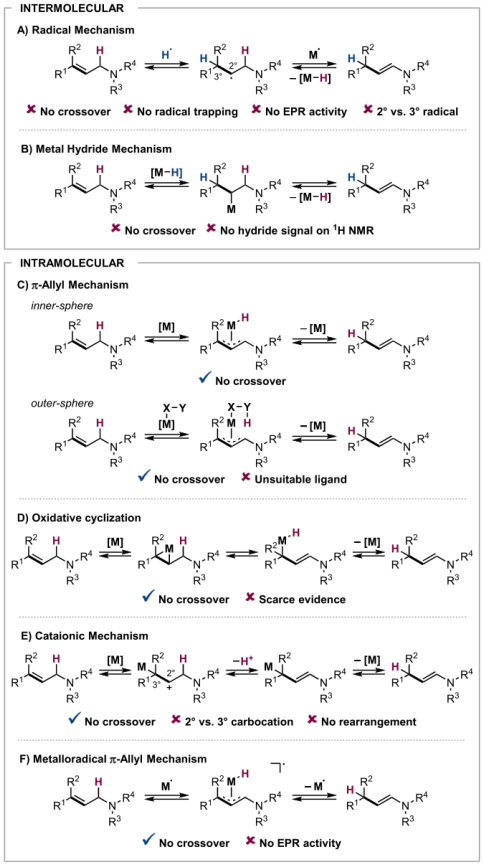

Distinguishing between these two required an additional experiment with the product addition, which indicated catalyst deactivation (Scheme 9B). For substantial variation in catalyst concentration, determining the substrate or catalyst order requires monitoring the catalyst concentration over time, which is impossible without knowing the actual active species.[33]

To elucidate the reason for the difference in activity and selectivity of ligands **L1** and **L15**, we hypothesized that the presence of a benzene ring in the tri(benzofuran-2-yl)phosphine contributes to the stability of the furyl moiety.[34] However, ^{31}P NMR analysis of the reaction mixtures did not reveal the presence of any additional phosphorus species except free ligands in both cases (SI section 9.6). Moreover, no change in the reaction with **L1** was observed after the addition of a mercury drop, excluding catalyst deactivation by nanoparticle formation.

Based on our mechanistic experiments and kinetic studies, we proposed the inner-sphere allyl mechanism (Scheme 10). The first step is the formation of the active Co species from $Co(acac)_2$ (a) or the defined **Co-2** precatalyst (b). Then, the

https://doi.org/10.1021/jacs.5c09017
J. Am. Chem. Soc. 2025, 147, 31859−31870

Scheme 9. Kinetic Studies[a]

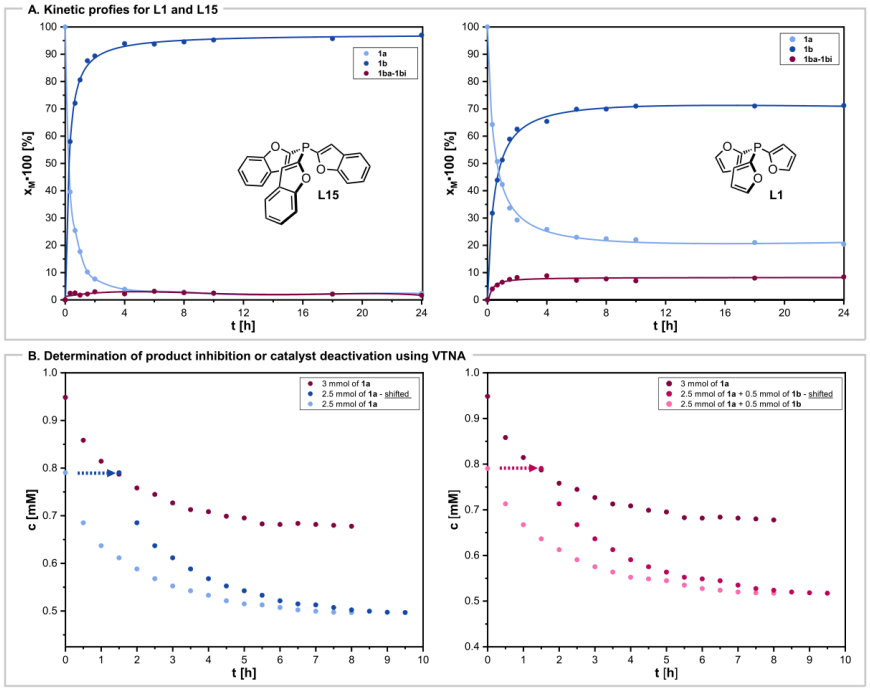

[a](A) Kinetic profile experiments, reaction conditions: 2.5 mmol of **1a**, 0.2 mol % $Co(acac)_2$, 0.4 mol % **L15**, and DIBAL-H, 2-MeTHF, 100 °C. (B) VTNA plots, modified reaction conditions: 2.5 mmol of **1a**, 0.5 mol % $Co(acac)_2$, 1 mol % **L15**, and DIBAL-H, 2-MeTHF, 60 °C.

Scheme 10. Proposed Mechanism for the Co-Catalyzed Isomerization of Allylamines

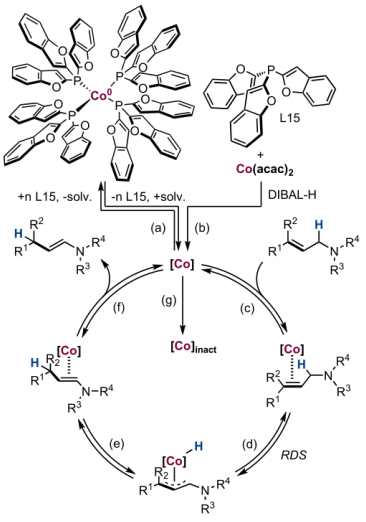

addition of an allylamine to the Co catalyst leads to a metal substrate intermediate (c) as evidenced by EPR measurements. In the next step, C−H activation of the allylic C−H bond occurs as a rate-determining step, which generates Co−H species (d). Subsequently, the Co−H complex undergoes reinsertion of the hydride into the allylic system, generating product intermediate (e), followed by the release of the desired enamine (f). During the reaction, the catalyst is transformed into an inactive species (g).

■ CONCLUSIONS

In summary, a series of novel monodentate phosphine ligands bearing furan- and benzofuran-substituents were synthesized and screened in the industry-relevant Co-based isomerization of allylamines. As a result, we discovered a highly active and selective system that provides similar activity compared to currently applied Rh catalysts. Moreover, the presented method allows the isomerization of structurally diverse substrates with up to quantitative yields, including terminal and internal (aliphatic and aromatic) allylamines, bearing various functionalities (e.g., Cl, F, CF_3). Potential industrial application of our system was substantiated by the scale-up experiment, which provided 311 g of citronellal in 96% yield. Furthermore, we observed that the catalyst activity was bound to the presence of furan-2-yl substituents of the phosphine ligand, while the selectivity increased with the number of benzofuran-2-yl groups.

https://doi.org/10.1021/jacs.5c09017
J. Am. Chem. Soc. 2025, 147, 31859−31870

These trends may be helpful in the context of designing new, efficient catalysts. Moreover, we managed to isolate and characterize the Co complex, serving as a precatalyst. Finally, we employed various analytical techniques such as TEM, EPR, and NMR to understand the nature of the isomerization process. Based on the above, in combination with deuterium labeling, radical trapping experiments, and kinetic studies, we postulated a plausible mechanism encompassing a 1,3-hydrogen shift.

■ ASSOCIATED CONTENT

Supporting Information

The Supporting Information is available free of charge at https://pubs.acs.org/doi/10.1021/jacs.5c09017.

Experimental procedures, mechanistic studies, computational studies and characterization of new compounds (PDF)

Accession Codes

Deposition numbers 2379866−2379870 contain the supplementary crystallographic data for this paper. These data can be obtained free of charge via the joint Cambridge Crystallographic Data Centre (CCDC) and Fachinformationszentrum Karlsruhe Access Structures service.

■ AUTHOR INFORMATION

Corresponding Authors

Matthias Beller − *Leibniz-Institut für Katalyse e.V., 18059 Rostock, Germany*; orcid.org/0000-0001-5709-0965; Email: matthias.beller@catalysis.de

Kathrin Junge − *Leibniz-Institut für Katalyse e.V., 18059 Rostock, Germany*; orcid.org/0000-0001-7044-8888; Email: kathrin.junge@catalysis.de

Haijun Jiao − *Leibniz-Institut für Katalyse e.V., 18059 Rostock, Germany*; orcid.org/0000-0002-2947-5937; Email: Haijun.Jiao@catalysis.de

Johannes Panten − *Symrise AG, 37603 Holzminden, Germany*; Email: johannes.panten@symrise.com

Authors

Sebastian Ahrens − *Leibniz-Institut für Katalyse e.V., 18059 Rostock, Germany*

Rafał Kusy − *Leibniz-Institut für Katalyse e.V., 18059 Rostock, Germany*; orcid.org/0000-0003-2700-6130

Anke Spannenberg − *Leibniz-Institut für Katalyse e.V., 18059 Rostock, Germany*

Thanh H. Vuong − *Leibniz-Institut für Katalyse e.V., 18059 Rostock, Germany*

Jabor Rabeah − *Leibniz-Institut für Katalyse e.V., 18059 Rostock, Germany; State Key Laboratory of Low Carbon Catalysis and Carbon Dioxide Utilization, Lanzhou Institute of Chemical Physics (LICP), Chinese Academy of Sciences, Lanzhou 730000, P. R. China*; orcid.org/0000-0003-2162-0981

Bernhard M. E. Russbueldt − *Symrise AG, 37603 Holzminden, Germany*

Complete contact information is available at: https://pubs.acs.org/10.1021/jacs.5c09017

Funding

We thank Symrise for funding this work.

Notes

The authors declare no competing financial interest.

■ ACKNOWLEDGMENTS

The authors thank Fairoosa Poovan for her support with the isotope labeling experiments and German Robledo Lopez for his help during the preparation of the manuscript. We are also grateful to Andreas Koch and Dr. Marcus Klahn for performing HRMS measurements and VT NMR measurements and PD Dr. Wolfgang Baumann and Susann Buchholz for NMR measurements.

■ REFERENCES

(1) (a) Massad, I.; Marek, I. Alkene Isomerization through Allylmetals as a Strategic Tool in Stereoselective Synthesis. *ACS Catal.* **2020**, *10* (10), 5793−5804. (b) Zhang, S.; Findlater, M. Cobalt-Catalyzed Isomerization of Alkenes. *Synthesis* **2021**, *53* (16), 2787−2797. (c) Liu, X.; Liu, Q. Catalytic asymmetric olefin isomerization: Facile access to chiral carbon-stereogenic olefinic compounds. *Chem. Catal.* **2022**, *2* (11), 2852−2864.

(2) (a) Gauthier, D.; Lindhardt, A. T.; Olsen, E. P. K.; Overgaard, J.; Skrydstrup, T. In Situ Generated Bulky Palladium Hydride Complexes as Catalysts for the Efficient Isomerization of Olefins. Selective Transformation of Terminal Alkenes to 2-Alkenes. *J. Am. Chem. Soc.* **2010**, *132* (23), 7998−8009. (b) Werner, E. W.; Mei, T.-S.; Burckle, A. J.; Sigman, M. S. Enantioselective Heck Arylations of Acyclic Alkenyl Alcohols Using a Redox-Relay Strategy. *Science* **2012**, *338* (6113), 1455−1458. (c) Larionov, E.; Lin, L.; Guénée, L.; Mazet, C. Scope and Mechanism in Palladium-Catalyzed Isomerizations of Highly Substituted Allylic, Homoallylic, and Alkenyl Alcohols. *J. Am. Chem. Soc.* **2014**, *136* (48), 16882−16894. (d) Singh, S.; Bruffaerts, J.; Vasseur, A.; Marek, I. A unique Pd-catalysed Heck arylation as a remote trigger for cyclopropane selective ring-opening. *Nat. Commun.* **2017**, *8* (1), No. 14200.

(3) (a) Mantilli, L.; Gérard, D.; Torche, S.; Besnard, C.; Mazet, C. Iridium-Catalyzed Asymmetric Isomerization of Primary Allylic Alcohols. *Angew. Chem., Int. Ed.* **2009**, *48* (28), 5143−5147. (b) Li, H.; Fiorito, D.; Mazet, C. Exploring Site Selectivity of Iridium Hydride Insertion into Allylic Alcohols: Serendipitous Discovery and Comparative Study of Organic and Organometallic Catalysts for the Vinylogous Peterson Elimination. *ACS Catal.* **2017**, *7* (3), 1554−1562.

(4) Scarso, A.; Colladon, M.; Sgarbossa, P.; Santo, C.; Michelin, R. A.; Strukul, G. Highly Active and Selective Platinum(II)-Catalyzed Isomerization of Allylbenzenes: Efficient Access to (*E*)-Anethole and Other Fragrances via Unusual Agostic Intermediates. *Organometallics* **2010**, *29* (6), 1487−1497.

(5) (a) Larsen, C. R.; Grotjahn, D. B. Stereoselective Alkene Isomerization over One Position. *J. Am. Chem. Soc.* **2012**, *134* (25), 10357−10360. (b) Wu, R.; Beauchamps, M. G.; Laquidara, J. M.; Sowa, J. R., Jr. Ruthenium-Catalyzed Asymmetric Transfer Hydrogenation of Allylic Alcohols by an Enantioselective Isomerization/Transfer Hydrogenation Mechanism. *Angew. Chem., Int. Ed.* **2012**, *51* (9), 2106−2110. (c) Clark, J. R.; Griffiths, J. R.; Diver, S. T. Ruthenium Hydride-Promoted Dienyl Isomerization: Access to Highly Substituted 1,3-Dienes. *J. Am. Chem. Soc.* **2013**, *135* (9), 3327−3330. (d) Larsen, C. R.; Erdogan, G.; Grotjahn, D. B. General Catalyst Control of the Monoisomerization of 1-Alkenes to trans-2-Alkenes. *J. Am. Chem. Soc.* **2014**, *136* (4), 1226−1229. (e) Bizet, V.; Pannecoucke, X.; Renaud, J.-L.; Cahard, D. Ruthenium-Catalyzed Redox Isomerization of Trifluoromethylated Allylic Alcohols: Mechanistic Evidence for an Enantiospecific Pathway. *Angew. Chem., Int. Ed.* **2012**, *51* (26), 6467−6470.

(6) (a) Yu, X.; Zhao, H.; Li, P.; Koh, M. J. Iron-Catalyzed Tunable and Site-Selective Olefin Transposition. *J. Am. Chem. Soc.* **2020**, *142* (42), 18223−18230. (b) Xu, S.; Geng, P.; Li, Y.; Liu, G.; Zhang, L.; Guo, Y.; Huang, Z. Pincer Iron Hydride Complexes for Alkene Isomerization: Catalytic Approach to Trisubstituted (*Z*)-Alkenyl Boronates. *ACS Catal.* **2021**, *11* (16), 10138−10147. (c) Woof, C. R.; Durand, D. J.; Fey, N.; Richards, E.; Webster, R. L. Iron Catalyzed Double Bond Isomerization: Evidence for an Fe(I) /Fe(III) Catalytic Cycle. *Chem.—Eur. J.* **2021**, *27* (19), 5972−5977.

https://doi.org/10.1021/jacs.5c09017
J. Am. Chem. Soc. 2025, 147, 31859−31870

(7) Liu, X.; Li, B.; Liu, Q. Base-Metal-Catalyzed Olefin Isomerization Reactions. *Synthesis* **2019**, *51* (06), 1293−1310.
(8) Raje, S.; Garhwal, S.; Młodzikowska-Pieńko, K.; Sheikh Mohammad, T.; Raphaeli, R.; Fridman, N.; Shimon, L. J. W.; Gershoni-Poranne, R.; de Ruiter, G. N_2 Dissociation vs Reversible 1,2-Methyl Migration in $PC_{NHC}P$ Cobalt(I) Complexes in the Stereoselective Isomerization (*E*/*Z*) of Allyl Ethers. *JACS Au* **2024**, *4* (11), 4234−4248.
(9) (a) Weber, F.; Schmidt, A.; Röse, P.; Fischer, M.; Burghaus, O.; Hilt, G. Double-Bond Isomerization: Highly Reactive Nickel Catalyst Applied in the Synthesis of the Pheromone (9*Z*,12*Z*)-Tetradeca-9,12-dienyl Acetate. *Org. Lett.* **2015**, *17* (12), 2952−2955. (b) Weber, F.; Ballmann, M.; Kohlmeyer, C.; Hilt, G. Nickel-Catalyzed Double Bond Transposition of Alkenyl Boronates for *in Situ* syn-Selective Allylboration Reactions. *Org. Lett.* **2016**, *18* (3), 548−551. (c) Yu, R.; Rajasekar, S.; Fang, X. Enantioselective Nickel-Catalyzed Migratory Hydrocyanation of Nonconjugated Dienes. *Angew. Chem., Int. Ed.* **2020**, *59* (48), 21436−21441. (d) Jiang, X.; Han, B.; Xue, Y.; Duan, M.; Gui, Z.; Wang, Y.; Zhu, S. Nickel-catalysed migratory hydroalkynylation and enantioselective hydroalkynylation of olefins with bromoalkynes. *Nat. Commun.* **2021**, *12* (1), No. 3792.
(10) Kapat, A.; Sperger, T.; Guven, S.; Schoenebeck, F. *E*-Olefins through intramolecular radical relocation. *Science* **2019**, *363* (6425), 391−396.
(11) Ludwig, J. R.; Schindler, C. S. Catalyst: Sustainable Catalysis. *Chem* **2017**, *2* (3), 313−316.
(12) (a) Liu, X.; Zhang, W.; Wang, Y.; Zhang, Z.-X.; Jiao, L.; Liu, Q. Cobalt-Catalyzed Regioselective Olefin Isomerization Under Kinetic Control. *J. Am. Chem. Soc.* **2018**, *140* (22), 6873−6882. (b) Zhang, S.; Bedi, D.; Cheng, L.; Unruh, D. K.; Li, G.; Findlater, M. Cobalt(II)-Catalyzed Stereoselective Olefin Isomerization: Facile Access to Acyclic Trisubstituted Alkenes. *J. Am. Chem. Soc.* **2020**, *142* (19), 8910−8917.
(13) Delgado, K. R.; Youmans, D. D.; Diver, S. T. Mild Isomerization of Conjugated Dienes Using Co-Mediated Hydrogen Atom Transfer. *Org. Lett.* **2020**, *22* (2), 750−754.
(14) Kim, D.; Pillon, G.; DiPrimio, D. J.; Holland, P. L. Highly *Z*-Selective Double Bond Transposition in Simple Alkenes and Allylarenes through a Spin-Accelerated Allyl Mechanism. *J. Am. Chem. Soc.* **2021**, *143* (8), 3070−3074.
(15) Zhao, P.; Huang, J.; Li, J.; Zhang, K.; Yang, W.; Zhao, W. Ligand-controlled cobalt-catalyzed remote hydroboration and alkene isomerization of allylic siloxanes. *Chem. Commun.* **2021**, *58* (2), 302−305.
(16) (a) Yamamoto, A.; Kitazume, S.; Pu, L. S.; Ikeda, S. Study of the fixation of nitrogen. Isolation of tris(triphenylphosphine)cobalt complex co-ordinated with molecular nitrogen. *Chem. Commun.* **1967**, No. 2, 79−80. (b) Yamamoto, A.; Kitazume, S.; Pu, L. S.; Ikeda, S. Synthesis and properties of hydridodinitrogen-tris-(triphenylphosphine)cobalt(I) and the related phosphine-cobalt complexes. *J. Am. Chem. Soc.* **1971**, *93* (2), 371−380. (c) Kumobayashi, H.; Akutagawa, S.; Otsuka, S. Metal-assisted terpenoid syntheses. 6. Enantioselective hydrogen migration in prochiral allylamine systems by chiral cobalt catalysts. *J. Am. Chem. Soc.* **1978**, *100* (12), 3949−3950.
(17) Raje, S.; Sheikh Mohammad, T.; de Ruiter, G. A Neutral $PC_{NHC}P$ Co(I)-Me Pincer Complex as a Catalyst for *N*-Allylic Isomerization with a Broad Substrate Scope. *J. Org. Chem.* **2024**, *89* (7), 4319−4325.
(18) Nicolaou, K. C.; Sorensen, E. J. *Classics in Total Synthesis: Targets, Strategies, Methods*; Wiley, 1996.
(19) Liu, X.; Zhang, W.; Wang, Y.; Zhang, Z. X.; Jiao, L.; Liu, Q. Cobalt-Catalyzed Regioselective Olefin Isomerization Under Kinetic Control. *J. Am. Chem. Soc.* **2018**, *140* (22), 6873−6882.
(20) Santelli-Rouvier, C.; Coin, C.; Toupet, L.; Santelli, M. Synthesis of the tertiaryphosphine derivatives of iron carbonyl phosphines: preparation of tetracarbonyl[tris(2-furyl)phosphine] iron(0), pentacarbonylbis[μ-bis(2-furyl)phosphido]-[tris(2-furyl) phosphine] diiron(0), tetracarbonyl[tris(2-benzofuryl) phosphine] iron(0) and pentacarbonylbis[μ-bis(2-benzofuryl) phosphido]-[tris(2-benzofuryl) phosphine]diiron-(0). *J. Organomet. Chem.* **1995**, *495* (1), 91−96.
(21) (a) Clarke, M. L.; Roff, G. J. A highly efficient procedure for hydroformylation and hydroamino-vinylation of methyl acrylate. *Green Chem.* **2007**, *9* (7), 792−796. (b) Kou, K. G. M.; Le, D. N.; Dong, V. M. Rh(I)-Catalyzed Intermolecular Hydroacylation: Enantioselective Cross-Coupling of Aldehydes and Ketoamides. *J. Am. Chem. Soc.* **2014**, *136* (26), 9471−9476. (c) Du, T.; Wang, B.; Wang, C.; Xiao, J.; Tang, W. Cobalt-catalyzed asymmetric hydrogenation of ketones: A remarkable additive effect on enantioselectivity. *Chin. Chem. Lett.* **2021**, *32* (3), 1241−1244.
(22) Chmielewska, E.; Miodowska, N.; Dziuk, B.; Psurski, M.; Kafarski, P. One-Pot Phosphonylation of Heteroaromatic Lithium Reagents: The Scope and Limitations of Its Use for the Synthesis of Heteroaromatic Phosphonates. *Molecules* **2023**, *28* (7), No. 3135.
(23) (a) Liu, H.; Cai, C.; Ding, Y.; Chen, J.; Liu, B.; Xia, Y. Cobalt-Catalyzed *E*-Selective Isomerization of Alkenes with a Phosphine-Amido-Oxazoline Ligand. *ACS Omega* **2020**, *5* (20), 11655−11670. (b) Liu, H.; Xu, M.; Cai, C.; Chen, J.; Gu, Y.; Xia, Y. Cobalt-Catalyzed *Z* to *E* Isomerization of Alkenes: An Approach to (*E*)-β-Substituted Styrenes. *Org. Lett.* **2020**, *22* (3), 1193−1198. (c) Garhwal, S.; Kaushansky, A.; Fridman, N.; de Ruiter, G. Part per million levels of an anionic iron hydride complex catalyzes selective alkene isomerization via two-state reactivity. *Chem. Catal.* **2021**, *1* (3), 631−647.
(24) Tani, K.; Yamagata, T.; Akutagawa, S.; Kumobayashi, H.; Taketomi, T.; Takaya, H.; Miyashita, A.; Noyori, R.; Otsuka, S. Metal-assisted terpenoid synthesis. 7. Highly enantioselective isomerization of prochiral allylamines catalyzed by chiral diphosphine rhodium(I) complexes. Preparation of optically active enamines. *J. Am. Chem. Soc.* **1984**, *106* (18), 5208−5217.
(25) (a) Chen, X.; Cheng, Z.; Guo, J.; Lu, Z. Asymmetric remote C-H borylation of internal alkenes via alkene isomerization. *Nat. Commun.* **2018**, *9* (1), 3939. (b) Hu, M.; Ge, S. Versatile cobalt-catalyzed regioselective chain-walking double hydroboration of 1,*n*-dienes to access *gem*-bis(boryl)alkanes. *Nat. Commun.* **2020**, *11* (1), No. 765.
(26) Lin, L.; Romano, C.; Mazet, C. Palladium-Catalyzed Long-Range Deconjugative Isomerization of Highly Substituted α,β-Unsaturated Carbonyl Compounds. *J. Am. Chem. Soc.* **2016**, *138* (32), 10344−10350.
(27) (a) Prima, D. O.; Kulikovskaya, N. S.; Galushko, A. S.; Mironenko, R. M.; Ananikov, V. P. Transition metal 'cocktail'-type catalysis. *Curr. Opin. Green Sustainable Chem.* **2021**, *31*, 100502. (b) Denisova, E. A.; Kostyukovich, A. Y.; Fakhrutdinov, A. N.; Korabelnikova, V. A.; Galushko, A. S.; Ananikov, V. P. "Hidden" Nanoscale Catalysis in Alkyne Hydrogenation with Well-Defined Molecular Pd/NHC Complexes. *ACS Catal.* **2022**, *12* (12), 6980−6996.
(28) Saraev, V. V.; Shmidt, F. K.; Larin, G. M.; Lipovich, V. G. Study of cobalt(0) complexes in catalytic systems by EPR method. *Bull. Acad. Sci. USSR, Div. Chem. Sci.* **1974**, *23* (1), 203−204.
(29) (a) Klein, H.-F. Trimethylphosphane Complexes of Nickel, Cobalt, and Iron—Model Compounds for Homogeneous Catalysis. *Angew. Chem., Int. Ed.* **1980**, *19* (5), 362−375. (b) Saraev, V. V.; Shmidt, F. K. EPR for catalysts based on nickel and cobalt complexes. *J. Mol. Catal. A: Chem.* **2000**, *158* (1), 149−154.
(30) Sen, A.; Lai, T. W. Catalytic isomerization of alkenes by palladium(II) compounds. An alternative mechanistic view. *Inorg. Chem.* **1981**, *20* (11), 4036−4038.
(31) (a) Kobayashi, T.; Yorimitsu, H.; Oshima, K. Cobalt-Catalyzed Isomerization of 1-Alkenes to (*E*)-2-Alkenes with Dimethylphenylsilylmethylmagnesium Chloride and Its Application to the Stereoselective Synthesis of (*E*)-Alkenylsilanes. *Chem.—Asian J.* **2009**, *4* (7), 1078−1083. (b) Gooßen, L. J.; Ohlmann, D. M.; Dierker, M. Silver triflate-catalysed synthesis of γ-lactones from fatty acids. *Green Chem.* **2010**, *12* (2), 197−200. (c) Pünner, F.; Schmidt, A.; Hilt, G. Up the Hill: Selective Double-Bond Isomerization of Terminal 1,3-Dienes towards *Z*-1,3-Dienes or 2*Z*,4*E*-Dienes. *Angew. Chem., Int. Ed.* **2012**, *51* (5), 1270−1273.
(32) Nielsen, C. D. T.; Burés, J. Visual kinetic analysis. *Chem. Sci.* **2019**, *10* (2), 348−353.

https://doi.org/10.1021/jacs.5c09017
J. Am. Chem. Soc. 2025, 147, 31859−31870

(33) Martínez-Carrión, A.; Howlett, M. G.; Alamillo-Ferrer, C.; Clayton, A. D.; Bourne, R. A.; Codina, A.; Vidal-Ferran, A.; Adams, R. W.; Burés, J. Kinetic Treatments for Catalyst Activation and Deactivation Processes based on Variable Time Normalization Analysis. *Angew. Chem., Int. Ed.* **2019**, *58* (30), 10189−10193.
(34) Cao, H.; Rupar, P. A. Recent Advances in Conjugated Furans. *Chem.—Eur. J.* **2017**, *23* (59), 14670−14675.



https://doi.org/10.1021/jacs.5c09017
J. Am. Chem. Soc. 2025, 147, 31859−31870

7.2 Development of highly efficient and selective palladium catalysts for telomerization of 1,3-butadiene with alcohols

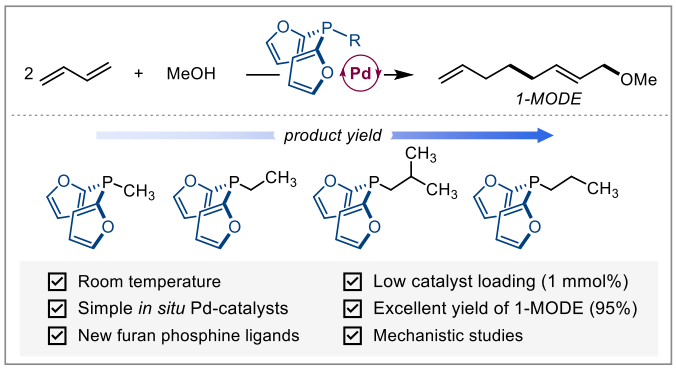

de Souza, E. L. S.‡; **Ahrens, S.**‡; Spannenberg, A.; Neumann, H.; Junge, K.; Correia, C. R. D.; Jackstell, R.; Beller, M. *Chem. Commun.* **2025**, 61, 9083.

DOI: 10.1039/d5cc01036e. Electronic supporting information is available online.

(‡Authors contributed equally.)

Author's Contribution

The author contributed to the conceptualization and design of the project, the synthesis and characterization of ligands, the optimization of reaction conditions, as well as catalytic and mechanistic studies. The author also contributed to the preparation of the initial manuscript draft and the supporting information. The author's contribution is estimated at approximately 40%.

Sebastian Ahrens
(PhD student)

Prof. Matthias Beller
(Supervisor)

ChemComm

COMMUNICATION

View Article Online
View Journal | View Issue

Open Access Article. Published on 02 May 2025. Downloaded on 10/17/2025 6:31:40 AM.
This article is licensed under a Creative Commons Attribution 3.0 Unported Licence.

Check for updates

Cite this: *Chem. Commun.*, 2025, **61**, 9083

Received 26th February 2025,
Accepted 2nd April 2025

DOI: 10.1039/d5cc01036e

rsc.li/chemcomm

Development of highly efficient and selective palladium catalysts for telomerization of 1,3-butadiene with alcohols†

Edson Leonardo Scarpa de Souza,‡[a] Sebastian Ahrens,‡[a] Anke Spannenberg,[a] Helfried Neumann,[a] Kathrin Junge,[a] Carlos Roque Duarte Correia,[b] Ralf Jackstell*[a] and Matthias Beller*[a]

Novel phosphine ligands based on (benzo)furylphosphines, enable the efficient palladium-catalyzed telomerization of 1,3-butadiene with methanol. The synthesis of industrially relevant 1-methoxy-2,7-octadiene (1-MODE) occurs in quantitative yields and excellent productivity (TON = 95.000), even at ambient temperatures.

1-Octene plays a pivotal role in industrial chemistry, with a multi-100 000-ton scale utilization as a monomer in the production of linear low-density polyethylene. Its significance extends to its role as a precursor for plasticizers, alcohols, and solvents, as well as in the production of fine chemicals, including corrosion inhibitors and herbicides.[1,2] Consequently, the synthesis of 1-octene has been a subject of interest for decades, and numerous methods have been developed to achieve this objective, including oligomerization of ethylene.[3,4] Among the industrial processes that have been applied, telomerization of 1,3-butadiene is noteworthy for its selectivity and environmental friendliness, exhibiting 100% atomic efficiency.[1,5–7]

The telomerization of 1,3-butadiene with methanol was first reported in 1967 independently by Smutny at Shell[8] and Takahashi at Osaka University.[9] In general, the telomerization can selectively afford 1-octene from inexpensive feedstocks through a three-step process (Scheme 1). Initially, the telomer 1-methoxy-2,7-octadiene (1-MODE, **2**) is produced *via* a palladium-catalyzed reaction. It is noteworthy that this step, apart from yielding the desired linear product (1-MODE), can also result in the formation of the branched product (3-MODE) and other byproducts. In the second step, hydrogenation of 1-MODE **2** furnishes 1-methoxyoctane **3**, which subsequently gives 1-octene **4** and methanol by thermal cracking.[1] The subsequent steps, namely hydrogenation and thermal cracking, are well-established processes that yield their respective products in a quantitative yield. Therefore, the efficiency of the overall process is determined by the telomerization reaction. Consequently, numerous researchers in both industry and academia have demonstrated a persistent interest in this transformation, with the objective of enhancing the yield, catalyst productivity, and selectivity for 1-MODE **2** synthesis.[10–17] To achieve high catalyst activity and regio- and chemoselectivity, a multitude of ligands, particularly mono- and bidentate phosphines, have been developed and evaluated in this transformation over the years.

As an example, in the presence of PPh_3, 1-MODE **2** is obtained in moderate to good yield, but poor linear/branched selectivity.[18–21] Derivatives of PPh_3 containing electron-donating methoxy substituents, especially in the *para* position, have been shown to yield superior results.[22–24] Intriguingly, ligands possessing bulky xanthene backbones have been observed to exhibit remarkable activity at low temperatures, and their oxygen coordination properties have been postulated to contribute to their enhanced performance.[25–27]

In addition, several trialkylphosphines were applied in the conversion of 1,3-butadiene into 1-MODE. It was observed that PEt_3 gave higher selectivity than PPh_3, while PCy_3 tended to give mainly undesired 1,3,7-octatriene instead of 1-MODE **2**.[23,28] Compared to PPh_3, bidentate phosphines showed better selectivity in the telomerization of 1,3-butadiene at lower temperature. Finally, it is worth mentioning that in the past two decades N-heterocyclic carbenes (NHCs) were introduced and studied in detail. These Pd–NHC-complexes afforded 1-MODE **2** in high selectivity in the presence of only ppm amounts of Pd (Scheme 1).[2]

While most prior research has been conducted with *in situ* generated Pd catalysts, some molecularly defined Pd complexes have also been examined in the telomerization reaction. Despite the necessity for additional synthesis steps and the potential increased sensitivity of the corresponding complexes,

[a] *Leibniz-Institut für Katalyse e.V., Albert-Einstein-Str. 29a, 18059 Rostock, Germany. E-mail: matthias.beller@catalysis.de*
[b] *Department of Organic Chemistry, Institute of Chemistry, University of Campinas, Rua Josué de Castro, 10384-612, Campinas, São Paulo, Brazil*

† Electronic supplementary information (ESI) available: CCDC 2339359. For ESI and crystallographic data in CIF or other electronic format see DOI: https://doi.org/10.1039/d5cc01036e

‡ These authors contributed equally to the development of this work.

Open Access Article. Published on 02 May 2025. Downloaded on 10/17/2025 6:31:40 AM.
This article is licensed under a Creative Commons Attribution 3.0 Unported Licence.

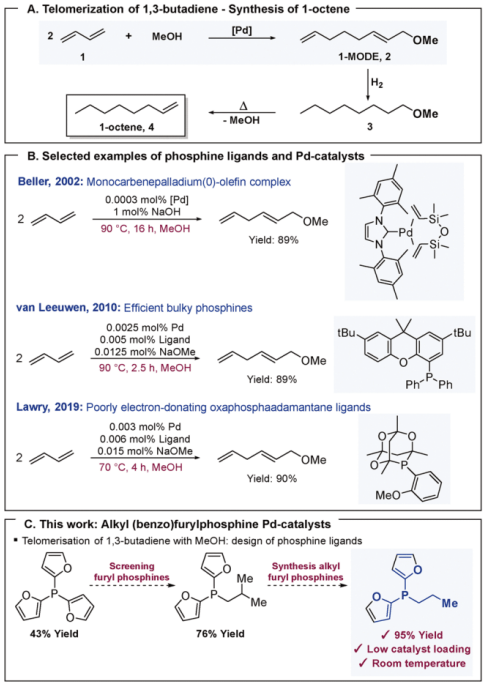

Scheme 1 (A) Synthesis of 1-octene **4** *via* Pd-catalyzed telomerization of 1,3-butadiene **1** with methanol. (B) Selected examples of ligands and Pd-complexes applied in the synthesis of 1-MODE **2**. (C) Design of alkyl (benzo)furylphosphine ligands for Pd-catalysts.

Table 1 Pd-catalyzed telomerization of 1,3-butadiene with methanol: testing different ligands[a]

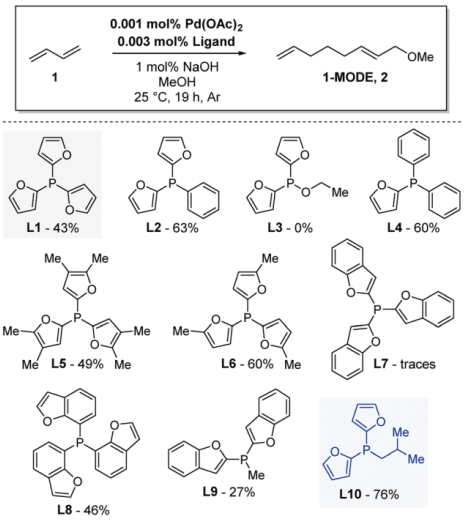

[a] Reaction conditions: $Pd(OAc)_2$ (0.001 mol%), ligand (0.003 mol%), NaOH (1 mol%), MeOH (1.5 mL/1.0 g 1,3-butadiene), condensed 1,3-butadiene, Ar, 25 °C, stirring at 750 rpm, 19 h. Yields calculated from GC-FID slope with isooctane as ISTD.

well-defined complex structures offer a distinct advantage in terms of enhanced catalyst activity. For instance, PPh_3–Pd–(η^2–η^2-allylether) was shown to be active even at −10 °C.[2,29,30]

Recently, our group prepared novel electron-rich furyl and benzofuryl phosphines for cobalt-catalyzed isomerization reactions. Building upon the above-mentioned previous works in the field of telomerization, we have postulated that the corresponding palladium complexes should be active in this transformation. Consequently, we have initiated a project to evaluate their performance. To enable proper activity evaluation and potential applications, all catalytic experiments were performed at low temperature (room temperature) and low Pd loading (0.001 mol%). Mechanistic studies showed that the active Pd species contains only one coordinated phosphine.[19,31,32] However, to ensure proper stabilization of the active metal species at low metal concentration, a metal : ligand ratio of 1 : 3 was applied. Utilizing PPh_3 as a ligand under these conditions gave 1-MODE **2** in 50% yield. In comparison, the use of tri(furan-2-yl)phosphine (TFP) **L1**, a commercially available ligand, resulted in 1-MODE **2**, albeit with a slightly lower yield (Table 1). It is also noteworthy that the majority of the previously examined monodentate ligands are symmetrical in nature. Interestingly, non-symmetric phosphine, obtained through the substitution of one or two phenyl groups with furyl groups, resulted in the telomerization product **2** in higher yields (**L2**, 60% and **L4**, 63%, respectively). In contrast, the more electron-rich TFP derivatives **L5** and **L6** provided 1-MODE **2** with yields of 49% and 60%, respectively. The evaluation of different tribenzofurylphosphines (**L7–L9**) demonstrated that the resulting orientation of the furan and benzofuran ring plays a crucial role in the coordination to the metal center, which is decisive for the catalytic activity.

While only traces of the desired product were observed with tri-2-benzofuranephosphine **L7**, tri-8-benzofuranephosphine **L8** gave a yield of 46% of 1-MODE **2**. Furthermore, we tested alkyl-substituted furyl and benzofurylphosphines and difuryl-isobutylphosphine **L10** provided the desired 1-MODE **2** in 76% yield. It is noteworthy that most of the catalytic experiments were performed at least twice and exhibited a very good degree of reproducibility. Considering the favorable outcome observed with **L10**, a systematic variation of the alkyl substituent on the difuryl phosphines was employed to enhance the activity of the respective palladium catalyst. A total of eight distinct alkyl difuryl phosphines were synthesized and utilized in the benchmark reaction (see Table 2 for details). The catalysis with the methyl-substituted phosphine **L11** furnished 1-MODE **2** in 53% yield, while the ethyl-substituted ligand **L12** yielded 70% of the product. Notably, the *n*-propyl-substituted difuryl phosphine **L13** achieved a remarkable 95% yield. Conversely, when iso-butyl- (**L10**) and *n*-butyl- (**L14**) substituted phosphines were utilized, the

 This journal is © The Royal Society of Chemistry 2025

Open Access Article. Published on 02 May 2025. Downloaded on 10/17/2025 6:31:40 AM.
This article is licensed under a Creative Commons Attribution 3.0 Unported Licence.

Table 2 Testing di-furyl alkyl phosphines in the Pd-catalyzed telomerization reaction: variation of the alkyl chain length of the ligand[a]

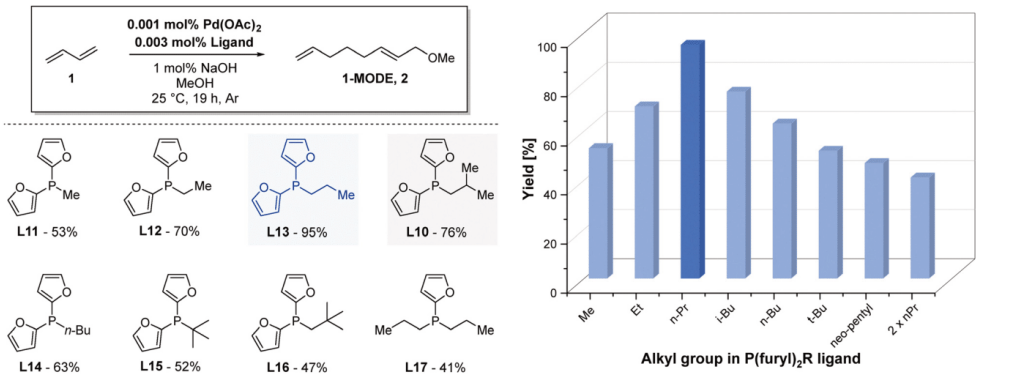

[a] Reaction conditions: $Pd(OAc)_2$ (0.001 mol%), ligand (0.003 mol%), NaOH (1 mol%), MeOH (1.5 mL/1.0 g butadiene), condensed 1,3-butadiene, Ar, 25 °C, stirring at 750 rpm, 19 h. Yields calculated from GC-FID slope with isooctane as ISTD.

yields were found to be considerably lower, at 76% and 63%, respectively. Ligands bearing alkyl groups with increased steric hindrance, such as *tert*-butyl **L15** and neopentyl **L16**, yielded 1-MODE in 52% and 47% yield, respectively. In the possession of the optimal ligand (**L13**), we proceeded to synthesize **L17**, which possess a single furyl group and two *n*-propyl chains attached to the phosphorus atom. When the telomerization reaction was performed with **L18**, the desired product was obtained in 41% yield, indicating the crucial role of the two furyl motifs and the propyl chain for the activity of the Pd catalyst.

As demonstrated in Table 2, a clear correlation exists between the size of the linear alkyl chain in the ligand and the yield of 1-MODE **2**, which attains an optimal level with *n*-propyl chains. Further increases in chain length (>*n*-propyl) and/or the bulkiness of the alkyl chains result in a decline in the desired product yield. It is noteworthy that the reaction in the presence of difuryl-alkyl-phosphine ligands proceeds with low catalyst loadings at room temperature towards the desired product with high selectivity, yielding exclusively the *Z*-isomer of 1-MODE **2**.

Nevertheless, even more active ligands could be expected by the proper combination of phosphine substituents, *e.g.* **L13** with methyl-furyl units.[33] Even though the yield of 1-MODE **2** was nearly quantitative with **L13** (95%, TON 95.000), further investigation was conducted into the role of the ligand (Table 3). In the absence of a ligand, no product was formed (Table 3, entry 1). Subsequent assessment of the ligand-to-metal ratio (L : M ratio) revealed a decline in yield for 1-MODE **2** when the L : M ratio was 1 : 1 or 5 : 1 (Table 3, entries 2 and 3). Furthermore, the effect of temperature on the telomerization reaction was investigated, and the catalytic system demonstrated optimal efficiency at 25 °C (Table 3, entry 5). Conversely, at 0 °C, the reaction yield was 10% (Table 3, entry 4). At 50 °C, the catalytic system exhibited a 93% yield. However, at elevated temperatures of 70 °C or 90 °C, the yield of 1-MODE 2 decreased to 52% and 58%, respectively (Table 3, entries 6–8). Notably, utilizing only 0.0005 mol% of

Table 3 Pd-catalyzed telomerization: influence of selected reaction parameters[a]

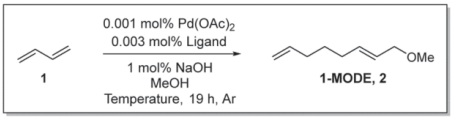

Entry	Changes from standard conditions	1-MODE (%)
1[b]	Without **L13**	0
2	0.001 mol% **L13**	50
3	0.005 mol% **L13**	42
4	0 °C	10
5	25 °C	95
6	50 °C	93
7	70 °C	52
8	90 °C	58
9[c]	0.0005 mol% $Pd(OAc)_2$	35

[a] Reaction conditions: $Pd(OAc)_2$ (0.001 mol%), L13 (0.003 mol%), NaOH (1 mol%), MeOH (1.5 mL/1.0 g 1,3-butadiene), condensed 1,3-butadiene, Ar, 25 °C, stirring at 750 rpm, 19 h. Yields calculated from GC-FID slope with isooctane as ISTD. [b] Reaction performed at 90 °C. [c] Ligand: 0.0015 mol% L13.

$Pd(OAc)_2$ produced the desired product in a moderate yield of 35%, as shown in Table 3, entry 9. Additionally, we investigated the air stability of **L13** and, to our surprise, the electron-rich phosphine **L13** (^{31}P NMR: −62.0 ppm) is considerably stable under aerobic conditions. More specifically, only 6% of the corresponding phosphine oxide **L18** (^{31}P NMR: 12.2 ppm, 1.0 : 0.06 ligand : ligand oxide ratio) was detected in a ^{31}P NMR spectrum after exposing **L13** to air at room temperature for an overnight period.

Following a week of storage in ambient air, the presence of approximately 21% phosphine oxide **L18** (with a ligand : ligand oxide ratio of 1.0 : 0.27) was ascertained through ^{31}P NMR analysis. The complete oxidation of **L13** to **L18** was only achieved using hydrogen peroxide as the oxidizing agent (for

Open Access Article. Published on 02 May 2025. Downloaded on 10/17/2025 6:31:40 AM.
This article is licensed under a Creative Commons Attribution 3.0 Unported Licence.

the crystal structure of **L18** see Fig. S4, ESI†). Notably, negligible amounts of 1-MODE **2** were observed with **L18**.

In the previous studies of telomerization reactions, the reactivity of the alcohol was often neglected. To examine the activity of this newly developed catalytic system towards different alcohols, the telomerization reaction was performed in a mixture of two alcohols with very similar structure and properties, namely methanol and ethanol. Notably, under standard conditions (Table 3), the catalytic system demonstrated a high degree of selectivity for methanol, yielding the products 1-MODE : 1-EtODE in a 10 : 1 ratio (ESI†). We assume that this selectivity is a result of the preferred protonation of the Pd–(η^3,η^1-octadienediyl)-complex, formed by the oxidative addition of 1,3-butadiene to the Pd(0)-complex. Notably, even when the percentage of ethanol in the solvent mixture was increased to a 1 : 1 ratio of methanol : ethanol, the reaction remained selective towards 1-MODE (ESI†). This observation led to the subsequent evaluation of the selectivity of the novel catalytic system for methanol in the presence of *n*-butanol. The resultant 1-MODE : 1-*n*BuODE ratio of 9 : 1 (ESI†) indicates the high degree of chemoselectivity of this system, which might be used for selective telomerizations of alcohol mixtures and substrates with more than one hydroxyl group. Finally, the mechanism of this reaction is believed to operate in a manner consistent with the findings of the original studies conducted by Jolly and colleagues[31] and subsequent investigations.[32,34–36]

In summary, we have synthesized and applied novel difuryl-alkyl-phosphines for the Pd-catalyzed telomerization reaction of 1,3-butadiene. Notably, the *n*-propyl derivative (**L13**) was identified as the optimal ligand for the synthesis of 1-MODE **2**. The newly developed catalytic system, as outlined in this report, enables the efficient synthesis of 1-MODE **2** with a high degree of purity using only 0.001 mol% of Pd at ambient temperature. Furthermore, experiments employing mixtures of alcohols in the telomerization reaction demonstrated a high degree of chemoselectivity for the optimal catalyst system.

Data availability

The data supporting this article have been included as part of the ESI.†

Conflicts of interest

There are no conflicts to declare.

Notes and references

1 S. Recker, C. M. Gordon, A. Peace, C. Redepenning and W. Marquardt, *Chem. Ing. Tech.*, 2017, **89**, 1479–1489.
2 R. Jackstell, M. G. Andreu, A. Frisch, K. Selvakumar, A. Zapt, H. Klein, A. Spannenberg, D. Röttger, O. Briel, R. Karch and M. Beller, *Angew. Chem., Int. Ed.*, 2002, **41**, 986–988.
3 J. Yang, P. Wang, H. Neumann, R. Jackstell and M. Beller, *Ind. Chem. Mater.*, 2023, **1**, 155–174.
4 T. A. Faßbach, A. J. Vorholt and W. Leitner, *ChemCatChem*, 2019, **11**, 1153–1166.
5 Y. Zong, C. Wang and Y. Zhang, *Polymers*, 2023, **15**, 1044.
6 M. Sharif, R. Jackstell, S. Dastgir, B. Al-Shihi and M. Beller, *ChemCatChem*, 2017, **9**, 542–546.
7 D. Peruzzo, M. Drelon, C. Dumont, A. Mortreux, I. Suisse and M. Sauthier, *Mol. Catal.*, 2021, **502**, 111369.
8 E. J. Smutny, *J. Am. Chem. Soc.*, 1967, **89**, 6793–6794.
9 S. Takahashi, T. Shibano and N. Hagihara, *Tetrahedron Lett.*, 1967, 2451–2453.
10 H. Zhang, C. Shen, Z. Xu, X. Tian and K. Dong, *Mol. Catal.*, 2021, **515**, 111883.
11 M. A. Topchiy, S. A. Rzhevskiy, L. I. Minaeva and A. F. Asachenko, *Pet. Chem.*, 2022, **62**, 1235–1241.
12 D. Peruzzo, M. Drelon, C. Dumont, A. Mortreux, I. Suisse and M. Sauthier, *Mol. Catal.*, 2021, **502**, 1–6.
13 D. S. Suslov, M. V. Bykov, M. V. Pakhomova, T. S. Orlov, Z. D. Abramov, A. V. Suchkova, A. A. Pavlova and P. A. Abramov, *J. Struct. Chem.*, 2023, **64**, 2235–2254.
14 S. Recker, C. M. Gordon, A. Peace and C. Redepenning, *Chem. Ing. Tech.*, 2017, 1479–1489.
15 Z. Wang, S. Hasegawa, K. Motokura, S. Kuang and Y. Yang, *Ind. Eng. Chem. Res.*, 2023, **62**, 3151–3156.
16 S. A. Rzhevskiy, M. A. Topchiy, V. N. Bogachev, A. A. Ageshina, L. I. Minaeva, G. K. Sterligov, M. S. Nechaev and A. F. Asachenko, *Mendeleev Commun.*, 2021, **31**, 478–480.
17 J. Colavida, J. A. Lleberia, A. Salom-Catala, A. Gual, A. Collado, E. Zangrando, J. M. Ricart, C. Godard, C. Claver, J. J. Carbo and S. Castillon, *ACS Catal.*, 2020, **10**, 11458–11465.
18 B. Estrine, S. Bouquillon, F. Hénin and J. Muzart, *Eur. J. Org. Chem.*, 2004, 2914–2922.
19 F. Vollmüller, J. Krause, S. Klein, W. Mägerlein and M. Beller, *Eur. J. Inorg. Chem.*, 2000, 1825–1832.
20 M. Drelon, D. S. Mérel, A. Mortreux, I. Suisse and M. Sauthier, *ChemCatChem*, 2019, **11**, 1742–1746.
21 J. Wang, X. Feng, J. Song, Z. Gao and W. Wang, *ChemistrySelect*, 2020, **5**, 9404–9408.
22 J. L. Klinkenberg and K. P. Lawry, *Org. Process Res. Dev.*, 2019, **23**, 1654–1658.
23 F. Benvenuti, C. Carlini, M. Lami, M. Marchionna, R. Patrini, A. M. Raspolli Galletti and G. Sbrana, *J. Mol. Catal. A: Chem.*, 1999, **144**, 27–40.
24 R. Palkovits, I. Nieddu, C. A. Kruithof, R. J. M. K. Gebbink and B. M. Weckhuysen, *Chem. – Eur. J.*, 2008, **14**, 8995–9005.
25 T. E. Barder, S. D. Walker, J. R. Martinelli and S. L. Buchwald, *J. Am. Chem. Soc.*, 2005, **127**, 4685–4696.
26 M. J. L. Tschan, H. Launay, H. Hagen, J. Benet-Buchholz and P. W. N. M. Van Leeuwen, *Chem. – Eur. J.*, 2011, **17**, 8922–8928.
27 M. J. L. Tschan, E. J. García-Suárez, Z. Freixa, H. Launay, H. Hagen, J. Benet-Buchholz and P. W. N. M. Van Leeuwen, *J. Am. Chem. Soc.*, 2010, **132**, 6463–6473.
28 F. Benvenuti, C. Carlini, M. Marchionna, R. Patrini, A. M. Raspolli Galletti and G. Sbrana, *J. Mol. Catal. A: Chem.*, 1999, **140**, 139–155.
29 J. Krause, G. Cestaric, K. J. Haack, K. Seevogel, W. Storm and K. R. Pörschke, *J. Am. Chem. Soc.*, 1999, **121**, 9807–9823.
30 A. Grotevendt, R. Jackstell, D. Michalik, M. Gomez and M. Beller, *ChemSusChem*, 2009, **2**, 63–70.
31 P. W. Jolly, *Angew. Chem., Int. Ed. Engl.*, 1985, **24**, 283–295.
32 C. F. Huo, R. Jackstell, M. Beller and H. Jiao, *J. Mol. Model.*, 2010, **16**, 431–436.
33 We thank one of the referees for pointing out this aspect.
34 F. Vollmüller, W. Ma, S. Klein, J. Krause and M. Beller, *Adv. Synth. Catal.*, 2001, 29–33.
35 N. D. Clement, L. Routaboul, A. Grotevendt and R. Jackstell, *Chem. – Eur. J.*, 2008, **14**, 7408–7420.
36 F. Vollmüller, J. Krause, S. Klein, W. Mägerlein and M. Beller, *Eur. J. Inorg. Chem.*, 2000, 1–7.

 This journal is © The Royal Society of Chemistry 2025

7.3 Synthesis of non-equivalent diamides and amido-esters via Pd-catalysed carbonylation

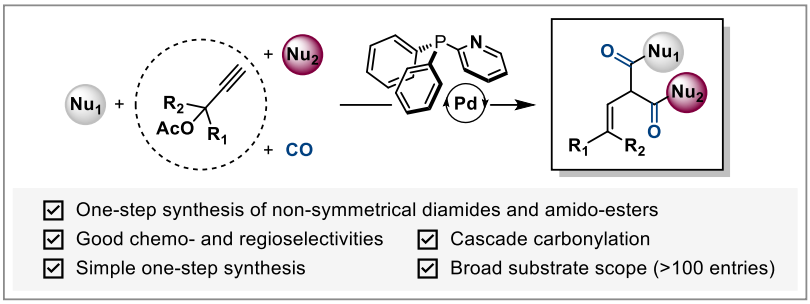

Ge, Y.; Huang, W.; **Ahrens, S.**; Spannenberg, A.; Jackstell, R.; Beller, M. *Nat. Synth.* **2024**, 3, 202–213.

DOI: 10.1038/s44160-023-00411-6. Electronic supporting information is available online.

Author's Contribution

The author contributed to the investigation of the substrate scope, the evaluation of the resulting data, and the performance of mechanistic experiments. The author also contributed to the preparation of the manuscript and the revision process. The author's contribution approximately accounts 20%.

Sebastian Ahrens
(PhD student)

Prof. Matthias Beller
(Supervisor)

nature synthesis

Article

https://doi.org/10.1038/s44160-023-00411-6

Synthesis of non-equivalent diamides and amido-esters via Pd-catalysed carbonylation

Received: 21 March 2023

Accepted: 1 September 2023

Published online: 5 October 2023

Check for updates

Yao Ge, Weiheng Huang, Sebastian Ahrens, Anke Spannenberg, Ralf Jackstell & Matthias Beller

Given the widespread use of amides in chemistry and biology, the development of methods for their synthesis remains important. Although the construction of amide bonds has in principle been known since Wöhler's urea synthesis, the direct and atom-efficient preparation of amides, especially with multiple amido groups, continues to be difficult. To address this challenge, we developed an efficient access to heterobifunctional compounds through linking amines as well as alcohols with specific molecular pincers in the presence of advanced carbonylation catalysts. In detail, we describe the synthesis of non-symmetrical diamides and amido-esters from available propargylic acetates using selective palladium-catalysed diamino- and amino-alkoxy carbonylations. Mechanistic studies and control experiments reveal a cascade process with allenoic amides, allylic amine and dienamide as crucial intermediates. The generality of this protocol is showcased by the highly selective synthesis of >100 heterobifunctional molecules including many pharmaceutically relevant products.

Amide bonds, as the backbone of proteins, not only play a crucial role in elaboration and composition of biological systems but are also present in most pharmacologically active compounds and materials, for example, hydrogels, artificial silks and biocompatible matrices for cell growth[1]. Indeed, amides are identified as the most frequently occurring functional group in ~40% of 420,000 bioactive molecules or two-thirds of drug candidates, and represent 25% of all pharmaceuticals currently on the market according to surveys in 2006 and 2020 (refs. 2–4). In addition, in 2014, >50% of the reported reactions in process chemistry of the pharmaceutical industry used amidation reactions[5]. This demand for amide synthesis encourages constant efforts towards the development of advanced synthetic methods and the construction of new amides. In this respect, diamide and amido-ester derivatives, which are widely distributed in many natural products, are also important in pharmaceutical chemistry[6–11]. For example, several top-selling drugs such as apixaban[6], penicillin[7] and diltiazem[8], as well as the oral anti-COVID-19 drug Paxlovid[9], possess diamide and amido-ester units (Fig. 1a).

Despite the importance of amides in organic chemistry, most of the well-established methods for their formation are relatively inefficient and co-produce large quantities of potentially hazardous waste products. In addition, the purification of the desired amide product can be tedious and difficult[12–15]. This is particularly true for the preparation of non-symmetrical diamide derivatives (Fig. 1b). Traditionally, multi-step synthesis and well-designed or previously functionalized specific starting materials are required for the synthesis of non-symmetrical diamides to avoid the generation of monoamides, symmetrical diamides and other undesirable by-products[16–19]. As an example, for preparation of non-symmetrical terephthaldiamides, it takes six steps to prepare the corresponding product, starting from commercially available *p*-phthaloyl chloride (Fig. 1c)[19]. Indeed, the simple treatment of *p*-phthaloyl chloride[20] with two different amines, for example, *n*-hexylamine and *N*-methylaniline, led to a complex mixture. Likewise, the direct preparation of non-symmetrical diamides of other dicarboxylic acids, for example, malonic acid[21] and phthalic anhydride[22], gave no desired diamides after common amide bond formation reactions (Supplementary Figs. 1–3). Thus, a straightforward and chemoselective synthesis of diamides by joining two different amines with similar reactivities is still in high demand.

In the field of proteomics and medical chemistry, the bio-orthogonal conjugation strategy of *N*-hydroxysuccinimide (NHS) esters with amines (famous as click chemistry and bio-orthogonal chemistry), highlighted by the Nobel Prize in 2022, allows linkage of chemical

Leibniz-Institut für Katalyse e.V., Rostock, Germany. e-mail: matthias.beller@catalysis.de

Article https://doi.org/10.1038/s44160-023-00411-6

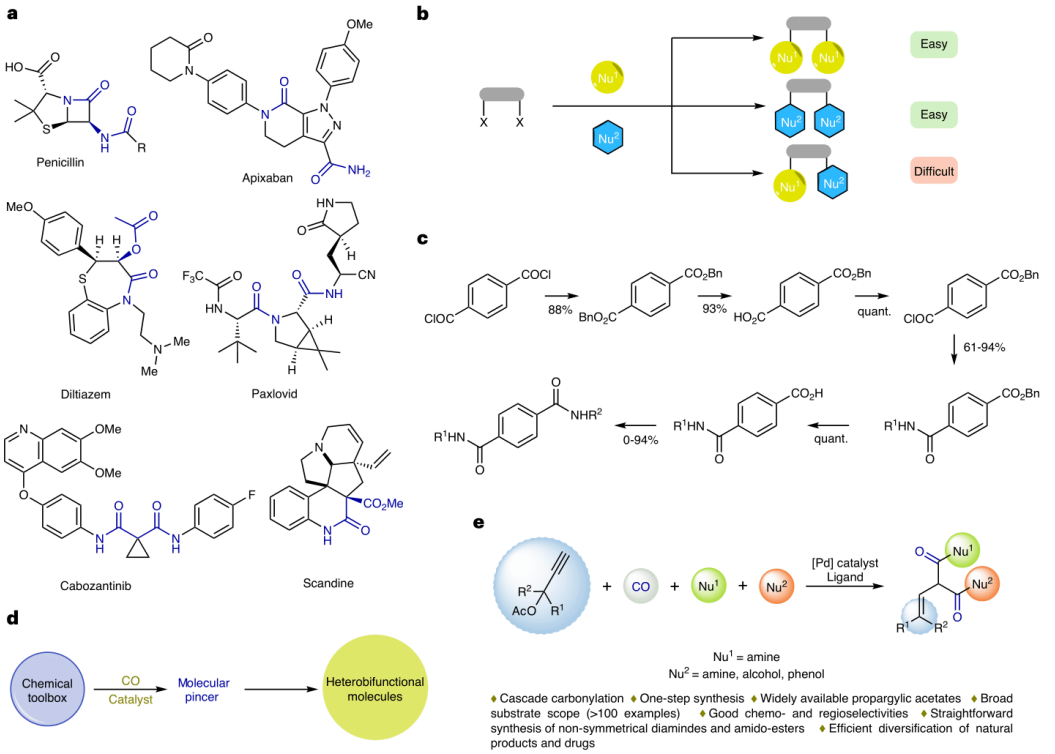

Fig. 1 | Reaction design and development. a, Selected examples of biologically active molecules and pharmaceuticals featuring diamide and amido-ester skeletons. **b**, Traditional ways of synthesizing non-symmetrical diamides **c**, An example for preparation of non-symmetrical terephthaldiamides, over six synthetic steps[19]. **d**, General concept for conversion of a chemical toolbox to heterobifunctional molecules through link chemistry. **e**, The method reported in the present study to access non-symmetrical diamides and amido-esters through dicarbonylation reactions.

fragments in a most efficient way; however, these methods make use of distinctly different molecules[23,24]. Inspired by this concept, we thought it would be appealing to develop a strategy for tethering two or more amines and/or alcohols selectively together with an appropriate molecular pincer as the cross-linking reagent (Fig. 1d). Such tethering of distinguished molecules, but with the same functional group, can be an efficient way to diversify chemical space[25]. As amino groups are omnipresent in pharmaceutically active compounds, their linkage by a molecular pincer can result in completely new biological activities[26–29].

To realize such transformations, the development of suitable linking reagents, which allow the selective connection of two different functional groups with similar reactivities, is crucial. As an extension to traditional link chemistry, which relies on high-throughput screening or iterative trial and error[25,29,30], we had the idea of selectively generating two different activated carboxylic acyl groups in situ via transition metal-catalysed carbonylation reactions (Fig. 1e), which are among the most important applications of industrial catalysis to produce a variety of bulk and fine chemicals[31–38].

Results

Reaction design and catalyst development

Recently, we demonstrated the usefulness of palladium (Pd)-catalysed mono- and dicarbonylation reactions of propargylic alcohols for the preparation of diverse heterocyclics. Notably, depending on the phosphine ligands, different reaction pathways can be controlled[39–41]. Thus, we had the idea that such transformations offer a unique way to utilize previously unexplored double carbonylations to tether amines using propargylic acetates as a molecular toolbox of the linkers. Challenges associated with such transformation are: (1) the catalyst must promote the different carbonylation reactions on the substrate; (2) the first amide bond must be formed selectively, despite the similar reactivities of diverse nucleophiles; and (3) side reactions such as monocarbonylation, isomerization and hydroamination must be suppressed too. Finally, it is worth mentioning that, specifically in the presence of amines and related substrates required for the synthesis of carboxamides, contradictory reactivity (acidic metal hydrides versus basic aliphatic amines) needs to be tolerated[42]. Thus, it is not surprising that, to the best of our knowledge, no such process has yet been reported. At the start, we selected 2-phenylbut-3-yn-2-yl acetate, **1a**, as a stable precursor for the molecular pincer. Its reaction with hexylamine, **2a**, and *N*-methylaniline, **3a**, was selected as a model system for connecting aliphatic and aromatic amines together and thereby providing an array of non-symmetrical malonamides (Table 1). Notably, malonamides are frequently found in retropeptidic derivatives, with the amide moiety serving as a functional linker to connect two fragments[10,16]. To control the chemo- and regioselectivity in this highly complicated reaction network, the selection of the catalyst system is crucial[31–36,39,43,44]. Thus, at the start of our study, we tested different mono- and bidentate phosphine

Article https://doi.org/10.1038/s44160-023-00411-6

Table 1 | Ligand optimization for Pd-catalysed dicarbonylation of 2-phenylbut-3-yn-2-yl acetate, 1a

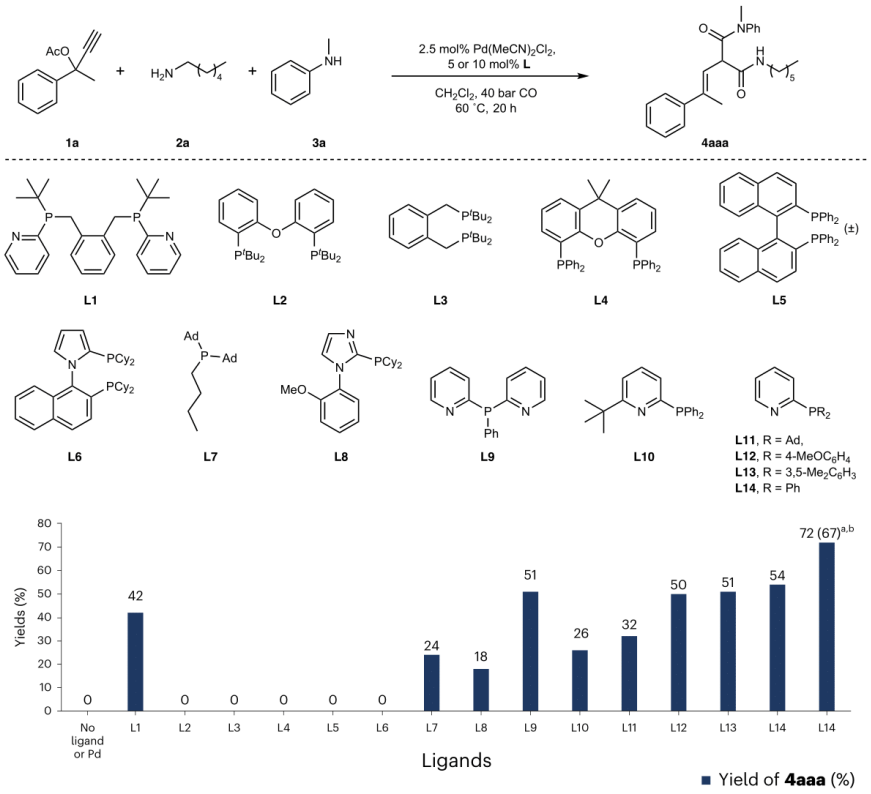

Reaction conditions: **1a** (0.2 mmol), **2a** (0.2 mmol), **3a** (0.2 mmol), $Pd(MeCN)_2Cl_2$ (2.5 mol%), bisphosphine ligand (5.0 mol%) or monophosphine ligand (10.0 mol%), CO (40 bar), CH_2Cl_2 (2.0 ml), 20 h at 60 °C. The yields of products were determined by crude ^1H NMR spectroscopic analysis using dibromomethane as the internal standard. [a]**2a** (0.3 mmol), **3a** (0.3 mmol). [b]Isolated yield. Ac, acetyl; Ad, adamantyl; Cy, cyclohexyl.

ligands (10 and 5 mol%, respectively) in the carbonylation of **1a** in the presence of 2.5 mol% $Pd(MeCN)_2Cl_2$, dichloromethane (solvent) and 40 bar CO at 60 °C (Table 1). As expected, no reaction occurred without ligand or Pd present. In the presence of our recently developed ligand **L1** (LIKATphos)[45] with 2-pyridyl-*tert*-butylphosphino groups, which proved to have unique reactivity in alkoxy carbonylations, full conversion occurred with the desired non-symmetrical malonamide **4aaa** as the main product (42% yield). Evaluating other commonly used bisphosphines, **L2**–**L6**, either provided complex reaction mixtures or did not give this product at all. Surprisingly, among the monophosphine ligands, **L7**–**L9** and **L9** gave an improved yield of **4aaa** (51%). Consequently, we studied the effect of analogous ligands **L10**–**L14** with different steric and electronic properties. When diphenyl(2-pyridyl)-phosphine, **L14** (ref. 46), was applied, the yield of this non-symmetrical dicarbonylation product reached 54%. The effectiveness of **L14** and related ligands is explained by the pyridine substituent on the phosphorous atom, which improved the rate of nucleophilic attack on the intermediate palladium acyl complex[39–41,45]. By variation of reaction parameters (catalyst precursor, temperature, pressure, etc.) in the presence of **L14**, the yield of **4aaa** was improved to 72% and only small amounts (<10%) of symmetrical diamides were formed (Supplementary Tables 1–8).

Mechanistic investigations

To understand the selectivity of this reaction in more detail, the dicarbonylation of **1a** with benzylamine, **2b**, and *N*-methylaniline, **3a**, was monitored under standard catalytic conditions; **2b** was used as a coupling partner because of the convenient characterization of the corresponding intermediates. As shown in Fig. 2a, the target product **4aba** was formed in 53% yield, whereas many species including allenoic amide **Int 1**, allylic amine **Int 2** and dienamide **Int 3** could be detected by ^1H nuclear magnetic resonance (NMR) spectroscopic analysis. At first, **1a** is converted into the allenoic amide, **Int 1**, which achieved a maximum yield of 42% after 45 min. Soon after, the starting material, **1a**, is fully converted and formation of allenoic amide, **Int 1**, allylic amine, **Int 2**, and dienamide, **Int 3**, took place. Then, **4aba** is generated along with the consumption of the reaction intermediates **Int 1**, **Int 2** and **Int 3**. After 8 h, the reaction is almost complete (Fig. 2b).

Next, control experiments were performed using **Int 1** and **Int 2** as starting materials (Fig. 2c). Indeed, the target compound **4aba** was produced in 42% and 53% yield, respectively, under standard conditions, which confirmed that **Int 1** and **Int 2** are active reaction intermediates in the overall process. Based on these findings and previous mechanistic studies of Pd-catalysed carbonylations[35,39–41,47–51], we propose the following main reaction pathway (Fig. 2d): initially, the stable Pd^{II} salt could

 https://doi.org/10.1038/s44160-023-00411-6

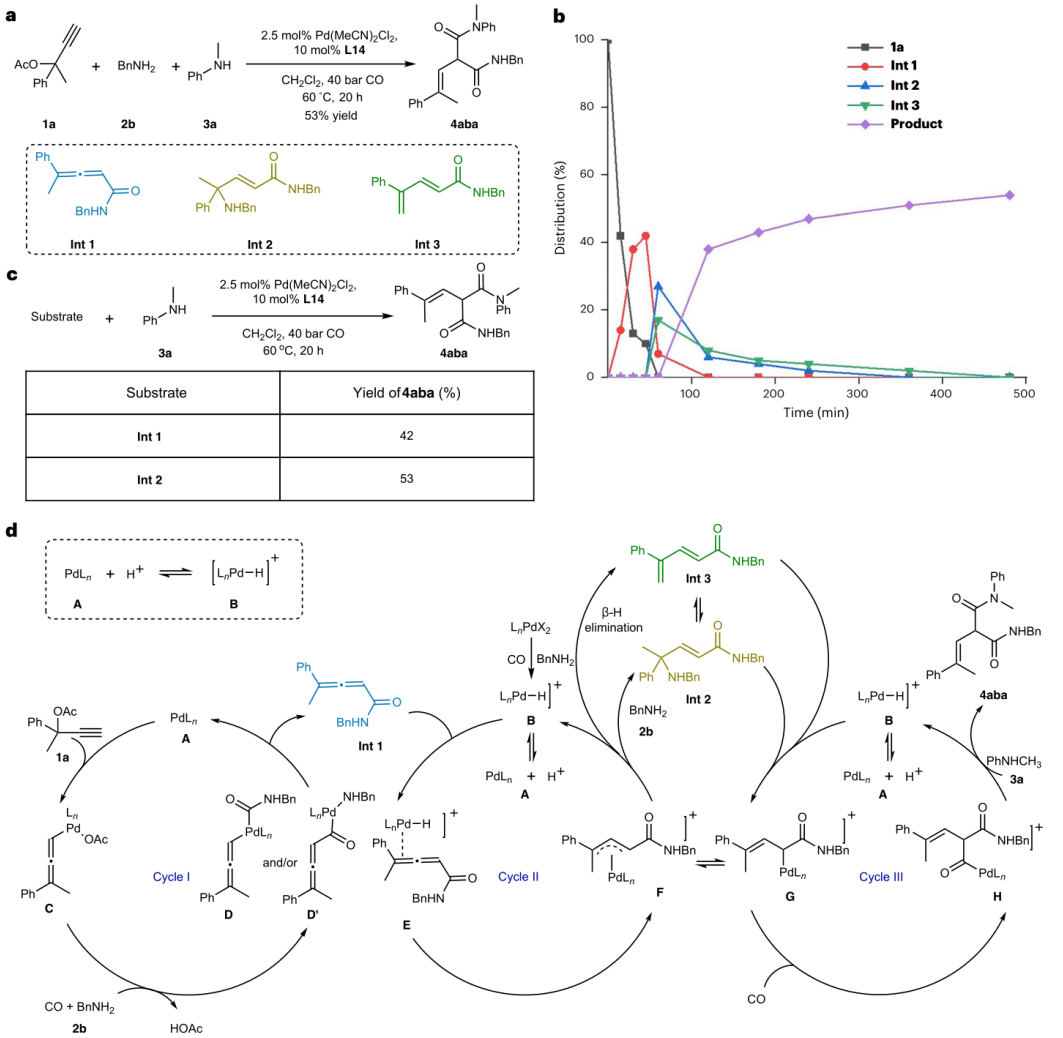

Substrate	Yield of **4aba** (%)
Int 1	42
Int 2	53

Fig. 2 | Kinetic study, control experiments and proposed catalytic cycle. **a**, Main species isolated from Pd-catalysed carbonylation of **1a** with **2b** and **3a**. **b**, Kinetic monitoring of intermediates over time by ^{1}H NMR spectroscopic analysis. **c**, Control experiments: **Int 1** and **Int 2** were transformed to **4aba**, which confirmed that **Int 1** and **Int 2** are active reaction intermediates in the overall process. **d**, Proposed mechanism for a catalyst-controlled strategy to deliver malonamide, **4ab**. The reaction of **1a** and **2b** affords **Int 1**. **Int 1** reacts with Pd and H affords π-allyl-palladium intermediate **F**, which undergoes equilibrium to give σ-palladium complex, **G**, β-H elimination to give **Int 3** and amination to give **Int 2**. Subsequent transformations of **G**, **Int 2** and **Int 3** lead to **4aba** and turn over the catalytic cycle. Bn, benzyl.

be in situ reduced to give the Pd^0 phosphine complex **A** in the presence of an excess amount of ligand[52,53]. In the presence of Pd^{II}, **2b** and high pressure of CO, the corresponding urea and cationic palladium hydride species, **B**, were formed, subsequently establishing an equilibrium with species **A**[49]. In cycle **I**, Pd^{0}Ln **A** will undergo S_N2'-type oxidative addition with propargylic acetate **1a** to give the allenylpalladium intermediate **C**, which reacts with CO and benzylamine, **2b**, to afford the carbonylation intermediates **D** or **D′**. Subsequently, reductive elimination affords the allenoic amide **Int 1** and regenerates the catalyst. **Int 1** is supposed to form complex **E** and subsequent olefin insertion regioselectively forms the π-allyl-palladium intermediate **F**. This species is in fast equilibrium with the corresponding σ-palladium complex **G**. Finally, CO insertion and aminolysis lead to the desired product, **4aba**. **F** is also prone to go through β-H elimination to form dienamide, **Int 3**, and amination to form allylic amine, **Int 2**.

Besides the possible balance between **Int 2** and **Int 3**, further reaction of the intermediates and Pd gives the σ-palladium complex **G**. In the same catalytic process, **4aba** is produced according to cycle III.

Article https://doi.org/10.1038/s44160-023-00411-6

Table 2 | Selective synthesis of non-symmetrical malonamides by Pd-catalysed carbonylation of propargylic acetates and amines

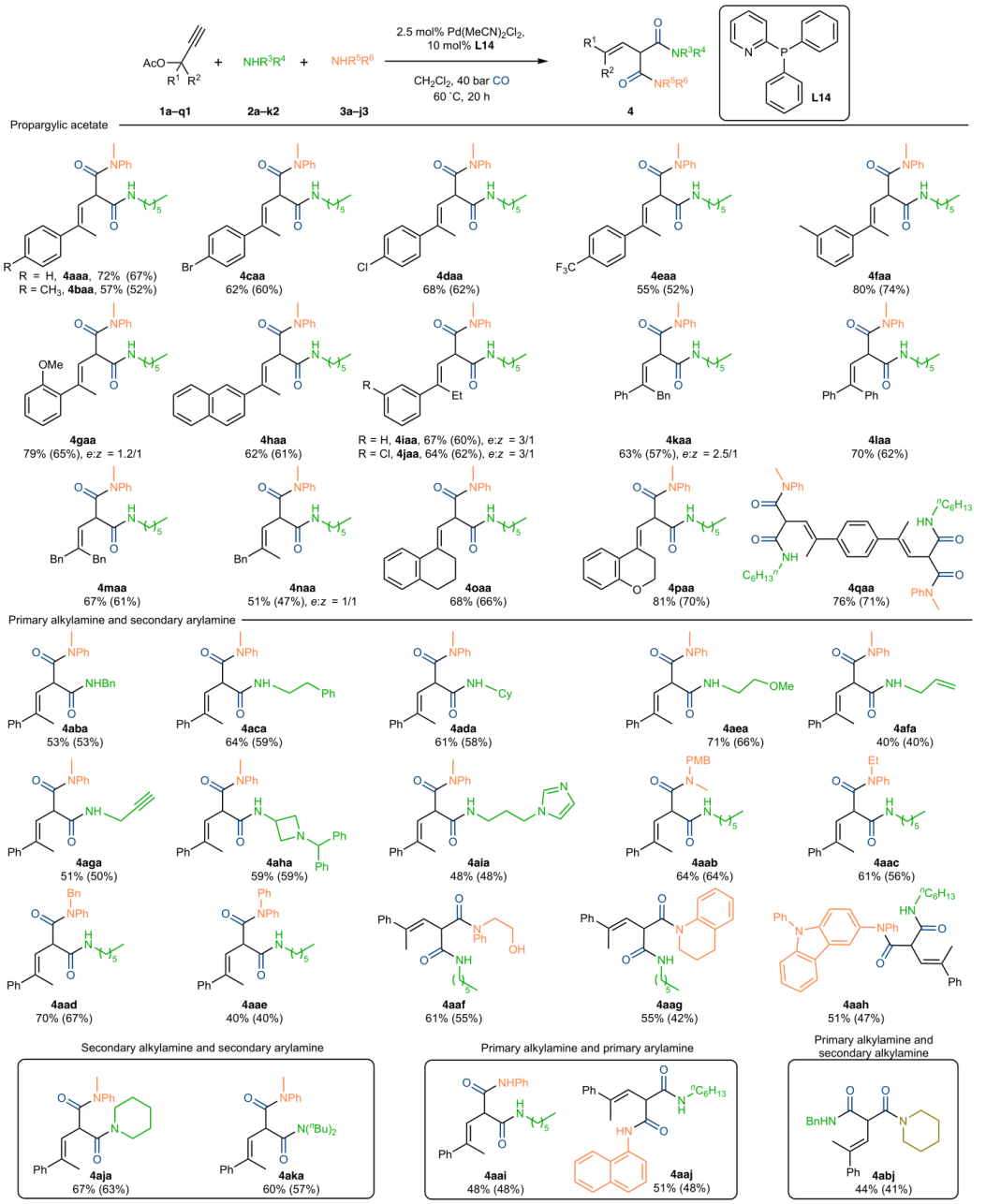

Standard reaction conditions: **1** (0.2 mmol), **2** (0.3 mmol), **3** (0.3 mmol), $Pd(MeCN)_2Cl_2$ (2.5 mol%), **L14** (10 mol%), CH_2Cl_2 (2.0 mL), CO (40 bar), 20 h at 60 °C. Isolated yields are given within parentheses. ^{1}H NMR spectroscopic yields (values before parentheses) and *z*/*e*-selectivities of **4** were determined by crude ^{1}H NMR spectroscopic analysis using dibromomethane as the internal standard. Unless otherwise noted, the *e*:*z* ratio is >20:1 in all cases.

The selective formation of the non-symmetrical diamides is controlled by both the reactivity of the nucleophile and the ligand effect. The more reactive nucleophile reacts with the initially formed Pd complex **C**, whereas the second amine undergoes amination of acyl palladium complex **H**. Deprotonation of the second amine by the built-in base of the ligand allows an efficient nucleophilic attack on the acyl palladium[45].

Substrate scope

With suitable conditions established for the model reaction, we examined the generality of this cascade, non-symmetrical, dicarbonylation process with respect to propargylic acetates as a molecular toolbox of tethering reagents. As shown in Table 2, diverse non-symmetrical malonamides can be conveniently prepared in the presence of the optimal catalytic system. Acetophenone analogues, **1b**–**1g**, and 2-acetonaphthone-derived propargylic acetate, **1h**, worked well to give the corresponding products **4baa**–**4haa** in 52–74% yields smoothly. In addition, other alkylated substrates led to the corresponding malonamides, **4iaa**–**4kaa**, in 57–62% yields with 2.5/1–3/1 selectivities. When 1,1-diphenylprop-2-ynyl acetate, **1l**, and **1m**–**1n** bearing benzyl and different alkyl groups were subjected to the optimized conditions, good activities and selectivities (47–62% yield) were achieved too. Furthermore, cycloalkyl-based propargylic acetates **1o**–**1p** can be transformed to the corresponding product **4oaa**–**4paa** in 66–70% yields. It is interesting that the highly functionalized product **4qaa** was obtained directly in 71% yield by multiple carbonylations of **1q**.

Next, we examined the general scope of the four-component process with respect to the reactivity of amines. Carbonylation reactions of **1a** with alkylamines and arylamines were performed in moderate-to-good yields. As shown in Table 2, primary alkylamines bearing alkyl chain (**2b** and **2c**), carbon ring (**2d**), functionalized groups (**2e**, **2f** and **2g**), heterocyclics (**2h and 2i**) and secondary alkylamines (**2j and 2k**) were all suitable partners in the reaction and gave the corresponding malonamides in 40–66% yields. Furthermore, diverse anilines (**3b**–**3j**), including the ones containing hydroxyl group (**3f**), heterocyclic motifs (**3g**) and hindered substituent (**3h**), underwent the desired transformation smoothly and the respective diamides **4aab**–**4aaj** were obtained in 40–67% yields. Notably, the more challenging combination of benzylamine (**2b**) and piperidine (**2j**) also worked selectively for this reaction, resulting in the formation of malonamide, **4abj**.

Tethering with proper linker chemistry provides new scaffolds for improved drug development[26,29]. Therefore, the combination of molecular pincer molecules with natural products or other biologically relevant molecules as reaction components offers many opportunities for the advancement of prodrug design. To showcase the applicability of the catalyst system to medicinal and complex organic chemistry, further functionalization of the molecular pincers was studied. As shown in Table 3, various functionalized primary alkylamines such as amino acid esters **2l** and **2m**, geranylamine (**2n**), oleylamine (**2o**), tryptamine (**2p**), myrtanylamine (**2q**), atorvastatin intermediate (**2r**), leelamine (**2s**), amlodipine (**2t**) and mexiletine (**2u**) were linked smoothly by carbonylation of **1a** and **3a** to the corresponding malonamides, **4ala**–**4aua**, in 40–63% yields. Numerous drugs or their derivatives containing secondary alkylamines (donepezil-related amine, **2v**, norquietapine, **2w**, buspirone-related amine, **2x**) as well as primary arylamines (vilazodone-related amine, **3k**, aminoglutethimide, **3l**) can be used in this multicomponent cascade process to furnish **4ava**–**4aal** in 47–64% yields in one step. The selective formation of **4ajt** in the presence of piperidine, **2j**, and amlodipine, **2t**, was also achieved despite their similar reactivities. The presented catalyst system is also well suited for generation of heterobifunctional compounds by bridging distinguished complex fragments or pharmacophores within one molecule. More specifically, geranylamine, **2n**, and vilazodone-related amine, **3k,** were coupled with **1a** to afford **4ank** in 51% yield. Similarly, the exploration of nucleophiles such as atorvastatin intermediate, **2r**, and sterically hindered amine, **3h**, amlodipine, **2t**, atorvastatin intermediate, **2r**, and aminoglutethimide, **3l**, showed that medicinally relevant molecules, **4arh, 4atl** and **4arl**, can be constructed in an efficient and selective manner, indicating the possibility of expanding the existing synthetic toolbox for chimeric molecule modification.

Amides are one of the most prolific moieties in pharmaceutical molecules, agrochemicals and natural products (see above)[1–9]. Therefore, there has been continuous interest in developing new amides that contain additional functional groups. In this respect, specifically amides with ester groups seemed interesting to us. Analogous to diamides, established approaches for synthesizing amido-esters encounter limitations owing to the low tolerance of functional groups under the reaction conditions used[54]. We thought that the developed double carbonylation reactions could be extended to provide the corresponding amido-esters. Again, to the best of our knowledge, such double-selective carbonylations have not been reported. The intrinsic challenges of such transformations are the possibilities of also forming diamides and diesters apart from the desired amido-esters. Furthermore, potential side reactions of propargylic acetates, which contain an unsaturated triple bond and an activated acetoxy group, increase the complexity of the system. Nevertheless, the reaction of propargylic acetate, **1a**, benzylamine, **2b**, and methanol, **5a**, provided amido-ester **6aba** in 41% yield, together with the diaminocarbonylation product **S9** and monocarbonylation products **Int 1** and **S10** under the previously developed conditions in the presence of **L14** as ligand. More detailed investigations of the chemo- and regioselectivity of this reaction allowed an increase in the yield of **6aba** up to 65% (Supplementary Tables 9–14).

As shown in Table 4, acetophenone analogues **1b**–**d** and **1f** and 2-acetonaphthone-derived propargylic acetate, **1h**, can be also used as connecting reagents providing the corresponding products **6bba**–**6hba** in 53–70% yields. The use of ethyl and benzyl-substituted substrates, **1i** and **1k**, led to amido-esters **6iba** and **6kba** in 67% (*e*:*z* = 3.9:1) and 59% yield (*e*:*z* = 3.3:1), respectively. In addition, 1-diphenylprop-2-ynyl acetate, **1l**, and dialkyl-substituted propargylic acetates, **1r** and **1m**, delivered the desired products smoothly. Finally, malonamides **6oba** and **6pba** were produced in 59–67% yields, starting from cycloalkyl-based propargylic acetates **1o** and **1p**.

Besides secondary amines (**2k**, **2A** and **2j**), primary ones (**2a**, **2c**, **2d**, **2e**, **2n**, **2y** and **2z**) are also suitable, giving the corresponding amido-esters in 48–68% yields. In addition, a variety of alcohols can be employed in this four-component reaction. Simple primary alcohols including ethanol (**5b**), *n*-butanol (**5c**), cyclopropylmethanol (**5d**) and halogen-containing alcohols (**5e**), as well as less reactive secondary alcohol, **5f**, and cholesterol, **5g**, gave the desired products **6abb**–**6abg**. As an example of a phenol derivative, vitamin E, **5h** was shown to be a suitable substrate in this transformation and provided **6abh** in 47% yield.

Recently, there has been increasing interest in so-called chimeric or multitargeting molecules, whereby the first component targets a specific cell or biological function and the second component exerts a different pharmacological activity. A stable or cleavable linker connects these two modules of a chimaera[27,29]. In this respect, the presented methodology also permits the simultaneous incorporation of two or more pharmaceutical elements. As shown in Table 5, various complex amines and alcohols are tethered with **1a** as the precursor of the linking unit. More specifically, Pd-catalysed selective carbonylation of **1a** progressed well with furfurylamine **2B** and furfurylalcohol, **5i**, glycine ethyl ester, **2l**, and nerol, **5j**, furnishing products **6aBi** and **6alj**. Furthermore, combination of cholesterol, **5g**, with oleylamine, **2o**, or amlodipine, **2t**, led to the formation of **6aog** and **6atg**. Steroid hormones such as pregnenolone, **5k**, stanolone, **5l**, and dehydroepiandrosterone, **5m**, participated with amlodipine, **2t**, oleylamine, **2o**, myrtanylamine, **2q**, atorvastatin intermediate, **2r**, and leelamine, **2s**, in this transformation, providing the target products **6aok**–**6asm** in 52–66% yields. Finally, the linkage of atorvastatin intermediate **2r** with

Article https://doi.org/10.1038/s44160-023-00411-6

Table 3 | Selective Pd-catalysed dicarbonylation for the synthesis of non-symmetrical malonamides with biologically relevant molecules

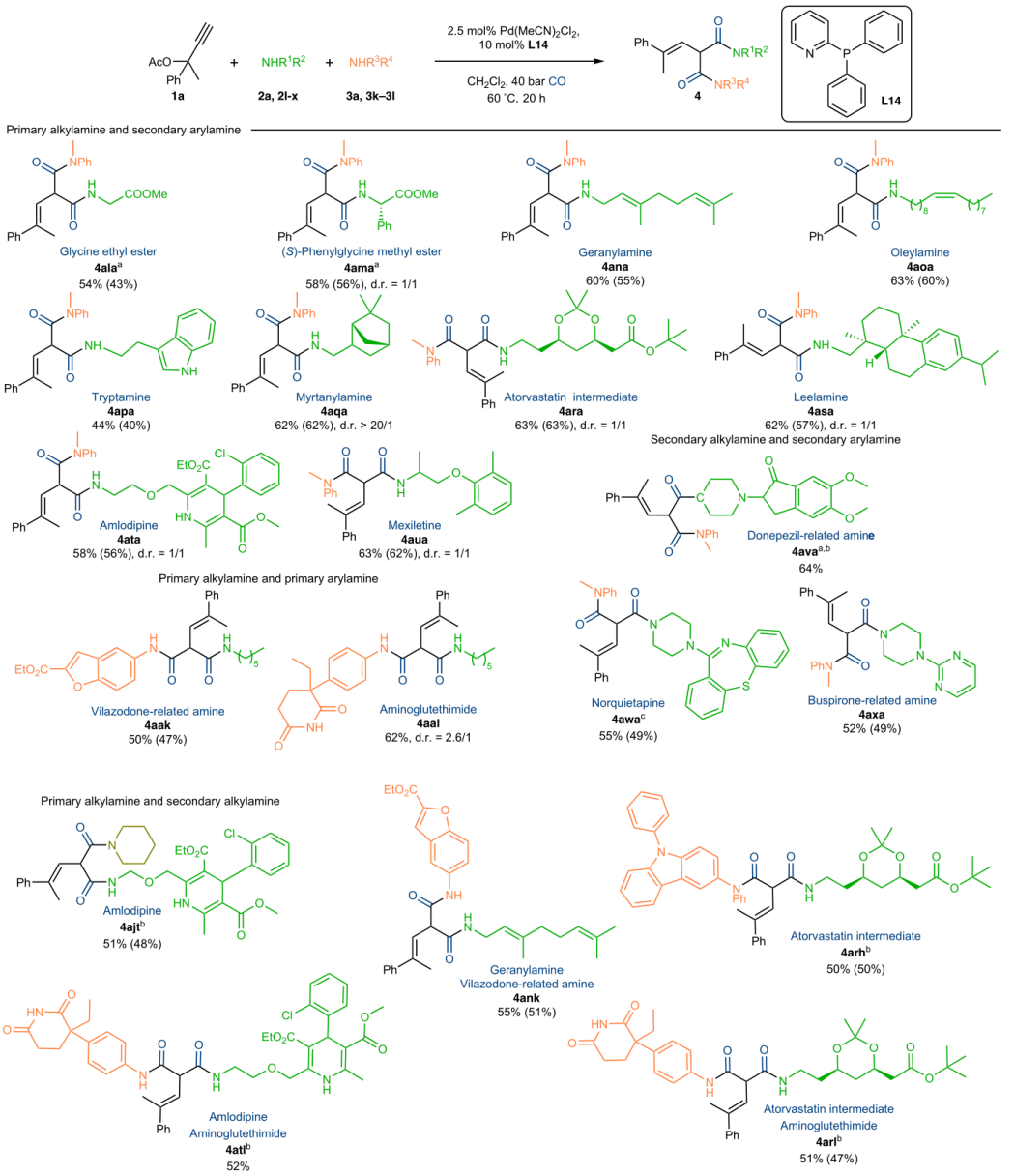

Standard reaction conditions: **1** (0.2 mmol), **2** (0.3 mmol), **3** (0.3 mmol), $Pd(MeCN)_2Cl_2$ (2.5 mol%), **L14** (10 mol%), CH_2Cl_2 (2.0 ml), CO (40 bar), 20 h at 60 °C. Isolated yields are given within parentheses. NMR spectroscopic yields (values before parentheses) and *z*:*e*-selectivities of **4** were determined by crude ^1H NMR spectroscopic analysis using dibromomethane as the internal standard. Unless otherwise noted, the *e*:*z* ratio is >20:1 in all cases. [a]0.3 mmol amino acid ester hydrochloride and 0.3 mmol Et_3N were used. [b]Isolated as mixture of diastereoisomers in an unknown ratio, the ratio could not be determined owing to overlapping signals in in the crude ^1H NMR spectra. [c]11-(Piperazin-1-yl)dibenzo[*b*,*f*][1,4]thiazepine dihydrochloride and 0.6 mmol Et_3N were used.

Article https://doi.org/10.1038/s44160-023-00411-6

Table 4 | Selective synthesis of amido-esters by Pd-catalysed dicarbonylation reactions

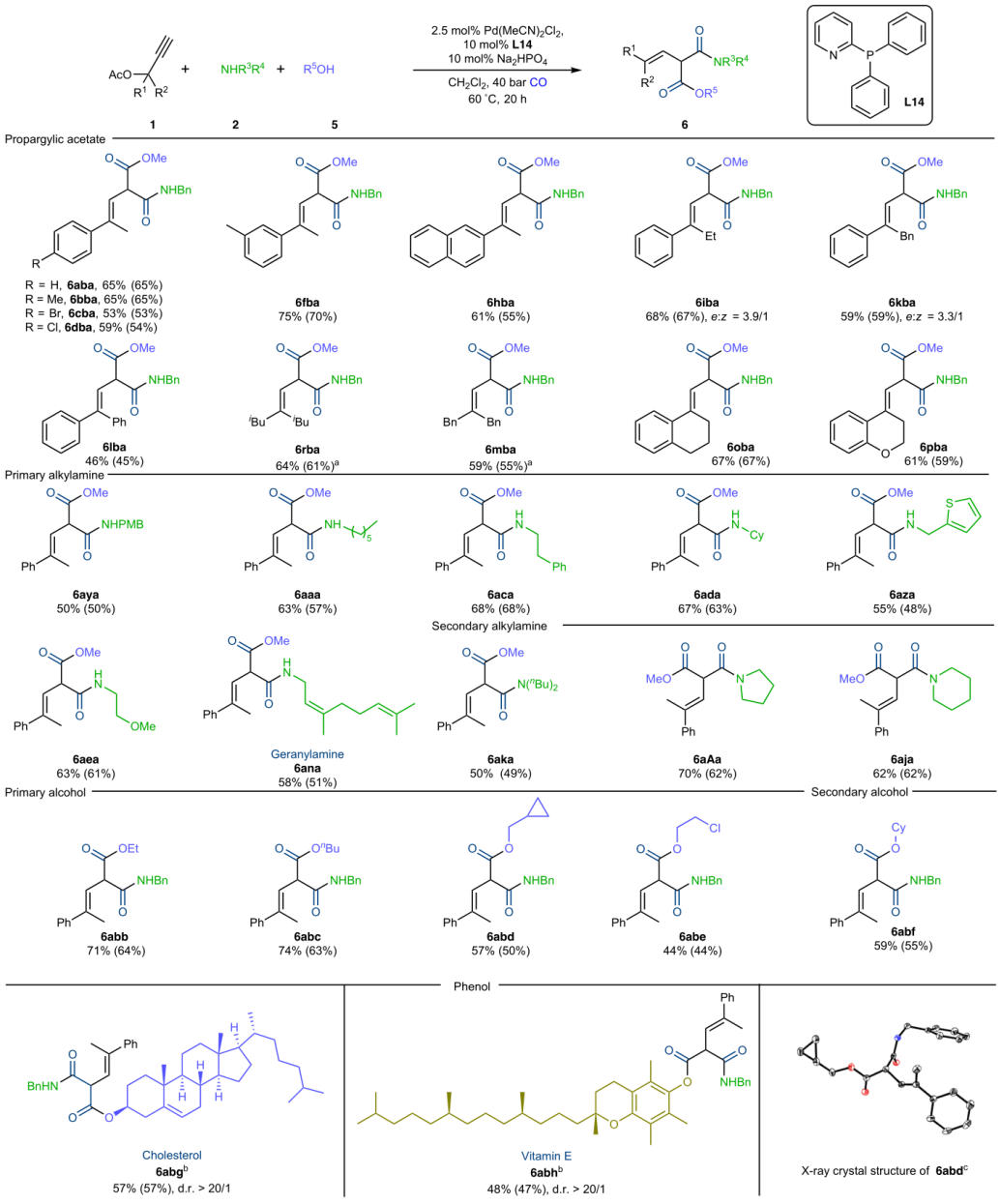

Standard reaction conditions: **1** (0.2 mmol), **2** (0.2 mmol), **5** (0.6 mmol), $Pd(MeCN)_2Cl_2$ (2.5 mol%), **L14** (10 mol%), Na_2HPO_4 (10 mol%), CH_2Cl_2 (2.0 ml), CO (40 bar), 20 h at 60 °C. Isolated yields are given within parentheses. NMR spectroscopic yields (values before parentheses) and *z*:*e*-selectivities of **6** were determined by crude ^1H NMR analysis using dibromomethane as an internal standard. Unless otherwise noted, *e*:*z* > 20/1 in all cases. [a]**2** (0.3 mmol); **5** (0.3 mmol). [b]**5** (0.2 mmol). [c]Displacement ellipsoid plot (30% probability level) of one molecule of the asymmetrical unit of **6abd** (without H).

Article https://doi.org/10.1038/s44160-023-00411-6

Table 5 | Pd-catalysed dicarbonylation for the synthesis of amido-esters with biologically relevant molecules

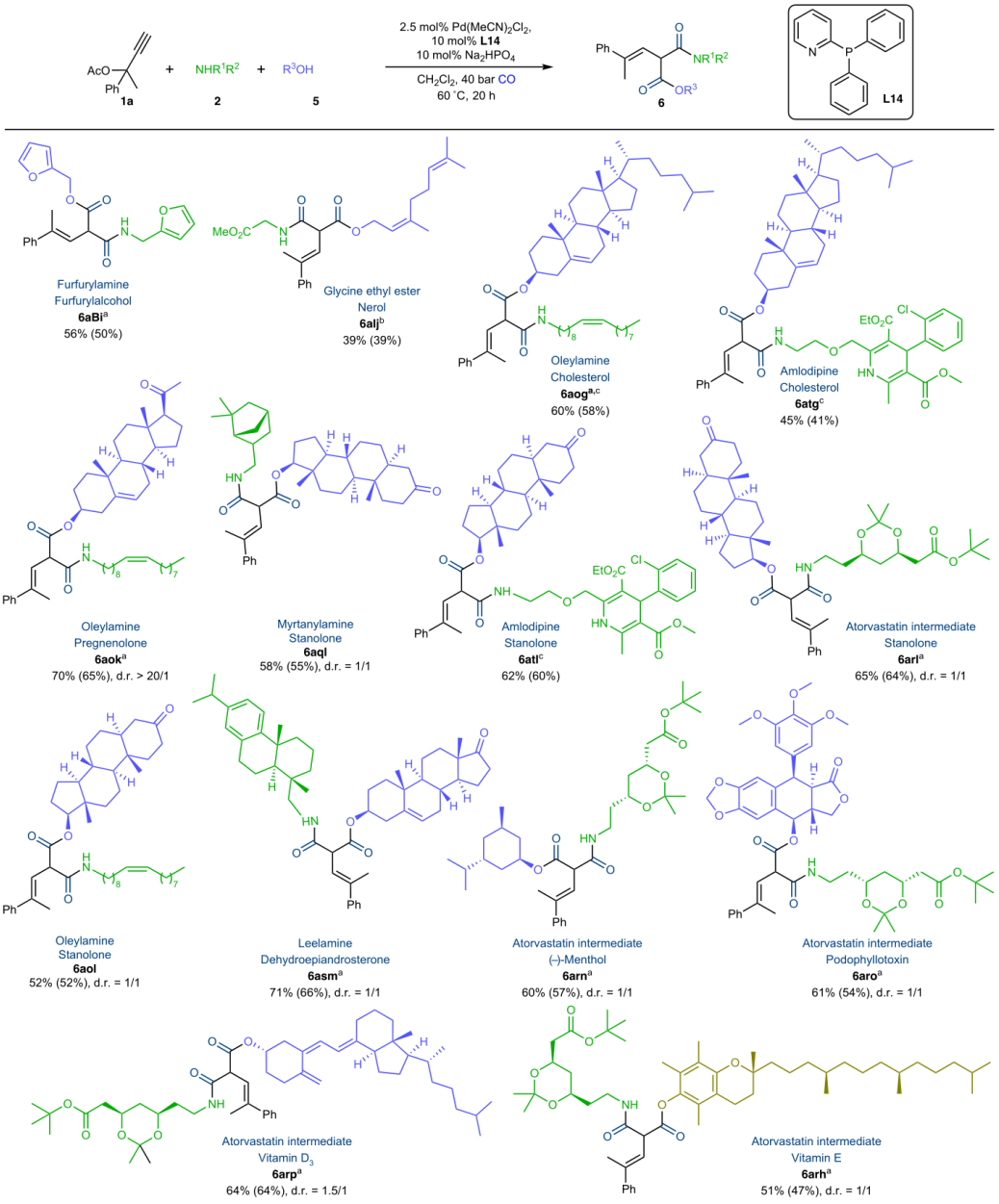

Standard reaction conditions: **1** (0.2 mmol), **2** (0.2 mmol), **5** (0.2 mmol), $Pd(MeCN)_2Cl_2$ (2.5 mol%), **L14** (10 mol%), Na_2HPO_4 (10 mol%), CH_2Cl_2 (2.0 ml), CO (40 bar), 20 h at 60 °C. Isolated yields are given within parentheses. NMR spectroscopic yields (values before parentheses) and *z*:*e*-selectivities of **6** were determined by crude ^1H NMR spectroscopic analysis using dibromomethane as an internal standard. Unless otherwise noted, *e*:*z* > 20/1 in all cases. [a]**2** (0.3 mmol), **5** (0.3 mmol). [b]0.3 mmol amino acid ester hydrochloride and 0.3 mmol Et_3N were used. [c]Isolated as mixture of diastereoisomers in an unknown ratio, the ratio could not be determined due to overlapping signals in in the crude ^1H NMR spectra.

(−)-menthol, **5n**, podophyllotoxin, **5o**, vitamin D_3, **5p**, and vitamin E, **5h**, was also achieved with this protocol, producing the corresponding amido-esters in 47–64% yields.

Conclusions

In summary, we report a general and atom-efficient, one-step synthesis of non-symmetrical diamides or amido-esters by using either two different amines or amines and alcohols, respectively. The presented methodology permits tethering of diverse amines, alcohols and phenols together with molecular pincers, thereby enabling the synthesis of heterobifunctional compounds in a completely new way. The selective linking reagent, the molecular pincer, is generated in situ by Pd-catalysed carbonylation of convenient and stable propargylic acetates. By using different propargylic acetates, a toolbox of different linking reagents can be easily created. Mechanistic studies of the diamino- and amino-alkoxy carbonylation reactions suggest a sequential carbonylation process with allenoic amide, allylic amine and dienamide as major intermediates. The development of development of the $Pd(MeCN)_2Cl_2$/diphenyl(2-pyridyl)-phosphine catalyst system was crucial for controlling the selectivity in the complex reaction network. The presented chemistry offers new ways for diversification in chemical space and the generality is demonstrated in >100 examples. To the best of our knowledge, the prepared molecules shown in the present study have not been described before.

Methods

General procedure for carbonylation

A 4-ml screw-cap vial was charged with $Pd(MeCN)_2Cl_2$ (1.3 mg, 0.005 mmol) and ligand (0.02 mmol). The synthesis of **4aaa** was achieved by adding **1a** (0.2 mmol), **2a** (0.3 mmol), and **3a** (0.3 mmol); the synthesis of **6aba** was achieved by adding **1a** (0.2 mmol), **2b** (0.2 mmol), **5a** (0.6 mmol), and Na_2HPO_4 (0.02 mmol); and an oven-dried stirring bar. The vial was closed by a poly(tetrafluoroethylene)/white rubber septum (Wheaton 13 mm Septa) and a phenolic cap and connected to the atmosphere with a needle. Then, the vial was evacuated under vacuum and recharged with argon 3×. After CH_2Cl_2 (2.0 ml) was injected by syringe, the vial was fixed in an alloy plate and put into a Parr 4560 series autoclave (300 ml) under an argon atmosphere. At room temperature, the autoclave was flushed with carbon monoxide 3× and CO was charged to 40 bar. The reaction was heated to 60 °C and stirred for 20 h. Afterwards, the autoclave was cooled to room temperature and the pressure was carefully released. The reaction mixture was filtered through a short pad of celite and concentrated via rotary evaporation. Dibromomethane (34.6 mg, 0.2 mmol) was added into the reaction as an internal standard. A sample of the mixture was analysed by ^{1}H NMR Spectroscopy. Pure product could be obtained by column chromatography on silica gel. Cautionary note: CO is harmful when breathed. Gas charging and releasing should be operated in a fume hood.

Data availability

All the data generated or analysed during the present study are included in this article and its Supplementary Information. Crystallographic data for the structure reported in this article have been deposited at the joint Cambridge Crystallographic Data Centre and Fachinformationszentrum Karlsruhe Access Structures service, under deposition no. CCDC 2190217 (**6abd**). Copies of the data can be obtained free of charge via https://www.ccdc.cam.ac.uk/structures.

References

1. de Figueiredo, R. M., Suppo, J. S. & Campagne, J. M. Nonclassical routes for amide bond formation. *Chem. Rev.* **116**, 12029–12122 (2016).
2. Ertl, P., Altmann, E. & McKenna, J. M. The most common functional groups in bioactive molecules and how their popularity has evolved over time. *J. Med. Chem.* **63**, 8408–8418 (2020).
3. Carey, J. S., Laffan, D., Thomson, C. & Williams, M. T. Analysis of the reactions used for the preparation of drug candidate molecules. *Org. Biomol. Chem.* **4**, 2337–2347 (2006).
4. Ghose, A. K., Viswanadhan, V. N. & Wendoloski, J. J. A knowledge based approach in designing combinatorial or medicinal chemistry libraries for drug discovery. 1. A qualitative and quantitative characterization of known drug databases. *J. Comb. Chem.* **1**, 55–68 (1999).
5. Todorovic, M. & Perrin, D. M. Recent developments in catalytic amide bond formation. *Pept. Sci.* **112**, 1–18 (2020).
6. Dabhia, R. C., Patela, U. P., Rathodb, V. B., Shahb, S. N. & Marua, J. J. Process optimization for acid-amine coupling: a catalytic approach. *Curr. Chem. Lett.* **12**, 133–140 (2023).
7. Urquhart, L. Top drugs and companies by sales in 2017. *Nat. Rev. Drug Discov.* **17**, 232–233 (2018).
8. Ananthanarayanan, V. S., Tetreault, S. & Saint-Jean, A. Interaction of calcium channel antagonists with calcium: spectroscopic and modeling studies on diltiazem and its Ca^{2+} complex. *J. Med. Chem.* **36**, 1324–1332 (1993).
9. Najjar-Debbiny, R. et al. Effectiveness of Paxlovid in reducing severe COVID-19 and mortality in high risk patients. *Clin. Infect. Dis.* https://doi.org/10.1093/cid/ciac443 (2022).
10. Wang, Q. et al. Discovery of 4-methyl-*N*-(4-((4-methylpiperazin-1-yl)methyl)-3-(trifluoromethyl)phenyl)-3-((1-nicotinoylpiperidin-4-yl)oxy)benzamide (CHMFL-ABL/KIT-155) as a novel highly potent type II ABL/KIT dual kinase inhibitor with a distinct hinge binding. *J. Med. Chem.* **60**, 273–289 (2017).
11. Padwa, A. et al. Intramolecular cycloaddition reactions of furo[3,4-b]indoles for alkaloid synthesis. *J. Org. Chem.* **79**, 3173–3184 (2014).
12. Constable, J. C. et al. Key green chemistry research areas-a perspective from pharmaceutical manufacturers. *Green Chem.* **9**, 411–420 (2007).
13. Valeur, E. & Bradley, M. Amide bond formation: beyond the myth of coupling reagents. *Chem. Soc. Rev.* **38**, 606–631 (2009).
14. Sperry, J. B. et al. Thermal stability assessment of peptide coupling reagents commonly used in pharmaceutical manufacturing. *Org. Process Res. Dev.* **22**, 1262–1275 (2018).
15. Lu, B., Xiao, W.-J. & Chen, J.-R. Recent advances in visible-light-mediated amide synthesis. *Molecules* **27**, 517 (2022).
16. Zhang, Z., Cao, X., Wang, G., Zhang, G. & Zhang, X. Straightforward synthesis of biologically valuable nonsymmetrical malonamides under mild conditions. *Green Chem.* **24**, 3035–3041 (2022).
17. Janikowska, K. & Makowiec, S. TMSCl as a rate-accelerating additive in acylations of amines with 5-(α-amino-α′-hydroxy) methylene meldrum acids. *Synth. Commun.* **42**, 975–988 (2012).
18. Yu, X., Wang, D.-S., Xu, Z., Yanga, B. & Wang, D. The synthesis of unsymmetric diamides through Rh-catalyzed selective C–H bond activation of amides with isocyanates. *Org. Chem. Front.* **4**, 1011–1018 (2017).
19. Khan, G. S., Dickson, B. D. & Barker, D. Synthesis of benzoic acids and polybenzamides containing tertiary alkylamino functionality. *Tetrahedron* **68**, 1790–1801 (2012).
20. Qian, H.-L., Meng, F.-L., Yang, C.-X. & Yan, X.-P. Irreversible amide-linked covalent organic framework for selective and ultrafast gold recovery. *Angew. Chem. Int. Ed.* **59**, 17607–17613 (2020).
21. Cai, L. et al. Asymmetric cyclization/nucleophilic tandem reaction of o-alkynylacetophenone with (diazomethyl) phosphonate for the synthesis of functional isochromenes. *Org. Lett.* **21**, 7597–7601 (2019).
22. Pignataro, L. et al. Rhodium-catalyzed asymmetric hydrogenation of olefins with PhthalaPhos, a new class of chiral supramolecular ligands. *Chem. Eur. J.* **18**, 1383–1400 (2012).
23. Clery, D. & Service, R. F. Molecular links snap up award. *Science* **378**, 125 (2022).

24. McKay, C. S. & Finn, M. G. Click chemistry in complex mixtures: bioorthogonal bioconjugation. *Chem. Biol.* **21**, 1075–1101 (2014).
25. Erlanson, D. A., Wells, J. A. & Braisted, A. C. Tethering: fragment-based drug discovery. *Annu. Rev. Biophys. Biomol. Struct.* **33**, 199–223 (2004).
26. Yang, X. et al. Making smart drugs smarter: the importance of linker chemistry in targeted drug delivery. *Med. Res. Rev.* **40**, 2682–2713 (2020).
27. Corson, T. W., Aberle, N. & Crews, C. M. Design and applications of bifunctional small molecules: why two heads are better than one. *ACS Chem. Biol.* **3**, 677–692 (2008).
28. Yamazoe, S. et al. Heterobifunctional molecules induce dephosphorylation of kinases-A proof of concept study. *J. Med. Chem.* **63**, 2807–2813 (2020).
29. Borsari, C., Trader, D. J., Tait, A. & Costi, M. P. Designing chimeric molecules for drug discovery by leveraging chemical biology. *J. Med. Chem.* **63**, 1908–1928 (2020).
30. Troup, R. I., Fallan, C. & Baud, M. G. J. Current strategies for the design of PROTAC linkers: a critical review. *Explor. Target Antitumor Ther.* **1**, 273–312 (2020).
31. Ali, B. E. & Alper, H. *Transition Metals for Organic Synthesis* (Wiley-VCH, 2008).
32. van Leeuwen, P. W. N. M. & Claver, C. *Rhodium Catalyzed Hydroformylation* Vol. 22 (Springer, 2002).
33. Franke, R., Selent, D. & Börner, A. Applied hydroformylation. *Chem. Rev.* **112**, 5675–5732 (2012).
34. Friis, S. D., Lindhardt, A. T. & Skrydstrup, T. The development and application of two-chamber reactors and carbon monoxide precursors for safe carbonylation reactions. *Acc. Chem. Res.* **49**, 594–605 (2016).
35. Wu, X. et al. Transition-metal-catalyzed carbonylation reactions of olefins and alkynes: a personal account. *Acc. Chem. Res.* **47**, 1041–1053 (2014).
36. Gabriele, B. *Carbon Monoxide in Organic Synthesis: Carbonylation Chemistry* (Wiley-VCH, 2021).
37. Zhu, C., Yang, B. & Bäckvall, J.-E. Highly selective cascade C–C bond formation via palladium catalyzed oxidative carbonylation-carbocyclization-carbonylation–alkynylation of enallenes. *J. Am. Chem. Soc.* **137**, 11868–11871 (2015).
38. Yang, B. et al. Enantioselective palladium-catalyzed carbonylative carbocyclization of enallenes via cross-dehydrogenative coupling with terminal alkynes: efficient construction of α-chirality of ketones. *Angew. Chem. Int. Ed.* **56**, 4535–4539 (2017).
39. Ge, Y. et al. Palladium-catalyzed domino aminocarbonylation of alkynols: direct and selective synthesis of itaconimides. *JACS Au.* **8**, 1257–1265 (2021).
40. Yang, J. et al. Direct synthesis of adipic acid esters via palladium catalyzed carbonylation of 1,3-dienes. *Science* **366**, 1514–1517 (2019).
41. Ge, Y. et al. Palladium-catalyzed cascade carbonylation to α,β-unsaturated piperidones via selective cleavage of carbon-carbon triple bonds. *Angew. Chem. Int. Ed.* **60**, 22393–22400 (2021).
42. Edward, P. L. H. & Sharon, G. L. Evaluated gas phase basicities and proton affinities of molecules: an update. *J. Phys. Chem. Ref. Data* **27**, 413–686 (1998).
43. Liu, J., Han, Z., Wang, X., Wang, Z. & Ding, K. Highly regio- and enantioselective alkoxycarbonylative amination of terminal allenes catalyzed by a spiroketal-based diphosphine/Pd^{II} complex. *J. Am. Chem. Soc.* **137**, 15346–15349 (2015).
44. Qi, H. et al. Bifunctional ligands for Pd-catalyzed selective alkoxycarbonylation of alkynes. *J. Catal.* **363**, 63–68 (2018).
45. Dong, K. W. et al. Cooperative catalytic methoxycarbonylation of alkenes: uncovering the role of palladium complexes with hemilabile ligands. *Chem. Sci.* **9**, 2510–2516 (2018).
46. Drent, E., Arnoldy, P. & Budzelaar, P. H. M. Efficient palladium catalysts for the carbonylation of alkynes. *J. Organomet. Chem.* **455**, 247–253 (1993).
47. Liu, J. et al. Selective palladium-catalyzed aminocarbonylation of olefins to branched amides. *Angew. Chem. Int. Ed.* **55**, 13544–13548 (2016).
48. Zheng, W. et al. Tetrasubstituted allenes via the palladium catalysed kinetic resolution of propargylic alcohols using a supporting ligand. *Nat. Catal.* **2**, 997–1005 (2019).
49. Fang, X., Li, H., Jackstell, R. & Beller, M. Selective palladium-catalyzed aminocarbonylation of 1,3-dienes: atom-efficient synthesis of β,γ-unsaturated amides. *J. Am. Chem. Soc.* **136**, 16039–16043 (2014).
50. Liu, Q. et al. Domino catalysis: palladium-catalyzed carbonylation of allylic alcohols to β,γ-unsaturated esters. *Angew. Chem. Int. Ed.* **52**, 8064–8068 (2013).
51. Liu, J. et al. Selective palladium-catalyzed carbonylation of alkynes: an atom-economic synthesis of 1,4-dicarboxylic acid diesters. *J. Am. Chem. Soc.* **140**, 10282–10288 (2018).
52. Amatore, C., Jutand, A. & M'Barki, M. A. Evidence of the formation of zerovalent palladium from $Pd(OAc)_2$ and triphenylphosphine. *Organometallics* **11**, 3009–3013 (1992).
53. Amatore, C., Carre, E., Jutand, A. & M'Barki, M. A. Rates and mechanism of the formation of zerovalent palladium complexes from mixtures of $Pd(OAc)_2$ and tertiary phosphines and their reactivity in oxidative additions. *Organometallics* **14**, 1818–1826 (1995).
54. Ramakrishna, K. & Sivasankar, C. Synthesis of amido esters and amido phosphonates through carbonylation of diazo compounds followed by nucleophilic addition reaction. *Eur. J. Org. Chem.* **2017**, 4035–4043 (2017).

Acknowledgements

We thank W. Baumann and P. Wang for help with NMR spectroscopy analysis and K. Junge for providing technical infrastructure. In addition, we thank the analytical team of LIKAT. We gratefully acknowledge the support from the Federal Ministry of Education and Research, the State of Mecklenburg-Vorpommern and the European Research Council (project NoNaCat 670986).

Author contributions

M.B. and Y.G conceived and designed the experiments. Y.G., W.H. and S.A. performed the experiments and analysed the data. A.S. performed the X-ray analysis. R.J. participated in the discussions and provided high-pressure infrastructure. M.B. and Y.G. prepared the manuscript with feedback from all authors.

Funding

Open access funding provided by Leibniz-Institut für Katalyse e.V. (LIKAT Rostock).

Competing interests

The authors declare no competing interests.

Additional information

Supplementary information The online version contains supplementary material available at https://doi.org/10.1038/s44160-023-00411-6.

Correspondence and requests for materials should be addressed to Matthias Beller.

Peer review information *Nature Synthesis* thanks Jan-Erling Backvall, Carmen Claver and the other, anonymous, reviewer(s) for their contribution to the peer review of this work. Primary Handling Editor: Thomas West, in collaboration with the *Nature Synthesis* team.

Article https://doi.org/10.1038/s44160-023-00411-6

Reprints and permissions information is available at www.nature.com/reprints.

Publisher's note Springer Nature remains neutral with regard to jurisdictional claims in published maps and institutional affiliations.

Open Access This article is licensed under a Creative Commons Attribution 4.0 International License, which permits use, sharing, adaptation, distribution and reproduction in any medium or format, as long as you give appropriate credit to the original author(s) and the source, provide a link to the Creative Commons license, and indicate if changes were made. The images or other third party material in this article are included in the article's Creative Commons license, unless indicated otherwise in a credit line to the material. If material is not included in the article's Creative Commons license and your intended use is not permitted by statutory regulation or exceeds the permitted use, you will need to obtain permission directly from the copyright holder. To view a copy of this license, visit http://creativecommons.org/licenses/by/4.0/.

© The Author(s) 2023

7.4 1,2-Bis(di(benzofuran-2-yl)phosphino)ethane

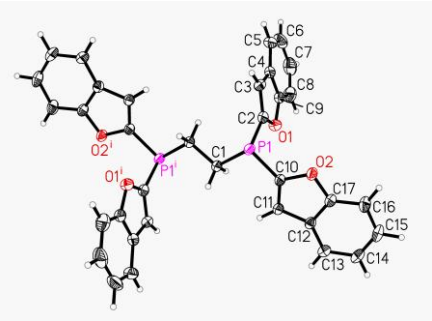

Ahrens, S.; Spannenberg, A.; Beller, M.; Junge, K. 1,2-Bis[di(benzofuran-2-yl)phosphanyl]ethane. IUCrData 2025, 10, x250916.

Author's Contribution

The author conducted the synthesis and characterization of the compounds, carried out the crystallization experiments, and prepared the initial manuscript draft. The overall contribution is estimated at approximately 80%.

Sebastian Ahrens
(PhD student)

Prof. Matthias Beller
(Supervisor)

data reports

IUCrData

ISSN 2414-3146

1,2-Bis[di(benzofuran-2-yl)phosphanyl]ethane

Sebastian Ahrens, Anke Spannenberg, Matthias Beller and Kathrin Junge*

Leibniz-Institut für Katalyse e. V., Albert-Einstein-Str. 29a, 18059 Rostock, Germany. *Correspondence e-mail: Kathrin.Junge@catalysis.de

Received 17 October 2025
Accepted 20 October 2025

Edited by L. Van Meervelt, Katholieke Universiteit Leuven, Belgium

Keywords: crystal structure; bidentate ligand; benzofuran; phosphine.

CCDC reference: 2496508

Structural data: full structural data are available from iucrdata.iucr.org

The title compound, $C_{34}H_{24}O_4P_2$, consists of an ethylene-bridged diphosphine with benzofuran residues, where the P—C—C—P backbone exhibits an *anti*-conformation. The asymmetric unit contains one half molecule, which is completed by inversion symmetry.

3D view

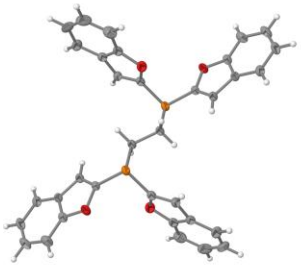

Chemical scheme

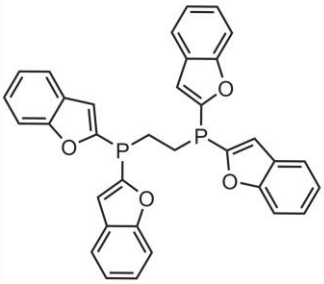

Structure description

Bidentate phosphine ligands play a pivotal role in homogeneous catalysis, where their chelation to a metal center enhances complex stability and allows precise control over electronic and steric properties (van Leeuwen *et al.*, 2000). Ethylene-bridged diphosphines, such as 1,2-bis(diphenylphosphanyl)ethane (dppe), are among the most widely used ligands owing to their versatile coordination behavior (Clevenger *et al.*, 2020). Variations in the substituents on phosphorus strongly influence catalytic activity, selectivity, and metal–ligand interactions. Consequently, structural modification of ethylene-bridged diphosphines remains a key strategy for the design of improved catalysts in transition-metal-mediated transformations. Numerous ethylene-bridged diphosphines have been synthesized, bearing alkyl substituents as well as aryl substituents (Dekker *et al.*, 1992).

Recently, our group demonstrated the potential of benzofuran-based phosphines in the Co-catalyzed isomerization of allylamines (Ahrens *et al.*, 2025). These studies revealed that benzofurylphosphines represent an alternative structural motif to conventional aryl phosphines, offering distinct electronic and steric properties that can significantly influence catalytic activity. Owing to their unique reactivity, structurally related phosphines have also been successfully applied in the Pd-catalyzed telomerization of butadiene (Souza *et al.*, 2025). In our previous work, only monodentate benzofuran phosphines were developed and evaluated in catalytic applications. To expand this ligand family, the corresponding bidentate analogue has now been synthesized. The new diphosphine 1,2-bis[di(benzofuran-2-yl)phosphanyl]ethane was prepared and its crystal structure determined.

OPEN ACCESS
Published under a CC BY 4.0 licence

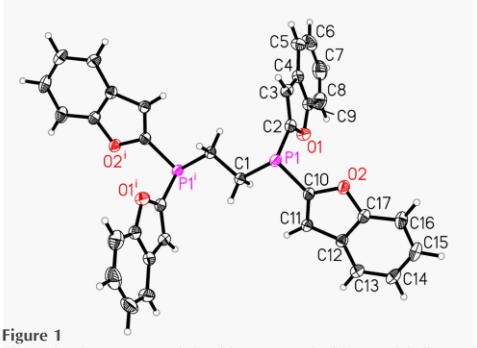

Figure 1
The molecular structure of the title compound with atom labeling and displacement ellipsoids drawn at 50% probability level [symmetry code: (i) $-x+1, -y+2, -z+1$].

The molecular geometry of the title compound reflects the characteristic features of ethylene-bridged diphosphines with the P–C–C–P backbone forming a zigzag chain and exhibiting an *anti*-conformation (Fig. 1). Each phosphorus atom displays a pyramidal arrangement with two benzofuran substituents and one CH_2 group of the ethylene bridge. The P—C—C—P torsion angle amounts to 180°, bond lengths and angles are in the expected range. The dihedral angle between the benzofuran rings is 84.94 (3)°. The asymmetric unit contains one half-molecule expanded by the symmetry operation $-x+1, -y+2, -z+1$.

Moreover, the electronic structure of the benzofuryl diphosphine differs significantly from that of dppe. In solution at room temperature, the ^{31}P NMR resonance is significantly upfield-shifted (–52.6 ppm compared to −12.6 ppm for dppe), indicating a higher electron density at the phosphorus atoms (Benny *et al.*, 2023). The increased shielding can be attributed to the greater π-donor strength and electron delocalization provided by the benzofuryl substituents. Therefore, the ligand shows an increased electron-donating character, altering the electron density and reactivity of its metal complexes relative to dppe.

Synthesis and crystallization

All synthetic procedures were carried out under argon atmosphere using standard Schlenk techniques. The anhydrous and oxygen-free solvents used (tetrahydrofuran, dichloromethane, diethyl ether, and *n*-pentane) were obtained from an Innovative Technology PS-MD-6 solvent purification system. The purified solvents were stored over 3 Å molecular sieves under argon. The reagents 1,2-bis(dichlorophosphanyl) ethane and benzofuran were obtained from Sigma-Aldrich and Fisher Scientific, respectively, and used as received.

NMR spectra were recorded on a Bruker Avance 300 spectrometer operating at 300 MHz for ^{1}H, 75 MHz for ^{13}C, and 121 MHz for ^{31}P. All chemical shifts (δ) are reported in ppm relative to tetramethylsilane (TMS). Solvent references for CD_2Cl_2 are δ = 5.32 ppm for ^{1}H and 53.84 ppm for ^{13}C. ^{31}P chemical shifts are reported relative to an external 85% H_3PO_4 standard.

Table 1
Experimental details.

Crystal data	
Chemical formula	$C_{34}H_{24}O_4P_2$
M_r	558.47
Crystal system, space group	Monoclinic, $P2_1/n$
Temperature (K)	150
a, b, c (Å)	5.6351 (5), 10.5372 (9), 22.7988 (19)
β (°)	93.696 (1)
V (Å^3)	1350.9 (2)
Z	2
Radiation type	Mo $K\alpha$
μ (mm^{-1})	0.20
Crystal size (mm)	0.35 × 0.17 × 0.11
Data collection	
Diffractometer	Bruker APEXII CCD
Absorption correction	Multi-scan (*SADABS*; Krause et al., 2015)
T_{min}, T_{max}	0.93, 0.98
No. of measured, independent and observed [$I > 2\sigma(I)$] reflections	23407, 3594, 3145
R_{int}	0.025
(sin $\theta/\lambda)_{max}$ (Å^{-1})	0.682
Refinement	
$R[F^2 > 2\sigma(F^2)]$, $wR(F^2)$, S	0.038, 0.102, 1.04
No. of reflections	3594
No. of parameters	181
H-atom treatment	H-atom parameters constrained
$\Delta\rho_{max}$, $\Delta\rho_{min}$ (e Å^{-3})	0.41, −0.28

Computer programs: *APEX2* (Bruker, 2014, *SAINT* (Bruker, 2013), *SHELXT* (Sheldrick, 2015*a*), *SHELXL* (Sheldrick, 2015*b*), *XP* in *SHELXTL* (Sheldrick, 2008) and *publCIF* (Westrip, 2010).

The synthesis of the title compound was carried out following literature procedures for ethylene-bridged diphosphines with minor modifications (Casey *et al.*, 1983). Under an argon atmosphere, anhydrous benzofuran (1.181 g, 10.0 mmol, 4 eq.) was charged in a Schlenk flask and dissolved in 20 ml of anhydrous THF. The solution was cooled to 253 K, and *n*-BuLi (2.5 *M*, 4.0 ml, 10.0 mmol, 4 eq.) was added dropwise. The reaction mixture was stirred for 2 h. Subsequently, 1,2-bis(dichlorophosphanyl)ethane (580 mg, 2.5 mmol, 1 eq.) was added slowly to the lithiated benzofuran solution. The reaction temperature was maintained at 253 K for 2 h before allowing the reaction mixture to warm to room temperature. After stirring overnight, the solvent was removed *in vacuo*, yielding a yellow solid. To remove lithium chloride, the yellow solid was dissolved in 60 ml of anhydrous diethyl ether and the resulting suspension was filtered under an inert atmosphere. 1,2-Bis[di(benzofuran-2-yl)phosphanyl] ethane was crystallized from a concentrated dichloromethane solution at 278 K to afford colorless, needle-shaped crystals (894 mg, 1.6 mmol, 64%). Crystals suitable for single-crystal X-ray diffraction were obtained by diffusion of *n*-pentane into a dichloromethane solution of the phosphine.

^{1}H NMR (300 MHz, CD_2Cl_2): δ = 7.55 (*ddd*, *J* = 7.5, 1.4, 0.7 Hz, 4H), 7.46–7.39 (*m*, 4H), 7.35–7.18 (*m*, 8H), 7.13 (*q*, *J* = 1.0 Hz, 4H), 2.54 (*dd*, *J* = 5.6, 5.0 Hz, 4H).

^{13}C NMR (75 MHz, CD_2Cl_2): δ = 158.17, 154.26 (*dd*, *J* = 11.0, 8.9 Hz), 128.29 (*t*, *J* = 3.2 Hz), 125.68, 123.29, 121.64, 117.50 (*t*, *J* = 15.5 Hz), 111.75, 21.43 (*dd*, *J* = 6.4, 5.0 Hz).

^{13}C-DEPT-135 NMR (75 MHz, CD_2Cl_2): δ = 125.12 (CH, pos.), 122.73 (CH, pos.), 121.08 (CH, pos.), 116.94 (CH, pos.), 111.19 (CH, pos.), 20.77 (CH_2, neg.).

^{31}P NMR (122 MHz, CD_2Cl_2): δ = −52.60.

HRMS (ESI): *m*/*z* calculated for $C_{34}H_{24}O_4P_2$: 558.1150 $[M+H]^+$, found: 559.1219.

Refinement

Crystal data, data collection and structure refinement details are summarized in Table 1.

References

Ahrens, S., Kusy, R., Spannenberg, A., Vuong, T. H., Rabeah, J., Russbueldt, B. M. E., Panten, J., Jiao, H., Junge, K. & Beller, M. (2025). *J. Am. Chem. Soc.* **147**, 31859–31870.

Benny, A., Sharma, D., Ankur, Rajeshkumar, T., Maron, L. & Venugopal, A. (2023). *Chem. Eur. J.* **29**, e202300588.

Bruker (2013). *SAINT*. Bruker AXS Inc., Madison, Wisconsin, USA.

Bruker (2014). *APEX2*. Bruker AXS Inc., Madison, Wisconsin, USA.

Casey, C. P., Bullock, R. M. & Nief, F. (1983). *J. Am. Chem. Soc.* **105**, 7574–7580.

Clevenger, A. L., Stolley, R. M., Aderibigbe, J. & Louie, J. (2020). *Chem. Rev.* **120**, 6124–6196.

Dekker, G. P. C. M., Elsevier, C. J., Vrieze, K. & Van Leeuwen, P. W. N. M. (1992). *Organometallics* **11**, 1598–1603.

Krause, L., Herbst-Irmer, R., Sheldrick, G. M. & Stalke, D. (2015). *J. Appl. Cryst.* **48**, 3–10.

Leeuwen, P. W. N. M. van, Kamer, P. C. J., Reek, J. N. H. & Dierkes, P. (2000). *Chem. Rev.* **100**, 2741–2770.

Sheldrick, G. M. (2008). *Acta Cryst.* A**64**, 112–122.

Sheldrick, G. M. (2015*a*). *Acta Cryst.* A**71**, 3–8.

Sheldrick, G. M. (2015*b*). *Acta Cryst.* C**71**, 3–8.

Souza, E. L. S., Ahrens, S., Spannenberg, A., Neumann, H., Junge, K., Correia, C. R. D., Jackstell, R. & Beller, M. (2025). *Chem. Commun.* **61**, 9083–9086.

Westrip, S. P. (2010). *J. Appl. Cryst.* **43**, 920–925.

data reports

full crystallographic data

IUCrData (2025). **10**, x250916 [https://doi.org/10.1107/S2414314625009162]

1,2-Bis[di(benzofuran-2-yl)phosphanyl]ethane

Sebastian Ahrens, Anke Spannenberg, Matthias Beller and Kathrin Junge

1,2-Bis[di(benzofuran-2-yl)phosphanyl]ethane

Crystal data

$C_{34}H_{24}O_4P_2$
M_r = 558.47
Monoclinic, $P2_1/n$
a = 5.6351 (5) Å
b = 10.5372 (9) Å
c = 22.7988 (19) Å
β = 93.696 (1)°
V = 1350.9 (2) Å^3
Z = 2
$F(000)$ = 580
D_x = 1.373 Mg m^{-3}
Mo $K\alpha$ radiation, λ = 0.71073 Å
Cell parameters from 9822 reflections
θ = 2.6–29.2°
μ = 0.20 mm^{-1}
T = 150 K
Needle, colorless
0.35 × 0.17 × 0.11 mm

Data collection

Bruker APEXII CCD diffractometer
Radiation source: fine-focus sealed tube
Detector resolution: 8.3333 pixels mm^{-1}
φ and ω scans
Absorption correction: multi-scan (SADABS; Krause et al., 2015)
T_{min} = 0.93, T_{max} = 0.98
23407 measured reflections
3594 independent reflections
3145 reflections with $I > 2\sigma(I)$
R_{int} = 0.025
θ_{max} = 29.0°, θ_{min} = 1.8°
h = −7→7
k = −14→14
l = −31→31

Refinement

Refinement on F^2
Least-squares matrix: full
$R[F^2 > 2\sigma(F^2)]$ = 0.038
$wR(F^2)$ = 0.102
S = 1.04
3594 reflections
181 parameters
0 restraints
Hydrogen site location: inferred from neighbouring sites
H-atom parameters constrained
$w = 1/[\sigma^2(F_o^2) + (0.0496P)^2 + 0.6701P]$ where $P = (F_o^2 + 2F_c^2)/3$
$(\Delta/\sigma)_{max}$ = 0.001
$\Delta\rho_{max}$ = 0.41 e Å^{-3}
$\Delta\rho_{min}$ = −0.28 e Å^{-3}

Special details

Geometry. All esds (except the esd in the dihedral angle between two l.s. planes) are estimated using the full covariance matrix. The cell esds are taken into account individually in the estimation of esds in distances, angles and torsion angles; correlations between esds in cell parameters are only used when they are defined by crystal symmetry. An approximate (isotropic) treatment of cell esds is used for estimating esds involving l.s. planes.

Fractional atomic coordinates and isotropic or equivalent isotropic displacement parameters (Å²)

	x	*y*	*z*	U_{iso}*/U_{eq}
P1	0.71188 (6)	0.84518 (3)	0.46075 (2)	0.02309 (10)
O1	0.49580 (18)	0.91096 (10)	0.35215 (4)	0.0306 (2)
O2	0.66914 (17)	0.61479 (9)	0.40832 (4)	0.0265 (2)
C1	0.4685 (2)	0.92984 (11)	0.49513 (6)	0.0236 (2)
H1A	0.320524	0.923062	0.469453	0.028*
H1B	0.439854	0.889731	0.533297	0.028*
C2	0.6973 (3)	0.92132 (12)	0.38979 (6)	0.0275 (3)
C3	0.8541 (3)	1.00332 (13)	0.36809 (6)	0.0280 (3)
H3	1.005756	1.025137	0.385828	0.034*
C4	0.7503 (3)	1.05138 (13)	0.31355 (6)	0.0273 (3)
C5	0.8159 (3)	1.14240 (15)	0.27287 (7)	0.0362 (3)
H5	0.963404	1.185957	0.277924	0.043*
C6	0.6589 (4)	1.16671 (17)	0.22517 (7)	0.0458 (4)
H6	0.698030	1.229013	0.197263	0.055*
C7	0.4426 (4)	1.1010 (2)	0.21721 (7)	0.0491 (4)
H7	0.339642	1.118676	0.183556	0.059*
C8	0.3754 (3)	1.01094 (17)	0.25715 (8)	0.0422 (4)
H8	0.229594	0.965882	0.251760	0.051*
C9	0.5312 (3)	0.99049 (13)	0.30494 (6)	0.0282 (3)
C10	0.5509 (2)	0.70025 (12)	0.44235 (5)	0.0227 (2)
C11	0.3408 (2)	0.65268 (12)	0.45784 (6)	0.0239 (3)
H11	0.229288	0.693672	0.480968	0.029*
C12	0.3194 (2)	0.52756 (12)	0.43237 (5)	0.0231 (2)
C13	0.1490 (3)	0.43112 (13)	0.43126 (6)	0.0284 (3)
H13	0.008549	0.439902	0.451813	0.034*
C14	0.1906 (3)	0.32213 (13)	0.39931 (7)	0.0326 (3)
H14	0.077800	0.255057	0.398549	0.039*
C15	0.3946 (3)	0.30903 (14)	0.36829 (7)	0.0347 (3)
H15	0.416334	0.233660	0.346410	0.042*
C16	0.5668 (3)	0.40349 (14)	0.36860 (7)	0.0327 (3)
H16	0.705679	0.395315	0.347393	0.039*
C17	0.5236 (2)	0.51025 (12)	0.40171 (6)	0.0245 (3)

Atomic displacement parameters (Å²)

	U^{11}	U^{22}	U^{33}	U^{12}	U^{13}	U^{23}
P1	0.02388 (17)	0.01797 (16)	0.02763 (18)	−0.00108 (11)	0.00324 (12)	−0.00143 (11)
O1	0.0314 (5)	0.0278 (5)	0.0333 (5)	−0.0038 (4)	0.0058 (4)	0.0004 (4)
O2	0.0255 (5)	0.0207 (4)	0.0339 (5)	0.0000 (4)	0.0059 (4)	−0.0060 (4)
C1	0.0272 (6)	0.0181 (5)	0.0259 (6)	−0.0009 (5)	0.0047 (5)	−0.0026 (5)
C2	0.0349 (7)	0.0203 (6)	0.0281 (6)	−0.0004 (5)	0.0073 (5)	−0.0034 (5)
C3	0.0339 (7)	0.0230 (6)	0.0273 (6)	−0.0057 (5)	0.0037 (5)	−0.0013 (5)
C4	0.0327 (7)	0.0240 (6)	0.0259 (6)	−0.0005 (5)	0.0072 (5)	−0.0028 (5)
C5	0.0399 (8)	0.0335 (8)	0.0367 (8)	−0.0043 (6)	0.0135 (6)	0.0027 (6)
C6	0.0671 (12)	0.0451 (9)	0.0267 (7)	0.0055 (8)	0.0143 (7)	0.0072 (7)

C7	0.0620 (12)	0.0565 (11)	0.0275 (7)	0.0084 (9)	−0.0089 (7)	−0.0055 (7)
C8	0.0405 (9)	0.0430 (9)	0.0419 (8)	−0.0020 (7)	−0.0059 (7)	−0.0096 (7)
C9	0.0317 (7)	0.0240 (6)	0.0296 (6)	−0.0012 (5)	0.0086 (5)	−0.0043 (5)
C10	0.0263 (6)	0.0172 (5)	0.0247 (6)	0.0020 (4)	0.0028 (5)	−0.0010 (4)
C11	0.0268 (6)	0.0186 (5)	0.0266 (6)	0.0008 (5)	0.0046 (5)	−0.0012 (4)
C12	0.0268 (6)	0.0188 (5)	0.0234 (6)	0.0015 (5)	−0.0017 (5)	0.0010 (4)
C13	0.0296 (7)	0.0239 (6)	0.0315 (7)	−0.0030 (5)	0.0006 (5)	0.0016 (5)
C14	0.0357 (7)	0.0211 (6)	0.0397 (8)	−0.0050 (5)	−0.0074 (6)	−0.0011 (5)
C15	0.0374 (8)	0.0231 (6)	0.0422 (8)	0.0044 (6)	−0.0077 (6)	−0.0110 (6)
C16	0.0299 (7)	0.0284 (7)	0.0396 (8)	0.0051 (5)	0.0003 (6)	−0.0103 (6)
C17	0.0248 (6)	0.0196 (6)	0.0288 (6)	0.0012 (5)	−0.0014 (5)	−0.0017 (5)

Geometric parameters (Å, º)

P1—C2	1.8028 (14)	C6—H6	0.9500
P1—C10	1.8117 (13)	C7—C8	1.384 (3)
P1—C1	1.8519 (13)	C7—H7	0.9500
O1—C2	1.3829 (18)	C8—C9	1.371 (2)
O1—C9	1.3887 (17)	C8—H8	0.9500
O2—C17	1.3758 (15)	C10—C11	1.3531 (18)
O2—C10	1.3869 (15)	C11—C12	1.4425 (17)
C1—C1^{i}	1.533 (2)	C11—H11	0.9500
C1—H1A	0.9900	C12—C17	1.3965 (19)
C1—H1B	0.9900	C12—C13	1.3971 (18)
C2—C3	1.3520 (19)	C13—C14	1.388 (2)
C3—C4	1.4321 (19)	C13—H13	0.9500
C3—H3	0.9500	C14—C15	1.394 (2)
C4—C9	1.394 (2)	C14—H14	0.9500
C4—C5	1.400 (2)	C15—C16	1.390 (2)
C5—C6	1.381 (2)	C15—H15	0.9500
C5—H5	0.9500	C16—C17	1.3850 (18)
C6—C7	1.404 (3)	C16—H16	0.9500
C2—P1—C10	100.04 (6)	C9—C8—H8	121.9
C2—P1—C1	99.98 (6)	C7—C8—H8	121.9
C10—P1—C1	97.50 (6)	C8—C9—O1	126.45 (14)
C2—O1—C9	106.27 (11)	C8—C9—C4	123.73 (14)
C17—O2—C10	106.06 (10)	O1—C9—C4	109.80 (12)
C1^{i}—C1—P1	110.79 (12)	C11—C10—O2	111.43 (11)
C1^{i}—C1—H1A	109.5	C11—C10—P1	133.26 (10)
P1—C1—H1A	109.5	O2—C10—P1	115.17 (9)
C1^{i}—C1—H1B	109.5	C10—C11—C12	106.59 (11)
P1—C1—H1B	109.5	C10—C11—H11	126.7
H1A—C1—H1B	108.1	C12—C11—H11	126.7
C3—C2—O1	110.67 (12)	C17—C12—C13	118.91 (12)
C3—C2—P1	128.31 (11)	C17—C12—C11	105.69 (11)
O1—C2—P1	120.64 (10)	C13—C12—C11	135.38 (13)
C2—C3—C4	107.70 (13)	C14—C13—C12	118.18 (14)

C2—C3—H3	126.1	C14—C13—H13	120.9
C4—C3—H3	126.1	C12—C13—H13	120.9
C9—C4—C5	119.42 (14)	C13—C14—C15	121.37 (13)
C9—C4—C3	105.53 (12)	C13—C14—H14	119.3
C5—C4—C3	134.98 (14)	C15—C14—H14	119.3
C6—C5—C4	117.75 (15)	C16—C15—C14	121.64 (13)
C6—C5—H5	121.1	C16—C15—H15	119.2
C4—C5—H5	121.1	C14—C15—H15	119.2
C5—C6—C7	121.14 (16)	C17—C16—C15	115.93 (14)
C5—C6—H6	119.4	C17—C16—H16	122.0
C7—C6—H6	119.4	C15—C16—H16	122.0
C8—C7—C6	121.67 (16)	O2—C17—C16	125.85 (13)
C8—C7—H7	119.2	O2—C17—C12	110.19 (11)
C6—C7—H7	119.2	C16—C17—C12	123.94 (13)
C9—C8—C7	116.23 (16)		

C2—P1—C1—C1^{i}	−66.72 (13)	C3—C4—C9—O1	1.48 (15)
C10—P1—C1—C1^{i}	−168.36 (12)	C17—O2—C10—C11	0.95 (14)
C9—O1—C2—C3	0.12 (15)	C17—O2—C10—P1	177.25 (9)
C9—O1—C2—P1	173.64 (9)	C2—P1—C10—C11	−113.82 (14)
C10—P1—C2—C3	−150.90 (13)	C1—P1—C10—C11	−12.23 (15)
C1—P1—C2—C3	109.56 (13)	C2—P1—C10—O2	70.91 (10)
C10—P1—C2—O1	36.84 (11)	C1—P1—C10—O2	172.49 (9)
C1—P1—C2—O1	−62.70 (11)	O2—C10—C11—C12	0.06 (15)
O1—C2—C3—C4	0.80 (16)	P1—C10—C11—C12	−175.35 (10)
P1—C2—C3—C4	−172.09 (10)	C10—C11—C12—C17	−1.02 (14)
C2—C3—C4—C9	−1.38 (15)	C10—C11—C12—C13	−179.30 (14)
C2—C3—C4—C5	175.51 (16)	C17—C12—C13—C14	−0.27 (19)
C9—C4—C5—C6	−0.7 (2)	C11—C12—C13—C14	177.84 (14)
C3—C4—C5—C6	−177.27 (16)	C12—C13—C14—C15	−0.9 (2)
C4—C5—C6—C7	−1.0 (2)	C13—C14—C15—C16	0.9 (2)
C5—C6—C7—C8	1.2 (3)	C14—C15—C16—C17	0.3 (2)
C6—C7—C8—C9	0.4 (3)	C10—O2—C17—C16	177.01 (13)
C7—C8—C9—O1	175.93 (14)	C10—O2—C17—C12	−1.61 (14)
C7—C8—C9—C4	−2.2 (2)	C15—C16—C17—O2	179.94 (13)
C2—O1—C9—C8	−179.39 (15)	C15—C16—C17—C12	−1.6 (2)
C2—O1—C9—C4	−1.02 (14)	C13—C12—C17—O2	−179.74 (11)
C5—C4—C9—C8	2.4 (2)	C11—C12—C17—O2	1.64 (14)
C3—C4—C9—C8	179.90 (14)	C13—C12—C17—C16	1.6 (2)
C5—C4—C9—O1	−176.00 (12)	C11—C12—C17—C16	−177.01 (13)

Symmetry code: (i) −*x*+1, −*y*+2, −*z*+1.

7.5 General and Anti-Markovnikov Selective Ni-Catalyzed Alkylation of Arenes and Heteroarenes with Non-Activated Olefins

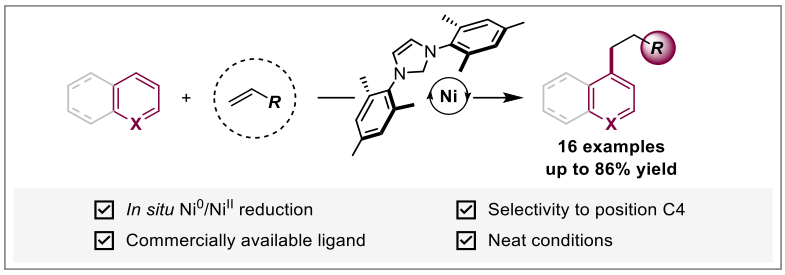

de Souza, E. L. S.; **Ahrens, S.**; Junge, K.; Quesada, J.; Beller, M. *Eur. J. Org.* **2025**, *28* (37), e202500590. DOI: 10.1002/ejoc.202500590. Electronic supporting information is available online.

Author's Contribution

The author optimized the reaction conditions and evaluated the substrate scope. The author also contributed to the preparation of the manuscript and to the revision process. The overall contribution is estimated at approximately 30%.

Sebastian Ahrens
(PhD student)

Prof. Matthias Beller
(Supervisor)

Check for updates

EurJOC
European Journal of Organic Chemistry

Research Article
doi.org/10.1002/ejoc.202500590

Chemistry Europe
European Chemical Societies Publishing

www.eurjoc.org

General and Anti-Markovnikov Selective Ni-Catalyzed Alkylation of Arenes and Heteroarenes with Non-Activated Olefins

Edson Leonardo Scarpa de Souza, Sebastian Ahrens, Kathrin Junge,* Jorge Quesada,* and Matthias Beller*

The majority of C–C coupling reactions between arenes and olefins result in the formation of branched isomer products, exhibiting what is known as Markovnikov selectivity. However, alternative catalytic strategies are required to modulate this selectivity, thereby yielding linear isomer products that are crucial for various significant applications. In this study, a straightforward Ni^0–*N*-heterocyclic carbene (NHC) catalyst is presented for the anti-Markovnikov hydroarylation of unactivated olefins with arenes (benzene) and heteroarenes (pyridine, indole, and imidazopyridine derivatives). The active catalyst species are *in situ* generated from NHC ligands and a stable Ni^{II} salt that is reduced by an alkaline hydride (NaH, LiH). This strategy circumvents the elaborate procedures that have been employed to synthesize and isolate Ni^0–NHC complexes. The assessment of >15 reactions between olefins and (hetero)arenes shows the formation of linear isomers as the predominant products, with yields ranging from moderate to excellent and exceptional selectivity.

1. Introduction

A classical method to prepare alkylated arenes is the Friedel–Crafts alkylation. Since the seminal report in 1877 by C. Friedel and J. Crafts,[1] this reaction became one of the cornerstones of organic chemistry,[2] and several Friedel–Crafts alkylation reactions are of considerable industrial significance. For instance, they play a pivotal role in the synthesis of ethylbenzene, which is a crucial precursor to polystyrene, and cumene, a vital intermediate in the production of styrene. Today, in most commercial applications, the alkylating agents employed are olefins, and the catalysts utilized are solid acids derived from zeolites. Despite many advancements over the past 150 years, Friedel–Crafts alkylation reactions still exhibit several drawbacks. Primarily, these transformations require harsh reaction conditions, which restrict the use of more advanced substrates. In addition, the reaction frequently fails with heteroarenes, such as pyridine, due to their intrinsic basicity. Conversely, alkylated heteroarenes, most notably pyridines, are significant motifs in numerous bioactive molecules, agrochemicals, and pharmaceuticals.[3–6] The synthesis of alkylated pyridines requires a substantial investment of time and resources and typically involves intricate synthetic methodologies, which are commonly based on coupling reactions catalyzed by transition metals.[7–11]

The functionalization of pyridine/(hetero)arene rings with alkyl substituents involves C—H bond activation processes, which are enabled by transition metal catalysis employing sophisticated ligands and additives. The C–H activation of the C-2 position in pyridine is comparatively less challenging than in C-3 or C-4 positions due to the reduced C–H acidity in this position,[12] and the strong coordination between the metal and the pyridine N-sp2. Nevertheless, functionalization of the C-4 position of pyridine has been achieved by obstructing the C-2 sites with bulky covalently bonded species at the pyridine nitrogen, as recently reported by Baran using a maleate-derived blocking group[13] and by Fier using an oxime-based pyridinium approach.[14] While these methods effectively produce the desired products with high yield and selectivity, they require multiple steps for the installation or removal of the blocking groups. Alternatively, *N*-oxides or *N*-alkyl/acyl-pyridinium derivatives can be used, as they facilitate electrophilic or nucleophilic substitution due to the increased polarity of the pyridine aromatic ring.[15–17] In contrast, C-4 functionalization of pyridines can be achieved directly using Lewis acids (LA).[18]

Hiyama and coworkers[18] as well as the group of Hartwig[19] demonstrated the hydroarylation of (hetero)arenes with olefins utilizing advanced Ni complexes. In these reactions, the respective C–H activation processes proceed via Ni^0 species. Typically, Ni species are stabilized by *N*-heterocyclic carbene (NHC)

E. L. Scarpa de Souza, S. Ahrens, K. Junge, J. Quesada,[+] M. Beller
Leibniz-Institut für Katalyse e.V.
Albert-Einstein-Str. 29a, 18059 Rostock, Germany
E-mail: Kathrin.Junge@catalysis.de
jorge.quesada@urjc.es
matthias.beller@catalysis.de

[+]*Present address: Department of Chemical, Energy, and Mechanical Technology, Universidad Rey Juan Carlos, C. Tulipán s/n, 28933 Móstoles, Madrid, Spain*

Supporting information for this article is available on the WWW under https://doi.org/10.1002/ejoc.202500590

© 2025 The Author(s). European Journal of Organic Chemistry published by Wiley-VCH GmbH. This is an open access article under the terms of the Creative Commons Attribution License, which permits use, distribution and reproduction in any medium, provided the original work is properly cited.

© 2025 The Author(s). European Journal of Organic Chemistry published by Wiley-VCH GmbH

EurJOC
European Journal of Organic Chemistry

Research Article
doi.org/10.1002/ejoc.202500590

Chemistry Europe
European Chemical Societies Publishing

19990690, 2025, 37, Downloaded from https://chemistry-europe.onlinelibrary.wiley.com/doi/10.1002/ejoc.202500590 by Leibniz-Institut fuer Katalyse, Wiley Online Library on [27/10/2025]. See the Terms and Conditions (https://onlinelibrary.wiley.com/terms-and-conditions) on Wiley Online Library for rules of use; OA articles are governed by the applicable Creative Commons License

ligands, and especially bulky ligands are beneficial in stabilizing the transition state, allowing selective anti-Markovnikov pathways. Nonetheless, the synthesis and subsequent isolation of such Ni^0–NHC complexes is often time-consuming and laborious. The *in situ* generation of active Ni^0 species by reduction of Ni^{II} precursors with metals (*e.g.*, Mn,^{0} Mg,^{0} Zn^0) or hydrides can circumvent these drawbacks. Following this idea, in this study a novel approach is proposed for the *in situ* formation of active Ni^0–NHC species for the selective alkylation of arenes and heteroarenes. This method involves combining NHC ligands with Ni^{II} salts in the presence of a reducing agent, using the reactants as the sole solvent. The generality of the concept is demonstrated by a set of 16 model reactions, in which various olefins and arenes/heteroarenes were tested. In all cases, the linear isomers were obtained with excellent regioselectivity in moderate to good yields. Notably, highly selective addition of pyridines at the C-4 position to unactivated olefins is possible without the need for blocking groups or additional chemical transformations of the pyridine motif.

The study was initiated with benzene (**1a**) and 3,3-dimethylbut-1-ene (**2a**) as model substrates. All experiments were conducted with the reactants acting as solvents, thereby avoiding the need to add other compounds to the reaction mixture (neat conditions). The complete tables that summarize the optimization procedure are provided, along with a discussion for each table, in the Supporting Information (SI, Table S1–S7). Different parameters of the reaction (NHC ligands, reducing agents, amounts of Ni salt and reducing agent, reaction temperature, and time) were thoroughly assessed. The most relevant data obtained from this screening of the reaction conditions are summarized in **Table 1**. First, the effect of combining $Ni(acac)_2$ with different NHC ligands was assessed to identify the ligand that would afford the best yield and selectivity at 80 °C over 24 h (Table 1, entries 1–3). No conversion of the starting materials into the desired products **3aa** and **3aa′** was observed when the NHC IPr (**L2**) and the bidentate ligand (**L3**) were used. Nevertheless, in the case of NHC IMes (**L1**), 43% conversion and 38% yield of the linear isomer **3aa** were detected. Increasing the temperature to 120 °C led to quantitative conversion and a 97% yield of the linear product, while no formation of the branched isomer was observed (entry 4).

The reduction of the Ni^{II} precursor to the active Ni^0 species is required for the catalytic reaction. For this purpose, several

Table 1. Screening of the reaction conditions for the hydroarylation of olefins catalyzed by Ni^0–NHC. Reaction conditions: 5 mol% Ni(acac)2, 5.5 mol% NHC, 10–50 mol% NaH, 1.05 mmol benzene (**1a**), benzene(**1a**):3,3-dimethyl but-1-ene(**2a**) = 11:1, 120 °C, 24 h, neat: absence of solvent. Yields were determined by gas chromatography with flame ionization detector (GC-FID).

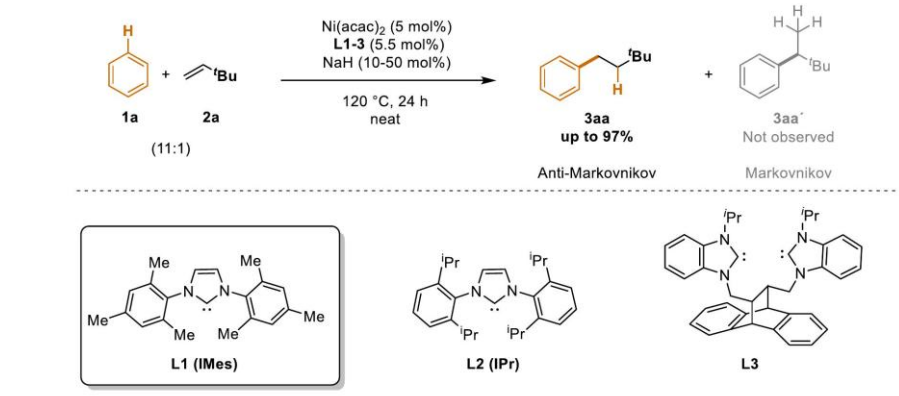

Entry	NHC	Varied parameter	Conv. [%]	Yield 3aa linear [%]	Yield 3aa′ branched [%]
1	**L1**	80 °C, 50 mol% NaH, 24 h, 11:1	43	38	not obs.
2	**L2**	80 °C, 50 mol% NaH, 24 h, 11:1	9	4	not obs.
3	**L3**	80 °C, 50 mol% NaH, 24 h, 11:1	13	Traces	not obs.
4	**L1**	120 °C, 50 mol% NaH, 24 h, 11:1	99	97	not obs.
5	**L1**	120 °C, 50 mol% NaH, 6 h, 11:1	99	97	not obs.
6	**L1**	120 °C, 20 mol% NaH, 6 h, 11:1	93	87	not obs.
7	**L1**	120 °C, 10 mol% NaH, 6 h, 11:1	40	33	not obs.
8	**L1**	120 °C, 20 mol% NaH, 6 h, 4:1	87	81	not obs.
9	**L1**	120 °C, 20 mol% NaH, 8 h, 4:1	**93**	**86**	not obs

© 2025 The Author(s). European Journal of Organic Chemistry published by Wiley-VCH GmbH

EurJOC
European Journal of Organic Chemistry

Research Article
doi.org/10.1002/ejoc.202500590

Chemistry Europe
European Chemical Societies Publishing

19990690, 2025, 37, Downloaded from https://chemistry-europe.onlinelibrary.wiley.com/doi/10.1002/ejoc.202500590 by Leibniz-Institut fuer Katalyse, Wiley Online Library on [27/10/2025]. See the Terms and Conditions (https://onlinelibrary.wiley.com/terms-and-conditions) on Wiley Online Library for rules of use; OA articles are governed by the applicable Creative Commons License

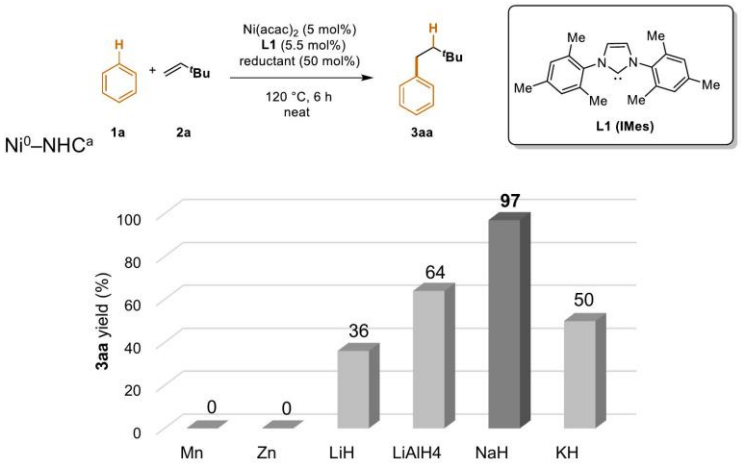

Figure 1. Screening of reductant agents in the hydroarylation of olefins catalyzed by Ni^0–NHC. a) Reaction conditions: 5 mol% $Ni(acac)_2$, 5.5 mol% IMes (**L1**), 50 mol% reductant, 1.05 mmol benzene (**1a**), benzene(**1a**):3,3-dimethyl but-1-ene(**2a**) = 11:1, 120 °C, 6 h, neat: absence of solvent. Yields were determined by GC-FID.

reductants (50 mol%) were assessed at 120 °C for 6 h. **Figure 1** shows the results obtained for the reaction between **1a** and **2a** using different reductant agents (Mn^0, Zn^0, LiH, $LiAlH_4$, NaH, and KH). Neither product formation nor reactant conversion was detected when Mn^0 or Zn^0 was used as reductant. In contrast, the desired linear isomer product **3aa** was observed as the sole product when alkaline hydrides were used. For instance, **3aa** was obtained in 97% yield with NaH as the reductant. The use of other alkaline hydrides led to the formation of **3aa** with yields in the range of 36–64% (36%, 50%, and 64% using LiH, KH, and $LiAlH_4$ as the reductants, respectively).

Following the identification of NaH as the optimal reducing agent, additional reaction parameters were screened. It was shown that after 6–8 h, the anti-Markovnikov product **3aa** was formed in high yields of up to 97%, depending on the loading of NaH (Table 1, entries 5 and 9). A further reduction in the amount of reducing agent to 20 mol% still provided satisfactory results, while catalytic efficiency decreased at 10 mol% (entries 6–7). The catalytic reaction also proceeded efficiently at a lower arene:olefin ratio of 4:1 (Table 1, entries 8–9), which reduces reactant consumption and facilitates product purification. Finally, under the optimized reaction conditions (5 mol% $Ni(acac)_2$, 5.5 mol% IMes (**L1**), 20 mol% NaH, arene:olefin ratio of 4:1, 120 °C, 8 h), 93% of the starting materials were smoothly converted into the linear anti-Markovnikov product **3aa** in 86% isolated yield.

The scope of the reaction was then investigated (**Figure 2**). Initially, substituted benzene derivatives such as *para*-xylene (**1b**) were tested, affording the corresponding anti-Markovnikov product **3ba** in 61% yield. Subsequently, various heteroarenes were assessed in the hydroarylation of olefins. Notably, pyridines, indole, and imidazopyridine furnished the linear products in good yields. In all examined cases, no formation of the branched isomer was detected.

After confirming that simple pyridine (**1c**) afforded the product **3ca** in 68% yield, the influence of different substituents was further examined. 2,5-Lutidine (**1d**) was converted to **3da** in 47% yield, while 2,6-lutidine (**1e**) led to **3ea** as a single isomer in 74% yield. Pyridines bearing bulkier groups, such as 2,6-di-*tert*-butylpyridine (**1f**), also reacted to yield the corresponding product **3fa** in 66% yield. Next, monosubstituted pyridines were examined, which could potentially lead to regioisomeric mixtures due to possible reactions at the C-2 and C-4 positions. The respective products **3ga** (ethyl), **3ha** (*i*Pr), and **3ia** (cyclopentyl) were obtained as single isomers resulting from C-4 functionalization of the pyridine ring, in moderate to good yields.

Pyridine bearing a phenyl substituent at the C-2 position underwent alkylation exclusively at the C-4 position, forming **3ja** in 57% yield. In this case, a slightly reduced chemoselectivity of the catalytic system was observed, resulting in small amounts (8%) of the phenyl hydroalkylation product. A similar outcome was observed with pyridine carrying a benzyl group at the C-2 position. Here, the anti-Markovnikov product **3ka** was obtained in 52% yield, while alkylation at the *para* position of the benzyl phenyl ring was detected in only 3% yield. Nevertheless, these two examples clearly show the preferential selectivity for the electron-poor aromatic ring compared to the phenyl and benzyl substituents. Hydroarylation products were also obtained from reactions with 2-methylquinoline, N-methylindole, and imidazo[1,2-a]pyridine, producing **3la** (44% yield), **3ma** (68% yield), and **3na** (42% yield), respectively.

© 2025 The Author(s). European Journal of Organic Chemistry published by Wiley-VCH GmbH

EurJOC
European Journal of Organic Chemistry

Research Article
doi.org/10.1002/ejoc.202500590

Chemistry Europe
European Chemical Societies Publishing

19990690, 2025, 37, Downloaded from https://chemistry-europe.onlinelibrary.wiley.com/doi/10.1002/ejoc.202500590 by Leibniz-Institut fuer Katalyse, Wiley Online Library on [27/10/2025]. See the Terms and Conditions (https://onlinelibrary.wiley.com/terms-and-conditions) on Wiley Online Library for rules of use; OA articles are governed by the applicable Creative Commons License

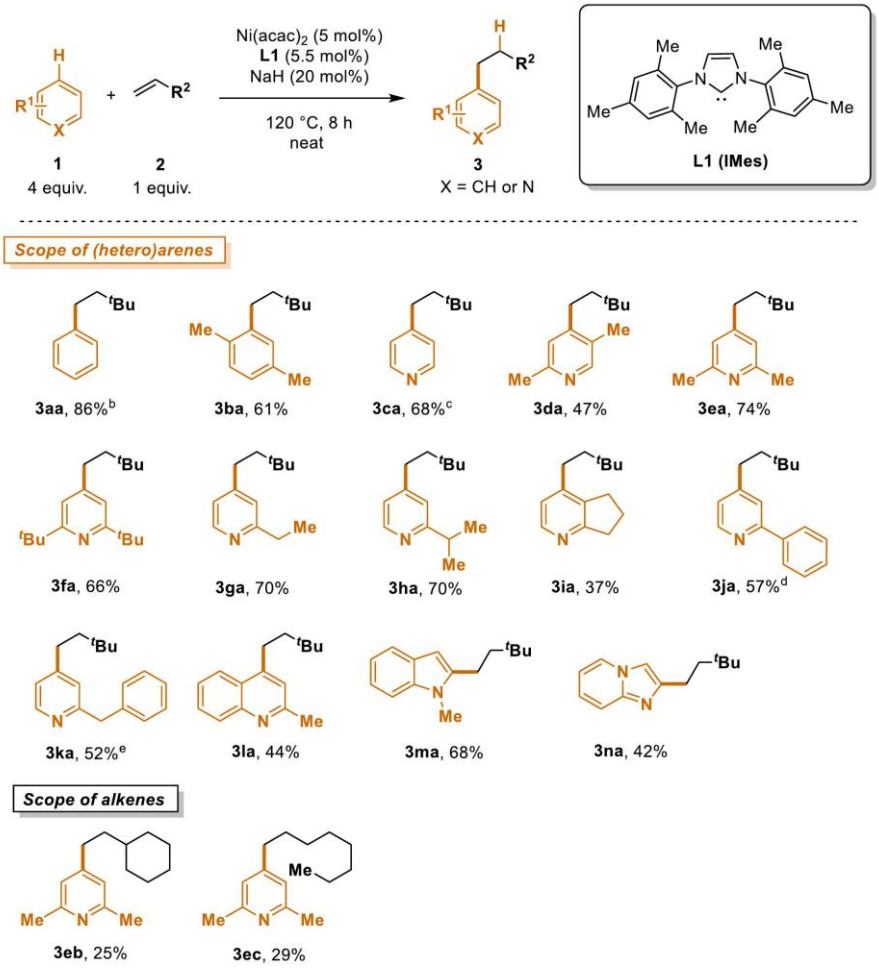

Figure 2. Scope of hydroarylation of olefins catalyzed by Ni^0–NHC. a) Reaction conditions: 5 mol% $Ni(acac)_2$, 5.5 mol% IMes (**L1**), arene:olefin ratio of 4:1 (4.2 mmol:1.05 mmol), 20 mol% NaH, 120 °C, 8 h, neat: absence of solvent. b) Yield was determined by GC-FID. c) Yield was determined by proton Nuclear Magnetic Resonance spectroscopy (^{1}H-NMR). d) 8% of the product was isolated from the reaction on the benzene ring. e) 3% of the product was isolated from the reaction on the benzene ring.

Next, the tolerance of the reaction toward different olefins was evaluated. Vinylcyclohexane was firstly considered, forming the desired product **3eb** in a moderate yield of 25%. The reaction using 1-octene as the olefin produced **3ec** in 29% yield. In both cases, neither double bond isomerization nor formation of branched products was detected.

In summary, a simple, practical, and resource-efficient protocol has been developed for the selective hydroarylation of unactivated olefins *via* an *in situ* generated Ni^0–NHC complex. The active catalytic system is formed by the reduction of the Ni^{II} precursor, $Ni(acac)_2$, and the IMes NHC ligand using simple NaH. The reported reaction exhibits high selectivity for the linear anti-Markovnikov product at the C-4 position of pyridines, without the need for additives or blocking groups. This enhances the sustainability of the transformation and contributes to a 100% atom economy.

© 2025 The Author(s). European Journal of Organic Chemistry published by Wiley-VCH GmbH

EurJOC
European Journal of Organic Chemistry

Research Article
doi.org/10.1002/ejoc.202500590

Chemistry Europe
European Chemical Societies Publishing

15990690, 2025, 37, Downloaded from https://chemistry-europe.onlinelibrary.wiley.com/doi/10.1002/ejoc.202500590 by Leibniz-Institut fuer Katalyse, Wiley Online Library on [27/10/2025]. See the Terms and Conditions (https://onlinelibrary.wiley.com/terms-and-conditions) on Wiley Online Library for rules of use; OA articles are governed by the applicable Creative Commons License

Acknowledgements

The authors acknowledge financial support from the German BMBF and the State of Mecklenburg-Western Pomerania. ELSS acknowledges financial support from the São Paulo Research Foundation (FAPESP grants: 2019/25657-9; 2022/14575-4). JQ acknowledges this project has received funding from the European Union's Horizon 2020 research and innovation program under the Marie Skłodowska-Curie grant agreement no. 101025659. The authors are also grateful to Dr. Soumyashree Jena for helpful discussions.

Open Access funding enabled and organized by Projekt DEAL.

Conflict of Interest

The authors declare no conflict of interest.

Author Contributions

The manuscript was prepared and written through contributions of all authors. All authors have given approval to the final version of the manuscript.

Data Availability Statement

The data that support the findings of this study are available in the supplementary material of this article.

Keywords: alkene hydroarylations · linear alkylbenzenes · *N*-heterocyclic carbenes · nickel catalysis · pyridine functionalization

[1] C. Friedel, J.-M. Crafts, *Compt. Rend.* **1877**, *84*, 1392.
[2] D. Lewis, *Synform* **2018**, 49, https://www.thieme.de/statics/bilder/thieme/final/en/bilder/tw_chemistry/CFZ-Synform-Charles-Friedel-James-Crafts-NRBio.pdf.
[3] L.S. Kishbaugh, *Curr. Top. Med. Chem.* **2016**, *16*, 3274.
[4] Y. Ling, Z. Y. Hao, D. Liang, C. L. Zhang, Y. F. Liu, Y. Wang, *Drug Des. Devel. Ther.* **2021**, *15*, 4289.
[5] S. De, S. K. Ashok Kumar, S. K. Shah, S. Kazi, N. Sarkar, S. Banerjee, S. Dey, *RSC Adv.* **2022**, *12*, 15385.
[6] K. Vaithegi, S. Yi, J. H. Lee, B. V. Varun, S. B. Park, *Commun. Chem.* **2023**, *6*, 1.
[7] R. Grigg, V. Savic, *Tetrahedron Lett.* **1997**, *38*, 5737.
[8] S.-J. Lou, L. Zhang, Y. Luo, M. Nishiura, G. Luo, Y. Luo, Z. Hou, *J. Am. Chem. Soc.* **2020**, *142*, 18128.
[9] J. Kwak, Y. Ohk, Y. Jung, S. Chang, *J. Am. Chem. Soc.* **2012**, *134*, 17778.
[10] M. Takimoto, M. Liu, M. Nishiura, Z. Hou, *ACS Catal.* **2022**, *12*, 13792.
[11] J. C. Lewis, R. G. Bergman, J. A. Ellman, *J. Am. Chem. Soc.* **2007**, *129*, 5332.
[12] K. Shen, Y. Fu, J. N. Li, L. Liu, Q. X. Guo, *Tetrahedron* **2007**, *63*, 1568.
[13] J. Choi, G. Laudadio, E. Godineau, P. S. Baran, *J. Am. Chem. Soc.* **2021**, *143*, 11927.
[14] P. S. Fier, *J. Am. Chem. Soc.* **2017**, *139*, 9499.
[15] R. Lavilla, *J. Chem. Soc. Perkin 1* **2002**, *2*, 1141.
[16] Y. Moon, B. Park, I. Kim, G. Kang, S. Shin, D. Kang, M. H. Baik, S. Hong, *Nat. Commun.* **2019**, *10*, 1.
[17] S. Jung, S. Shin, S. Park, S. Hong, *J. Am. Chem. Soc.* **2020**, *142*, 11370.
[18] Y. Nakao, Y. Yamada, N. Kashihara, T. Hiyama, *J. Am. Chem. Soc.* **2010**, *132*, 13666.
[19] N. I. Saper, A. Ohgi, D. W. Small, K. Semba, Y. Nakao, J. F. Hartwig, *Nat. Chem.* **2020**, *12*, 276.

Manuscript received: June 3, 2025
Revised manuscript received: July 21, 2025
Version of record online: August 6, 2025

© 2025 The Author(s). European Journal of Organic Chemistry published by Wiley-VCH GmbH

7.6 Manganese *N,N,N*-pincer complex-catalyzed epoxidation of unactivated aliphatic olefins

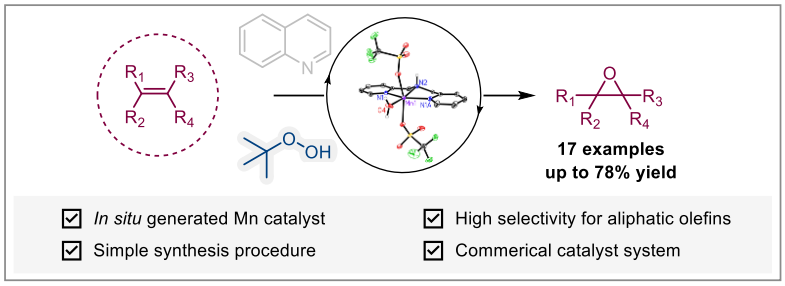

Verspeek, D.; **Ahrens, S.**; Spannenberg, A.; Wen, X.; Yang, Y.; Li, Y. W.; Junge, K.; Beller, M. *Catal. Sci. Technol.* **2022**, 12, 7341-7348.

DOI: 10.1039/D2CY01472F. Electronic supporting information is available online.

Author's Contribution

The author contributed to the conceptualization of the mechanistic studies and performed the crystallization experiments. The author also contributed to the preparation of the initial manuscript draft and the supporting information. The overall contribution is estimated at approximately 20%.

Sebastian Ahrens
(PhD student)

Prof. Matthias Beller
(Supervisor)

Published on 17 October 2022. Downloaded by Leibniz-Institut für Katalyse e. V. (LIKAT Rostock) on 10/17/2025 6:41:48 AM.

Catalysis Science & Technology

ROYAL SOCIETY OF CHEMISTRY

PAPER

View Article Online
View Journal | View Issue

Check for updates

Cite this: *Catal. Sci. Technol.*, 2022, **12**, 7341

Received 19th August 2022,
Accepted 17th October 2022

DOI: 10.1039/d2cy01472f

rsc.li/catalysis

Manganese *N,N,N*-pincer complex-catalyzed epoxidation of unactivated aliphatic olefins†

Dennis Verspeek, [a] Sebastian Ahrens, [a] Anke Spannenberg, [a] Xiaodong Wen, [bc] Yong Yang, [bc] Yong-Wang Li, [bc] Kathrin Junge *[a] and Matthias Beller *[a]

A practical *in situ* generated manganese(II) catalyst system with the commercially available bis(2-picolyl) amine ligand enables epoxidation of terminal aliphatic olefins in good yields with *tert*-butyl hydroperoxide as oxidant. Crystallization experiments revealed the formation of two manganese solvent complexes with MeCN and H_2O, respectively. Furthermore, a detailed investigation of the quinoline additive identified its crucial role in this transformation as being both essential for the epoxide formation while simultaneously being detrimental to its stability.

Introduction

Metal-catalyzed epoxidation reactions of aliphatic olefins are widely used and studied tools in organic synthesis and the chemical industry.[1–4] More specifically, the selective epoxidation of terminal aliphatic olefins under environmentally benign conditions is desired as the corresponding 1,2-epoxides are valuable building blocks for a variety of daily life products ranging from epoxy resins, paints, surfactants to health care.[1,5–7] Thus, numerous epoxidation protocols based on a variety of different transition-metals, such as Sc,[8] Ti,[9–11] Mn,[12–16] Fe,[17–19] Nb,[20] Mo,[21] Ru,[22–24] and Rh[25,26] have been published in the past four decades. However, until now terminal olefins are difficult to be epoxidized in high yields.[27,28] With respect to the catalyst system, the use of non-noble metal complexes to enable such reactions would be preferred due to their non-toxic and ecologically friendly traits as well as their abundance and therefore inexpensive price.[29]

Among the non-noble metals, especially catalysts based on manganese have the potential for further applications in epoxidation reactions.[3] Despite all the advantages of non-noble metal catalysts, in general cost-effectiveness and robustness remain major unsolved problems with

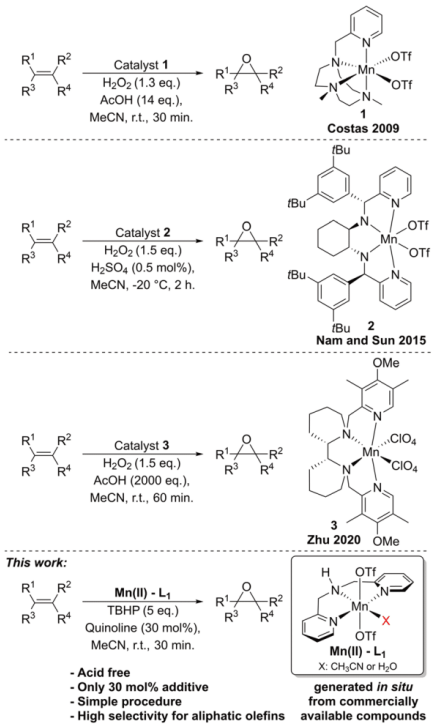

Scheme 1 Manganese(II) complexes applied in epoxidation reactions of alkenes.

[a] Leibniz-Institute für Katalyse e.V., Albert-Einstein-Straße 29a, 18059 Rostock, Germany. E-mail: kathrin.junge@catalysis.de, matthias.beller@catalysis.de
[b] State Key Laboratory of Coal Conversion, Institute of Coal Chemistry, Chinese Academy of Sciences, Taiyuan, 030001, China
[c] National Energy Center for Coal to Liquids, Synfuels China Co., Ltd, Huairou District, Beijing, 101400, China

† Electronic supplementary information (ESI) available. CCDC 2187359 and 2187360 contain the supplementary crystallographic data for this paper. For ESI and crystallographic data in CIF or other electronic format see DOI: https://doi.org/10.1039/d2cy01472f

View Article Online

Published on 17 October 2022. Downloaded by Leibniz-Institut für Katalyse e. V. (LIKAT Rostock) on 10/17/2025 6:41:48 AM.

established manganese-catalyzed methodologies. Interestingly, in 2008 the group of Wong showed that even terminal aliphatic olefins can be epoxidized in high yields following a simple procedure, though they relied on the use of peracetic acid as the oxidant, which results in undesirable side-products.[6]

One year later, Costas and co-workers demonstrated that high yields can also be achieved in these reactions utilizing environmentally friendly H_2O_2 as oxidant, but a large excess of acetic acid is needed to achieve decent yields (Scheme 1).[30]

In 2015, Nam and Sun reported the asymmetric epoxidation of olefins, which also included terminal aliphatic olefins.[31] However, the requirement of rather complex procedures and elaborate ligand syntheses renders their protocol unsuitable for industrial application of inexpensive bulk chemical syntheses. Although further, valuable contributions were made in the field of manganese-catalyzed epoxidation reactions,[32–37] there is still a general lack of a method that focuses on a combination of the following points: 1) a protocol that specifically addresses the epoxidation of terminal aliphatic olefins, which is of interest for bulk and fine chemical syntheses, 2) the employment of a cheap catalytic system that does not require complicated procedures or elaborate ligand syntheses, and 3) the use of an environmentally benign oxidant without the necessity of large excesses of acids or similarly corrosive, toxic or otherwise unbenign compounds. In this paper, we present our development of a simple and accessible *in situ* manganese(II)-catalyzed reaction that is designed for the environmentally friendly and cost-effective epoxidation of terminal aliphatic olefins. Furthermore, we provide a detailed investigation of this system, its advantages and ultimately, its limitations.

Results and discussion

Catalytic experiments

Based on our previous works with non-noble metal pincer catalysts,[18,38] we started our investigations by probing the reactivity of the *in situ* catalytic system of manganese(II) – triflate as precursor and bis(2-picolyl amine) $\mathbf{L_1}$ as the employed *N*,*N*,*N* – pincer ligand for the epoxidation of the model substrate 1-octene **4a**. As the terminal oxidant, an aqueous solution of *tert*-butyl hydroperoxide (TBHP) was used, which is also industrially applied in the epoxidation of propylene (Halcon process).[39] Employing 1 equivalent of TBHP at room temperature and 5 mol% of manganese precursor only trace amounts of the desired product 1,2-epoxyoctane **5a** were detected by GC analysis (Table 1). Here, no major product could be identified assuming that the starting material mainly underwent oxidative degradation to CO_2. However, the addition of *N*-heterocyclic compounds as co-ligands, which are known for their beneficial effects in selected metal-catalyzed oxidation reactions,[18,40,41] surprisingly improved the reaction to a significant degree. Selected results of the influence of different *N*-containing compounds on the reaction outcome are shown in Table 1.

Table 1 Screening of different additives and ligands

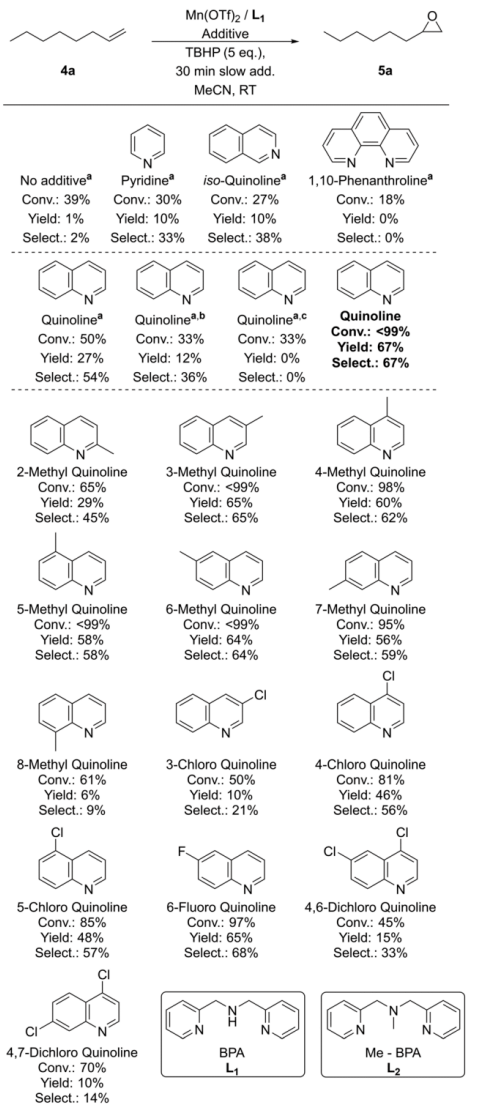

Conversion and yield determined by GC analysis with hexadecane as IST. Reaction conditions: 0.5 mmol substrate (0.125 M), 5 mol% $Mn(OTf)_2$, 6 mol% $\mathbf{L_1}$, 30 mol% quinoline derivative, MeCN (4 mL), 25 °C, 30 min slow addition of TBHP (70% aq., 5 eq.) *via* syringe pump. [a] 1 eq. of TBHP employed. [b] 6 mol% $\mathbf{L_2}$. [c] No ligand employed.

 This journal is © The Royal Society of Chemistry 2022

View Article Online

Published on 17 October 2022. Downloaded by Leibniz-Institut für Katalyse e. V. (LIKAT Rostock) on 10/17/2025 6:41:48 AM.

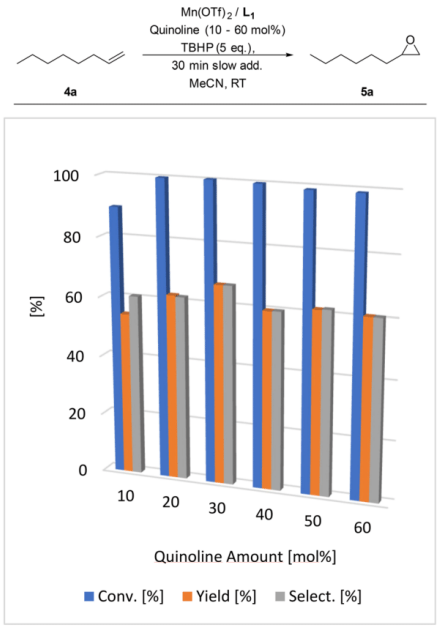

Fig. 1 Variation of the quinoline amount for epoxidation reaction. Conversion and yield determined by GC analysis with hexadecane as IST. Reaction conditions: 0.5 mmol substrate (0.125 M), 5 mol% $Mn(OTf)_2$, 6 mol% L_1, 10–60 mol% quinoline, MeCN (4 mL), 25 °C, 30 min slow addition of TBHP (70% aq., 5 eq.) *via* syringe pump.

For example, in the presence of 30 mol% of pyridine, 10% of the corresponding epoxide was formed. Notably, switching from pyridine to quinoline to test other aromatic heterocycles, showed a significant improvement of this result, giving 27% yield of 1,2-epoxyoctane **5a** under the applied reaction conditions. Here, *iso*-quinoline yielded very similar results to pyridine, and the bidentate 1,10-phenanthroline was not suitable for this reaction. Interestingly, applying 5 eq. of TBHP led to full conversion of **4a** giving 67% yield of the desired epoxide **5a** with simple quinoline as the additive. Therefore, the effect of different substituted and commercially available quinolines was investigated in the model reaction. In a first set of experiments, we used methylated quinolines as additives.

While 2-methyl- and 8-methylquinoline led to a significantly reduced catalytic performance, all other methylated quinolines provided similar or slightly lower yields compared to unsubstituted quinoline. Next, halogenated quinolines with electron-withdrawing substituents were investigated in the epoxidation reaction. Here, 6-fluoroquinoline yielded the epoxide **5a** in good yield, and 4- and 5-chloroquinoline provided more moderate yields. On the other hand, 3-chloroquinoline and di-chlorinated quinolines caused lower conversions and low selectivity towards the desired epoxide (see Table 1). Obviously, there is no clear structure–activity relationship of the influence of the substituted quinolines on the reaction outcome. Since none of the tested quinoline derivatives increased the product yields, the parent quinoline was the additive of choice for further optimization studies. As expected, no reaction occurred without employing a pincer ligand. Applying the *N*-methylated bis(2-picolyl amine) L_2 had a detrimental effect on the reactivity of this system, giving only 12% epoxide **5a** after GC analysis.

Next, the amount of the quinoline additive was varied (Fig. 1 and Table S1†). Employing only 10 mol% of quinoline led to a slightly reduced conversion and an accordingly lower yield. Similar conversions were obtained with loadings of quinoline between 20 and 40 mol%, while 30 mol% of quinoline seemed to be the reactions "sweet-spot".

In contrast, higher amounts of the additive (up to 60 mol%) do not further improve the reaction outcome giving yields around 60%.

Subsequently, different manganese precursors were tested for this reaction. To identify differences in the reactivity more easily, we employed only 1 eq. of TBHP. As shown in Table 2 and Fig. S1,† only precursors with weakly coordinating anions were effective for the epoxidation reaction. Optimal results were obtained in the presence of manganese(II) perchlorate, manganese(II) triflimide and manganese(II) triflate (Table 2, entries 1, 5 and 7). Using an iron(II) pre-catalyst was found to be not compatible with the present protocol, demonstrating the unique reactivity of manganese under these conditions (Table 2, entry 4). Next to TBHP, we tested hydrogen peroxide as final oxidant, which provided only low amounts of the desired product (12%) (Table 2, entry 3). Interestingly, no difference applying the *in situ* generated catalyst system compared to using the isolated complexes **Mn-1** and **Mn-2** as catalyst was observed (Table 2, entry 13). It should be noted that no extra time for pre-stirring of the *in situ* system is required.

Here, the full catalytic potential is achieved shortly after mixing the precursor, the ligand, and the additive, indicating a fast complexation of the pincer ligand to the metal. Further screening efforts revealed that MeCN is the most suitable solvent for this reaction, as it is often observed in epoxidation reactions (Table S2†).[3] Any deviations from these optimized reaction conditions within the numerical parameters of this system, *e.g.*, reaction time, temperature, catalyst loading or the amount of employed oxidant, either had no positive effect on the yield, or gave (slightly) worse results (Table S3†).

Catalyst characterisation

Following the investigations of the model reaction, we focused our attention on synthesizing the defined manganese(II) complex catalyst. Therefore, manganese(II) triflate and bis(2-picolyl amine) L_1 were mixed under inert conditions in dry MeCN and subsequently layered with dry Et_2O.

View Article Online

Published on 17 October 2022. Downloaded by Leibniz-Institut für Katalyse e. V. (LIKAT Rostock) on 10/17/2025 6:41:48 AM.

Table 2 Screening of different metal-precursors and amounts of peroxide

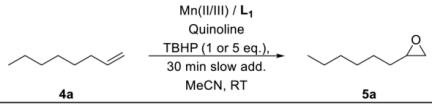

Entry	Precursor	TBHP [eq.]	Conv.[a] [%]	Yield[a] (**5a**) [%]	Sel. (**5a**) [%]
1	$Mn(OTf)_2$	1	50	27	54
2	$Mn(OTf)_2$	5	>99	67	67
3	$Mn(OTf)_2$	H_2O_2 (5 eq.)	21	12	57
4	$Fe(OTf)_2$	5	12	1	8
5	$Mn(ClO_4)_2$	1	43	24	55
6	$Mn(ClO_4)_2$	5	99	59	60
7	$Mn(NTf_2)_2$	1	42	26	62
8	$Mn(NTf_2)_2$	5	99	61	62
9	$MnCl_2$	1	17	1	6
10	$Mn(OAc)_2$	1	22	0	0
11	$Mn(acac)_2$	1	14	0	0
12	$Mn(acac)_3$	1	21	0	0
13	**Mn-1** or **Mn-2**	5	>99	67	67

[a] Conversion and yield determined by GC analysis with hexadecane as IST. Reaction conditions: 0.5 mmol substrate (0.125 M), 5 mol% manganese precursor, 6 mol% $\mathbf{L_1}$, 30 mol% quinoline, MeCN (4 mL), 25 °C, 30 min slow addition of oxidant *via* syringe pump.

Gratifyingly, **Mn-1** was obtained as colourless needles after crystallization. The complex crystallizes in the triclinic space group $P\bar{1}$ with two molecules in the unit cell and a distorted octahedral geometry. Here, one MeCN molecule is coordinated to the manganese(II) center in addition to the three nitrogen atoms of the pincer ligand and two triflate groups with the ligand coordinating in an equatorial fashion (Fig. 2). There are reports known where the employed ligands coordinate in a facial manner to the transition metal, especially when a twofold excess of ligand is used.[42–45] Elemental analysis confirms the formation of $Mn(II)(OTf)_2$ – $\mathbf{L_1}$ as the coordinating MeCN is removed *in vacuo* when drying the crystals before measurement. Accordingly, HRMS shows $[M\text{-}OTf]^+$. In a second set up, the above procedure was repeated, however, in this case undried MeCN was used to mimic the reaction conditions, where aqueous TBHP solution is applied. Here, layering the MeCN solution of the complex with benzene led to the formation of a different solvent complex **Mn-2**, which was obtained as colourless prismatic needles. In contrast to **Mn-1**, the usage of undried MeCN led to an exchange of the additional coordinating MeCN with a water molecule. This complex crystallizes in the monoclinic space group $P2/n$ with two molecules in the unit cell and a distorted octahedral geometry. The pincer ligand and the triflates coordinate in a similar fashion to **Mn-1** (Fig. 3). Here, elemental analysis and HRMS also confirm the formation of $Mn(II)(OTf)_2$ – $\mathbf{L_1}$ and $[M\text{-}OTf]^+$, respectively.

Obviously, **Mn-1** is converted to **Mn-2** during the catalytic reaction, which would also explain the similar catalytic performance of the isolated complexes **Mn-1** and **Mn-2** and the *in situ* system. A detailed discussion about the bond length and angles of **Mn-1** and **Mn-2** is not possible because

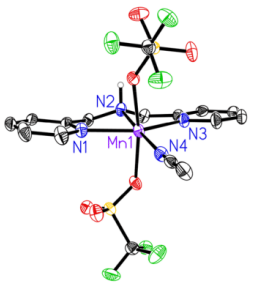

Fig. 2 ORTEP representation of **Mn-1**. (S yellow, O red, F green). Displacement ellipsoids correspond to 30% probability. C-bound hydrogen atoms and one position of the disordered triflate ligands are omitted for clarity.

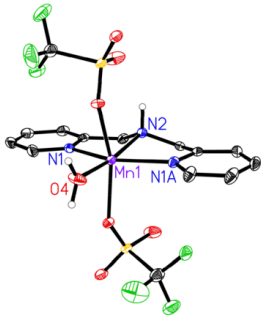

Fig. 3 ORTEP representation of **Mn-2**. (S yellow, F green). Displacement ellipsoids correspond to 30% probability. C-bound hydrogen atoms and one position of the disordered parts of the complex are omitted for clarity.

This journal is © The Royal Society of Chemistry 2022

View Article Online

Published on 17 October 2022. Downloaded by Leibniz-Institut für Katalyse e. V. (LIKAT Rostock) on 10/17/2025 6:41:48 AM.

the triflate groups of both complexes as well as the ligand backbone of **Mn-2** are disordered over two sites (see ESI†).

Mechanistic studies and scope

With the optimized reaction conditions and two crystal structures in hand, we focused on a more profound understanding of this catalytic system. Therefore, we started to investigate the reaction pathway by recording the kinetic profile of the epoxidation of the model substrate 1-octene **4a** (Fig. 4). When plotting the selectivity *versus* the reaction time, we found that it stays rather constant at approx. 60–67% after the starting period. Intriguingly, we also observed that the quinoline is partially consumed during the reaction, as only 39% of the initially employed amount is detected by GC analysis after 30 minutes.

To shed light on the nature of the reaction and possible side or follow-up reaction as well as on the intriguing role of quinoline, many control experiments were performed (Scheme 2): first, the radical scavenger TEMPO (1 eq.) was applied in the model reaction under optimized conditions, which completely inhibited product formation and pointed towards the importance of radical intermediates in this novel reaction. When adding 1 eq. of BHT to the reaction mixture, a similar yet less pronounced effect was observed with 45% conversion and 26% yield.

Furthermore, the product 1,2-epoxyoctane **5a** was subjected under the standard reaction conditions to test its stability. Interestingly, only 72% of **5a** and 19% of the employed quinoline were detected by GC analysis after 30 minutes. This clearly suggests that the product is not entirely stable under reaction conditions and that the inherent limitation of this system is more likely a follow-up reaction of the product with the quinoline rather than a side reaction of the starting material. Repetition of this experiment in the presence of 1 eq. TEMPO revealed that both the product **5a** and the quinoline remain completely unreacted, which indicates that the presumed follow-up reaction of the epoxide with the quinoline is also of radical nature. Unfortunately, all efforts to isolate the decomposition product (more than 20 attempts, see below) failed and it was not possible to identify its structure. In addition, we subjected the product to our standard reaction protocol without the addition of quinoline. Indeed, 100% of the epoxide could be recovered after 30 minutes reaction time, also indicating that these two compounds could react together in a follow-up reaction. Further control experiments revealed that a simple Lewis-acid catalyzed reaction between the quinoline and the epoxide can be excluded. Additionally, no reaction occurs in the absence of TBHP, revealing that the decomposition reaction only takes place under oxidative conditions. Interestingly, even the presence of the pincer ligand is also necessary for the decomposition step. Summarizing all these results, we can conclude that the

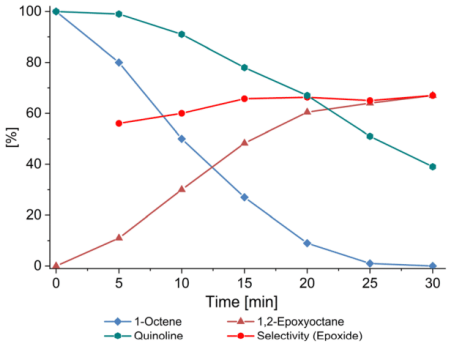

Fig. 4 Kinetic profile of epoxidation of 1-octene **4a**. Conversion and yield determined by GC analysis with hexadecane as IST. Reaction conditions: 0.5 mmol substrate **4a** (0.125 M), 5 mol% $Mn(OTf)_2$, 6 mol% L_1, 30 mol% quinoline, MeCN (4 mL), 25 °C, 30 min slow addition of TBHP (70% aq., 5 eq.) *via* syringe pump. Six reactions were set up in parallel and at every 5-minute mark one reaction was stopped and analyzed.

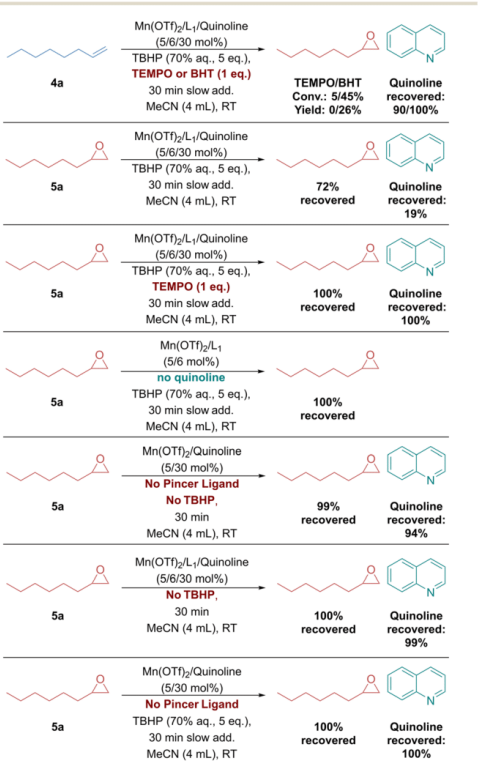

Scheme 2 Mechanistic experiments with 1-octene and 1,2-epoxyoctane. Conversion and yield determined by GC analysis with hexadecane as IST. Reaction conditions: 0.5 mmol 1-octene **4a** or 1,2-epoxyoctane **5a** (0.125 M), 5 mol% $Mn(OTf)_2$, 6 mol% L_1, 30 mol% quinoline, MeCN (4 mL), 25 °C, 30 min slow addition of TBHP (70% aq., 5 eq.) *via* syringe pump.

View Article Online

Published on 17 October 2022. Downloaded by Leibniz-Institut für Katalyse e. V. (LIKAT Rostock) on 10/17/2025 6:41:48 AM.

presence of quinoline or related heterocycles is essential for the desired product formation, while on the other hand it also promotes an unwanted follow-up reaction with the formed epoxide, which both are mediated by our manganese-pincer catalyst under oxidative conditions.

Further attempts were made to identify potential side products such as the mono-hydroxylated octenes **6** and **7**, 1,2-octanediol **8**, octanal **9** or octanoic acid **10**. Also, the formation of olefin cleavage products, such as heptanoic or hexanoic acid was considered (ESI†). However, none of them could be detected by GC and LC-MS analysis of the reaction mixture. Also, neither of these compounds appears to be an intermediate in the reaction, as their employment as starting materials did not yield the desired epoxide as product. Additionally, LC-MS analysis of reaction mixtures did not reveal the formation of quinoline-*N*-oxide, which could be formed under these oxidizing reaction conditions (Scheme S1 and Table S4†).

Besides, Browne and co-workers[15,16] describe the oxidative degradation of the ligand scaffolds to 2-picolinic acid which forms the active catalyst. Hence, several control experiments were realized, applying 2-picolinic acid or 2-picolyl amine as ligands in the model reaction. However, no catalytic activity was observed demonstrating that this reaction likely occurs through a different mechanism. Furthermore, the addition of picolinic acid in the presence of the pincer ligand BPA had only minor (6 mol% acid) or detrimental effect (15 mol% acid) on the reaction outcome. Based on these findings the involvement of 2-picolinic acid in the formation of the active catalyst can be excluded.

Furthermore, the potential formation of quinoline-*N*-oxide and its involvement in the catalytic reaction was explored. Using quinoline-*N*-oxide as additive only 18% of epoxide were formed underlining the beneficial role of quinoline for our catalytic protocol (see Table S5†).

Based on these results the following catalytic cycle was postulated (Scheme 3): in the first step (**A**), quinoline acts as a base deprotonating TBHP to facilitate the oxidation of $L_1Mn(II)(OTf)_2$ to $L_1Mn(III)(OTf)_2OOtBu$. A similar behaviour is reported by the group of Todisco using imidazole for the activation of TBHP in a manganese-catalyzed oxidation reaction.[46] Then, the manganese(III) species undergoes homolysis generating the oxo-species $L_1Mn(IV)=O(OTf)_2$ and a *tert*-butyl radical (step **B**). In the last step (**C**), the olefin **4** is oxidized to the epoxide **5** by the previously formed Mn(IV)=O species. As quinoline is partly consumed during the reaction, the following pathway **D** is proposed: The protonated quinoline can react with a *tert*-butyl radical, generating *tert*-butanol (observed by GC) and an oxidized quinolyl radical. Tertiary alkoxy radicals are known to eliminate methyl radicals and to generate the corresponding ketone.[31] Such methyl radicals can be responsible for quinoline degradation.

Notably, in the presence of TEMPO quinoline is fully recovered, while the formation of the alkylated adduct 1-methoxy-2,2,6,6-tetramethylpiperidine is observed by GC-MS (step **F**).

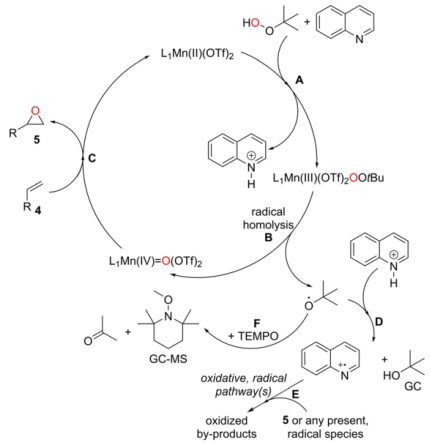

Scheme 3 Proposed catalytic cycle and quinoline degradation pathways of the epoxidation of simple olefins.

Finally, we studied the scope of this catalytic protocol applying other aliphatic olefins (Table 3). Both, linear and terminal epoxides bearing shorter alkyl chains **5b** and **5c** were obtained in moderate yields of 49% and 45%, respectively, possibly due to higher volatility of the corresponding products. Linear olefins with longer alkyl chains gave similar epoxide yields around 60% (see Table 3). Notably, the presented catalyst system is also suitable for the epoxidation of internal olefins. Switching to this class of substrates, we found that 2-methyl-1-heptene (**4i**) and 2-methyl-2-heptene (**4j**) gave epoxide yields of 59% and 53%, respectively. Applying cyclic alkenes, *e.g.*, cyclohexene (**4m**), less selective oxidizations occurred under these conditions, as an allylic oxidation also happens as a competing reaction, giving both products in a one-to-one ratio.

On the other hand, cyclooctene was epoxidized in good yield of 61%. Next, we subjected the more challenging substrate 4-vinyl cyclohexene to our optimized conditions to probe the selectivity of ring epoxidation *versus* epoxidation of the vinyl side chain. To our delight we observed an overall yield of epoxidation products of 78% with a selectivity of 2.2 : 1 (double epoxidation : ring epoxidation). Only trace amounts of the vinyl chain epoxidation product were observed.

Lastly, we tested the epoxidation of few selected aromatic olefins, which are in most epoxidation procedures more reactive substrates than terminal aliphatic olefins.[47] However, with the here presented catalytic protocol only 26% of styrene oxide were formed. Analogously, allylbenzene also led to a rather moderate epoxide yield of 27%. In both cases no major side product was observed by GC analysis. Furthermore, we found that the naturally occurring 1-octene-3-ol or the corresponding ketone are not well tolerated under our reaction conditions. In both cases only trace amounts of product (<5%), and much lower conversions were obtained (see Table S6†).

This journal is © The Royal Society of Chemistry 2022

View Article Online

Published on 17 October 2022. Downloaded by Leibniz-Institut für Katalyse e. V. (LIKAT Rostock) on 10/17/2025 6:41:48 AM.

Table 3 Manganese-catalyzed epoxidation with aliphatic olefins

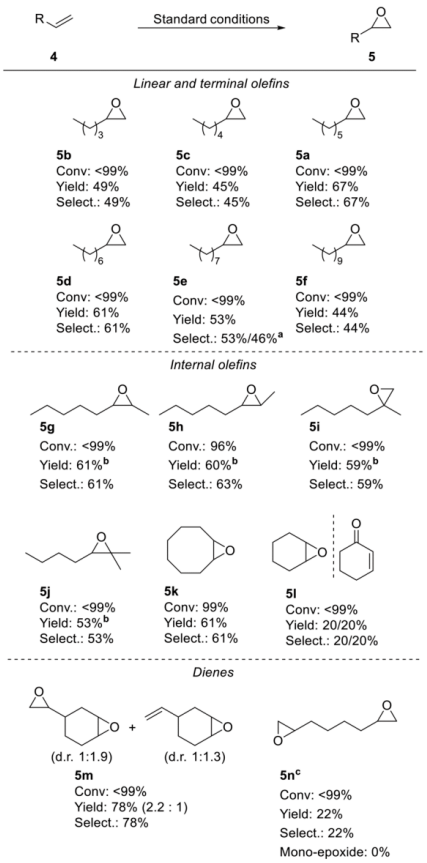

Conversion and yield determined by GC analysis with hexadecane as IST. [a] Isolated yield. [b] Yield determined by NMR analysis with dibromomethane as IST. [c] 0.25 mmol substrate. Reaction conditions: 0.5 mmol substrate (0.125 M), 5 mol% $Mn(OTf)_2$, 6 mol% $\mathbf{L_1}$, 30 mol% quinoline, MeCN (4 mL), 25 °C, 30 min slow addition of TBHP (70% aq., 5 eq.) *via* syringe pump.

Conclusions

In summary, we present a novel non-noble metal catalyst system for the epoxidation of industrially relevant aliphatic olefins. Key features of this system are the use of the commercially available tridentate *N*,*N*,*N*-ligand BPA and quinoline as additive. The active catalyst can be conveniently generated *in situ* from several cationic manganese salts, *e.g.*, $Mn(OTf)_2$ and BPA. Crystal structures of the formed pincer complexes are also provided. Mechanistic experiments underlined the crucial role of the addition of quinoline for this catalytic reaction as being essential for product formation, but also detrimental to product stability. Although the detailed influence of quinoline on these reactions is not entirely clear, we assume these results will inspire other researchers using quinoline and related derivatives in related reactions, too. Under optimized conditions, epoxide yields up to 67% could be achieved, which provides potential for further applications.

Experimental

General procedure for epoxidation of simple olefins

An 8 mL glass vial equipped with a Teflon coated stirring bar was charged with stock solutions of $Mn(OTf)_2$ (0.025 mmol, 8.8 mg, 5 mol% catalyst loading), bis(2-picolyl amine) (0.03 mmol, 6.0 mg, 6 mol%) and freshly distilled quinoline (0.15 mmol, 19.4 mg, 30 mol%). The resulting mixture was further diluted with MeCN to a total volume of 4 mL and stirred for 5 minutes. Then, 1-octene (0.5 mmol, 56.1 mg, 0.125 M) was added. Next, a solution of *tert*-butyl hydroperoxide (TBHP) (2.5 mmol, 5 eq., 340 μL, 70% aq.) in MeCN (660 μL) was added *via* a syringe pump to the reaction mixture over the course of 30 minutes. Afterwards, the reaction was terminated by the addition of a few drops of a saturated aqueous $Na_2S_2O_3$ solution (note: in most cased the addition of $Na_2S_2O_3$ is not necessary as all TBHP was already consumed at this point).

For GC analysis the reaction mixture was then diluted with EtOAc, filtered, and analyzed using hexadecane (30 μL) as an internal standard to determine conversion and yield.

Author contributions

M. B., K. J., and D. V. conceived and designed the project; D. V. and S. A. performed the experiments and analyzed the data; A. S. was responsible for the SC-XRD needed for the project; K. J., and M. B., supervised the research activities at the corresponding institutions, X. W., Y. Y. and Y.-W. L. supported the project with funding acquisition, M. B., K. J., and D. V. coedited the manuscript; D. V., S. A., K. J., and M. B. cowrote the paper.

Conflicts of interest

There are no conflicts to declare.

Acknowledgements

We thank Shuxin Mao and Prof. Haijun Jiao for valuable scientific discussions and the analytical department of LIKAT for their excellent services. In addition, we acknowledge funding from Synfuels China.

Notes and references

1 H. Adolfsson, *Transition Metal-Catalyzed Epoxidation of Alkenes*, Wiley-VCH, 2010.
2 J. Chen, Z. Jiang, S. Fukuzumi, W. Nam and B. Wang, *Coord. Chem. Rev.*, 2020, **421**, 213443.

View Article Online

Published on 17 October 2022. Downloaded by Leibniz-Institut für Katalyse e. V. (LIKAT Rostock) on 10/17/2025 6:41:48 AM.

3 R. M. Philip, S. Radhika, C. M. A. Abdulla and G. Anilkumar, *Adv. Synth. Catal.*, 2021, **363**, 1272–1289.
4 M. Costas, in *Green Oxidation in Organic Synthesis*, 2019, pp. 123–157, DOI: **10.1002/9781119304197.ch4**.
5 K. Junge, G. Wienhöfer and M. Beller, *Applied Homogenous Catalysis with Organo-metallic Compounds*, Wiley-VCH, 2018.
6 K. P. Ho, W. L. Wong, K. M. Lam, C. P. Lai, T. H. Chan and K. Y. Wong, *Chemistry*, 2008, **14**, 7988–7996.
7 M. V. B. S. Lane, V. J. DeRose and K. Burgess, *J. Am. Chem. Soc.*, 2002, **124**, 11946–11954.
8 H. Zhang, Q. Yao, L. Lin, C. Xu, X. Liu and X. Feng, *Adv. Synth. Catal.*, 2017, **359**, 3454–3459.
9 T. Katsuki and K. B. Sharpless, *J. Am. Chem. Soc.*, 1980, **102**, 5974–5976.
10 K. Matsumoto, Y. Sawada, B. Saito, K. Sakai and T. Katsuki, *Angew. Chem., Int. Ed.*, 2005, **44**, 4935–4939.
11 A. Berkessel, T. Guenther, Q. Wang and J. M. Neudörfl, *Angew. Chem., Int. Ed.*, 2013, **52**, 8467–8471.
12 R. Irie, K. Noda, Y. Ito and T. Katsuki, *Tetrahedron Lett.*, 1991, **32**, 1055–1058.
13 W. Zhang, J. L. Loebach, S. R. Wilson and E. N. Jacobsen, *J. Am. Chem. Soc.*, 1990, **112**, 2801–2803.
14 E. N. Jacobsen, W. Zhang, A. R. Muci, J. R. Ecker and L. Deng, *J. Am. Chem. Soc.*, 1991, **113**, 7063–7064.
15 D. Pijper, P. Saisaha, J. W. de Boer, R. Hoen, C. Smit, A. Meetsma, R. Hage, R. P. van Summeren, P. L. Alsters, B. L. Feringa and W. E. Browne, *Dalton Trans.*, 2010, **39**, 10375–10381.
16 P. Saisaha, J. J. Dong, T. G. Meinds, J. W. de Boer, R. Hage, F. Mecozzi, J. B. Kasper and W. R. Browne, *ACS Catal.*, 2016, **6**, 3486–3495.
17 K. Schröder, B. Join, A. J. Amali, K. Junge, X. Ribas, M. Costas and M. Beller, *Angew. Chem., Int. Ed.*, 2011, **50**, 1425–1429.
18 S. Mao, S. Budweg, A. Spannenberg, X. Wen, Y. Yang, Y.-W. Li, K. Junge and M. Beller, *ChemCatChem*, 2021, e202101668, DOI: **10.1002/cctc.202101668**.
19 O. Cussó, M. Cianfanelli, X. Ribas, R. J. M. Klein Gebbink and M. Costas, *J. Am. Chem. Soc.*, 2016, **138**, 2732–2738.
20 H. Egami, T. Oguma and T. Katsuki, *J. Am. Chem. Soc.*, 2010, **132**, 5886–5895.
21 Y. Shen, P. Jiang, P. T. Wai, Q. Gu and W. Zhang, *Catalysts*, 2019, **9**, 31.
22 W.-C. Cheng, W.-H. Fung and C.-M. Che, *J. Mol. Catal. A: Chem.*, 1996, **113**, 311–319.
23 M. K. Tse, C. Döbler, S. Bhor, M. Klawonn, W. Mägerlein, H. Hugl and M. Beller, *Angew. Chem., Int. Ed.*, 2004, **43**, 5255–5260.
24 M. K. Tse, S. Bhor, M. Klawonn, G. Anilkumar, H. Jiao, A. Spannenberg, C. Döbler, W. Mägerlein, H. Hugl and M. Beller, *Chem. – Eur. J.*, 2006, **12**, 1875–1888.
25 K. Barry Sharpless, *Chem. Commun.*, 1997, 1565–1566.
26 A. K. Yudin and K. B. Sharpless, *J. Am. Chem. Soc.*, 1997, **119**, 11536–11537.
27 J. R. Coombs and J. P. Morken, *Angew. Chem., Int. Ed.*, 2016, **55**, 2636–2649.
28 A. Murphy, G. Dubois and T. D. P. Stack, *J. Am. Chem. Soc.*, 2003, **125**, 5250–5251.
29 R. J. M. K. Gebbink and M.-E. Moret, *Non-Noble Metal Catalysis – Molecular Approaches and Reactions*, Wiley-VCH, Weinheim, 2019.
30 I. Garcia-Bosch, X. Ribas and M. Costas, *Adv. Synth. Catal.*, 2009, **351**, 348–352.
31 C. Miao, B. Wang, Y. Wang, C. Xia, Y. M. Lee, W. Nam and W. Sun, *J. Am. Chem. Soc.*, 2015, **138**, 936–943.
32 F. Zhu, G. Yang, A. J. Zoll, E. V. Rybak-Akimova and X. Zhu, *Catalysts*, 2020, **10**, 285–293.
33 D. Shen, C. Saracini, Y. M. Lee, W. Sun, S. Fukuzumi and W. Nam, *J. Am. Chem. Soc.*, 2016, **138**, 15857–15860.
34 M. Fontanet, M. Rodríguez, C. Viñas, F. Teixidor and I. Romero, *Eur. J. Inorg. Chem.*, 2017, **2017**, 4425–4429.
35 V. V. Fomenko, O. V. Bakhvalov, V. F. Kollegov and N. F. Salakhutdinov, *Russ. J. Gen. Chem.*, 2017, **87**, 1675–1679.
36 L. Vicens, G. Olivo and M. Costas, *ACS Catal.*, 2020, **10**, 8611–8631.
37 R. A. Moretti, J. Du Bois and T. D. P. Stack, *Org. Lett.*, 2016, **18**, 2528–2531.
38 S. Budweg, K. Junge and M. Beller, *Chem. Commun.*, 2019, **55**, 14143.
39 H. Mimoun, M. Mignard, P. Brechot and L. Saussine, *J. Am. Chem. Soc.*, 1986, **108**, 3711–3718.
40 Q.-W. Zhang, J. A. A. W. Elemans, P. B. White and R. J. M. Nolte, *Chem. Commun.*, 2018, **54**, 5586–5589.
41 B. Meunier, *Chem. Rev.*, 1992, **92**, 1411–1456.
42 K. Visvaganesan, R. Mayilmurugan, E. Suresh and M. Palaniandavar, *Inorg. Chem.*, 2007, **46**, 10294–10306.
43 A. Malassa, C. Agthe, H. Görls, M. Friedrich and M. Westerhausen, *J. Organomet. Chem.*, 2010, **695**, 1641–1650.
44 J. T. Simmons, Z. Yuan, K. L. Daykin, B. T. Nguyen, R. J. Clark, M. Shatruk and L. Zhu, *Supramol. Chem.*, 2014, **26**, 214–222.
45 A. Das, A. Rajeev, S. Bhunia, M. Arunkumar, N. Chari and M. Sankaralingam, *Inorg. Chim. Acta*, 2021, **526**, 120515.
46 A. Neshat, M. Kakavand, F. Osanlou, P. Mastrorilli, E. Schingaro, E. Mesto and S. Todisco, *Eur. J. Inorg. Chem.*, 2020, **2020**, 480–490.
47 A. M. Al-Ajlouni and J. H. Espenson, *J. Am. Chem. Soc.*, 1995, **117**, 9243–9250.

 This journal is © The Royal Society of Chemistry 2022

8 Appendix

8.1 Curriculum Vitae

Sebastian Ahrens

Personal Details

Date of Birth	16.01.1996 in Güstrow, Germany
Nationality	German
Address	John-Brinckman-Straße 13, 18055 Rostock, Germany
E-Mail	sebastian.ahrens@catalysis.de
ORCID	0000-0001-8365-0276

Education & Research Experience

10/2021-Present	Doctoral Researcher, Leibniz Institute for Catalysis, Rostock, Germany Supervisor: Prof. Dr. Matthias Beller Doctoral Thesis: *Rational Design and Synthesis of Phosphine Ligands and Their Application in Transition Metal-Catalyzed Reactions*
10/2018-03/2021	M.Sc. Biochemistry, University Greifswald Master Thesis, Group of C. Schulzke *Modification of mono-dithiolene complexes towards active catalysts for the small molecule activation*
10/2015-10/2018	B.Sc. Biochemistry, University Greifswald Bachelor Thesis, Group of C. Schulzke *Synthesis of oxo- and sulfido-complexes of molybdenum and tungsten bearing a maleonitriledithiolate ligand*
07/2015	Abitur, John-Brinckman-Gymnasium Güstrow

8.2 Publication List

1. Ahrens, S.; Kusy, R.; Spannenberg, A.; Vuong, T. H.; Rabeah, J.; Rußbüldt, B. M. E.; Panten, J.; Jiao, H.; Junge, K.; Beller, M. Cobalt(0)-Catalyzed Isomerization of Allylamines Promoted by Monodentate Benzofuran Phosphines. *J. Am. Chem. Soc.* **2025**, 147 (35), 31859–31870.

2. de Souza, E. L. S.[‡]; Ahrens, S.[‡]; Spannenberg, A.; Neumann, H.; Junge, K.; Correia, C. R. D.; Jackstell, R.; Beller, M. Development of Highly Efficient and Selective Palladium Catalysts for Telomerization of 1,3-Butadiene with Alcohols. *Chem. Commun.* **2025**, 61, 9083.

3. Ahrens, S.; Spannenberg, A.; Beller, M.; Junge, K. 1,2-Bis[di(benzofuran-2-yl)phosphanyl]ethane. *IUCrData* **2025**, 10, x250916.

4. Ge, Y.; Huang, W.; Ahrens, S.; Spannenberg, A.; Jackstell, R.; Beller, M. Synthesis of Non-Equivalent Diamides and Amido-Esters via Pd-Catalyzed Carbonylation. *Nat. Synth.* **2024**, 3, 202–213.

5. de Souza, E. L. S.; Ahrens, S.; Junge, K.; Quesada, J.; Beller, M. General and Anti-Markovnikov Selective Ni-Catalyzed Alkylation of Arenes and Heteroarenes with Non-Activated Olefins. *Eur. J. Org. Chem.* **2025**, 28 (37), e202500590.

6. Verspeek, D.; Ahrens, S.; Spannenberg, A.; Wen, X.; Yang, Y.; Li, Y. W.; Junge, K.; Beller, M. Manganese *N*,*N*,*N*-Pincer Complex-Catalyzed Epoxidation of Unactivated Aliphatic Olefins. *Catal. Sci. Technol.* **2022**, 12, 7341–7348.

7. Verspeek, D.; Ahrens, S.; Wen, X.; Yang, Y.; Li, Y. W.; Junge, K.; Beller, M. A Manganese-Based Catalyst System for General Oxidation of Unactivated Olefins, Alkanes, and Alcohols. *Org. Biomol. Chem.* **2024**, 22, 2630.

[‡] Authors contributed equally.

8.3 Conference Presentations

1. Poster “Electron-Rich Benzofuran Phosphines – Realizing Highly Efficient Cobalt-Catalyzed Isomerization of Allylamines” at the XXIII International Symposium on Homogeneous Catalysis. University of Trieste 2024, Italy.

2. Poster “Cobalt(0)-Catalyzed Isomerization of Allylamines Promoted by Monodentate Benzofuran Phosphines” at the 58th Annual Meeting of German Catalysts. Weimar 2025, Germany.